OPTIMISATION OF PETALOID BASE DIMENSIONS AND PROCESS OPERATING CONDITIONS TO MINIMISE ENVIRONMENTAL STRESS CRACKING IN INJECTION STRETCH BLOW MOULDED PET BOTTLES

A dissertation submitted for the degree of

Doctor of Philosophy

by

BILAL DEMIREL

M.Sc. Chemical Engineering
B.Sc. Chemical Engineering

School of Aerospace, Mechanical, and Manufacturing Engineering
RMIT University
Melbourne
Australia

September 2008

DEDICATION

To my mother who recently passed away and whom I respected and will always love

DECLARATION

The author declares that:

(1) To the best of my knowledge, this thesis does not contain any material previously written or published by another person except where reference is made;

(2) The thesis has not been submitted previously, in whole or in part, to qualify for any other academic award;

(3) The content of the thesis is the result of work which has been carried out since the official commencement date of the approved research program.

Bilal Demirel

<u>ACKNOWLEDGEMENT</u>

Last but not least, I would like to acknowledge my friends Baris Koca, Ali Turgut, Ismail Atas and Mustafa Uzkar for their valuable discussion, recommendations and guidance regarding bottle mould design and stress analysis.

TABLE OF CONTENTS

Page

Page

ABBREVIATIONS AND SYMBOLS

ABBREVIATIONS

ASCRU	Accelerated stress crack test unit
ASTM	American standard test methods
CAD	Computer aided design
CAM	Computer aided manufacturing
CHDM	Cyclohexane dimethanol
CSD	Carbonated soft drink
DMA	Dynamic mechanical analysis
DOT	Design optimization tools
DSC	Differential scanning calorimetry
ESC	Environmental stress cracking
ESCR	Environmental stress crack resistance
ESEM	Environmental scanning electron microscopy
FEA	Finite element analysis
FEM	Finite element method
FT-IR	Fourier transformed infrared
HDPE	High-density polyethylene
IMI	Industrial materials institute
ISBM	Injection stretch blow molding
IRS	Internal reflectance spectroscopy
MD	Machine direction
MDSC	Modulated differential scanning calorimerty
NMR	Nuclear magnetic resonance

PC	Polycarbonate
PET	Poly ethylene terephthalate
RER-PET	Reactive extruded recycled PET
RSBM	Reheat stretch blow molding
R-PET	Recycled PET
SAXS	Small angle X-ray scattering
SPC	Stored program control
SQC	Statistical quality control
SQP	Sequential quadratic programming
TA	Thermal Analysis
TD	Transverse direction
WAXS	Wide angle X-ray scattering

SYMBOLS

a	Wall thickness
b	Half-thickness of part
$C_{i,j}$	Mooney-Rivlin constants
$C_{o,i}$	Dimensionless coefficients
Cp	Specific heat
E	Young modulus
F	Fourier number or dimensionless time
f	Friction coefficient
h	Heat transfer coefficient
J(o)	Elastic compliance

K	Stress intensity factor
k	Thermal conductivity
T_a	Ambient temperature
T_{av}	Average temperature
T_C	Cold crystallization temperature at the first heating stage in MDSC
T_{C1}	Cold crystallization temperature at the cooling stage in MDSC
T_e	Ejection temperature of plastic part
T_f	Mould temperature
Tg	Glass transition temperature
T_i	Initial temperature of polymer melts
T_m	Melting point
T_m	Mid-plane temperature
$T(y, t)$	Temperature as function of thickness and time
t	Time
t_c	Cooling time
$U(\varepsilon)$	Strain energy potential
X	Weight of acid
X_c	Polymer crystallinity
W	Bottle base weight
Wc	Critical value for inelastic tensile strain energy density
Y	Carbonation Required (Gas Volumes)
y	Distance from mid-plane of part
Z	Brimful capacity of container
ΔH	Measured enthalpy of melting sample

ΔH_u	Enthalpy of fusion per mole of PET
ΔH_{100}	Enthalpy of melting a 100 % crystalline sample
τ_{xy}	Shear stress
γ_{xy}	Shear strain
υ	Poisson's ratio
α	Thermal diffusivity
λ	Principal stretch ratio
σ	Applied stress
σ_c	Critical stress
$\sigma(o)$	Instantaneous maximum stress
ε	Tensile strain
ε_c	Total critical tensile strain
ρ	Measured density of PET sample
ρ_a	Amorphous PET density
ρ_c	Crystalline PET density

LIST OF FIGURES

Page

Page

Page

Page

Page

LIST OF TABLES

LIST OF PUBLICATION ARISING FROM THIS WORK

Demirel, B., Daver, F., Kosior E. (2007). "Optimum design of PET bottle bases against environmental stress cracking", Conference Proceedings, 23rd Annual Meeting of the Polymer Processing Society, (PPS-23), Salvador, Brazil, 27-31

Demirel, B., Daver, F., Kosior E. (2007). "Petaloid bases of PET bottles: Design and process optimization against environmental stress cracking ", Conference Proceedings, SPE ANTEC, Cincinnati, OH, 2159-2164

Demirel, B., Daver, F., Kosior E. (2008). "The optimization of petaloid base dimensions and operating conditions for injection stretch blow moulded PET bottles", Conference Proceedings, 24th Annual Meeting of the Polymer Processing Society, (PPS-24), Salerno, Italy

Daver, F., Demirel, B. (2009)."Optimization of PET bottle via numerical modeling: A statistical design of experiment approach", Journal of Applied Polymer Science **(Submitted)**

Demirel, B., Daver, F. (2009) **"**Effects of the geometrical modification of the petaloid base on the final physical properties of the PET bottles", Journal of Applied Polymer Science **(Submitted)**

Demirel, B., Daver, F. (2009) **"**Simulation of stress in the base of the PET bottles under different processing conditions", Journal of Applied Polymer Science **(in preparation)**

ABSTRACT

Injection stretch blow moulded PET bottles are the most widely used container type for carbonated soft drinks. PET offers excellent clarity, good mechanical and barrier properties, and ease of processing. Typically, these bottles have a petaloid-shaped base, which gives good stability to the bottle and it is the most appropriate one for beverage storage. However, the base is prone to environmentally induced stress cracking and this a major concern to bottle manufacturers.

The object of this study is to explain the occurrence of stress cracking, and to prevent it by optimising both the geometry of the petaloid base and the processing parameters during bottle moulding.

A finite element model of the petaloid shape is developed in CATIA V5 R14, and used to predict the von Mises stress in the bottle base for different combinations of three key dimensions of the base: foot length, valley width, and clearance. The combination of dimensions giving the minimum stress is found by a statistical analysis approach using an optimisation and design of experiments software package ECHIP-7.

A bottle mould was manufactured according to the optimum base geometry and PET bottles are produced by injection stretch blow moulding (ISBM). In order to minimize the stresses at the bottom of the bottle, the ISBM process parameters were reviewed and the effects of both the stretch rod movement and the temperature profile of the preform were studied by means of the process simulation software package (Blow View version

8.2). Simulated values of the wall thickness, stress, crystallinity, molecular orientation and biaxial ratio in the bottle base were obtained. The process parameters, which result in low stress and uniform material in the bottle base, are regarded as optimum operating conditions.

In the evaluation process of the optimum bottle base, bottles with standard (current) and optimized (new) base were produced under the same process conditions via a two-stage ISBM machine. In order to compare both the bottles, environmental stress crack resistance, top load strength, burst pressure strength, thermal stability test as well as crystallinity studies via modulated differential scanning calorimetry (MDSC) and morphology studies via environmental scanning electron microscopy (ESEM) and optical microscopy were conducted.

In this study carried out, the new PET bottle with the optimised base significantly decreased the environmental stress cracking occurrence in the bottom of the bottle. It is found that the bottle with optimised base is stronger than the bottle with standard base against environmental stress cracking. The resistance time against environmental stress cracking are increased by about % 90 under the same operating process conditions used for standard (current) bottles; and by % 170 under the optimised process conditions where the preform re-heating temperature is set to 105 ^{o}C.

Chapter 1

INTRODUCTION

1.1 PET MATERIAL AND BOTTLES FOR CARBONATED SOFT DRINKS

Polyethylene terephthalate (PET) is a versatile and commercially important polymer. It is the preferred resin for containers of carbonated soft drink, juice, and many other beverages. PET also has many applications in medical and pharmaceutical, household and chemical, electronic and automotive, as well as food packaging markets. This widely used material can be found in rigid and flexible packaging, composite molded structures, and tapes and discs of various kinds. Markets for PET are increasing rapidly; the world market is expected to reach 20 million tones in the near future.

Efforts have intensified to improve the barrier properties and hot-fill capabilities of PET in order to extend its applications to include even more food and oxygen-sensitive products. These technologies include new high barrier resins, coatings, multilayer structures with oxygen scavengers, heat settings and blending [Jabarin, 2003].

It is commonly accepted that plastic packaging has a number of advantages over glass packaging; namely, they are lighter, cheaper, and unbreakable [Rosato, 1998]. Furthermore, less energy is required to produce a plastic bottle and the environmental footprint is reduced still further if the plastic packaging is properly recycled. Of course, plastic has limitations, particularly in food packaging. These may involve load bearing strength (e.g. when the product must be stacked during storage and transportation), low vacuum resistance and high permeability. A particular limitation is that pressuration from the contents the plastic bottle can result in substantial deformation [Van Dijk, 1997]. This phenomenon is demonstrated as paneling and results in an unaesthetic packaging that gives the consumer the impression that something has happened to the contents.

PET is the most commonly used material for carbonated soft-drink bottling [BSDA, 2000] since it offers excellent clarity, good mechanical and barrier properties, and ease of processing [Martin, et al., 1999].

The petaloid base is the widely used bottle design. The alternative is a two-piece bottle in which a separate flat-bottomed cup is fitted over the hemispherical base of the as-moulded bottle. The petaloid-shaped base gives a self-standing feature to the bottle and the production cost is less than that of two-piece bottle. However, the base is prone to stress cracking under pressure from the carbonation content, when the bottle is exposed to line lubricants or stored at hot and humid environments for long periods; and this a major concern to bottle manufacturers.

There is a number of parametric modeling in the literature for the ISBM process, which is used for the processing of polymer materials, especially for PET bottle production. Computer aided design (CAD) and computer aided manufacturing (CAM) software programs are needed to produce bottle-mould initial design with minimal modeling and production time as processing and mould design are time consuming and expensive [Chua and Lye, 1998]. It is convenient to use blow molding systems in the manufacture of hollow plastic items like containers and bottles due to favorable cost factors, possibility of variable wall thicknesses, and low stresses [Rosato and Rosato, 1989].

Processes utilized for fabrication of commercial PET products include injection molding, blow molding, extrusion, thermoforming, and film blowing. The ease of fabrication, the quality of the fabricated products, and the end-use properties are all dependent on basic material properties and specific responses during the various steps of each of the processing methods used to convert the resin into the final product. It is obvious that PET occupies an increasingly strong share of the

plastics market and also demonstrates a strong potential for application and property enhancements through selection and modification of material and processing variables [Jabarin, 2003].

1.2 CRACKING AT THE BOTTO M OF THE BOTTLE

The main problem with the one-piece bottle is stress cracking in the petaloid shaped base during the storage of the soft-drink, causing major inconvenience for carbonated soft drink producers and distributors. For this reason, bottle and petaloid shaped base need to be redesigned by using computer programs employing Finite Element Analysis (FEA) techniques to prevent cracking at the base of the bottles before being produced with the injection stretch blow molding (ISBM) process. So far, a few computer simulation programs have been used for this purpose [Rosato and Rosato, 1989]. Both the bottle design and the ISBM process parameters are optimised by means of these programs, improving resistance to stress cracking, and reducing the time and cost of bottle production.

PET is subject to environmental stress cracking (ESC) and a brittle failure initiated by surface imperfection. In general, ESC occurs when the glassy polymer is exposed to an aggressive medium and loaded at low stress for long periods of time [Wright, 1996; Joao et al., 2000; Howard, 1959]. Since at least 15% of all plastics failures in service are caused by ESC [Wright, 1996], the investigation of the phenomena is very important for the applications of engineering plastics.

Some researchers [Chevalier et al., 1999] have focused on crystallinity as the main contributor to the cracking problem. Processing temperature, pressure and environment have been known to affect crystallinity [Jabarin, 1998].

1.3 THE MAIN OBJECTIVES OF THE RESEARCH

The objectives of the research are as follows:

(1) To review the standard (current) design of various PET bottles in terms of strength, stretching ratio and peak stresses when filled.

(2) To determine the mechanism of crack formation experimentally.

(3) To systematically conduct numerical modeling and finite element analysis of a PET bottle in order to examine the effect of changes to geometry and key dimensions of the petaloid base.

(4) To develop a more rational design process that can be applied to the design of other PET products by means of advanced finite element analysis and experimental verifications.

(5) To optimise ISBM process via simulation and verify optimum process parameters experimentally.

(6) To test the optimized bottles, which are produced under optimum ISBM operating conditions, against the environmental stress crack resistance.

1.4 SPECIFIC RESEARCH QUESTIONS TO BE ADDRESSED

The specific research questions to be addressed are as follows:

(1) What effect does the geometry of the petaloid base have on stress cracking?

(2) What are the effects on stress cracking of process conditions, such as preform reheat temperature, pre-blow and final blow pressure

(3) What is the relationship between the stretching and blowing stages?

(4) Do the material properties play a role in stress cracking?

(5) At what conditions are the current PET bottles cracking when filling with carbonated soft drink?

(6) How will the newly designed PET bottles perform in terms of the quality?

(7) What type of tests should be carried out on both the standard (current) bottles and the newly designed (optimum) bottles?

(8) Will the commercial finite element package CATIA respond to detailed stress analysis?

(9) Will the outcomes of numerical methods comply with the newly produced PET bottles?

(10) What are the effects of the preform temperature on bottle properties?

1.5 STRUCTURE OF THE THESIS

In the literature review, the principal characteristic properties of PET, including chemical and physical properties, and the factors affecting these properties are reviewed in detail with respect to the proposed research questions. The processes utilized in the production of PET bottle and the parameters pertaining to these processes are reported. Some detailed explanation is made regarding the material models used in simulation programs.

In the third chapter of this study, the geometrical design process of the petaloid base of the 1.5 lt. bottle, on the base of which the environmental stress cracking occur, is discussed. Here, a new design is proposed that aims to minimise the stresses induced in the base by the carbonation pressure of the bottle content. Since the analysis of the stress was done using the Catia, all steps associated with this process are explained in detail. The knowledge related to the design parameters of the petaloid shaped base and the optimization process via ECHIP-7 software program are also given in detail.

Fourth chapter describes the ISBM process optimization via the Blow View 8.2 software program. The most appropriate process conditions are identified for the bottle design according to the FEM optimisation. These are defined by considering the effects of both the stretch rod movement used for stretching the preform, the temperature of the preform and the preform weight on the physical

properties of the material in the bottle base section. The properties, such as thickness, crystallization, molecular orientation, stress, biaxial ratio are obtained through the Blow View 8.2 simulation software program and these values are assessed with the aim of defining appropriate process conditions.

In the fifth chapter, the new bottle base is obtained by optimising both the bottle base design and process parameters which are used in fabrication of the bottles. The bottles with the standard base and the optimum base are produced under the same process conditions and the performance tests are performed for both bottles with the aim of comparison. The results of top load strength, environmental stress crack resistance, burst pressure, material, thermal stability and percent crystallinity are presented in this chapter. In this chapter, crack morphology is studied for current and new bottles, based on Environmental Scanning Electron Microscopy (ESEM) and optical microscopy images of the cracks.

The overall project conclusions are given in chapter 6. Suggestions for further study are also included in this chapter.

Chapter 2

LITERATURE REVIEW

2.1. INTRODUCTION

PET has the most application among plastics and is found most commonly in daily life. It is used especially in containers produced for storing and carrying food and liquids; in particular carbonated soft drinks (CSDs). However, some cracking problems have been observed at the bottom of bottles; due to either the geometrical shape of the petaloid base or the process parameters.

In this literature review the development of the PET bottle is reviewed, followed by a discussion of physical and chemical properties of PET and the factors that affect these properties. In the third section the problem of cracks occurring in the bottle base is reviewed and its causes investigated. In the fourth section, detail information is presented on PET bottle manufacturing. In the fifth section, the material models that are used in simulation programs are explained. The process parameters of the injection stretch blow molding (ISBM) such as blow pressure and timings and their effects on PET bottle production are investigated in the sixth section. In the last section, attention is focused on the optimization process in relation to the process parameters and bottle base design, as well as preform design. Some explanations about the design process are also presented.

2.2. DEVELOPMENT OF THE PET BOTTLE

PET poly (ethylene terephthalate) was developed in the 1940's and since then it has played an important role in the food and beverage packaging industry [Bjorksten et al., 1956]. Due to its popularity the use of PET in carbonated soft drinks bottles has been studied extensively [Bonnebat et al., 1981; Erwin et al., 1983; Cakmak et al., 1984; Leigner, 1985]. Initially, PET bottles consisted of two pieces; the blown bottle section, and a separate 'cap'section fitted over

the over the hemispherical bottle base. The polyethylene cap section-made the bottle self-standing. In recent times, PET bottles have been made in one piece with a self-standing petaloid-shaped base [Lyu and Pae, 2003].

The desirable properties of PET (clear, lightweight, high strength, stiffness, favorable creep characteristics, low flavor absorption, high chemical resistance, barrier properties and low price) [Bjorksten et al., 1956; Dominghaus, 1993] make it the material of choice for carbonated soft drinks containers [Wang et al., 1998], fibers and films. Due to low cost, better aesthetic appearance, and better handling, PET is being preferred over polycarbonate (PC) polymers [VanderPlaats, 1999].

PET has been also known for many years as a textile fiber forming material. But lately, it has started to be used in extrusion foam processing for textile fibers because of its elastic nature [Yilmazer et al., 2000]. PET is also used as a recyclable polymer, and the markets for recycled PET (R-PET) are growing by the year.

2.3. PET MATERIAL AND PROPERTIES

PET is commonly obtained through a polycondensation process by re-acting a dicarboxylic acid (terephthalic acid) with a diol (ethylene glycol) and eliminating methanol, as shown below (fig. 2-1) [Joel, 1995].

n[H$_3$COOC —⬡— COOCH$_3$]   +   n[HO(CH$_2$)$_2$OH]

　　　　Dimethyl terephthalate　　　　　　　　Ethylene glycol

$$[-OOC-\langle O \rangle - COOCH_2—CH_2O—]_n \quad + \quad 2n[CH_3OH]$$

Polyethylene terephthalate   Methanol
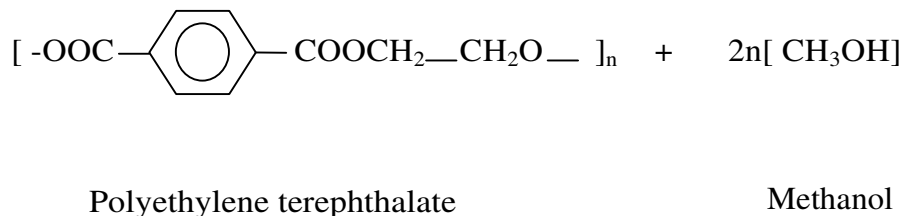
Fig.2-1. PET synthesis reactions

The polymers obtained usually have high molecular weight, low carboxyl, and acetaldehyde content, and they can be used for beverage bottle or industrial yarns [Chang et al., 1983]. Most of the physical and mechanical properties of polymers improve as molecular weight increases. PET follows this same trend and its organic repeat unit is as in fig. 2-2. End uses dictate the molecular weight of the polyester. As the requirements of mechanical properties become more stringent, higher molecular weight becomes necessary. The PET soft drink bottles should have an intrinsic viscosity of 0.72 dl/g, a density greater than 1.38 g/cm^3 and crystallinity greater than 40 percent [Cobbs et al., 1953]. High molecular weight PET is produced by one of the following three methods [Chang et al., 1983].

    (1) Continuation of the melt polymerization of PET,

    (2) Chemical coupling (interlinking) reaction,

    (3) Solid state polymerization of PET
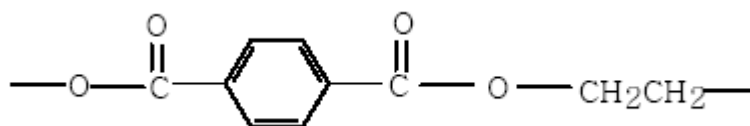
Fig.2-2. The repeat unit of Polyethylene terephthalate

A project of solid-stating of PET at low molecular temperature was carried out by [Chang et al., 1983]. PET polymerization is carried out by heating the pre-polymer containing higher carbon content at temperatures below its melting point but above its glass transition temperature.

2.3.1. Crystallization behavior of PET

'Crystalline' means that the polymer chains are parallel and closely packed, and 'amorphous' means that the polymer chains are disordered [Robertson, 1993]. Most polymers exist as complex structures made up of crystalline and amorphous regions. Crystallinity is usually induced by heating above the glass transition temperature (Tg) and is often accompanied by molecular orientation [Jabarin, 1984]. It is impossible to reach 100 % crystallinity with the lowest free energy because polymers do not have a uniform molecular weight. Instead, the polymers can only react to produce partly crystalline structures, usually called "semicrystalline" [Strobl, 1997].

The degree of polymer crystallinity depends on both intrinsic and extrinsic factors. Narrow molecular weight, linear polymer chain structure, and high molecular weight are very important pre-conditions in terms of obtaining high crystallinity [Robertson, 1993]. Crystallinity is also affected by extrinsic factors, like stretch ratio, mode of extension and crystallization temperature in the preparation of polymer films [Varma et al., 1998]. Below the glass transition temperature, polymer chains are rigid; after reaching the glass transition temperature, the chains become more flexible and are able to unfold under stress. If the temperature is above Tg and stretching is carried out, the randomly coiled and entangled chains begin to disentangle, unfold, and straighten and some of them even slide over their nearest neighbor chains [Benning, 1983].

PET is a crystallizable polymer because of its regularity in chemical and geometric structures. It is either in the semi-crystalline state or in the amorphous state. The levels of crystallinity and

morphology significantly affect the properties of the polymers [Groeninckx, et al., 1976; Starkweather, et al., 1956; Dixon and Jackson, 1968]. Even with limitations in its barrier properties and mechanical strength, crystalline PET is still widely used. Polymers with high crystallinity have a higher glass transition temperature Tg (Tg is 67° C for amorphous PET and 81° C for crystalline PET) [Collins et al., 1973] and have higher modulus, toughness, stiffness, tensile strength, hardness and more resistance to solvents, but less impact strength [Groeninckx, et al., 1976; Starkweather, et al., 1956; Dixon and Jackson, 1968].

Crystallinity in PET is usually induced by thermal crystallization and/or by stress or strain-induced crystallization. Thermally induced crystallization occurs when the polymer is heated above Tg and not quenched rapidly enough. In this condition the polymer turns opaque due to the spherulitic structure generated by thermal crystallization aggregates of un-oriented polymers [Jabarin, 1982]. In stress-induced crystallization, stretching or orientation is applied to heated polymer and the polymer chains are rearranged in a parallel fashion and become closely packed [Salem, 1998]. The crystallization process is composed of nucleation and spherulitic crystallization, and may occur at temperatures above Tg and below the melting point T_m [Miller, 1966]. Quenching the melt quickly results in a completely amorphous PET [Collins et al., 1973].

Crystalline polymers have a heterogeneous structure due to the interspersed amorphous regions while amorphous polymers in all their forms (melts, rubbers, glasses, etc.) have a homogeneous structure. Polymers are characterized by a glass transition temperature Tg and a melting temperature T_m [Mark et al., 1985]. The glass transition behavior of semi-crystalline polymers are greatly affected by the factors affecting degree of crystallinity such as molecular weight, amount of crystalline phase and morphology [Groeninckx et al., 1976; Miller, 1966; Munk and Aminabhavi, 2002; Newman and Cox, 1960; Illers and Breuer, 1963; Ito, 1974; Lee and Min,

1999; Struik, 1978]. The glass transition temperature of semi-crystalline polymer is higher and broader than that of the amorphous polymer [Groeninckx et al., 1976; Newman and Cox, 1960; Illers and Breuer, 1963; Struik, 1978].

Crystalline polymers are characterized by a T_m and amorphous polymers are characterized by a Tg. At the melting point, polymers are like a rubber-liquid. For crystalline polymers, the following relationship between Tg and Tm has been described [Robertson, 1993].

Tg $\longrightarrow$ $2/3T_m$ (for unsymmetrical chains)   (Equation 1)

and

Tg $\longrightarrow$ $1/2T_m$ (for symmetrical chains)   (Equation 2)

PET has a Tg between 340 to 353 K (67 to 80 °C) and a T_m of 540 K (267 °C).

The crystallization of PET has been widely investigated. The Avrami equation was adopted by [Keller and Lester, 1954], with using the density balance method, where the amorphous fraction was calculated from the final density at that condition, rather than the density of 100% crystalline PET. X-ray analyses and polarizing microscopy were used to observe crystalline structures. Different structures could be obtained by adjusting crystallization temperature or previous melt conditions. The maximum rate of crystallization occurs at 180°C. Further research in this subject has also been reported [Rybnikar, 1960; Lu and Hay, 2001; Misra and Stein, 1972].

Studies have been conducted on the kinetics of crystallization of different commercial PET materials in terms of the Avrami equation with a Differential Scanning Calorimetry (DSC) method and confirmed that the rate constant k is very sensitive to crystallization temperature

[Jabarin, 1987]. Different PET samples have different crystallization mechanisms. With increasing crystallization temperature, spherulite diameter increases [Keller, 1955].

Ozawa studied the kinetics of dynamic crystallization of PET**.** He obtained crystallization curves through DSC at different cooling rates [Ozawa, 1971]. A modified Avrami equation was applied to the primary crystallization in a non-isothermal situation. Jabarin compared the crystallization rate parameters of both isothermal and dynamic processes, and found that they are similar to each other in terms of mechanisms of crystallization. A method was developed to predict the minimum cooling rate required to obtain non-crystalline PET [Jabarin, 1987].

In addition to time and temperature, many other factors such as pressure, the degree of molecular orientation [Alfonso et al., 1978] and environment [Jabarin, 1998] have influence on crystallization mechanism, morphology, and final properties of PET. Nucleating agents also affect the crystallization of PET. Some studies have investigated the effect of the additives on crystallization behavior [Groeninckx et al., 1974; Mitra and Misra, 1988].

The crystallization behavior of PET with and without catalysts has been compared by [Asano et al., 1989]. They found that nucleation has a great influence on overall crystallization rate at low temperatures near Tg. Moisture and molecular weight have a great effect on crystallization [Jabarin, 1987a; 1987b]. It is found that the kinetics of crystallization depends on molecular weight and that with increasing percentage of moisture, the half-time crystallization and induction time of crystallization decrease. Spherulite growth rate was independent of water absorbed [Jabarin, 1987a].

Stress is an important factor, affecting crystallization. The effect of stress-induced crystallization of PET has been investigated with density measurements, wide-angle X-ray diffraction and

small-angle light scattering measurements [Misra and Stein, 1975]. Amorphous PET films were stretched at constant strain rates below and above Tg. The stress-induced crystallization has also been analyzed as a function of time and orientation level [Venkateswaran et al., 1998].

[Marco et al., 2002] focused on the crystallinity induced by stretching PET at temperatures above the glass transition, and on the influence of stretch and blow molding parameters on the properties of the final product.

A study has been conducted with PET material and found that reducing the shot size (amount of material injected into the mould cavity) will minimize crystallinity while hold time (length of time the gate remains open allowing more material to be pushed into the mold cavity) has no effect at the lower shot size. However, with a larger shot size, a low hold time is necessary to reduce crystallinity. The least crystallinity occurs with minimum hold time and minimum shot size [Zagarola, 1998].

In a study conducted by [Hanley et al., 2006], it was found that the extent of the orientation and crystallinity depends upon the geometry of the bottle base, and that there is an abrupt change from the amorphous region to the crystalline regions. The valley and the transition region to the foot are the most biaxially oriented regions of the base. The orientation in the middle of the foot is more circular and the crystallization is less. This shows that the stretch in this region is more uniaxial (or less biaxial), but crystalline lamellae are still observed.

Some experimental works has been conducted on the orientation and crystallization of PET films subjected to uniaxial or biaxial drawing under industrial processing conditions [Chevalier et al., 1999; Yang et al., 2004; Blundell et al., 1999; 2000; Mahendrasingam et al., 1999; 2000]. The

changes in the degree of orientation and crystallinity have been investigated using the wide-angle

X-ray scattering (WAXS) technique [Blundell et al., 2000]. By analyzing the crystalline

diffraction patterns, they found that the orientation of the developing crystals depends on the

relation of the draw rate and temperature to the chain relaxation process, and that the

crystallization rate is highly temperature dependent. Everall et al. used polarized attenuated

reflection infrared spectroscopy to quantify biaxial orientation in PET films and stretch blow

molded bottles [Everall et al., 2002].

Crystallization may be due to many nuclei centres forming small spherulites at low temperatures.

Larger crystal structures may be obtained when the material is crystallized at higher temperatures

or by slow cooling from the melt, but 100% crystallinity is never possible in normal processing

conditions [Miller, 1966; Munk and Aminabhavi, 2002]. Usually the percentage crystallinity is

lower than 90% [Munk and Aminabhavi, 2002]. In general, polymeric materials are semi-

crystalline with crystalline and amorphous phases co-existing [Boyer, 1975]. Schematic diagrams

of the completely amorphous phase and the morphology of semi-crystalline polymers are shown

in fig. 2-3 and 2-4 respectively [Boyer, 1975] [Joel, 1995].
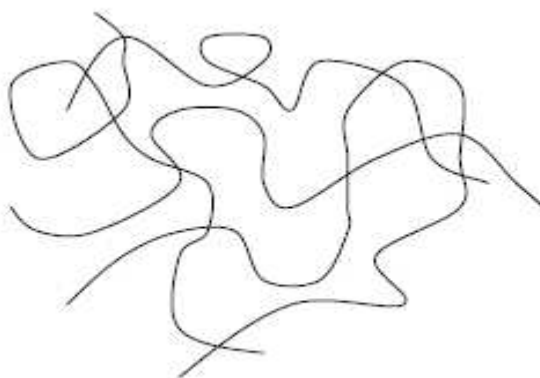
Fig.2-3. Schematic diagram of completely amorphous phase [Boyer, 1975]
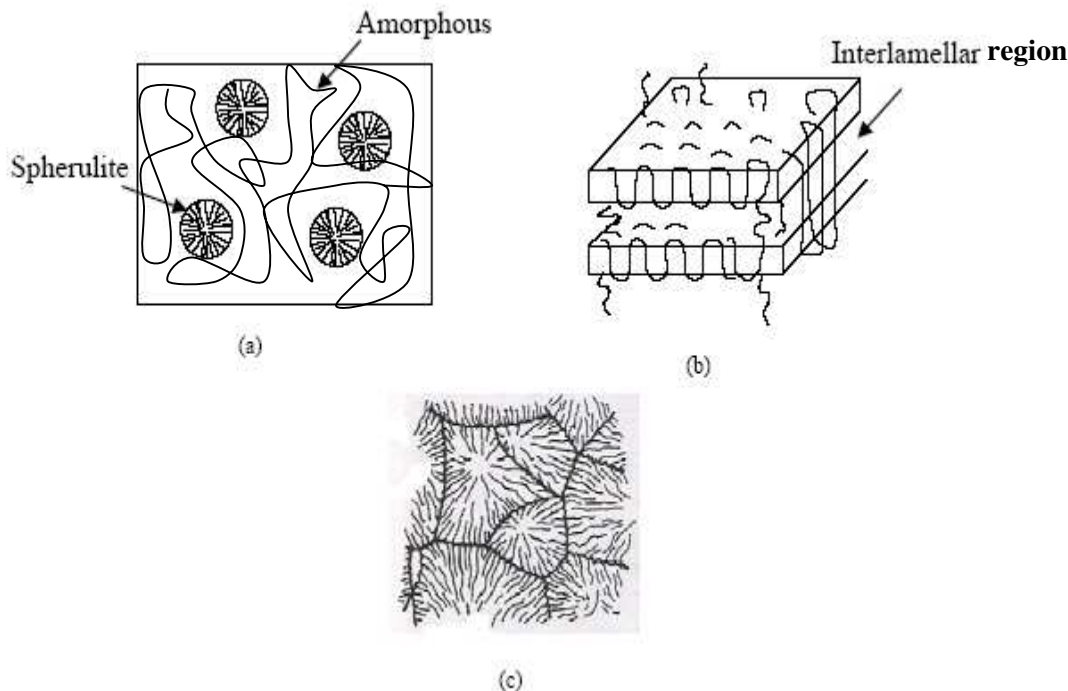
Fig.2-4. Schematic morphology of semi-crystalline polymers [Joel, 1995]

a) Schematic appearance b) Alignment of semi-crystalline layers c) Microscopic appearance

The morphology is described by the spherulite radius, lamellar thickness and long period; distance between two adjacent lamellae. Small angle light scattering, microscopy, and X-ray analyses are usually applied to obtain these parameters [Miller, 1966]. Even at the same crystallinity content, samples crystallized at higher temperature are more opaque and brittle [Keller and Lester, 1954]. Samples with smaller spherulite sizes have higher yield stress, lower ultimate elongation and high brittleness temperature [Starkweather et al., 1959] and higher impact strength [Ohlberg et al., 1959].

2.3.1.1. Crystallinity calculation

Several methods have been used to determine the amount of crystallinity [Chua and Lye, 1998;

Jabarin, 1998]. They include density measurement, X-ray diffraction, infrared absorption, nuclear magnetic resonance (NMR), and differential scanning calorimetry (DSC). However, the calculated results may vary with the methods used [Miller, 1966].

Density measurement is one of the best methods of quantifying percent crystallinity [Cobbs et al., 1953]. The crystallinity of a polymer can be easily calculated using this method because there are differences of density between crystalline and amorphous regions in polymers, and the relationship is in proportion to the degree of crystallization. The first method is given at [ASTM, 2000]. Here, calculation is made by comparing sample weights in air and in isopropanol using the following equation:

$$\chi_c = \frac{(\rho - \rho_a)}{(\rho - \rho_c)} \qquad \text{(Equation 3)}$$

Where χ_c is the polymer crystallinity; ρ is the measured density of PET sample; ρ_a is the density of amorphous PET; and ρ_c is the density of crystalline PET.

A second method to calculate crystallinity is an estimate based on the measured density using carbon tetrachloride and n-heptane in a density gradient column [Maruhashi, 2001].

$$\% \chi_c = \frac{\rho_c (\rho - \rho_a)}{\rho (\rho_c - \rho_a)} \times 100 \qquad \text{(Equation 4)}$$

Where is X_c the % crystallinity; ρ is the measured PET sample density; ρ_c is the crystalline PET density; and ρ_a is the amorphous PET density.

Another method, which is widely used, to analyze thermally induced property changes of a polymer is Differential Scanning Calorimetry (DSC). This is based on recording the heat flow that

is added to either the sample or the reference [Brody, 2001]. The initial crystallinity can be calculated by determining the total enthalpy change in the temperature range of glass transition and the equilibrium melting temperature between the sample and perfectly crystallized material [Reading et al., 2001].

$$\chi_c = \frac{\Delta H}{\Delta H_{100}}$$ (Equation 5)

Where ΔH is the measured enthalpy of melting the sample; and ΔH_{100} is the enthalpy of melting a 100 % crystalline sample of the same material. In practice, a 100 % crystalline polymer cannot be achieved, so ΔH_{100} is replaced by the enthalpy of fusion per mole of PET (ΔH_u) [Hatakeyama and Quinn, 1994].

Infrared absorption is based on the observation that infrared intensity changes accompany crystallization. A method has been developed to study the isothermal crystallization process of PET film [Cobbs and Burton, 1953]. Schmidt [1963] demonstrated that the band intensity change of stretched PET can be interpreted by orientation and structural factor. Lofgren and Jabarin used polarized internal reflectance spectroscopy (IRS) to evaluate molecular orientation and crystallinity of PET film surfaces and found that this technique can be used for characterization of the structure of oriented and crystalline PET when the sample is not restricted by its thickness and clarity [Lofgren and Jabarin, 1994].

For beverage bottles with the volumes greater than 2 litres, PET 1 is preferred because when subjected to an elongational deformation, at a certain true strain, the material becomes much stiffer, so that it resists further deformation [Wang et al., 1999].

The amorphous phase of PET contains both trans and gauche isomers; while the crystalline phase is in the trans form only (fig. 2-5a, b). At any given levels of crystallinity, the amount of conformational structure may be different [Schmidt, 1963].
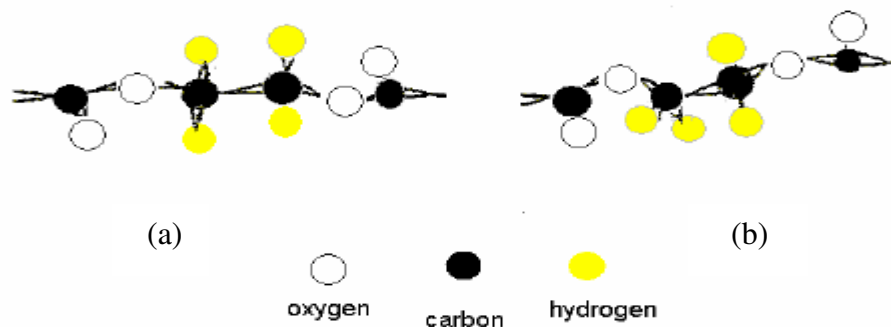
Fig.2-5. Three dimensional structures of rotational isomers of PET [Schmidt, 1963]

(a) Trans, (b) Gauche

2.3.2. Physical aging

Physical aging which is also called internal aging [Ehrenstein, 2001] is a time-dependent behavior of glassy systems; which include both polymeric and low molecular weight materials [Struik, 1978; Tant and Wikes, 1981; Hutchinson, 1995]. It is generally observed in amorphous polymers and partially crystalline PET. Physical aging is a reversible process causing no permanent modification of the structure [Struik, 1978]. This is different from chemical aging and biological aging in which the polymer structure is permanently affected.

Physical aging causes some material property changes. These include thermal, mechanical, and electrical properties. Aging will generally cause glass transition temperatures to shift to higher positions, brittle failure to increases, and density and enthalpy of relaxation values to increase [Tant and Wikes, 1981]. In the studies carried out, it is found that during aging, density, yield stress, drawing stress and elastic modulus increase, while impact strength, fracture energy,

ultimate elongation and creep rate decrease [Tant and Wikes, 1981; Jabarin and Lofgren, 1992; Azar et al., 1983].Various techniques have been used for in-depth studies of property changes due to aging [Tant and Wikes, 1981; Hutchinson, 1995; Lu and Hay, 2000; Moore et al., 1981]. Dynamic Mechanical analysis (DMA) [Tant and Wikes, 1981], Differential Scanning Calorimetry (DSC) [Lu and Hay, 2000], Fourier Transform Infra-red (FTIR) spectroscopy [Moore et al., 1981] are frequently used to test mechanical property responses to aging. Recently, a positron lifetime annihilation technique has been used to study the physical aging process [Sathyanarayana et al., 2002].

Lu and Hay studied the effect of physical aging on the rate of cold crystallization of PET by DSC [Lu and Hay, 2000]. They found that aging accelerates the crystallization rate. In amorphous PET during volume recovery by FTIR, the changes in conformation have been characterized by [Moore et al., 1981]. They suggested that changes detected with FTIR spectroscopy may have a correlation with the onset of brittleness. Tant and Wilkes studied the physical aging of semicrystalline PET of various crystallinities by stress-strain behavior, stress relaxation, and DSC measurement. They concluded that semicrystalline polymer undergoes physical aging and with increasing crystallinity, the extent and rate of physical aging decreases [Tant and Wilkes, 1981]. As aging time increases the glass transition peak rises to higher temperatures [Canadas et al., 1998]. However, it was found that the whole amount of the amorphous phase was almost constant during the aging for the small change of density [Zhao et al., 2002].

Gas permeation is also sensitive to physical aging. With increasing aging time, gas permeability decreases [Dorkenoo and Pfromm, 1999]. The decrease of the gas permeability is often attributed to the loss of free volume [McCaig and Paul, 2000].

2.3.2.1. Factors affecting aging

There are many factors that may affect the aging process. These are water absorption [Zelkó et al., 2000; Sűvegh and Zelkó, 2002; Sun et al., 1999; Berens and Hodge, 1984; Han and McKenna, 1997; Jabarin and Lofgren, 1986; 1986; Launay, 1999] sample thickness [Dorkenoo and Pfromm, 1999; McCaig and Paul, 2000; Pfromm and Koros, 1995; McCaig et al., 2000], stress [Berens and Hodge, 1984] and molecular weight. On the other hand, aging time and temperature are controlling factors [Mark et al., 1985]. It was found that the glass transition temperature, crystallization temperature, degree of orientation and yield stress decreased because of the absorbed water [Jabarin and Lofgren, 1986; 1986; Jabarin, 1998] and the diffusion coefficient increases with temperature [Launay, 1999].

2.3.3. Mechanical property changes

Temperature and strain history are important factors for the mechanical properties of PET [Yang et al., 2004]. Its stress-strain curve shows strong strain-softening followed by strain-hardening under large strains. It is also found that a relatively broad molecular weight provides good physical properties and processibility [Strebel and Benson, 1996].

2.3.3.1. Orientation

Orientation is a process of stretching the polymer material under heat to align the molecular chains [Robertson, 1993]. Orientation improves the strength and durability to polymer material [Stuart, 2002]. In addition, other physical properties such as tensile and impact strengths, stiffness, clarity, resistance to crazing (cracking), and barrier characteristics may also be significantly enhanced in oriented films. On the other hand, orientation may cause detrimental effects on elongation. Common commercially oriented films include PET, low density polyethylene, polyamide, polypropylene.

Polymers can be oriented in either one direction (uniaxial orientation) or in two directions (biaxial orientation). Biaxial orientation is more widely used in film manufacture. Polymers are stretched at a temperature above the glass transition temperature but below the melt temperature. This is the method most used in practice to orient the polymer material. Below the glass transition temperature, polymer chains are rigid; they become more flexible at the glass transition temperature and are able to unfold under stress. If stretching is above T_g, the polymer chains, which are randomly coiled and entangled, begin to disentangle, unfold, and straighten [Benning, 1983]. Orientation ensures more crystallization while the chains and crystalline structure align in the direction of stretching. The best process conditions are where maximum chain uncoiling and alignment, and minimum viscous flow, or chain slippage, are achieved [Munk and Aminabhavi, 2002].

Some studies have been conducted on the molecular structure of PET [. Brooks and explored the molecular organization of PET molecules in the petaloid bases of high quality bottles, and bottles that had split under load under a range of controlled experimental conditions (e.g., temperature, shear, and chain composition) through small-angle X-ray scattering (SAXS) technique [Brooks and Giles, 2002]. It was found by the symmetry of the SAXS pattern that there is no preferred orientation of the molecular chains. However, Hanley et al. found that biaxial orientation of the PET crystallites occurred across a foot and down a corresponding valley in the base of the petaloid shaped bottles [Hanley et al., 2006].

Hoop extension in the bottle walls is achieved by pressure applied to the inner wall of the preform in the blowing stage. Differences in hoop extension in the inner and outer surfaces of a bottle wall result in differences in morphological properties of the inner and outer surfaces of the bottles [Everall et al., 2002].

In a project titled "visualization study and analysis on preform growth in polyethylene terephthalate stretch blow molding" Huang et al. compared the profiles of different preform types; dolphin, sandpile, and two-bubble-type. They concluded that the inflating speed of the stretched preform for the dolphin-type preform growth was higher than that of the sandpile-type and two-bubble-type preform growths [Huang et al., 2006]. Uniformity of thickness in the final bottle is very important in mitigating against environmental stress cracking, and since preform shape directly influences thickness the design of the preform is very important.

The central region of the bottle base does experience some thinning during the stretch blow molding process, but this region should be amorphous for good bottles after processing. However, reduced thickness leads to reduced strength of the base, until the material is stretched far enough for strain hardening to occur, at which point there is a dramatic increase in overall strength [Hanley et al., 2006].

2.3.3.2. Influence of orientation conditions on PET films

A way of enhancing PET mechanical properties is to orient the material by controlling polymer morphology. When the force is increased to stretch the film stretch ratio, chain orientation, and elastic modulus increase along the stretch direction. However, the relation between drawing parameters, polymer structure, and mechanical properties of oriented films is very complex [Ward, 1975].

Most of the commercially used PET is biaxially drawn at a constant extension rate in two modes: sequential or simultaneous. For simultaneous drawing, the temperature is normally between 80 and 95°C. For sequential drawing the temperature in the forward draw is generally in the 80-95°C range, and in the transverse draw it is usually 5-10°C higher [Salem, 1999]. Satoto et al. [1999]

have focused on molecular mobility in PET films that were unstretched and biaxially stretched at 90°C and 95°C, and found that the unstretched sample had less thermal stability to temperature change than the stretched samples.

A number of studies on the effect of orientation on the barrier properties of PET are reported in the literature [Fan et al., 2000; Osborn and Jenkins, 1992; McEvoy et al., 1998; Chevalier et al., 1999; Chevalier, 1999]. Fan et al., [2000] have conducted a significant study of biaxial stretch ratio effects on PET film permeability and showed that the carbon dioxide permeability of oriented PET film was much more influenced by the stretch ratio in the machine direction (MD) than the stretch ratio in the transverse direction (TD). They also stated that there is a slight decrease in permeability with an increase in the TD stretch ratio and also that the best stretch ratio pair for reducing carbon dioxide permeability was 3.5 MD x 3.0 TD in this condition.

Some studies have been made of the effect of changes in the degree of PET orientation and crystallinity over a wide range of drawing rates and draw ratios using the wide-angle X-ray scattering (WAXS) technique to analyze the crystalline diffraction patterns [Blundell et al., 1999; 2000; Mahendrasingam et al., 1999; 2000]. They have found that the orientation of the developing crystals depends on the relation of the draw rate and temperature to the chain relaxation process, and that the crystallization rate is highly temperature dependent.

The biaxial orientation in PET films and stretch blow molded bottles has been examined using polarized attenuated reflection infrared spectroscopy [Everall et al., 2002] and it was found that there were significant gradients in orientation through the film thickness and bottle walls. They also reported that the bottles exhibited complex orientation patterns that depend on preform and mold design, which may be associated with the temperature non-uniformity and changes in the

preform during stretch-blow molding.

A series of studies on the structure and properties of biaxially stretched PET sheets under different temperatures and orientation rates were conducted by [Maruhashi, 2001; Maruhashi and Asada, 1996]. The results showed that thermal shrinkage was very small at 85°C, which is hot-filling temperature, for sheets stretched at both high temperature and high speed. Sheets stretched at a higher temperature and a lower speed, were easy to soften at 85°C because molecular segment relaxation occurred under these conditions, instead of crystallization. Sheets stretched at a lower temperature (85°C) showed large thermal shrinkage, although there was high crystallinity in the sheets due to the large increase in strain during stretching.

Some researchers [e.g. Jabarin, 1984; 1992] also carried out numerous studies of orientation and stress-induced crystallization of PET. Their research indicated that the mechanical and transport properties of PET are directly dependent on the degree of orientation, and that stress-induced crystallization of annealed, stretched PET can be processed depending on the residual degree of orientation. A super-molecular structure is also found by [Evstatiev et al., 1992]. This structure is formed by cold-drawing of rapidly quenched PET films that were highly organized and consisted of a relatively large number of maximally extended chains in the amorphous regions.

Various measurement techniques are currently available in industry to examine and interpret the structures and properties of the polymer based on different macromolecular or morphologic characteristics. They include light scattering, wide-angle X-ray and small-angle X-ray diffraction [Sathyanarayana et al., 2002].

2.4. ENVIRONMENTAL STRESS CRACKING

Studies of environmental stress cracking (ESC) began in the 1950s when it was observed in polyethylene natural gas pipes [Howard, 1959]. (ESC) is a brittle failure initiated by surface imperfections and occurs when the glassy polymer is exposed to an aggressive medium and loaded at low stress for a long period of time [Howard, 1959]. At least 15% of all plastic failures in service are due to ESC [Wright, 1996].

ESC has a number of causes. It is a time-dependent brittle failure process, which depends on environmental factors such as chemical solution and stress [Jabarin, 1998]. In general, studies made have been focused on the mechanism of crazing: from craze initiation and craze growth until failure, because a craze is the precursor of ESC behavior. The failure mechanism of polystyrene thin film was investigated by means of electron microscopy [Wellinghoff and Baer, 1975]. It was found that the heterogeneous surface initiates small voids (< 30nm in diameter) which coalesce in response to stress concentrations. Crazing is as a result of a repetition of the above two processes.

There are two simple viscoelastic criteria to predict craze initiation. According to Wright and Gotham, the total critical tensile strain is composed of two components under constant stress [Wright and Gotham, 1983]. These are elastic strain and inelastic strain:

$$\varepsilon_c = \varepsilon_{(elastic)} + \varepsilon_{(inelastic)} = J(0)\sigma + K \qquad \text{(Equation 6)}$$

Where J (o) is the elastic compliance and σ is the applied stress.

Under constant strain (ε) conditions,

$$\sigma_c = \sigma(0) \cdot \left(1 - \frac{K}{\varepsilon}\right)$$
(Equation 7)

Where σ_c is the critical stress and $\sigma(o)$ is the instantaneous maximum stress generated under stress relaxation conditions.

The inelastic strain contains both delayed elastic and viscous elements. Crazing occurs as the inelastic strain reaches a critical value (K). For many polymer- environment combinations, K is lower than 0.1%.

For the second criterion; under constant stress conditions,

$$\varepsilon_c = \frac{J(0)\sigma + W_c}{\sigma}$$
(Equation 8)

Moreover, under constant strain conditions:

$$\sigma_c = \frac{W_c}{(\sigma(0) - \sigma_c)}$$
(Equation 9)

Crazing is observed as the inelastic tensile strain energy density exceeds a critical value W_c, which has a typical order of 0.1 N mm/mm.

Surface energy mechanisms and plasticization are two widely held theories to explain the role the environment plays in stress cracking [Yaffe and Kramer, 1981; Bernier and Kambour, 1968; Kefalas, 1995]. The first theory postulated that the ESC agents reduce surface tension and are adhesive on polymer surface, and thus reduce the surface energy for craze initiation. In the plasticization theory, ESC agents act as plasticizers to reduce-resistance to craze formation.

Material structure variables, including molecular weight, lamellar orientation and branch length have great influence on ESC behavior. As polymers with high molecular weight have long chains in their molecular structure, their ESC resistance is usually high [Joao et al., 2000; Lustiger, 1986]. Whilst craze initiation is independent of molecular weight craze development and breakdown increase with molecular weight according to Fellers and Kee. [Fellers and Kee, 1974].

Crystalline content and its nature also affect ESC. Whilst many studies have been conducted into ESC, the conclusions on this phenomenon are not consistent. It is generally agreed that amorphous plastics are more susceptible to ESC than semi-crystalline plastics because of their poor permeation barrier [Wright, 1996]. However, for polyethylene, ESC resistance decreases as crystallinity increases [Howard and Martin, 1960]. A graphic model for the brittle failure of semi-crystalline polymers was presented by [Lustiger and Markham, 1983] under ESC conditions. When a low level of stress is applied tie molecule chains, which begin and end in adjacent lamellae, are stretched. The stretching can be maintained for a long while without breaking the chain because it is under low stress. After a certain time, as most tie molecules begin to untangle, brittle failure occurs. If the polymer molecules are in a liquefied environment, the tie molecules are "lubricated" and failure is accelerated.

Hittmair and Ullman [1962] studied ESC in polyethylene and found that crazing occurred along the spherulite diameter. That the ESC of semi-crystalline polymer is an "interlamellar failure process" is confirmed by other researchers [Lustiger and Markham, 1983; Peterlin, 1975].

A study has been conducted using X-ray diffraction, optical microscopy and constant strain rate tensile tests [Shanahan et al., 1980]. It was found that the greater ESC resistance occurs at the

same degree of crystallinity, as spherulite size gets smaller, and that craze propagation is hindered by the presence of spherulites.

Thermal history is another factor affecting ESC resistance of polymers. Arnold studied the effects of physical aging on the brittle fracture behavior of polystyrene [Arnold, 1995]. He found that longer physical aging time reduced the lifetimes of all samples, because physical aging reduced the toughness and reduced the craze strength, resulting in brittle fracture. The crazes formed in ethanol were examined by means of transmission optical microscopy and scanning electron microscopy and it was found that longer aging time will delay craze formation, but that these crazes are less stable than those formed at the early stage.

Resin properties have effects on resistance to ESC. In general, lowering density increases crack resistance and copolymers have higher crack resistance than homopolymers [Strebel and Benson, 1996]. Jabarin and Lofgren [1992] studied the environmental aging and stress-cracking behavior of homopolymer and copolymer PET at 30°C. They found the number of crazes which developed under stress increased as exposure time increased. At equivalent conditions, the higher the copolymer concentration (in terms of cyclohexane dimethanol (CHDM)) the more crazes are formed. However, without a stress cracking agent more samples exhibited brittle failure during tensile testing. When no stress acted on the samples no crazes developed. Brittle failure occurred in these samples when aging time was long enough. They concluded that brittle failure may be related to crazing, but it must be caused by other factors, such as enthalpies of relaxation.

The ESC behavior of amorphous PET in aqueous NaOH at ambient conditions was investigated by Moskala [1998]. In that study, creep crack growth rate was determined as a function of the applied stress intensity factor (K). It was found that the crazing growth was discontinuous and

was due to the virgin polymer and the hydrolysis effect. At same value of K, crack growth rate increased with increased NaOH concentration.

2.4.1. Environmental stress cracking in PET bottles

High environmental stress crack resistance is one of the primary requirements of PET bottles used for commercial and industrial containers. In an aggressive environment, these bottles must withstand low stresses for long periods without cracking [Strebel and Benson, 1996].

Both resin and processing variables affect crack resistance. Strebel and Benson conducted a study to determine the effects of blow-molding process variables on crack resistance in high-density polyethylene (HDPE) bottles. They focused on the effects of mold temperature, melt temperature, die temperature, molding time, blow time and drop time (the time in which the bottle is released). Tests were carried out using internal pressure for bottles blown at each condition, and it was found crack resistance decreased with increasing die temperature, mold temperature and mold time, increased with increasing drop time [Strebel and Benson, 1996]. However, George and O'Shea reported an increase in crack resistance with decreasing mold temperature [George and O'Shea, 1990].

It could be conjectured that increased die temperature reduces the viscosity of the PET resulting in increase in the bottle base weight. However, for one type of polycarbonate, it was found that increasing the die temperature actually increased stress crack resistance [Roseblade, 1983].

The use of a petaloid shape for the base of carbonated PET bottles is widespread, but sharp angles in the complex geometry of this shape become stress concentrators, and environmental stress cracking mostly occurs in the bottle base. Because PET is less oriented near the injection

gate and is most exposed to stress crack agents [Zagarola, 2000] unfortunately, this phenomenon

has been little studied and it is not accurately understood [Brooks and Giles, 2002].

In general, two types of cracking are encountered; radial and circumferential. Radial cracks (fig.

2-7a) begin at the center of the base and go outwards, whereas circumferential cracks (fig 2-7b),

are located some distance from the base center [Lyu and Pae, 2003].
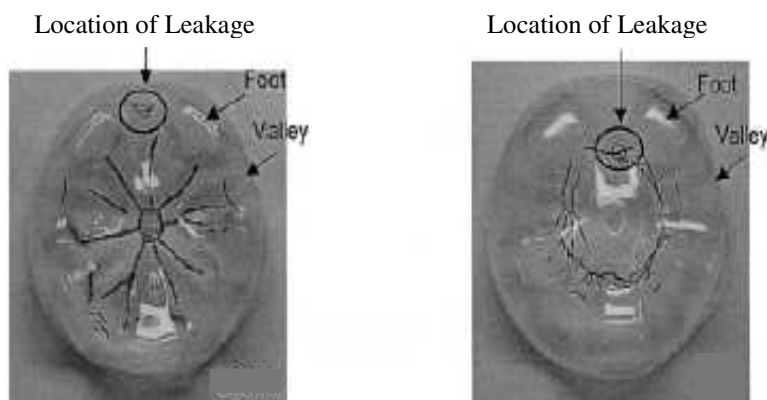
(a) Cracks in radial direction   (b) cracks in circumferential direction

Fig.2-6. Cracks in the petaloid bottom of the bottle [Lyu and Pae, 2003]

A study using Small-Angle X-Ray Scattering has been conducted by Hanley et al. [2006] on the

molecular morphology of the petaloid bases of PET bottles. They have said that the likelihood of

failure by cracking is directly related to the polymer morphology in the petaloid base and that,

therefore, the production process can significantly influence cracking susceptibility. They found

that the polymer chains in the central region of the bottle base are circumferentially aligned but

also non-crystalline and also assumed that the alignment happens during the stretch blow molding

stage and the morphology is fixed by quenching the temperature before the chains have time to

relax. They concluded that the maximum principle stress was located in the valleys of the petaloid

base and that crazing strongly influenced crack formation.

It is also reported that crazing occurs in brittle materials under tensile stress [McCrun et al., 1997; Sternstein et al., 1968] and that high temperatures accelerate the stress crack development so that cracking failures typically occur more often in warmer climates [Zagarola, 2000; Hanley et al., 2006]. Thus, the crazing is strongly related to ambient temperature as well as the tensile principal stresses.

A further study has been concluded by Lyu and Pae [2003] and found that there are three key design parameters (fig. 2-8 and 2-9) affecting circumferential cracking in the bottle base; foot length, valley width and clearance (the distance from the centre of the base to the surface that the bottle stands on).
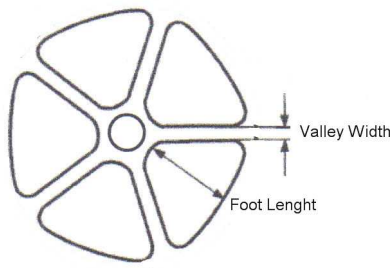
Fig.2-7. Valley width and foot length   Fig. 2-8. Clearance
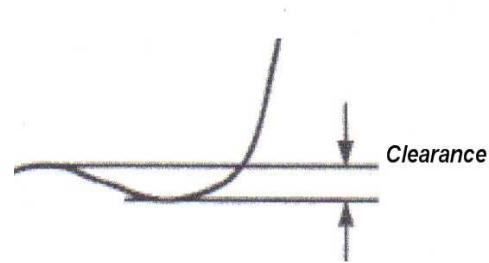
Cracks occur in the transition region [Zagarola, 2000; Lyu and Pae, 2003; Hanley et al., 2006] because of thinning of the base, but only in regions where the stretch ratio was not yet great enough to induce strain hardening and crystallization [Lyu and Pae, 2003]. The region where the cracks do not occur corresponds to the amorphous region [Hanley et al., 2006].

Lyu and Pae redesigned the petaloid shape in a 2 lt PET bottle using results from a study of the maximum principal stress in the bottle [Lyu and Pae, 2003]. They observed base cracking in a

solvent cracking test, and analyzed the effective stress and the maximum principal stress in a carbonated bottle using computer simulation. They concluded that the cracks were due not only to insufficient strength of material (because of insufficient stretching of the PET), but were also due to the design of the petaloid shape. The highest maximum principal stress occurred at the valley of the petaloid, in a circumferential direction, and was a major cause of the cracking.

Because the geometry of the base is complicated, it is difficult achieve a stretch ratio above the natural draw ratio in this area [Bonnebat et al., 1981]. Some researchers therefore performed their work by changing the dimensions of the parameters on the petaloid base [Lyu and Pae, 2003].

Stretching and temperature are only two of the parameters important to the arrangements of polymer chains [Yang et al., 2004]. The increments of the stress were found to be very small for low stretch ratios in PET stretched at elevated temperature [Venkateswaran et al., 1998; Dumbleton, 1968; Rietsch, 1990]. The polymer chains are arranged in the stretching direction as the stretch ratio increases. Subsequently, the stress increases drastically as the stretch ratio increases after a certain point of the stretch ratio.

Abrupt thickness reductions without compensating increases in the material strength cause the structural weakness in the bottle base. Therefore, to prevent cracking, the stretch ratio in bottle blowing should be higher than the hardening point so that mechanical properties relevant to the molecular orientation can be at the acceptable level, and at the same time, the maximum principal tensile stress should be lowered or minimized at the valleys of the petaloid [Lyu and Pae, 2003]. The same authors have also concluded that a large foot length, large clearance, and narrow valley width can be used to prevent the circumferential cracks on the bottle base regardless of the bottle size.

There are many methods developed for ESC testing [Wright, 1996]. Single cantilever or three-point bending for rigid materials, bent- strip test for flexible materials, tensile, creep rupture and tensile creep methods are widely used. Micro-hardness measurement has been accepted as a new test method.

Choi et al. investigated the ESC mechanism and cracking failure characterization of high density polyethylene (HDPE) by means of scanning electron microscopy [Choi et al., 2007]. They have observed differences in morphology of the cracks and they concluded that the samples with fibrillar cracks showed high stress crack resistance whereas samples with sharp, straight cracks showed low stress crack resistance values.

The role of injection and blow molding set-up in reducing the bottles' vulnerability to stress cracking has been discussed by [Zagarola, 2000]. He discussed process optimization for stress crack resistance and illustrated typical key process variables affecting stress cracking; including interactions with injection molding variables. He concluded that crude bottle base design, the size of bottles with greater diameters, and abrupt transitions at the bottle base make the bottle vulnerable to stress cracking and also that the injection process, the blow process, and the age of the preform (older is more susceptible) affect bottle durability.

Zagarola lists the key factors , affecting vulnerability to stress crack failures as follows: crystallinity in the preform gate that penetrates through the end cap surface; crystallinity rings in the end cap; contamination; too low intrinsic viscosity; excessive injection packing; abrupt thickness transition from thick to thin as in the base from the gate to the foot; poor molecular orientation in the base or neck , usually reflected as excessive base thickness; brittle bases from excessive preform or bottle storage.

[Zagarola, 2000] has demonstrated in his study that one of the key control factors was the hold time for the injection process. He also found that most stress resistance was achieved with the lower weight (less packed) preform, and that the greater stretch pressure consistently increased ESCR.

Perhaps the most important finding from Zaragola's investigation was that thickness and base clearances have no relation with good or poor resistance. He illustrated all obtained results through scatter diagrams.

The literature provides some leads to improving the stress crack resistance properties of blow-moulded bottles. The following are a selection:

- Since cooling rate affects the morphology and properties of the product, the mold should be quickly quenched to reduce crack propagation rates. [Shanahan et al., 1980; George and O'Shea, 1990; Strebel and Moet, 1995].

- It is not necessary to cool blow-molded bottles with liquid nitrogen because this does not affect stress crack resistance [ASTM, 2005], and only slightly improves top-load resistance [Gibbs, 1989].

- Bottle contact with the mold should be only long enough to solidify the melt [Strebel and Benson, 1996].

- The injection speed should be slowed or the barrel temperature reduced for polycarbonate [Roseblade, 1983] and also processing of fluoropolymers under high temperatures or high shear decreases stress crack resistance [Imbalzano et al., 1991].

- PET bottle preforms should be firstly injection molded in batches and cooled to room temperature so that the preform is virtually amorphous. For the stretch blow moulding stage preforms should be reheated above the glass transition temperature, but below the cold crystallization temperature. Hereby, the crystallinity and molecular orientation are to be induced [Rosato and Rosato, 1989].

2.5. MANUFACTURE OF PET BOTTLES FOR CARBONATED SOFT DRINKS

PET bottles for carbonated beverages started to be produced in the mid 1970's by the Dupont Company, from PET resin by biaxially orientating it [Rosato and Rosato, 1989]. Since then, PET bottles are now widely used in packaging carbonated beverages, bottled water and other beverages such as juices and liquor, because of the excellent mechanical properties, gas barrier, chemical resistance, clarity and gloss [Marco et al., 2002].

There are two main types of PET bottle used commercially in the beverage industry; one for carbonated beverages and one for hot-filled drinks [Maruhashi and Asada, 1996]. Carbonated beverage bottles require strength to withstand the higher internal pressure of typical carbonated soft drinks, and hot-filled bottles, greater thermal stability with less shrinkage at a temperature of 85°C [Robertson, 1993; Briston, 1992].

In the industry, there are a few kinds of processing methods developed to process polymer materials. These methods vary depending on the quality of polymer material to be produced, the type of polymer resins used, the quality of the production desired. In general, there are currently three kinds of processing methods and these are as follows; (1) Extrusion Blow Molding (2) Injection Blow molding (3) Injection Stretch Blow Molding

2.5.1. Injection stretch blow molding

The injection stretch blow molding process is used for the production of containers having biaxial molecular orientation, such as for beverages, food, household, industrial and pharmaceutical products. The most commonly used material is PET, since it offers excellent clarity, good mechanical and barrier properties, and ease of processing [McEvoy et al., 1998; Thibault et al., 2007; Martin et al., 1999].

There are two distinct stretch blow molding techniques; the one-stage process; and the two stage process. In the one-stage process the preform (shaped like a test tube, Fig. 2-11) is injection molded, conditioned to the appropriate temperature, and blown into a container; all in one continuous process [McEvoy et al., 1998].

In the two-stage process, there are three steps (Fig. 2-10). The Preform is injection molded separately and stored at ambient temperature until the time necessary. It is then reheated using infrared heating elements to the desired forming temperature range (90 to 110°C) and blown to the final shape. During blowing the sides of the bottle are stretched bi-orientational (longitudinal then radial); whereas the shoulders and base of the bottle are not stretched as much. A typical bottle profile is shown in Fig. 2-11. Finally, the stretched and blown bottle is removed from the mold and kept at ambient temperature for solidification. During the blowing stage, the preform is stretched in the vertical direction by a cylindrical rod. A pre-blow pressure is applied inside the preform to prevent contact between the stretching rod and the inside wall of the preform; which may lead to container defects, When the stretch rod reaches to the base of the bottle, a high blow pressure is applied in the radial direction to complete the final bottle shape and maximize cooling efficiency. The blow pressure air is applied for few seconds and the product is finally taken out of the mold [McEvoy et al., 1998; Thibault et al., 2007; Baczek, 2003].

Because of the relatively high cost of the molding and equipment, this technique is best for producing high-volume items such as carbonated beverage bottles. If no stretch rod motion is included the bottle formation process is known as blow molding [McEvoy et al., 1998]. [Wang et al., 1999] have used a two-stage model for PET material processing because it evaluates the strain hardening and the strain rate hardening in a proper way.
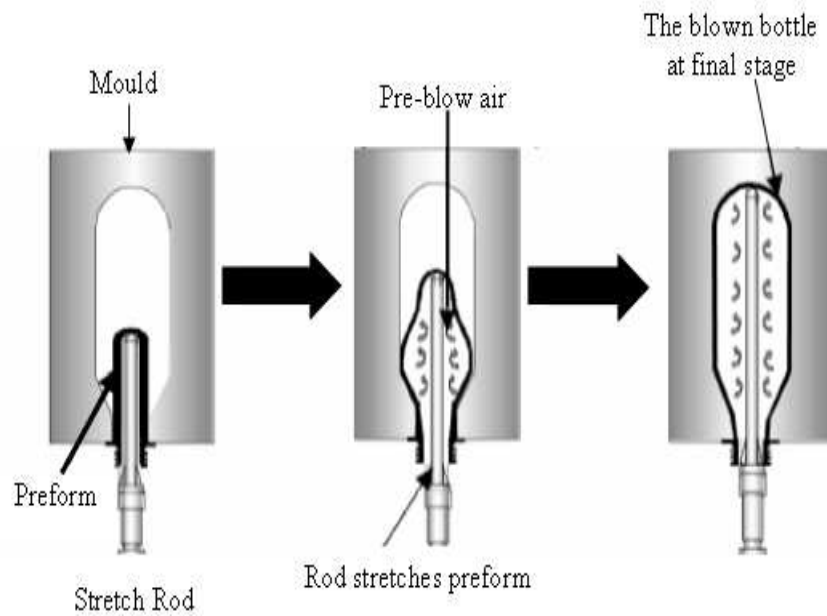
Fig.2-9. Stretch-blow molding of PET bottles [McEvoy et al., 1998].
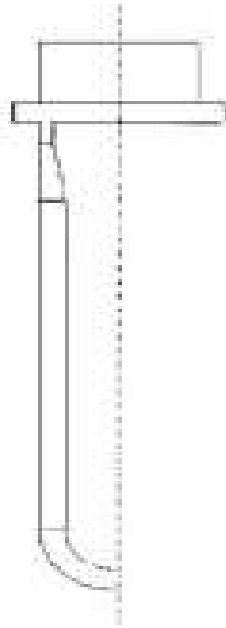
Fig.2-10. The preform design used in ISBM process [VanderPlaats, 1999]

2.5.2. Extrusion blow molding

This process comprises the conventional extrusion of a parison, or tube, using a die very similar to that used for making pipe or tubing [Crawford, 1987]. The tube is extruded downward between the two halves of an open mould until parison reaches a certain length, when the mould closes and pinches off the parison at the top and bottom end. For products with a natural opening such as bottles, the parison in the mould is blown by means of pressured air at the neck end. For products without a natural opening, the blowing air is injected to the inside from any convenient point of the parison by piercing it. After cooling, the mould is opened, the part is ejected, and any excess material is trimmed [Menary, 2001].

2.5.3. Injection blow molding

In this process, the material is injection moulded around a core pin [Crawford, 1987]. The molten polymer material on the core pin is indexed to the blow moulding station where it is

blown, cooled, and stripped from the core pin. In this method, the amount of trim scrap is not much more than that in extrusion blow moulding. More detail can be achieved in the neck and finish area (thread area) and control of wall thickness is easier than in extrusion blow moulding. However unlike injection stretch blow moulding this method is not effective improving material properties and orientation. Generally, this method is used only for the production of relatively small bottles [Menary, 2001].

2.6. PROCESS CONDITIONS

A critical development step in simulation technologies is the ability to use the process set-up as input for the simulation. This can be done by integrating the successive simulation steps from preform reheat to part cooling [Martin et al., 1999]. Since process conditions have significant effects on the final thickness, crystallinity, biaxial orientation and consequently final material properties, the initial preform temperature, the heat transfer, the balance between stretching and blowing rate, the cooling rate of the product as well as the initial preform shape must be optimized in order to achieve good bottle wall thickness in the produced products [Pham et al., 2004; Schmidt et al., 1966; 1998].

There are numerous experimental studies on this subject in the literature, to find out the effects of processing conditions on wall thickness, crystallinity, stress and the other mechanical properties of the final product.

It is understood from the studies carried out so far that the types of preform growth in the stretching and blowing stage in ISBM process depends on the geometry and sizes of the preform, the hoop and longitudinal stresses within it, and the temperature along it. However, the critical

factor is surely the delay time of the pre-blow influencing the thickness along the sidewall of the

PET bottles [Huang et al., 2006].

A study on the design of the PET preform has been presented by [Zagarola, 1998]. He asserted

that the process conditions such as small cushion, low hold pressure, and minimum hold times

reduce gate crystallinity and residual stresses, whereby lightweight preforms could be achieved.

An experimental work has been conducted on a properly instrumented ISBM machine to define

the effects of processing parameters on the bottle performance [Schmidt et al., 1998]. They tried

to understand the pressure effects and also processed with preform free inflation. Findings are

compared with a simple thermodynamic model and they also developed a numerical model for

the thermo mechanical simulation of the ISBM process. One of the results they achieved is that

an increase in the pre-blowing delay induces more material displacement from the neck to the

bottom of the bottle.

Cracking problems in carbonated soft drink bottles have been investigated and it is reported that

the ISBM set-up played a key role in stress crack resistance and that optimum process design

could double or triple stress crack resistance. So the best method for maximum stress crack

resistance is with the study of the process parameters; it is not sufficient to improve stress crack

resistance only via specifications of the bottle parameters [Zagarola, 2000]. He suggested that

since the process effects were typically highly interactive and complex, the best way to discover

the optimum set-up was to use statistically designed experiments and to control all processes in

the manufacturing system so that stress crack resistance is kept constant. He noticed that a small

change in average weight of the preforms by as little as 0.3 grams, introduced in injection stage

of the ISBM process, could significantly affect environmental stress crack performance.

2.6.1. Preform temperature

One of the most important process parameters is the preform temperature, which defines the ultimate performance of the bottle [Monteix et al., 2001]. The ability to control the temperature profile on the preform as well as blow pressure and the stretch rod sequence during stretching and inflation is critical [Martin et al., 1999]. Reheating and the temperature of the preform are achieved by means of infrared radiation supplied by an array of lamps in conjunction with convection. Generally, the temperature range of the preform is between 90 and 115°C. This is the range preferred in industrial scale production because it avoids pearlescence (stress whitening due to microvoiding) and haziness in the bottle. The axial temperature profile along the preform should be controlled because both the neck region above the support ring and the bottom region of the preform should remain cooler than the main body temperature; the bottle closure region can be distorted due to being over heated and the bottom of the bottle can be ruptured by the stretched rod. However, the body temperature profile of the preform may vary because of tapering in the thickness of the wall. Moreover, when the temperature in the preform is wrong, too much material may reside in the sidewall and not in the base [Wang et al., 1998]. The temperature profile of the preform base is important for the final morphology of the petaloid base [Hanley et al., 2006].

Lebaudy and Grenet [2001] have stated, based on experiments on PET, that it is essential to have the preform temperature either below or close to the glass transition (Tg) to achieve principally oriented glassy structure and that the crystalline structure could be enhanced as well by drawing or thermal treatments [Lebaudy and Grenet, 2001]. Zagarola has also stated that reducing reheat temperature increased top-load strength for both light and heavy weight preforms and that the lighter weight preform was also better at both reduced reheat temperature and increased reheat temperature [Zagarola, 1998]. Moreover, he has also obtained the greatest base clearance at low

re-heat temperature for the light weight preform and at high reheat temperature for the heavy weight preform.

The temperature range between the bottom and the neck region of the preform prior to the stretching is between 15-20°C. The average temperature along the length of the preform is shown in fig. 2-12 [McEvoy et al., 1998]. The temperature profile is also important in terms of clarity and material in the bottle. Lower temperatures require higher blowing pressures and vice versa.
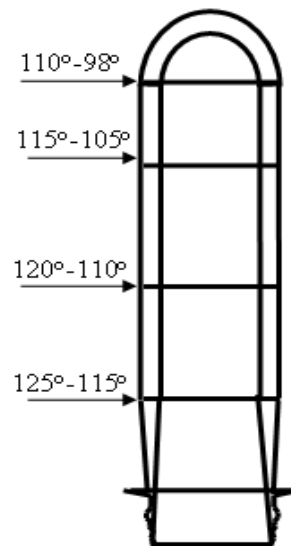
Fig.2-11. Temperature along the length of the preform [McEvoy et al., 1998]

The subsequent inflation of the preform is strongly dependant on the design of the preform and the temperature on the preform. The hot zones of the preform are to blow faster and consequently become thinner, on the contrary of this, the colder and stiffer zones are to blow slower and remain thicker [Martin et al., 1999].

Monteix et al. have completed an experimental study with numerical simulation of a preform that was exposed to infrared radiative heating [Monteix et al., 2001]. They found that the final

thickness of the part was dependant on the initial temperature inside the preform which is determined at the re-heating stage.

It has been demonstrated by other researchers that a temperature exists through the thickness [Wang et al., 1998] and that it is at least as important as temperature along the preform. However, measurement of the temperature profile on or through the preform is extremely difficult because the heat transfer rate from the outer surface of the preform to the environment is too high [Nyugen and Prystay, 1978]. But temperature is very important since it determines how well material is distributed between the sidewall and the base of the moulded bottle [Wang et al., 1998]. Wang et al. measured the temperature on the preform experimentally using an infrared camera but they could not measure the temperature through the thickness. The infrared camera gives a good indication of the relative temperature along the length of the preform, but is unable to determine the temperature through the thickness. There have been some attempts to measure temperature profile through the thickness direction with methods such as fluorescence spectroscopy [Bur et al., 1994; Migler and Bur, 1998], ultrasonic [Konno et al., 1993; Wadley et al., 1986] and infrared pyrometry [Rietveld and Lai, 1994; Lai and Rietveld, 1996].

A method called inversion technique has been developed to measure the temperature through the preform thickness by using surface temperature measurement [Nyugen and Prystay, 1978].

Some researchers have simulated the heating of the preform and subsequently used the results to predict temperature [Hartwig and Michaeli, 1995]. Other researcher attempted to determine the 3D temperature of preform by using a 'zone' method in a new heating simulation employed in the blow moulding process [Walter, 2004].

2.6.2. Heat transfer

Strain-induced crystallinity is highly dependant on the temperature reduction rate, so optimization of the cooling system in the mold to achieve the desirable mechanical properties in material is essential. This is because the heat transfer coefficient has significant effect on the temperature reduction rate. However, significant nonlinear differentials exist in the temperature, temperature reduction rate and strain, both through the thickness and length directions throughout the process, especially in the neck areas and relatively thick bottle base [Yang et al., 2004]. The thermal properties and the density of PET are shown in table 2-1.

Table 2-1. Thermal properties and density of PET [Schmidt et al., 1998]

Density	1336 kg/m^3
Conductivity	0.25 W/m/^{o}K
Specific Heat (at 296 ^{o}K)	1130 J/kg/ ^{o}K

In the last two decades extensive studies have been made in heat transfer modeling of extrusion blow molding and thermoforming. Since both mold cooling time and cooling temperature directly affect the part solidification rate and average part ejection temperature, and consequently the final part properties such as residual stresses and the level of crystallinity. However, the heat transfer question has been neglected in almost all published numerical studies of ISBM with the exception of the studies conducted by Schmidt [Schmidt et al., 1998]. Researchers have assumed temperatures remain constant during the process. The grounds for this assumption are as follows:

- The process time in stretch-blow molding is generally much shorter (typically within 2.0 seconds) than in extrusion blow molding and thermoforming [McEvoy et al., 1998; Menary, 2001; Wang et al., 2000; Menary et al., 2000].

- The preform temperature in stretch-blow molding is not high enough to produce thermally induced crystallinity.

- There is a lack of relevant experimental data and history of temperature, which is very difficult to measure because of the closed mold and short process time.

- Stretch-blow molding is characterized by strain-induced crystallization due to its critical effects on the performance of the final bottle [Yang et al., 2004].

The relationship between heat transfer and thickness in the PET bottle have been studied via non-isothermal finite element model and parametric studies of contact conditions and heat transfer coefficients [Yang et al., 2004]. It was found that lower friction coefficients and heat transfer coefficients between the stretch rod and the preform both lead to a thinner bottle base.

The available heat transfer equations have been reviewed by various researchers [Yu and Sunderland, 1992; Liang and Ness, 1996]. Stelson has conducted a study on calculating cooling times for polymer injection molding, comparing all available formulae from a theoretical stand-point, and discussing their derivations for both thin and thick parts [Stelson, 2003]. He has also clarified which equations are theoretically correct, and concluded that if the ejection criterion is based on mid-plane temperature, equation (13) is correct [Busch et al., 1988], but if the ejection criterion is based on average temperature, equation (14) is correct. [Xu and Kazmer, 1999]. Dietzel and Menges have listed cooling formulae for many simple shapes such as cylinders,

spheres, and parallelepipeds [Dietzel et al., 1991; Menges et al., 2001]. However, the most used

formulae are those for a flat plate of infinite length but and finite thickness.

$$t_c = \frac{a^2}{\pi^2 \alpha} \ln\left(\frac{4}{\pi} \left(\frac{T_i - T_f}{T_e - T_f} \right) \right) \dots\dots\dots\dots\dots\dots\dots\dots\dots\dots\dots\dots\dots\dots\dots\dots\dots\dots\dots\dots\dots\dots\text{Equation 10}$$

$$t_c = \frac{a^2}{\pi^2 \alpha} \ln\left(\frac{8}{\pi^2} \left(\frac{T_i - T_f}{T_e - T_f} \right) \right) \dots\dots\dots\dots\dots\dots\dots\dots\dots\dots\dots\dots\dots\dots\dots\dots\dots\dots\dots\text{Equation 11}$$

The cooling time formula for plates is as follows; in its most used form.

$$t_c = \frac{C_0 a^2}{\alpha} \ln\left(C_1 \left(\frac{T_i - T_f}{T_e - T_f} \right) \right) \dots\dots\dots\dots\dots\dots\dots\dots\dots\dots\dots\dots\dots\dots\dots\dots\dots\dots\text{Equation 12}$$

Where,

t_c is the cooling time,

a is the thickness,

α is the thermal diffusivity of the polymer,

T_i is the initial temperature of the polymer melt,

T_f is the mould temperature

T_e is the ejection temperature of the part.

The heat deflection temperature of the material is often taken as an acceptable value for T_e.

In the solution of the equation (16) the assumptions are that the mould is maintained at a

constant temperature, T_f, the polymer has a constant initial temperature, T_i, thermal contact

between the polymer and mould is perfect, and thermal diffusivity of the cooling polymer is constant [Carslaw and Jaeger, 1959; Bird et al., 1960].

$$\frac{T_{(y,t)} - T_f}{T_i - T_f} = 2\sum_{n=0}^{\infty} \frac{(-1^n)}{\left(n+\frac{1}{2}\right)\pi} e^{-\left(n+\frac{1}{2}\right)^2 \frac{\pi^2 \alpha t}{b^2}} \times Cos\left(n+\frac{1}{2}\right)\frac{\pi y}{b} \quad \dots\dots\dots\dots\dots\dots\dots\dots \text{(Eq. 13)}$$

Where

a is the part thickness,

b is the part half-thickness,

c_0 and ci are the dimensionless coefficients of equations (1) and (2) respectively,

F is the Fourier number or dimensionless time,

t is the time (s),

t_c is the cooling time (s),

T_{av} is the average temperature,

T_e is the ejection temperature,

T_f is the final temperature,

T_i is the initial temperature,

T_m is the mid-plane temperature,

$T(y, t)$ is the temperature,

y is the distance from mid-plane of part (m),

α is the thermal diffusivity (m^2/s) where temperatures are given in degrees.

Dubay and Bell have investigated the cooling cycle of injection molding for cylindrical shaped plastics components and formulated a numerical model by using the full conservative form of the energy equation with temperature dependent polymer properties having continuous equations of

state [Dubay and Bell, 1998]. They concluded that the cooling time predictions from the numerical method were in good agreement with experimental results and that the model they proposed predicted shorter cooling times than the often used non-conservative heat conduction model, which uses constant polymer properties or a temperature dependent thermal diffusivity. They also realized that for parts which had a thickness of 3 mm, [Ballman and Shusman, 1959] and the conservative model have given very good agreement in cooling time but the statistical cooling time model of Busch was more suitable for plastics parts [Busch et al. ,1988].

An inverse method has been proposed for estimation of the initial temperature profile of a preform for polymer processing [Nyugen and Prystay. 1978]. Since the wall thickness of the preform is usually small compared to its height or width, it is reasonable to assume that heat transfer is one-dimensional. Moreover, as the mold temperature is controlled approximately at the same temperature on both sides, the temperature through the thickness is considered symmetric. The equation governing the temperature evolution in the preform can then be simplified as follows; this differential equation solution has been given by Carslaw and Jaeger [Carslaw and Jaeger, 1959]

$$\rho C_p \frac{dT}{dt} = \frac{d}{dt} k \frac{dT}{dX}$$ …………...……………………………………………...……………Equation 14

with the following boundary and initial conditions:

$$\frac{dT}{dX} = 0 \text{ at } X = 0$$ (on the plane of symmetry) …………...……..…Equation 15

$$-k \frac{dT}{dX} = h(T - T_a)$$ at   X=d   (on the surface)……………………………….Equation 16

$T(x, t = 0) = f(x)$ ………………………………………...…………………...………Equation 17

Where

T is the temperature,

T_a is the ambient temperature,

ρ is the density,

C_p is the specific heat,

k is the thermal conductivity,

h is the heat transfer coefficient,

t and x denote time and spatial coordinate, respectively

d is the half thickness of the part.

2.6.3. Blow pressure – Time

The sequence of the stretching and blowing has a considerable effect on preform growth [Huang et al., 2006] and blow pressure determines the total processing time of the bottles [Wang et al., 1998]. The deformation of the preform imposed by stretch rod and blow pressure has been studied during the stretching and blowing stages. Three types of preform growth have been observed 'dolphin-type', 'sandpile-type', and 'two bubble-type' [Huang et al., 2006].

Wang et al. have conducted blow molding simulations in three regimes; blowing without stretching, complete stretch followed by blowing, and partial stretch followed by blowing to completion [Wang et al., 1998]. The results have shown that the last method yields the best thickness in the final product. McEvoy et al. have obtained the same result in their studies; that applying a pre-blow pressure does over-predict the side wall thickness of the bottle in simulations [McEvoy et al., 1998]. They have worked with AOKI ISBM machines and applied around 0.1–

0.2 MPa as a pre-blow pressure and 4 MPa as a blow pressure. The fig.2-13 shows the ideal

pressure development rates as a function of time for a 2 lt bottle.
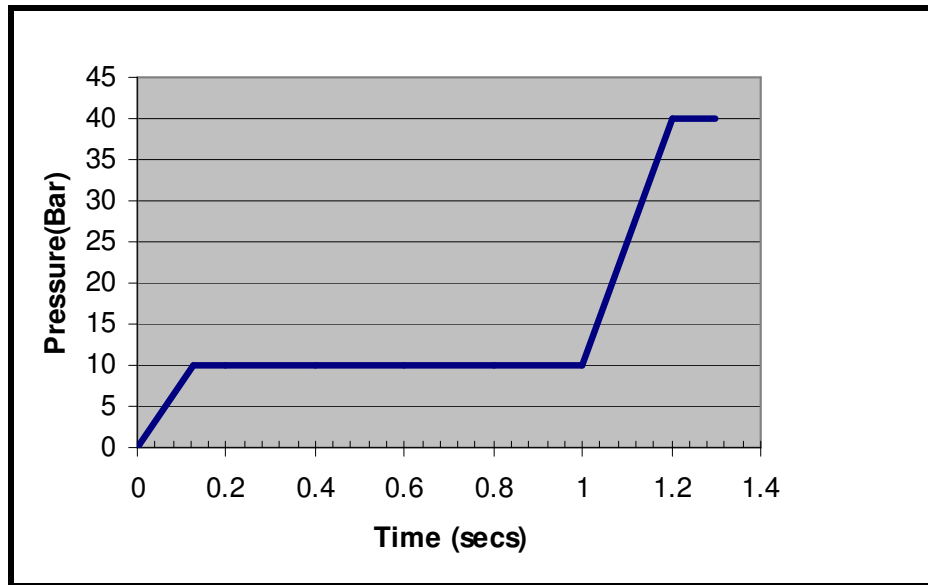
Fig.2-12. Pressure vs. time for 2 lt bottles

2.6.4. Stretch rod displacement as a function of time

Correct stretch rod ensures the desired strain hardening of PET in the side walls and hence a

constant wall thickness in this area. If the movement is too slow relative to the pre-blow

activation or when there is no stretch rod movement, the preform can go off-centre and cause non

uniform wall thicknesses. If the movement is too rapid, the preform may rupture [McEvoy et al.,

1998].

The base of the bottle is stretched very little, the temperature range around that section is lower

(around 80°C) than in the upper areas, and the rod may also stick to the bottom of the bottle

[Hanley et al., 2006]. That is why; the bottom section of the bottle demonstrates weakness in

terms of stress cracking resistance. After stretching stops near the base, the rest of the areas

continue to be stretched first by the 'pre-blow' pressure and then the 'final-blow' pressure.

Consequently, compression may occur at the bottom area [Yang et al., 2004]. The fig.2-14 shows

the typical stretch rod displacement vs. time relationship. McEvoy et al. have simulated the

stretch blow molding process of PET bottles in AOKI-ISBM machine according to this model

[McEvoy et al., 1998].
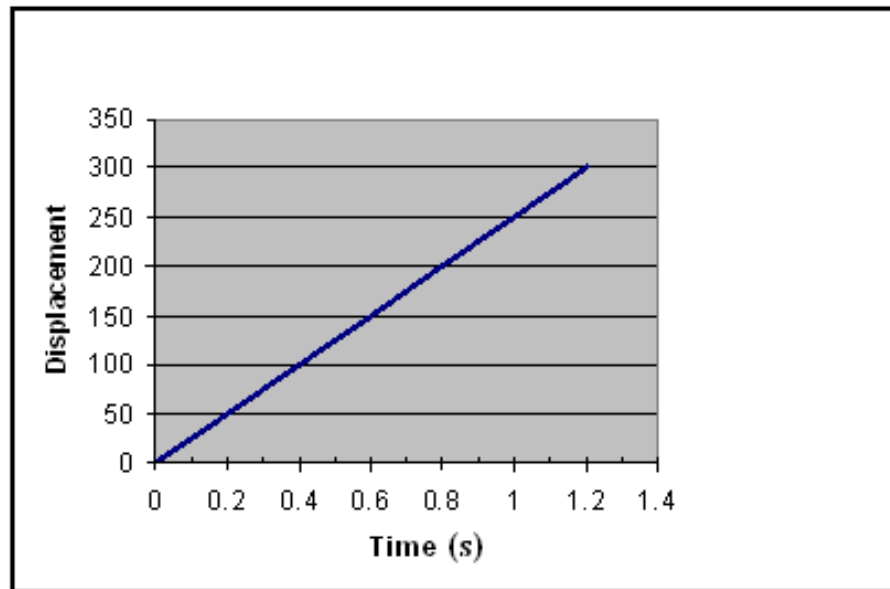
Fig. 2-13 Stretch Rod Displacement *vs.* Time for AOKI blow molder [McEvoy et al., 1998]

Pham et al. have demonstrated a model describing the mechanical behavior of PET [Pham et al.,

2004]. They have also explained that PET undergoes strain hardening when it is stretched;

stretching of the preform is essential to achieving uniform wall thickness in the formed bottle.

Because strain hardening depends on the temperature profile and strain-rate; at any given strain,

increasing the temperature reduces the strain hardening properties and vice versa. In contrast, at a

fixed temperature increasing strain rate causes the polymer to strain-harden, particularly at large

strain values. So, if the preform being blown touches the mould before strain hardening occurs, the

material does not reach its natural draw ratio and consequently the desired uniform wall thickness can

not be achieved [Wang et al., 1998].

2.7. OPTIMIZATION INJECTION STRETCH BLOW MOULDING PROCESS

The design of a PET preform is highly complex especially from a numerical optimization point of view. The ISBM process sequence is complex and coupled. However, the rheological behavior of the material during the stretching and blowing stages is highly nonlinear and thermally dependent. In short, optimization of the ISBM process is very complicated [Thibault et al., 2007].

There is limited work in the literature in terms of numerical modeling for design optimization; the only work conducted in this subject is the study which Lee and Soh have made for ISBM [Lee and Soh, 1996]. They developed a finite element method to determine the optimal thickness profile of a preform for a blow-molded part and tried to find the required wall thickness. They assumed that the preform was not axially stretched during the forming stage.

A study related to extrusion blow molding has been conducted, and it is proposed that a closed-loop optimization approach analogous to classical process control system can be used to manipulate the process parameters in order to determine the thickness of the inflated part [Laroche et al., 1995].

Gauvin et al. [2003] have revised the previous work by means of a gradient-based approach in order to minimize the design objective function by fixing the processing parameters. In polymer injection molding, in order to minimise the filling time of the polymer material, some researchers have attempted to optimise the gate location through a design sensitivity analysis coupled with a gradient-based approach [Smith et al., 1997; Kabanemi et al., 2002]. There are several papers in metal forming [Xinhai et al., 2006], which propose different algorithms to optimise the preform mould design.

Some studies have been carried out with the intention of developing a design optimisation environment for the design of preforms and container moulds, and two complementary optimisation algorithms have been proposed [Thibault et al., 2007].

Since thickness in a preform affects blown container performance specifications such as top load, pressurization, and vacuum loads, prediction of preform thickness is emphasised in a performance optimization process [VanderPlaats, 1999]. On the other hand, there are different types of preform available in industry, and the choice depends on the bottle to be produced and the desired final thickness. These preform models are shown in Fig. 2-15.

Three different types of stretch ratios are considered in the preform design: axial, hoop and end-cap thickness ratio. The detailed expressions on the preform design have been provided [Vander Plaats, 1999]. A number of numerical optimisation techniques are found in the literature, such as traditional gradient techniques of zero, first, and second-order or soft computing methods. Vander Plaats has used a second order method because of this method's strong track record**.**

Outside taper   Inside taper   Dual side taper   Base step design
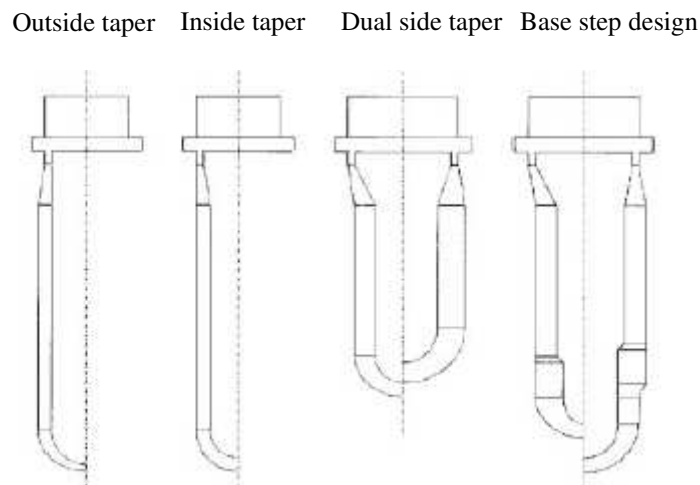
Fig.2-14. Different types of preform geometry used in the industry [VanderPlaats, 1999]

2.7.1. Bottle base weight

Over-thickening in the base of the PET bottle is a commonly encountered problem in ISBM process. More material is piled up at the base due to this problem and thus material waste arises. The problem also results in under-straining and, consequently, less crystallization and orientation. Optimizing preform design and process conditions is therefore crucially important to achieving thinner, highly orientated, and more crystallized bottle bases [Yang et al., 2004].

The packing pressure of the injection molded preform [Brooks and Giles, 2002; Zagarola, 1998] and the temperature of the preform during stretch blow molding [Venkateswaran et al., 1998] determine the final properties of the bottle. In the 'injection stage' of the material into the mold, the 'hold time', which is the length of time the gate remains open allowing more material to be pushed into the mold cavity, relates to the preform weight. For this reason, the hold time and the shot size should be kept as short as possible in order to force less material into the end of the preform; which finally forms the base of the bottle. However, the cooling efficiency of the body and neck of the preform is also important because these regions in the mold resist the addition of more material [Hanley et al., 2006].

In order to observe heat transfer and contact conditions in the ISBM process and to define friction and heat transfer coefficients, Yang et al. [2004] have developed a model. They concluded that the friction coefficient and heat transfer coefficient between the stretch rod and the preform affected only the bottom area, and also that both lower friction coefficients and lower heat transfer coefficients led to a thinner bottle base since only in this condition the bottom remains relatively softer to stretch.

Some researchers have assumed that the hemispherical base of the PET bottle would not significantly affect the wall thickness along the neck, shoulder, and side-wall regions and conducted their study under this assumption [Wang et al., 1998]. It has been reported that in extrusion blow molding systems the bottle base weight was affected by 'drop time' and 'parison sag' [Strebel and Benson, 1996]. As the drop time and parison sag increase the bottle base weight also increases; this is why the weight of the bottle base affects the crystallinity, consequently affecting potential for cracking.

2.7.2. Bottle and petaloid base design

The petaloid base shape currently used in commercial applications is shown in fig. 2-16.
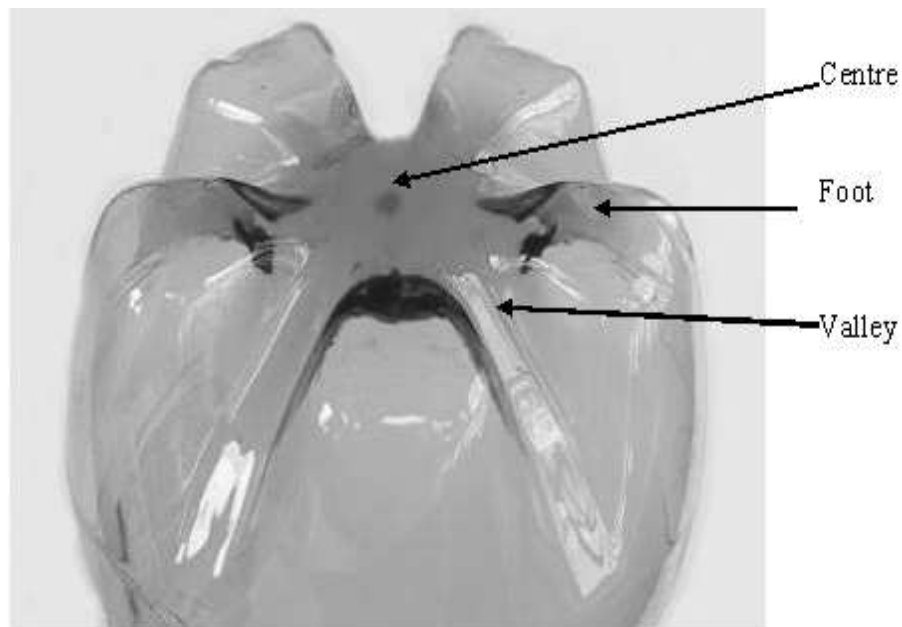
Fig.2-15. CAD drawing of a typical petaloid base of a bottle

There are many types of bottles in use, and their shape varies depending on the usage, material type and blow molding machine [Chua and Lye, 1998]. Preforms should be well designed in

terms of both the desired bottle wall thickness and the bottle shape to be produced. In the literature, there are valuable guidance regarding preform and bottle design [Masood and Keshavamurthy, 2005; Zagarola, 1998]. The bottle's collapsibility is highly dependant on its wall thickness [Masood and Keshavamurthy, 2005] and the draw ratio on the parallel (hoop) direction should be about 35% more than the perpendicular (axial) direction [Rosato and Rosato, 1989].

Some useful suggestions regarding the factors which should be considered in the design of blow-moulded bottles can be listed as follows:

1. It should be considered that wall thickness vary from side panels to corners.

2. Rounding and filleting of edges and corners is very important because this increases resistance to higher levels of stress.

3. There should be a harmony among the sections of the bottle. Abrupt thickness changes between sections causes cracking. So very narrow or very wide bottoms and tops are not recommended.

4. The neck section of the bottle has to withstand both handling and liquid pressure inside the bottle. Therefore, the thickness of this section is highly important.

5. The shoulder of the bottle should be strong, but flexible enough to withhold the liquid pressure and also be resistant to cracking.

6. The bottle base is the most important section of the bottle from a functional point of view and should be slightly concave because it absorbs external shocks and improves impact strength [Zagarola, 1998].

Chapter 3

BOTTLE BASE DESIGN

AND

OPTIMIZATION

3.1 INTRODUCTION

The goal of the study presented in this chapter is to determine the petaloid geometry and dimensions in the base of the bottle that will maximise resistance to environmental stress cracking.

A finite element model of a standard 1500 ml bottle is developed in CATIA. In the optimization process, another design of experiment and optimization program called ECHIP-7 was utilized. The relative parameters of the bottle base and the optimization range of these parameters were defined, and hereby combinations of the base dimensions to be used in the optimization process were generated by ECHIP. Stresses in the base are calculated by means of the finite element analysis according to these combinations of base dimension; finally, the base dimensions which result in the minimum von Mises stress are identified as the optimum base dimensions.

Furthermore, the optimization was conducted at two different wall thickness of the PET in the bottle base under two different internal pressure applied from the inside of the bottle; and the optimisation studies were systematically repeated under these conditions.

3.2 CURRENT BOTTLE DESIGN

The PET bottle in consideration is a 1500 ml. carbonated soft drink bottle A dimensioned drawing of the bottle design is shown in fig. 3-1; taken from a production drafting supplied by a bottle manufacturer, The bottle dimensions are given. The bottle's respective specifications relevant to CSD packaging requirements are given in table 3-1. The two sets of dimensions are given in Table 3-1, along with weight and capacity specifications.

Table 3-1. 1500 ml Billboard CSD-Stock dimensions and specifications

Preform Weight	40 g.					
	Immediately after production			72 hours after production		
Characteristics	**Min.**	**Target**	**Max.**	**Min.**	**Target**	**Max.**
Preform Weight (g)	39.8	40.0	40.2	-	-	-
Section Weights (g)						
Top (194.3 mm)**	13.2	13.7	14.2	-	-	-
Centre	14.2	14.7	15.2	-	-	-
Base (53.3 mm)**	11.1	11.6	12.1	-	-	-
Dimensions (mm)	**Min.**	**Target**	**Max.**			
Overall Height	295.3	296.4	297.6	294.8	296.0	297.2
Label Panel Height	140.7	141.2	141.8	140.4	141.0	141.6
Major Top Diameter	92.3	93.0	93.6	92.1	92.7	93.4
Label Panel Diameter	90.8	91.5	92.1	90.6	91.2	91.8
Base Diameter	92.3	93.0	93.6	92.1	92.7	93.4
Base Clearance	-	6.1	-	-	-	-
Capacity (ml) Average*						
Fill point	1510	1518	1525	1502	1510	1518
Brimful	1535	1543	1550	1527	1535	1543

** Sectional cuts are measured from the base.

* Fill point capacity at 42.5mm down inside
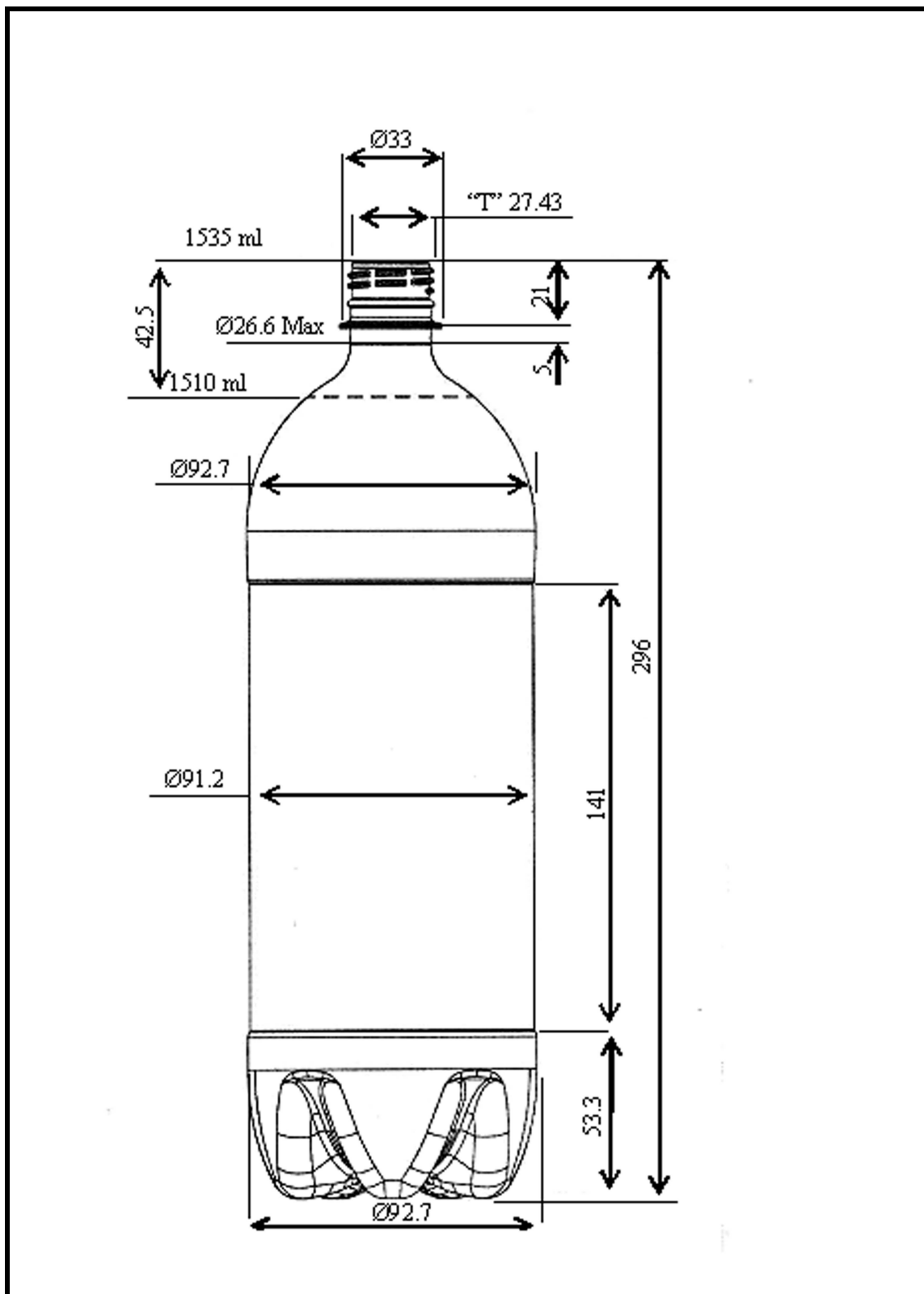
Fig.3-1. 1500 ml PET bottle drawing and dimensions

In the CATIA model the top, centre and base sections are generated separately and then joined together to form the whole bottle as shown in fig. 3-2. The bottle base is further divided into five 72° segments. The CATIA model of a single 72° segment is shown in fig 3-3, and the completed base in fig. 3-4.

Fig.3-2. The CATIA drawing of the standard (current) PET bottle
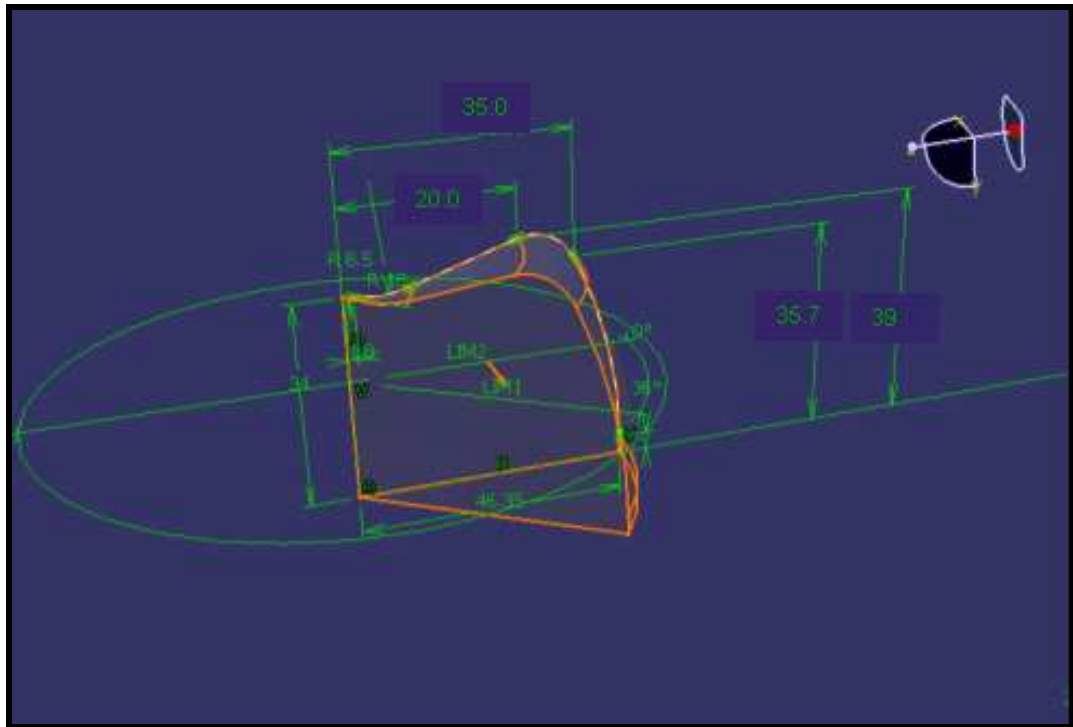
Fig.3-3. Dimensioned CATIA model of one segment of the bottle base
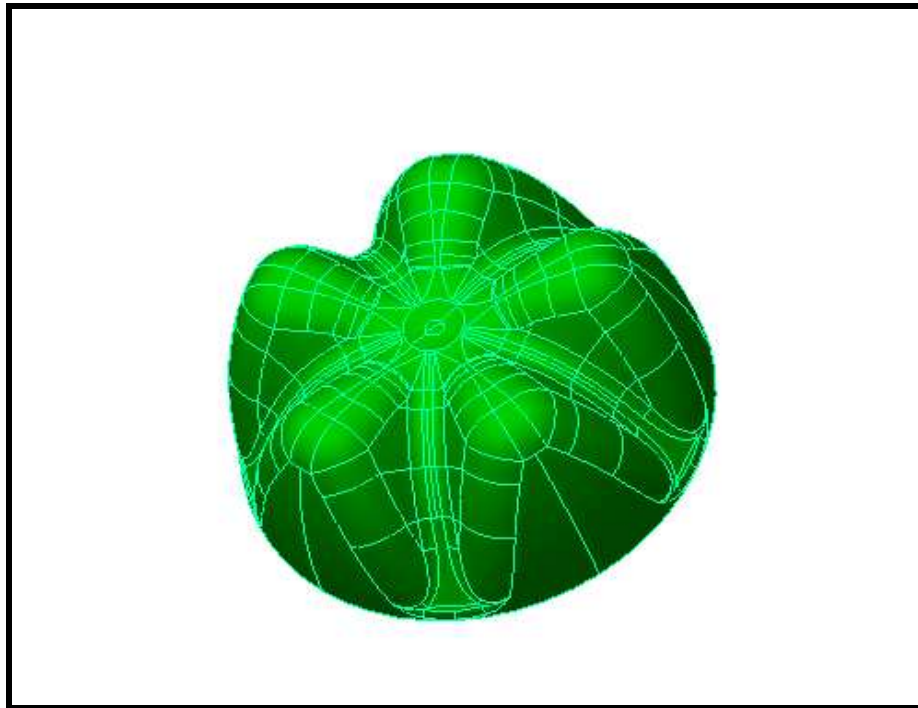
Fig.3-4. CATIA model of the current bottle base

All studies related to optimization of the bottom of the bottle are conducted on the base section. Although the wall thickness varies through the base, in order to test the effect of base dimensions on the stress observed, a uniform wall thickness of 2 mm. throughout the bottle was assumed; and all optimization analysis was done according to this assumption. The analysis was repeated for wall thicknesses of 1 mm. and 0.5 mm.

3.3 FINITE ELEMENT ANALYSIS

In the FEA method the structure is modelled as a network of small elements interconnected at their nodes. The fact that a real structure can be sub-divided into relatively small elements each of a simple shape is fairly basic but it is the most important principle of the finite element analysis method (fig. 3-5). The displacement or stress patterns around these very small elements can be represented by a relatively simple mathematical equation such as a linear or quadratic function, and has a set of 'nodes' at each end of a line element or at each corner of a quadrilateral element. In order to form a mesh that is a mathematical model of the design, each element is joined together at adjacent nodes. In principle, the applied loads and the direction on which the model is supported should be defined. The nodes are points at which different elements are joined together; nodes are the locations where values of unknowns (usually displacements) are to be approximated. The mathematical equations of the models generated in simple geometrical shapes are resolved by FEM and these resolved thousands of simultaneous equations are combined in a sum. This sum is the total of the solution across the element. The shape and size of the element mesh are very important parameters in terms of the accuracy of the result. There are not any certain rules about what constitutes a good mesh but there are guidelines.
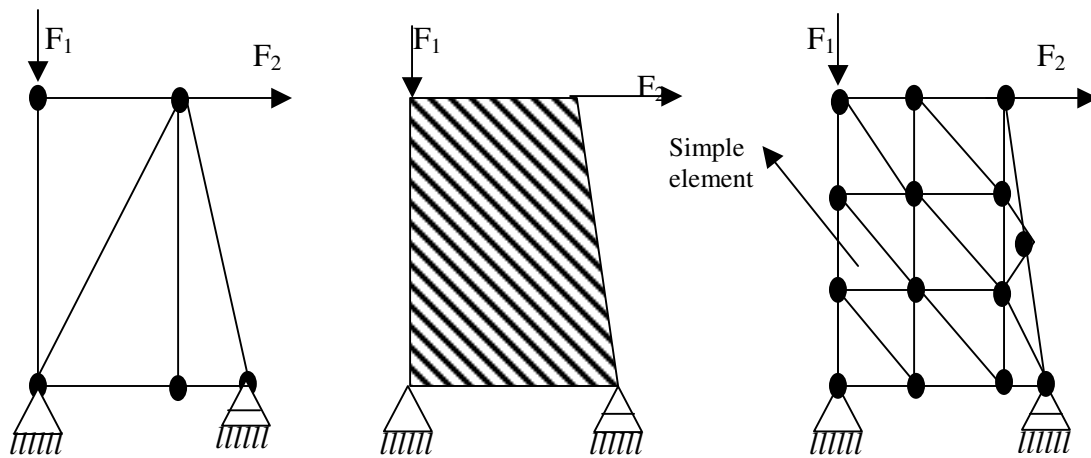
Fig.3-5. Finite element structure

The software programs currently in use are used to develop and analyze some physical properties of the model studied. The development usually contains three stages.

1. Pre-processing stage: In this stage, the model or the component to be studied is drawn like in the conventional CAD drawing. The drawings will define the geometry of the component although often some additional geometrical information will be required. In addition, the material properties, the applied loads and supports or restraints on the structure should be defined to complete the finite element modeling.

2. Analysis stage: The software program solves the mathematical equations relating forces to stress, displacement etc. within the timeframe of a few minutes or several hours, even days. For the simple model and good conditioned computer, the analysis time is very small, but for the complex model and small size computer analysis time becomes long.

3. Post-processing stage: In this stage, the numerical results achieved from the analysis are shown in order to assist the assessment of the numerical data. For example, stress results achieved can be plotted using colors to represent different levels of stress [McEvoy, 1997].

3.3.1 Generation of a model for finite element analysis

All commercial computer FEM programs have a library of element types and these elements can be selected automatically by the program, as well as manually. These are one dimensional (lines such as shells, beams), two-dimensional (surfaces) and three- dimensional (blocks). Moreover, these may also be of the straight or curved sides. Two-dimensional elements are of rectangles, squares, triangles, or other quadrilaterals. Three dimensional elements are tetrahedral or triangular prisms, hexahedral bricks (fig. 3-6). There are normally nodes at the corners of the elements. Each element has certain degrees of freedom; i.e. freedom to move in given directions. The simplest elements have only one or two degrees, the movement in the x and/or y directions can be regarded as of them and also the movement in the z axis and rotations about the x, y and z axes can be added for more complex elements which have multiple freedom degrees. In some instances, more than one type of element can be used for the model considered.

The mesh element shape should fairly represent its basic shape because highly distorted elements results in poor results. In case that the number of elements is required to be increased, engineering experience is of course important. The elements to be selected in mesh are matched to the geometry of the structure, the accuracy, and type of result required. Generally, the number of elements in a model should be enough and the mesh size and shape should be defined so as to represent the model so that the model can represent the actual behavior and lead to better and accurate results. However, increasing the number of elements increases computer time and cost [McEvoy, 1997].

3 Element Beam Element

3 Noded 2D Triangular   8 Noded 2D solid

Quadrilateral Element

4 Noded 3D solid

Tetrahedral Element

20 Noded 3D Solid

Hexahedral Element

6 Noded 3D solid

Tetrahedral Element
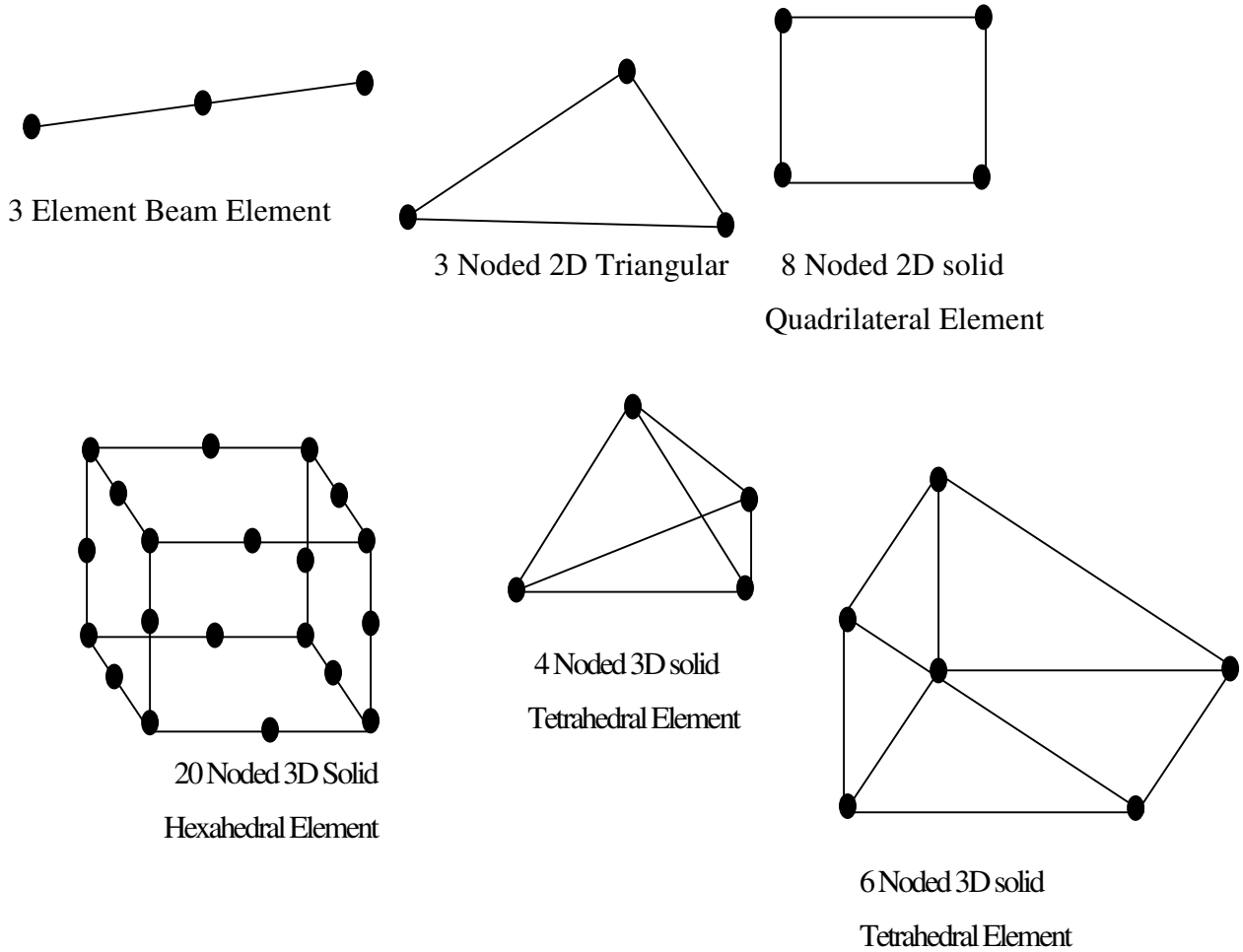
Fig.3-6. Various finite elements

3.3.2. Stress analyses of solid bodies

Stress strain relationship: For a two-dimensional plane stress element, stresses and strains are related by the following equations;

$$\sigma_x = \frac{E}{\left(1-v^2\right)} \cdot \left(\varepsilon_x + v \cdot \varepsilon_y\right)$$

$$\sigma_y = \frac{E}{\left(1-v^2\right)} \cdot \left(\varepsilon_y + v \cdot \varepsilon_x\right)$$

$$\tau_{xy} = \frac{E}{2(1+\upsilon)}\gamma_{xy}$$

Where

σ_x, σ_y are tensile stress in x and y direction respectively.

ε_x, ε_y are the strain in x and y direction respectively.

υ is poisson's ratio

E is Young modulus,

τ_{xy} is shear stress

γxy is shear strain.

These equations may be expressed in matrix form as;

$$\begin{Bmatrix} \sigma_x \\ \sigma_y \\ \tau_{xy} \end{Bmatrix} = \frac{E}{(1-\upsilon^2)} \begin{bmatrix} 1 & \upsilon & 0 \\ \upsilon & 1 & 0 \\ 0 & 0 & (1/2)(1-\upsilon) \end{bmatrix} \cdot \begin{Bmatrix} \varepsilon_x \\ \varepsilon_y \\ \gamma_{xy} \end{Bmatrix}$$

or in shorthand form as;

$$\{\sigma\} = |D| \cdot \{\varepsilon\}$$

where |D| expresses the material stiffness of the element. For example, for a spring element of modulus E this would be given by

$$D = \begin{bmatrix} E & 0 \\ 0 & E \end{bmatrix}$$

The computations and the design procedures involved in the finite element analysis are both very complicated and time consuming and are impossible for manual calculations. However, these calculations have been possible through software programs like CATIA, Abaquous, and Pro-Engineer etc.

3.4 VON MISES STRESS ANALYSIS AND SIMULATION PROCEDURE

The conditions that the product might experience in use should be defined correctly in the analysis and simulation stage. The bottle model generated in the mechanical design section of CATIA was automatically transferred into the 'Analysis and Simulation Work Bench'. The material properties of PET are then required for the stress and deformation analysis step.

The von Mises yield criterion [Von mises, 1913] suggests that the yielding of materials begins when the second deviatoric stress invariant reaches a critical value (k). For this reason, it is sometimes called the plasticity or flow theory. It is part of a plasticity theory that applies best to ductile materials, such as metals. Prior to yield, material response is assumed to be elastic.

In material science and engineering the von Mises yield criterion can be also formulated in terms of the von Mises stress or equivalent tensile stress, (σ_v), a scalar stress value that can be computed from the stress tensor. In this case, a material is said to start yielding when its von Mises stress reaches a critical value known as the yield strength, (σ_y). The von Mises stress is used to predict yielding of materials under any loading condition from results of simple uniaxial tensile tests. The von Mises stress satisfies the property that two stress states with equal distortion energy have equal von Mises stress.

Because the von Mises yield criterion is independent of the first stress invariant, it is applicable for the analysis of plastic deformation for ductile materials such as metals, as the onset of yield for these materials does not depend on the hydrostatic component of the stress tensor.

3.4.1 Setting the material properties

As PET material properties vary depending on the conditions exposed to, the material properties in the actual production conditions should be used to achieve the best performance. The properties for PET are given in table 3-2.

Table 3-2. Material properties for virgin PET

Young Modulus	2.9 GPa
Poisson Ratio	0.4
Density	1200 kg/m^3
Thermal Expansion	0.00007 1/ $^{\circ}$C
Yield Strength	55 MPa

3.4.2 Static solution parameters

For static case solutions, problems are defined as either linear or non-linear. A linear problem is where there is no contact feature (virtual or real), no pressure fitting property, and where the displacement is a linear function of the load. Non-linear is the condition that there is at least one contact feature (virtual or real) or pressure fitting property, and the displacement is a non linear function of the load.

A new Analysis Case is a set of object corresponding to a new set of specifications of simultaneous environmental actions on a given system. To create object sets for the new specifications, a new Static Case should be inserted. This cause a static solution procedure for the computation of the system response according to applied static loads under given restraints. The static solution parameters can be set as shown in fig. 3-7.
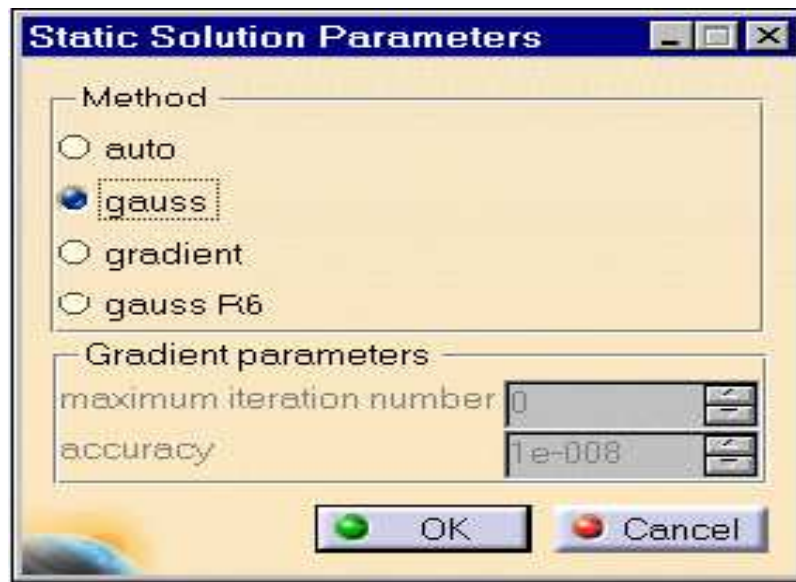
Fig.3-7 CATIA dialog box for 'static solution parameters'

The method is selected depending on the type of model; small, medium or complex. For small models it is recommended, that the method be set as auto; whereby the stresses can be computed automatically. In this study, the Gauss Method was chosen. The Gauss Method is a direct method which is mainly recommended for computing stresses in small to medium models.

3.4.3 Application of restraints

Restrains must be applied to the body to be analysed so that static analysis such as stress, deformation analysis can be carried out. These restraints may be in either one, two, or three

dimensions. There are different types of restraints in the 'Generative Structural Analysis Workbench' and the isostatic restraints were selected out of them.

The restraints were applied to the bottom of the bottle because the deformations during filling are taken into consideration in the upright standing position. So clamps were held to the parts of the bottom of the bottle where it touches the ground in 8 faces as indicated in CATIA dialog box shown in fig. 3-8. Once the surfaces are selected, the program automatically chooses restraints (fig. 3-9). The body is prevented from rigid-body translations and rotations by means of the boundary condition.
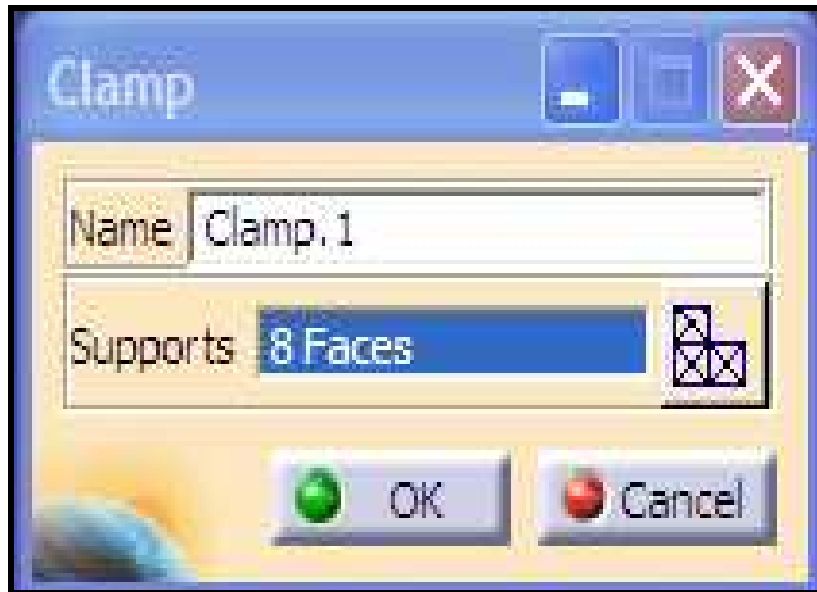
Fig.3-8. CATIA dialog box for clamp type and number of faces supported
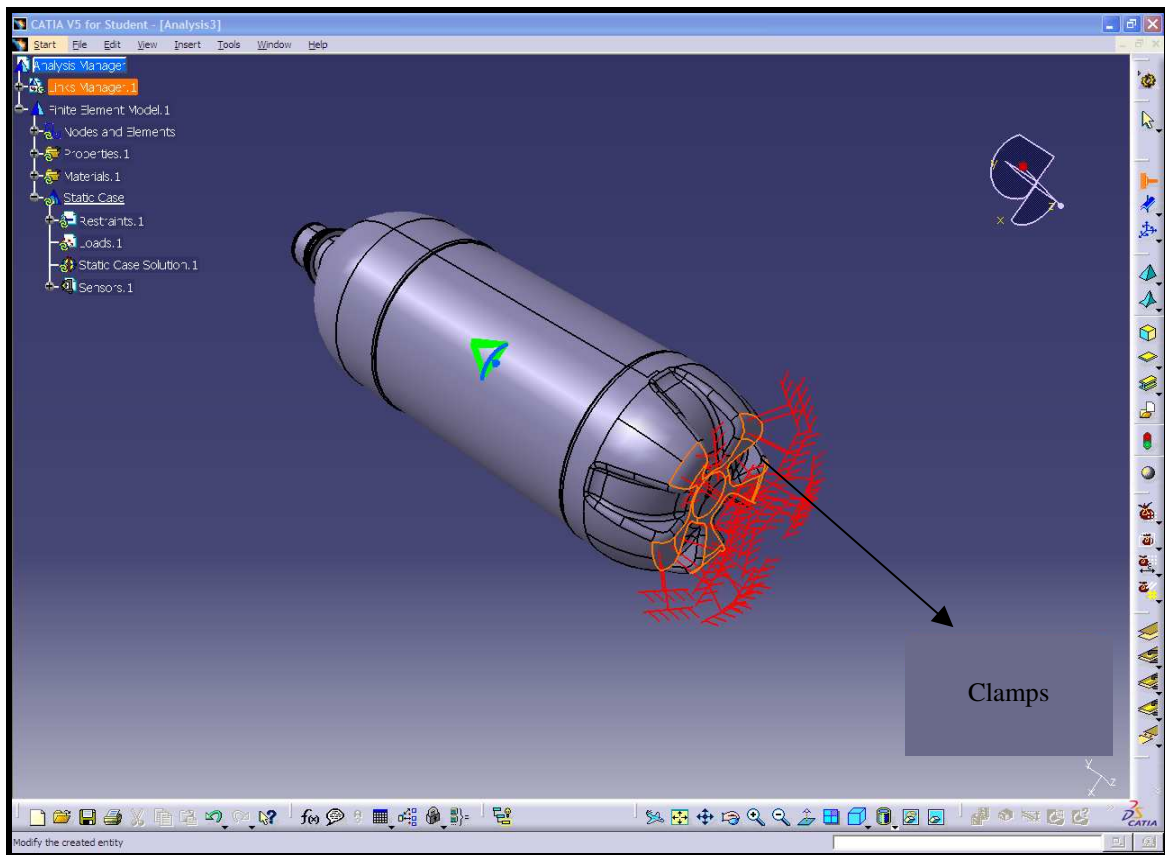
Fig.3-9. Application of restraints to the base of the bottle

3.4.4 Application of pressure

The stresses due to the pressure of the carbonation of the content are simulated and applied in the Generative Structural Analysis Workbench of CATIA. On this workbench, pressures can be applied onto the selected surfaces and the magnitude and direction of the pressure can be given as the input.

According to the information obtained from bottle manufacturers and the studies investigated, the pressure applied by the carbonation pressure of the content ranges between 400,000 and 600,000 N/m^2. According to the CATIA dialog box shown in fig. 3-10, these pressures were applied to the inner surfaces of the PET bottle (fig. 3-11) and then stress analyses were conducted.
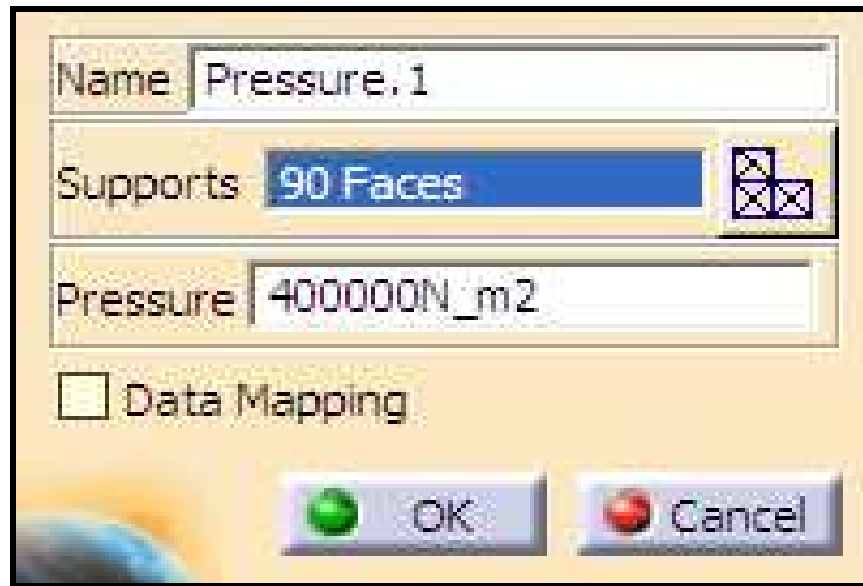
Fig.3-10. CATIA dialog box for applied pressure
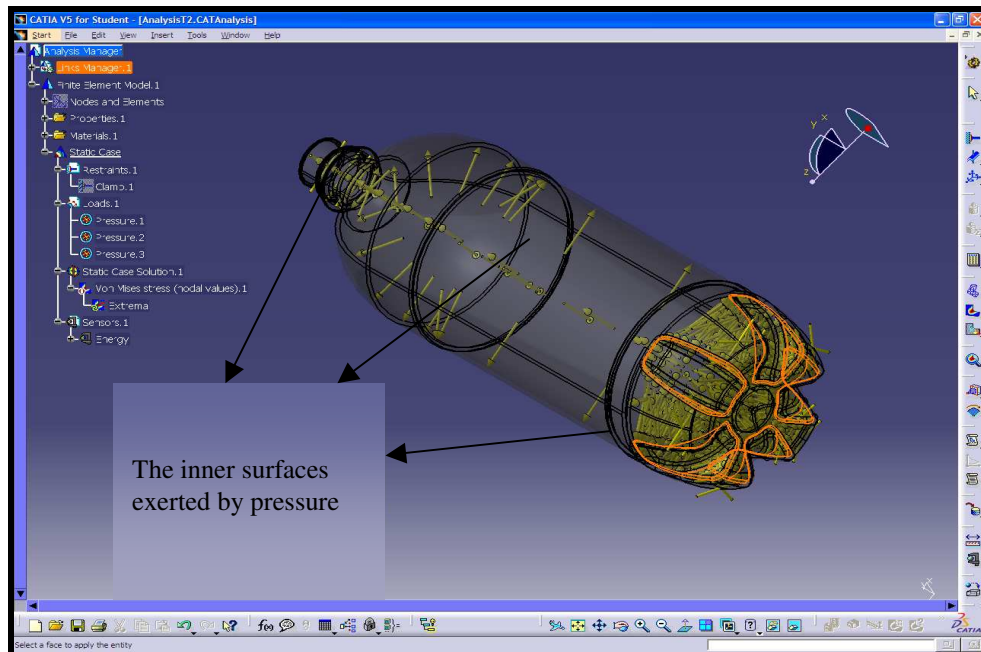
Fig.3-11.The application of pressures on the inner surfaces of the bottle

3.4.5 Mesh generation

Once the pressure and constraints are set up, the program automatically starts the computation to calculate the stresses occurring on the bottle surface and to identify the areas where the maximum and minimum stresses arise. However, prior to this step, the elements and the nodes, required for the stress calculations must be generated. This is referred to as 'meshing' or mesh generation. Generating suitable mesh geometry is very important to achieving more accurate results. CATIA supports two types of mesh: 'Linear Tetrahedron' and 'Parabolic Tetrahedron'. In this study, the Linear Tetrahedron mesh type was used because it covers more surface than the parabolic tetrahedron and it is a much simpler. The complete meshed bottle is shown in fig. 3-12. The mesh geometry and dimensions are shown in fig. 3-13. When all input parameters are set up, von Mises Stress values and displacements can be computed.
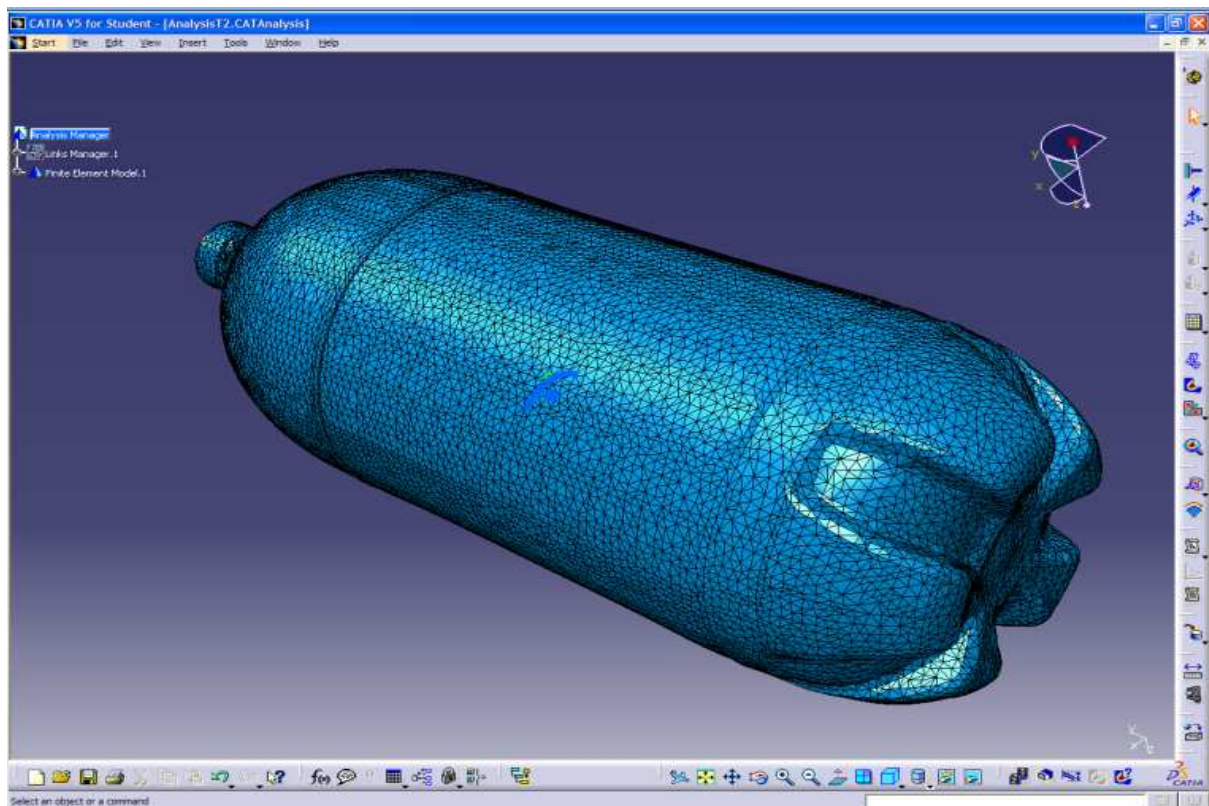
Fig.3-12. The meshed surface of the bottle
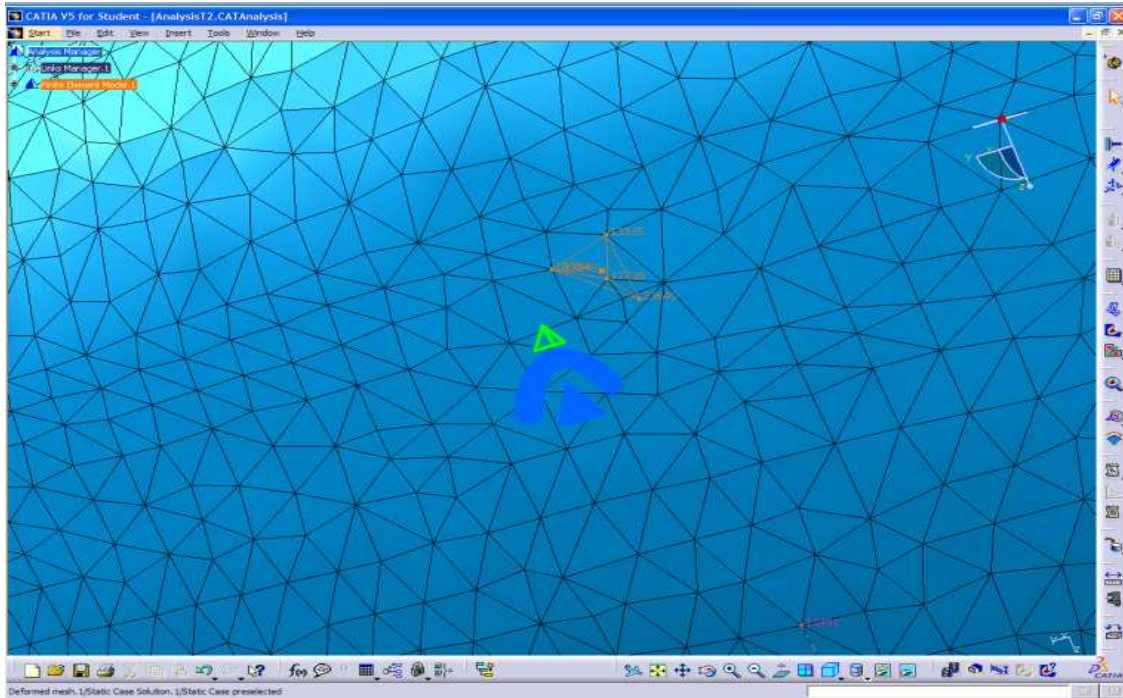
Fig.3-13. The mesh geometry and dimensions of elements on the bottle surface

Fig.3-14. The mesh size used in the stress analysis

The petaloid base of the bottle being geometrically a very complicated shape has made the proper selection of mesh geometry difficult. Linear Tetrahedron mesh geometry was therefore selected but the mesh size was kept as small as possible by depending on the capacity of the computer studied on. But, the time consumed for computation increased as the mesh size got small. In this study, 2.527 mm. was considered as the smallest mesh size to be studied (Fig. 3-14).

The fact that the computer processor is fast and the other components of the computer used in the study are suitable for CATIA program is highly important. The size of the mesh form is also important from the accuracy of the stress point of view. In this study, the mesh size is kept as small as possible, because the smaller the mesh size the more accurate the stress values.

Meshing time may vary depending on the size and geometry shape of the surface on which computation is made. Once the meshing is over, the computation is completed and the program shows the time elapsed and the memory used in the computation. Then the report for post-analysis is automatically generated and the deformed mesh form and the stress on the bottle surface are shown (fig. 3-15). The colour coded scale on the top left corner of the computer screen indicates the magnitude of the stress.

When the inner wall of the bottle is subjected to pressure exerted by the carbonated soft drink, three dimensional stresses are created. They are combined into 'Equivalent' or von Mises stresses. If the von Mises stress exceeds the yield stress, then the material is considered to be at a failure condition. The von Mises stress obtained from the analysis is given in fig. 3-16 and fig. 3-17.
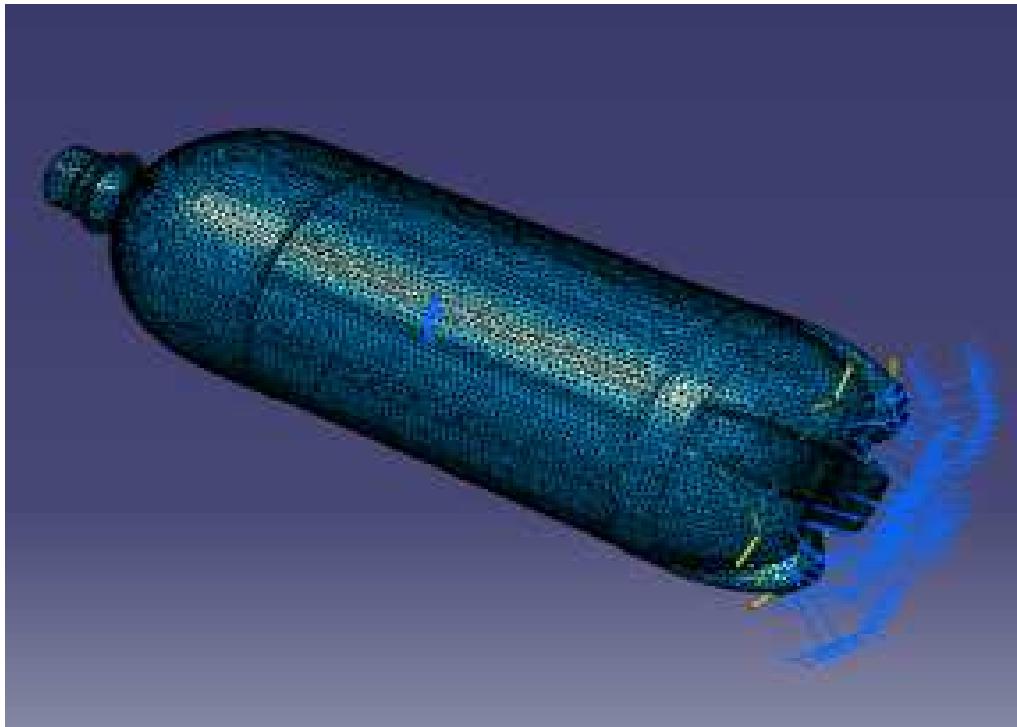
Fig.3-15. The deformed mesh with the restraints and loads as a result of the deformation
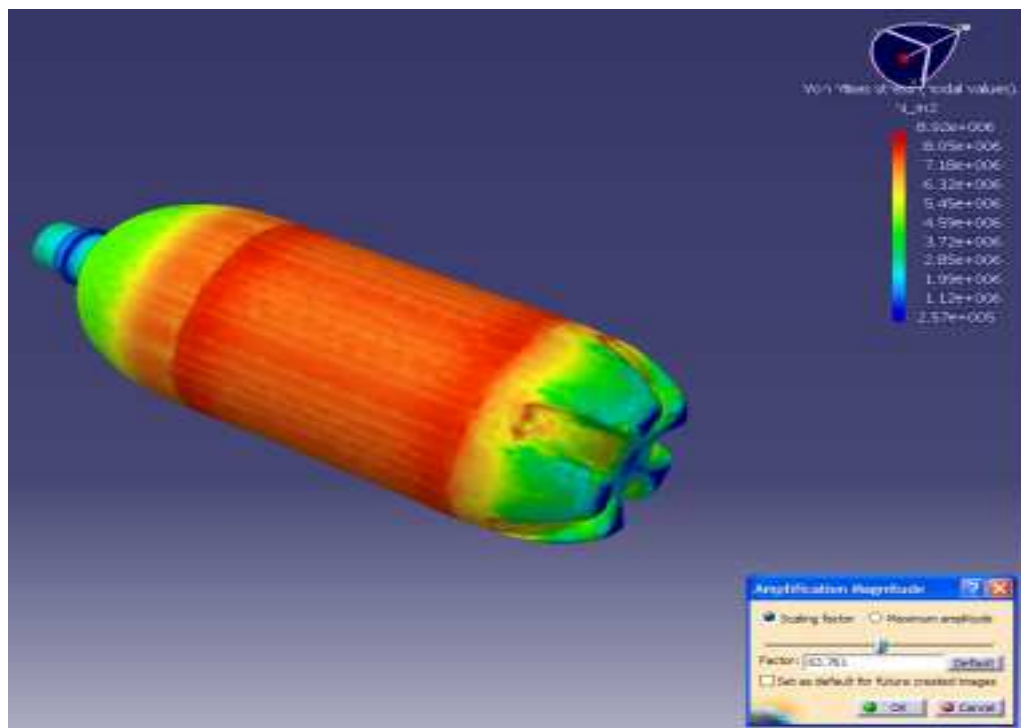
Fig.3-16. The von Mises stress on amplification magnitude of 63.7
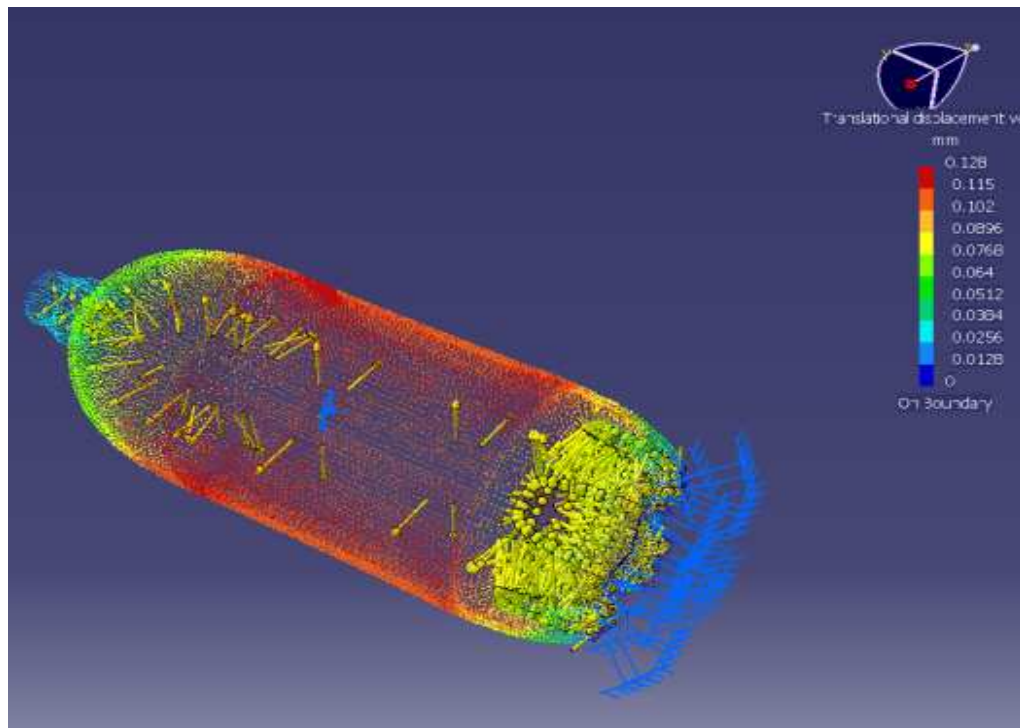
Fig.3-17. Translational displacement vectors as a result of the pressure inside the bottle

3.5 RESULTS AND DISCUSSION

To establish the optimum base parameters the data obtained from the stress analysis in CATIA were input to the ECHIP-7 design of experiments and optimization software program, and optimization was achieved based on statistical analysis of the simulated stress results via ECHIP. Following can be said about the simulated stress in the bottle.

- The stresses are most intense in the middle sidewall section of the bottle. But, whilst the stresses on the base of the bottle are low, those on the edges between the base and sidewall are found to be rather high. That is to say, the high stresses are recorded on the sidewall at which the bottle is the most sound and the low stresses are on the base section where the bottle is the weakest.

- The maximum stress values were taken into consideration in the optimization process. Increases in the maximum stress values are almost the same for the pressure of both 0.4 MPa and 0.6 MPa. At some combinations of petaloid base parameters resulted in the material yielding in the base by becoming convex. To ensure for the bottle to be self-standing, some constraints were applied for the clearance settings for the optimisation process in ECHIP-7.

- Small foot length and small clearance are required for a sound base design to achieve low simulated stress values. Valley width does not seem to have considerable effect on the stress. Nevertheless, wall thickness also needs to be minimised to reduce material cost.

Clearance: 1mm
Max Stress: 8.64 MPa
(a)

Clearance: 6 mm
Max Stress: 10.1 MPa
(b)

Clearance: 12 mm
Max Stress: 11.7 MPa
(c)
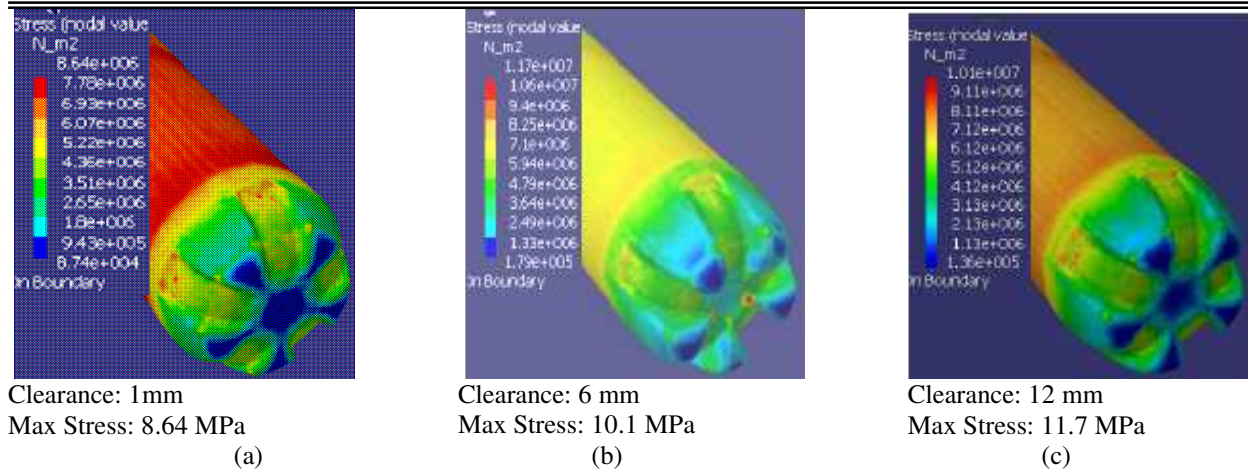
Fig.3-18. The highest von Mises stress as a function of clearance

Valley width: 4.85mm
Max Stress: 10.6 MPa
(a)

Valley width: 16.17mm
Max Stress: 9.86 MPa
(b)

Valley width: 27.49mm
Max Stress: 10.2 MPa
(c)
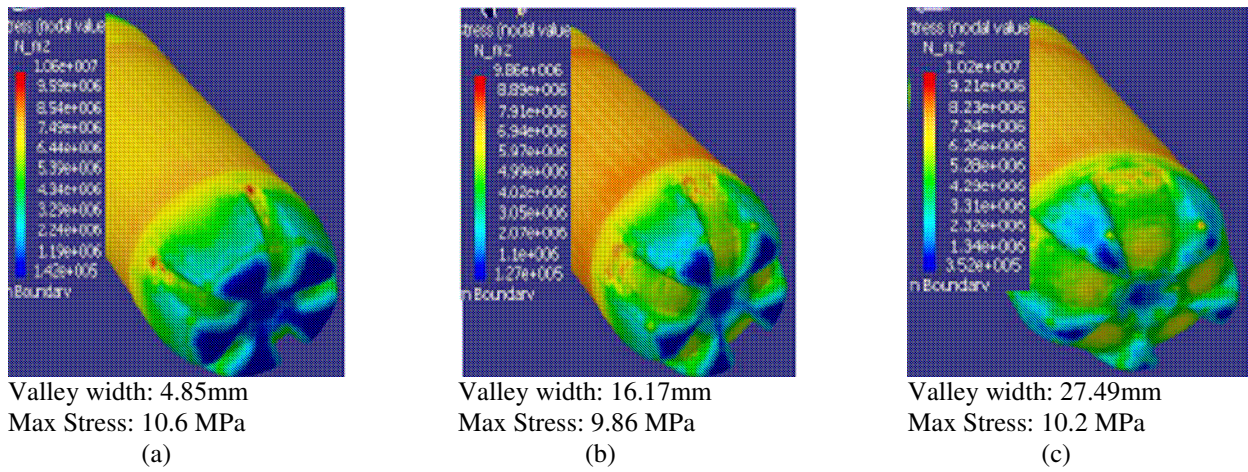
Fig.3-19. The highest von Mises stress as a function of valley width

Foot Length: 16 mm
Max Stress: 10.3 MPa
(a)

Foot Length: 28 mm
Max Stress: 8.9 MPa
(b)

Foot Length: 41 mm
Max Stress: 10.3 MPa
(c)
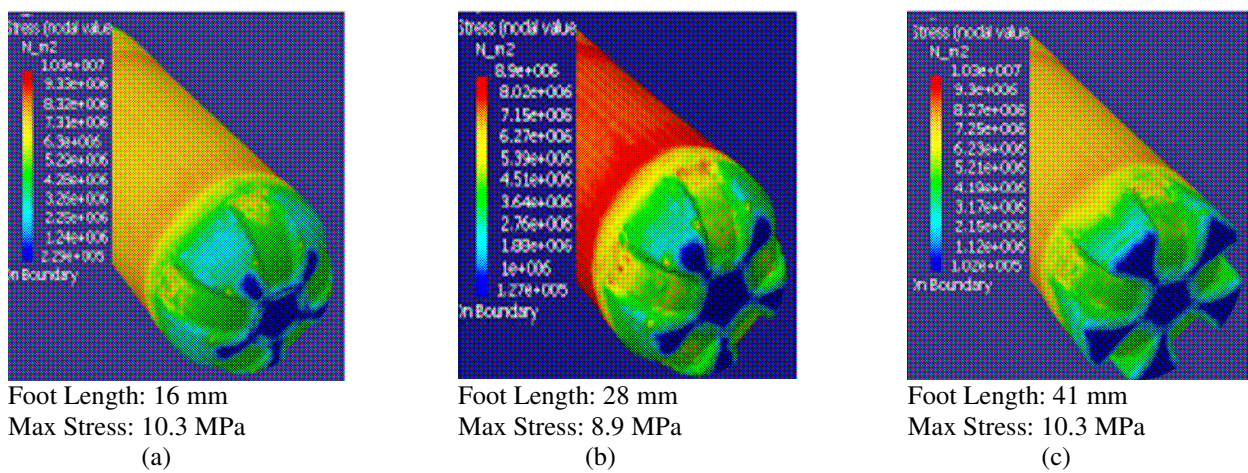
Fig.3-20.The highest von Mises stress as a function of foot length

Fig. 3-18, 3-19, and 3-20 respectively, show the effects of clearance, valley width, and foot length dimension on the max von Mises stress in the bottle base. It is clear that valley width has no significant influence. Fig. 3-21 shows the effects of wall thickness on these stress relationships. Increased wall thickness results in lower maximum stress values for all optimization parameters. On the other hand, the maximum stress values comperatively decreased along with the increasing wall thickness and the average maximum stress values for the 1 mm and 2 mm are around 2.00 x 10^7 N/m^2 and 1.00 x 10^7 N/m^2 respectively. Ideally, wall thickness should be optimised as a function of stress, production cost, burst strength and other physical properties such as gas permeation.
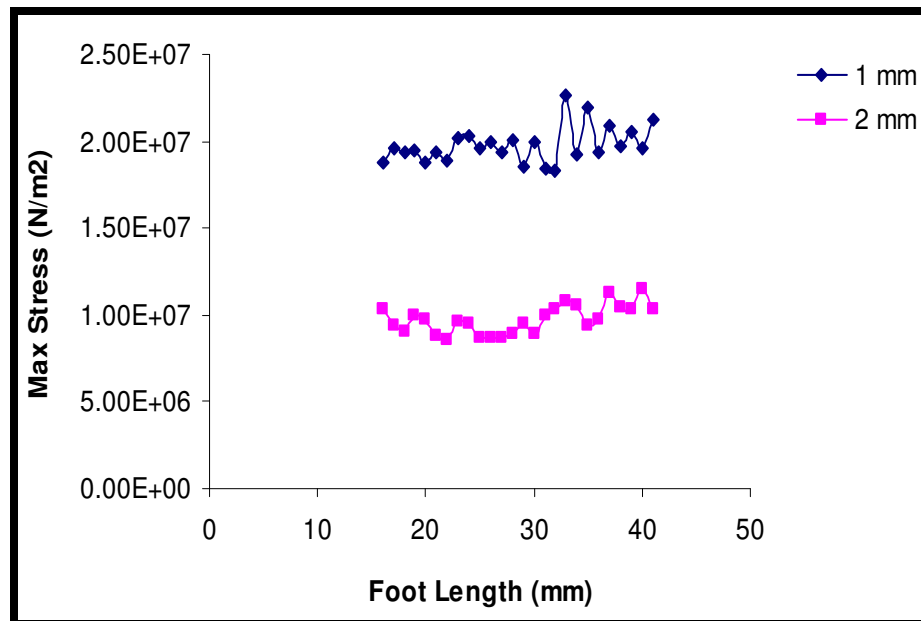
(a)
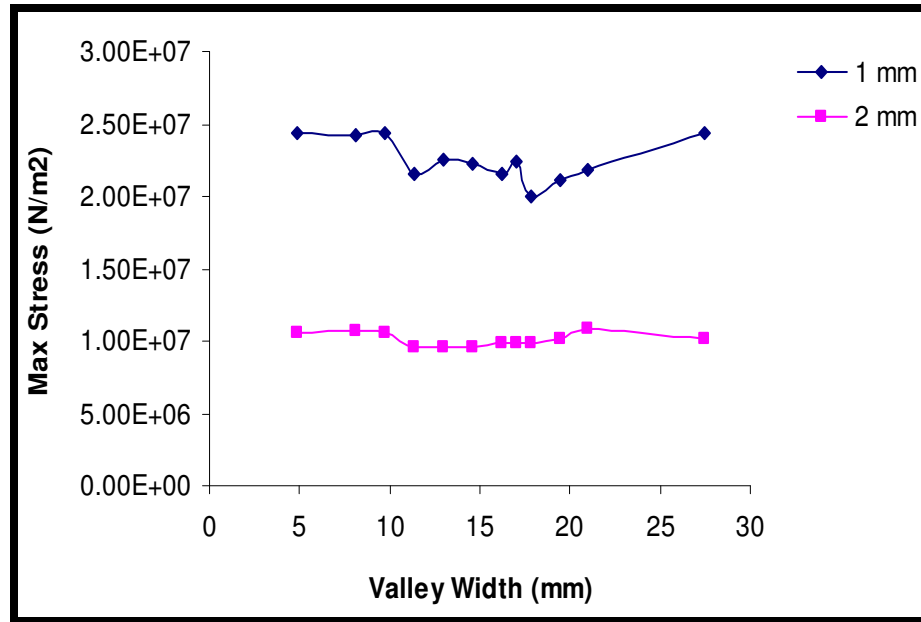
(b)
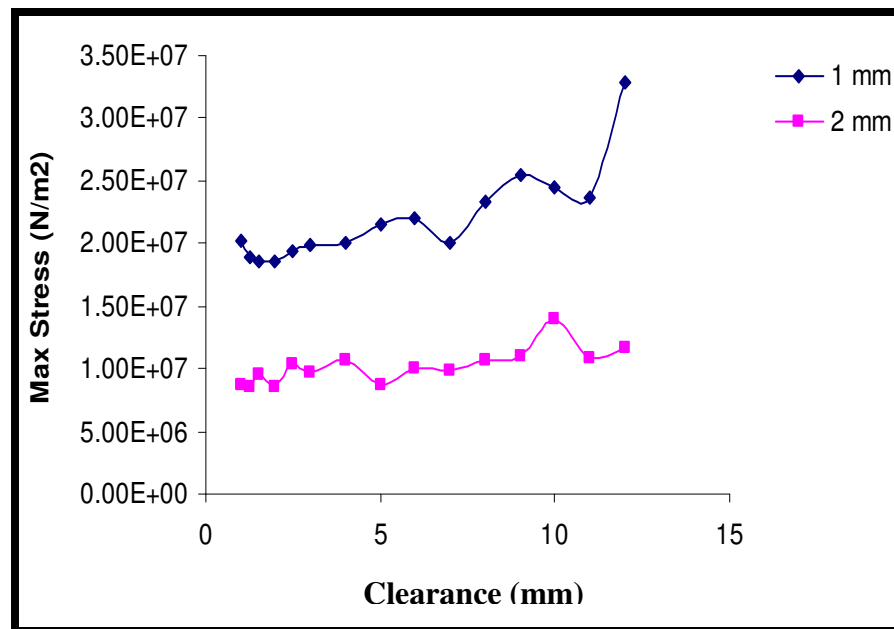
(c)

Fig.3-21. Max stress at two different wall thicknesses

for the bottle base parameters (a) foot length (b) valley width (c) clearance

3.6 OPTIMIZATION OF BASE GEOMETRY

In this study, the bottom of the PET bottle of 1500 ml. is optimized against environmental stress cracking. As in the previous study conducted by Lyu and Pae [2003], three parameters of the bottle base are regarded as to having the most influence on stress crack resistance: foot length, valley width, and clearance (fig. 3-22).
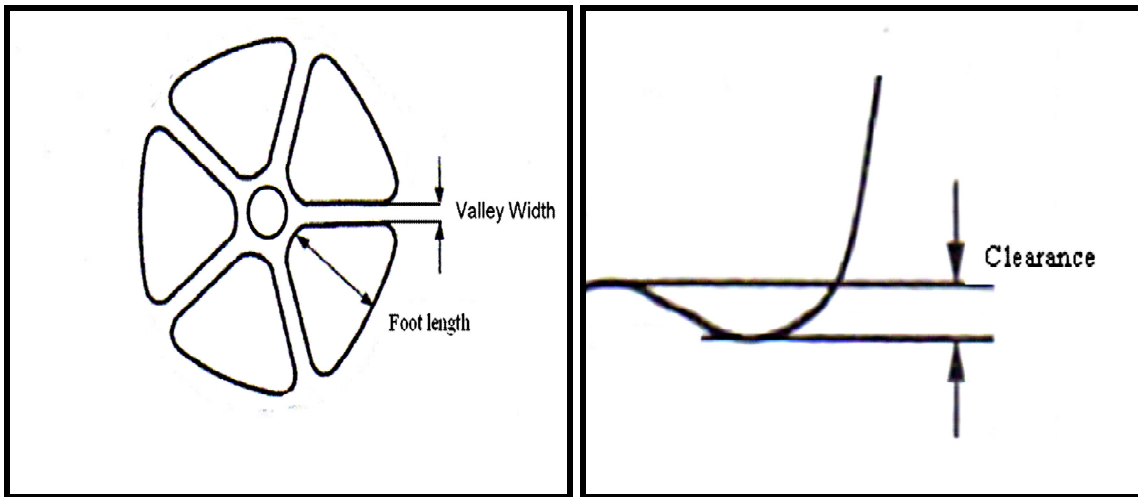
Fig.3-22. Design parameters of the petaloid base

In the standard PET bottle, foot length, valley width, and clearance dimensions are 36.0, 7.0 mm and 6.1 mm respectively. The minimum and maximum values identify the optimization range for each parameter.

3.6.1 Experimental design with ECHIP-7

The optimisation process was carried out by ECHIP-7 experimental design and optimization program. Hereby, both the time required for calculation and the numbers of stress analysis step were significantly reduced; and the optimisation process was based on a scientific approach.

The maximum and minimum values of the design parameters (table 3-3) are chosen so as the petaloid base was not deformed and stayed upright position.

Table 3-3. Design parameters

Design Parameters	Minimum	Maximum
Foot length (mm)	16	41
Clearance (mm)	1	12
Valley Width (degree)	3	17

Echip-7, a design of experiment and optimization program provides the user with the 'standard' and 'algorithmic' design options; model specifications such as quadratic, interaction, central composite in cube, partial cubic, central composite in sphere and Box-Behnken. The algorithmic design in partial cubic was regarded as a suitable model for this study, because there is one block variable for clearance parameter and three input variables; on the other hand algorithmic design is not linear but flexible in terms of using the results obtained from the stress tests; and the experimental region on the stress analysis has also a few constraints.

After three design variables mentioned above are entered, the type of design was defined (fig. 3-23); and the number of trials is calculated through the 'make design' command (fig. 3-24). A maximum of 21 total trials are carried out according to the experimental design generated by ECHIP-7 and von Mises stress values obtained from CATIA V5-R14 are input as the response variable as shown in fig. 3-25. If the 21 trials are equal to or less than the number calculated through the 'How many trials?' command, the model generated by the program is then feasible for the stress analysis test in CATIA V5-R14, otherwise, the model can not be applied.
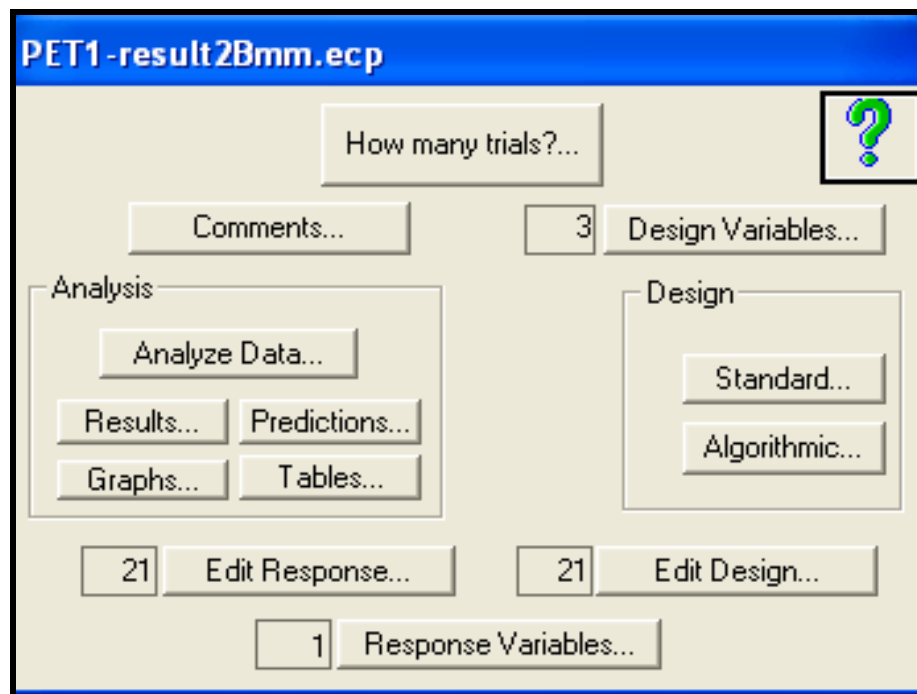
Fig.3-23. Experimental design via ECHIP; design and response variables, design type
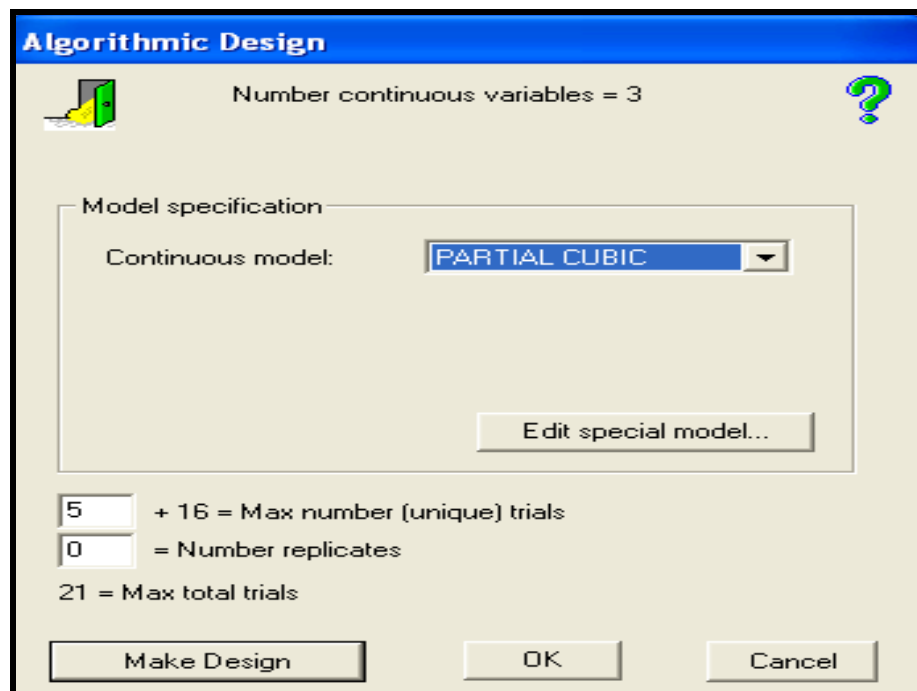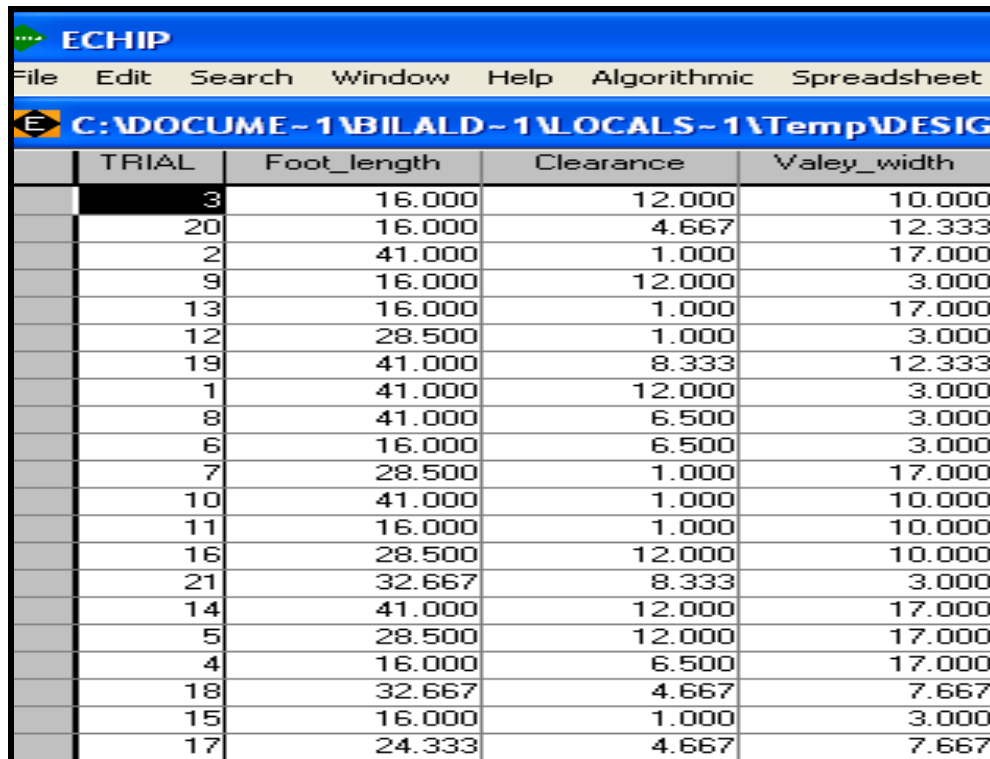
Fig.3-24. Making a design via ECHIP; model specification, max of trials

In order to verify the suitability of the model generated by the ECHIP-7 program to this study, for stress analysis tests, standard deviation of the stress analysis tests should be estimated properly. That is why, some stress analysis were made for some selected combinations of the design parameters of the petaloid shaped base and the standard deviation is then found to be 0.5×10^6 N/m^2 as calculated by the Windows EXCEL program (Table 3-4). This value refers to the standard deviation resulting from the stress analysis calculated through the CATIA software. As to the least important difference which is the smallest change in the response that one desires to detect, is accepted to be 1.5×10^6 N/m^2.

TRIAL	Foot_length	Clearance	Valey_width
3	16.000	12.000	10.000
20	16.000	4.667	12.333
2	41.000	1.000	17.000
9	16.000	12.000	3.000
13	16.000	1.000	17.000
12	28.500	1.000	3.000
19	41.000	8.333	12.333
1	41.000	12.000	3.000
8	41.000	6.500	3.000
6	16.000	6.500	3.000
7	28.500	1.000	17.000
10	41.000	1.000	10.000
11	16.000	1.000	10.000
16	28.500	12.000	10.000
21	32.667	8.333	3.000
14	41.000	12.000	17.000
5	28.500	12.000	17.000
4	16.000	6.500	17.000
18	32.667	4.667	7.667
15	16.000	1.000	3.000
17	24.333	4.667	7.667

Fig.3-25. The combinations of trials generated for stress analysis

Table 3-4. Von Mises stress values for standard deviation of the study

Von Mises Stress Values of the 1500 lt. Bottles			Applied Pressure		0.6 MPa		
			Bottle wall Thickness		1 mm		
			Von Mises Stress Values (N/m^2)				
X (mm)	Y (mm)	Z (mm)	Test1	Test2	Test3	Test4	Test5
22	17.79	1.5	2.82×10^7	2.79×10^7	2.89×10^7	2.87×10^7	2.77×10^7
					Average Standard Deviation: 0.5×10^6		

X: Foot length   Y: Clearance Z: Valley width

As can be seen from table 3-4, at these conditions the standard deviation for this experimental study is 0.5 E+6, the least important difference is 1.5 E+6; and the continuous model is partial cubic, the number of trials was calculated by the ECHIP-7 program as 18 (fig. 3-26). Since the trial numbers defined in the algorithmic design function and 'How many trials?' menu are very close to each other, the proposed design model shown in fig. 3-25 is feasible for the stress analysis test on CATIA. This is why, after obtaining the test results from CATIA, the results were imported back into the ECHIP-7 under 'response variables'. Then, the results were analyzed by ECHIP-7.
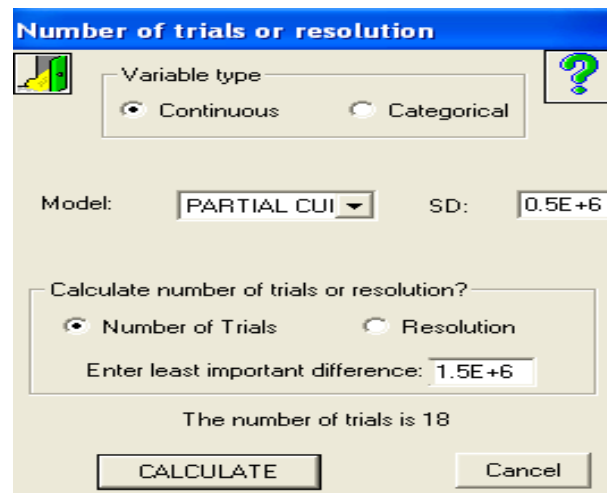
Fig.3-26. The number of trials or resolution for the experimental test on CATIA

3.6.2 Assessment of the response variables with ECHIP-7

The results obtained from the analysis made in CATIA, according to the experimental design generated in the ECHIP-7 are entered to the software program as response variables for the assessment. But, reforming the base geometry by abiding to the generated bottle base parameter combinations at times has been difficult. Some minor adjustments in bottle base parameters other than the foot length, valley width, and clearance have been necessary in order for the base geometry not to be deformed. That is why, there have been slight deviations of the combinations generated by ECHIP-7 and of the corresponding stress values, but these were taken into consideration during the calculation of standard deviation used with the ECHIP-7 software.

The ECHIP-7 program automatically analyzes the variables loaded into the program and the results are given on graphs and tables. Furthermore, the effects of input variables on the output variables can be investigated through the 'Analyze Data' menu. The simulated stress results are obtained by CATIA according to the combinations shown in fig. 3-25 and they are given in table 3-5 and table 3-6 for the pressures values of 0.40 MPa and 0.60 MPa respectively.

Table 3-5. 1500 ml. PET bottle von-Mises stress values for the pressure of 0.40 MPa

				0.5 mm		1 mm		2 mm	
No	X (mm)	Y (mm)	Z (deg)	Max (10^7)	Min (10^5)	Max (10^7)	Min (10^5)	Max (10^7)	Min (10^5)
15	16	1	3	6.04	1.73	2.73	1.96	1.29	2.39
11	16	1	10	5.86	1.50	3.00	2.24	1.30	3.76
13	16	1	17	5.97	2.59	3.32	4.99	1.52	4.14
20	16	4.67	12.33	7.37	2.16	3.50	3.07	1.40	3.09
6	16	6.5	3	7.22	0.79	3.39	2.08	1.44	0.71
4	16	6.5	17	6.96	9.14	3.42	17.5	1.63	10.4
9	16	12	3	8.28	1.43	4.15	2.35	1.73	1.31
3	16	12	10	8.22	2.71	3.58	4.01	1.59	2.45
17	24.33	4.67	7.67	6.65	1.08	3.41	1.84	1.34	1.86
12	28.5	1	3	5.97	1.55	3.29	2.01	1.35	1.92
7	28.5	1	17	6.04	4.87	2.92	9.80	1.46	5.95
16	28.5	12	10	7.45	1.44	3.35	3.82	1.66	4.72
5	28.5	12	17	6.90	17.2	3.87	7.47	1.62	9.31
18	32.67	4.67	7.67	7.42	1.77	3.47	1.98	1.46	2.10
21	32.67	8.33	3	7.80	1.69	4.06	2.07	1.70	1.86
10	41	1	10	7.37	1.42	3.16	1.97	1.49	2.17
2	41	1	17	7.27	2.99	3.63	2.46	1.73	5.22
8	41	6.5	3	8.59	1.11	4.30	1.91	1.76	2.08
19	41	8.333	12.333	8.18	1.86	4.03	2.05	1.59	1.99
1	41	12	3	9.04	1.40	4.82	1.97	2.04	2.30
14	41	12	17	7.71	3.85	3.83	2.88	1.70	2.29

X: Foot length   Y: Clearance Z: Valley width

Table 3-6. 1500 ml. PET bottle von-Mises stress values for the pressure of 0.60 MPa

No	X (mm)	Y (mm)	Z (deg)	0.5 mm		1 mm		2 mm	
				Max (10^7)	Min (10^5)	Max (10^7)	Min (10^5)	Max (10^7)	Min (10^5)
15	16	1	3	6.04	1.73	2.73	1.96	1.29	2.39
11	16	1	10	5.86	1.50	3.00	2.24	1.30	3.76
13	16	1	17	5.97	2.59	3.32	4.99	1.52	4.14
20	16	4.67	12.33	7.37	2.16	3.50	3.07	1.40	3.09
6	16	6.5	3	7.22	0.79	3.39	2.08	1.44	0.71
4	16	6.5	17	6.96	9.14	3.42	17.5	1.63	10.4
9	16	12	3	8.28	1.43	4.15	2.35	1.73	1.31
3	16	12	10	8.22	2.71	3.58	4.01	1.59	2.45
17	24.33	4.67	7.67	6.65	1.08	3.41	1.84	1.34	1.86
12	28.5	1	3	5.97	1.55	3.29	2.01	1.35	1.92
7	28.5	1	17	6.04	4.87	2.92	9.80	1.46	5.95
16	28.5	12	10	7.45	1.44	3.35	3.82	1.66	4.72
5	28.5	12	17	6.90	17.2	3.87	7.47	1.62	9.31
18	32.67	4.67	7.67	7.42	1.77	3.47	1.98	1.46	2.10
21	32.67	8.333	3	7.80	1.69	4.06	2.07	1.70	1.86
10	41	1	10	7.37	1.42	3.16	1.97	1.49	2.17
2	41	1	17	7.27	2.99	3.63	2.46	1.73	5.22
8	41	6.5	3	8.59	1.11	4.30	1.91	1.76	2.08
19	41	8.33	12.33	8.18	1.86	4.03	2.05	1.59	1.99
1	41	12	3	9.04	1.40	4.82	1.97	2.04	2.30
14	41	12	17	7.71	3.85	3.83	2.88	1.70	2.29

Table header: **1500 ML BOTTLE von MISES STRESS VALUES (N/m²)** **Pressure: 0.6 MPa**

X: Foot length   Y: Clearance Z: Valley width

The response surfaces in 2-D and then 3-D are shown in fig. 3-27, and 3-28 respectively. The optimum dimensions of the foot length, valley width, and clearance which minimize the stresses on the bottle surface are found to be 29.00 mm, 8.40 mm, and 5.80 mm. Stress values are plotted as a function of foot length versus valley width at a clearance dimension of 5.8 mm. In this optimization process, the clearance dimension is constrained in order to prevent the bottle base deforming/yielding to a convex shape. This is why the minimum clearance was set to 5.8 mm. The optimized bottle base shape to be used in the further study is shown in fig. 3-29.
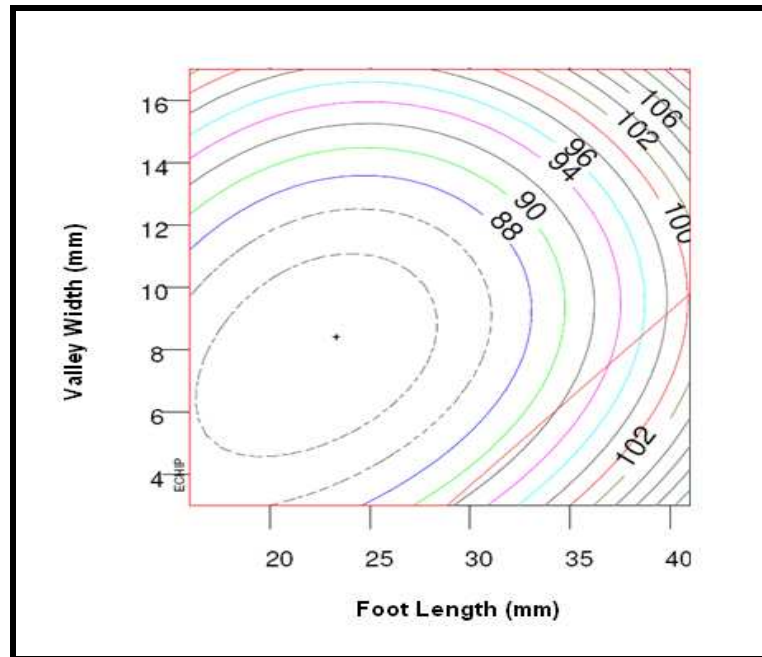
Fig.3-27. Optimization 'response surface' in 2-D without constraint
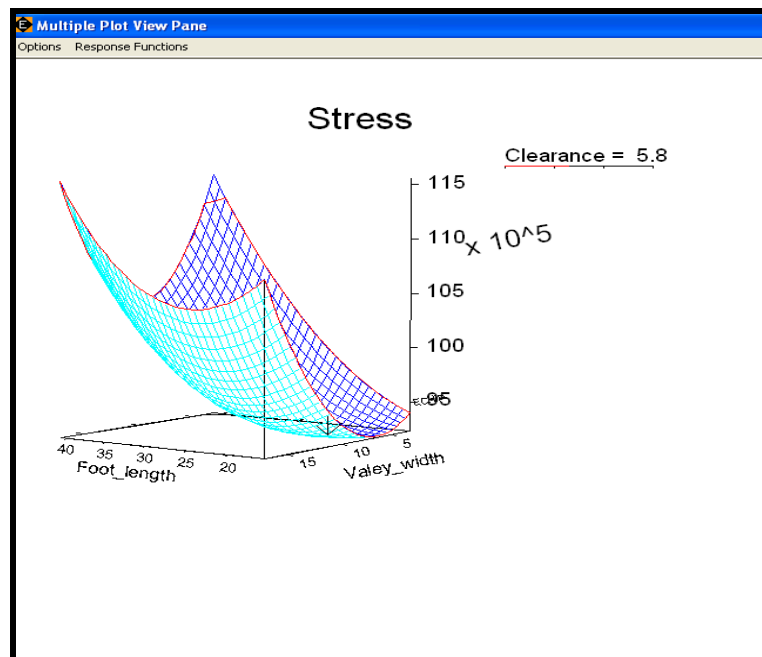
Fig.3-28. Optimization 'response surface' in 3-D with constraint
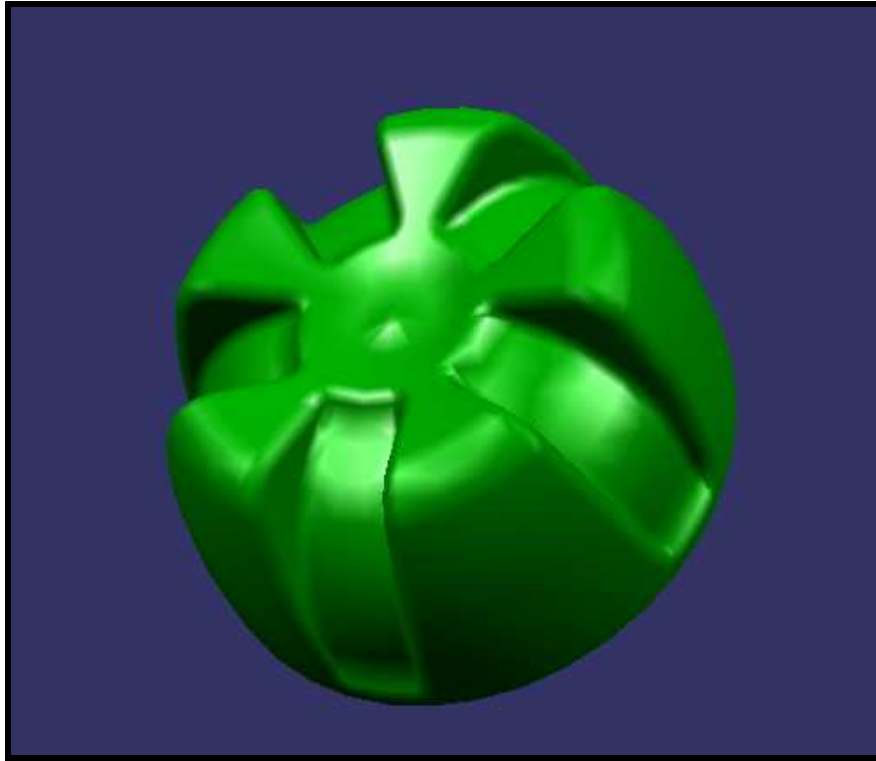
Fig.3-29. CAD drawing of the optimum bottle base

3.7 CONCLUSION

In this chapter, in order to minimize the cracking occurred on the base of the PET bottle of 1500 ml, the optimization process of the petaloid base geometry was carried out by using CATIA and ECHIP-7 software programs. As a result, the existing petaloid base of the standard bottle was reformed and the parameters of the bottle base currently being used, such as the valley width, foot length, and clearance, the numerical values of which are 4.25 mm, 20 mm, and 5 mm respectively, are optimized with the new values of 8.40 mm, 29 mm, and 5.80 mm, respectively. In this case, the maximum stress value of 1×10^7 N/m^2 of the standard (current) bottle has been optimized to 8.92×10^6 N/m^2 in new (optimised) bottle.

Table 3-7. The base dimensions of the current and proposed bottles

	Standard (Current) Design	Optimised (New) Design
Foot Length (mm)	20	29
Valley Width (mm)	4.25	8.40
Clearance (mm)	5	5.80
Resultant Stresses for an internal pressure of 0.4 MPa.	10 MPa	8.9 MPa

Chapter 4

ISBM PROCESS DESIGN WITH

BLOW VIEW 8.2

4.1 INTRODUCTION

This chapter describes a simulation study of the injection stretch blow moulding of the PET bottle using the Blow View 8.2 simulation program. The study investigated the effects of selected process parameters on, wall thickness, stress, crystallization, molecular orientation, and biaxial ratio.

Three process parameters were investigated:

1. Preform weight; 34 g and 40 g

2. Preform temperature; 93-110 ^{o}C and 98-115 ^{o}C

3. Degree of stretching applied by the stretch rod and the accompanying 'free-blow' pressure profile as a function of time

Three degrees of stretching were simulated:

• Zero stretching. The stretch rod was not applied; i.e. the bottle was free-blown.

• 50% stretch. The stretch rod was applied to stretch the bottle to half its final length; thereafter, the bottle was formed only by blow pressure.

• Full stretch. The stretch rod was applied for the whole of the moulding period followed by blowing.

Degree of stretching applied by the stretch rod and the accompanying 'free-blow' pressure profile as a function of time define three different processing conditions, namely model-1, model-2 and model-3.

The CATIA file of the bottle is first converted to the IGES format and then transferred to the Blow View 8.2 program as a patran file for use as the ISBM mold, along with a patran file of the

stretch rod. The preform design was generated through Blow View's 'Preform Design Menu'.

The preform weight was 40 g, as required for a 1.5lt bottle. Throughout the study the preform is

blown into the mold gradually so as to represent the 'free-blowing' conditions. That is why, the

magnitude of pressure required to blow the preform, has been adjusted accordingly.

4.2 SIMULATION SETTING FOR THE PROCESS OPTIMIZATION

4.2.1 Process and material model

This study is based on two-stage blow molding processes; the preform is produced separately, and then blown after re-heating to the blow temperature. Accordingly, the injection stage, which produces the preform, is not considered in this study.

For the material model, the visco-hyperelastic model was chosen due to its demonstrated credibility in ISBM simulation studies. The material selected was PET Eastapak 9921 (Eastman Company), which is available in the Blow View database. The material's rheological properties and relevant model coefficients are given in fig. 4-1.

Fig.4-1. PET Eastapak 9921 rheological properties and relevant model coefficients

4.2.2 Alignment of the bottle mould and stretch rod

This process is rather important because an error in this alignment can cause wrong deformation motion in the stretching and blowing stage. Stretch rod and mold alignment in Blow View 8.2 is shown in fig. 4-2.
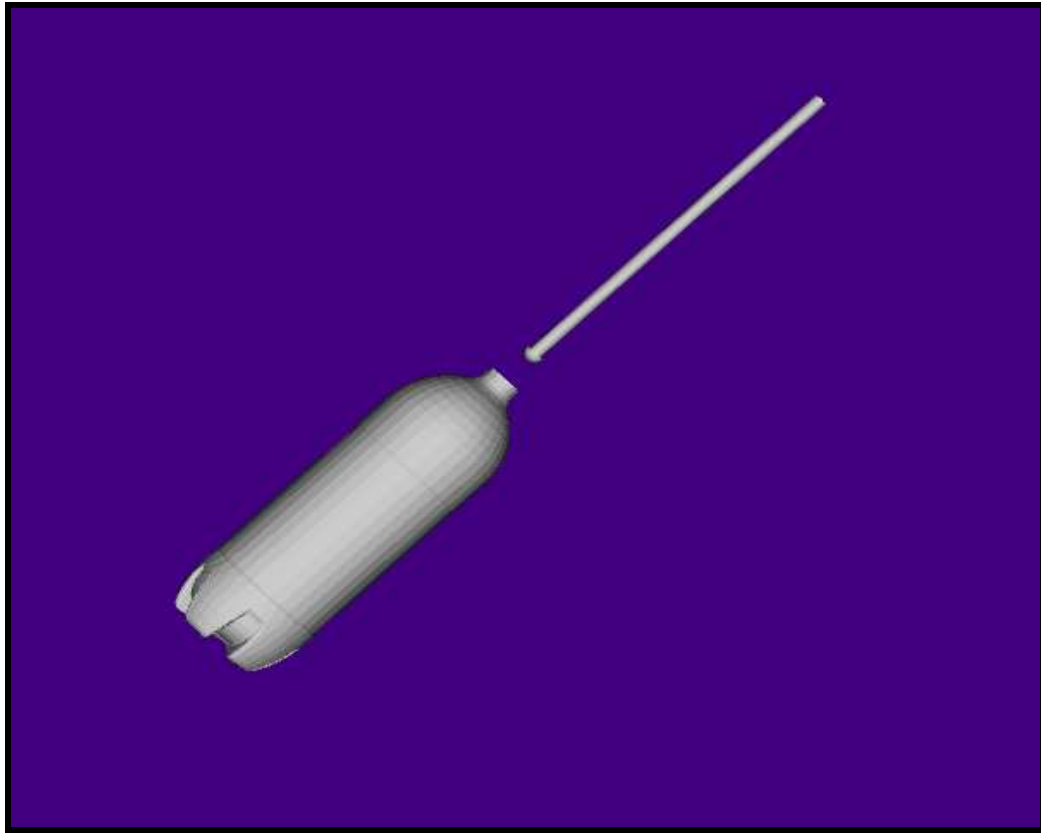
Fig.4-2. Stretch Rod and Bottle alignment in Blow View

4.2.3 Preform thickness profile

The thickness profile of the preform is one of the most important parameters that affect the thickness of the final bottle. Hereby, the desired thickness in the bottle is ensured by the preform design. While the uniformity of the bottle base thickness could be targeted, because the abrupt thickness changes in the base is claimed to be the source of the crack development at the bottom of the bottle [Lyu and Pae, 2003] more importantly, thickness profile which will minimize the stress and also reduce the variations in stress along the bottle base is targeted. Therefore, thickness profile which minimizes the stress with minimum variation produces the optimum processing conditions.

The preform design can be imported to the simulation program, however, in this study the preform design was generated by the simulation program's own design menu (fig. 4-3). The study is conducted based on the preform design currently used in the industry which weighs 40 g. as shown in fig. 4-4. Process optimisation is also considered for preform design where the preform weight is reduced to 34 g. by changing preform wall thickness (fig. 4-5 and fig. 4-6).
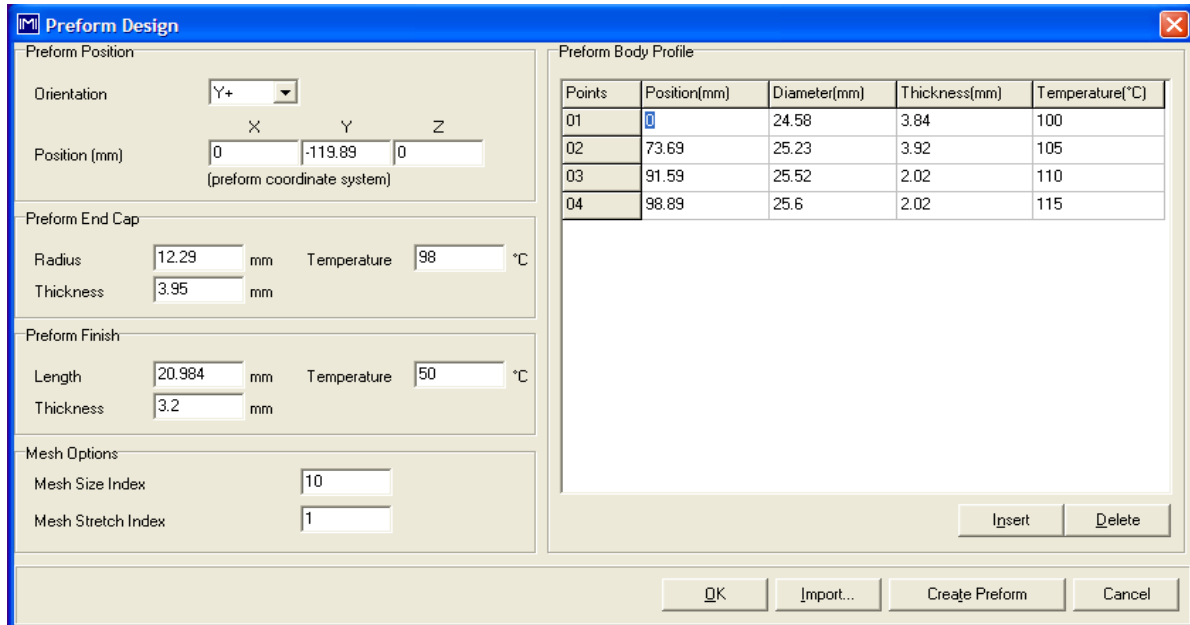
Fig.4-3. Preform design menu in Blow View 8.2 for the 40 g. preform
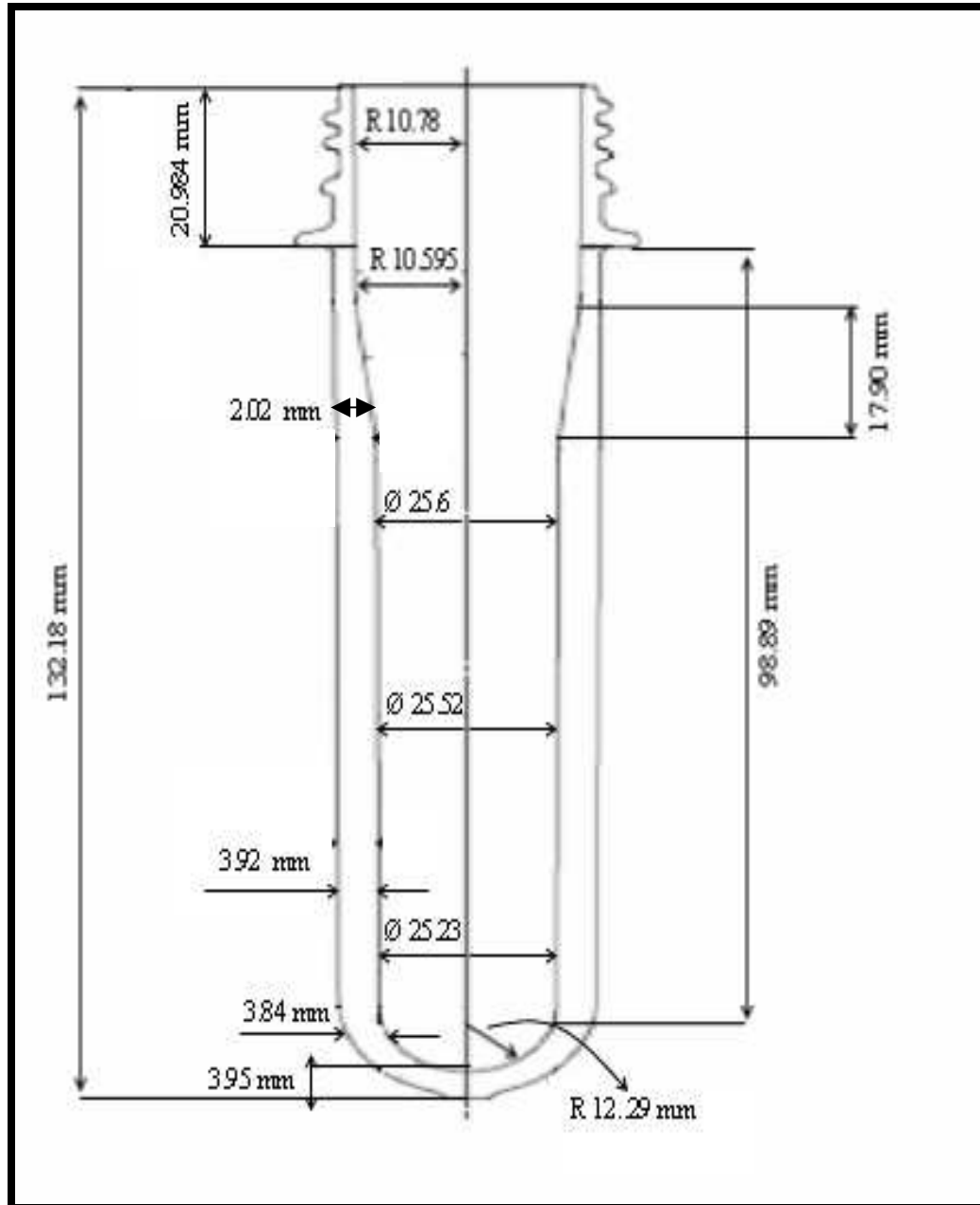
Fig.4-4. Design currently used in industry for the 40 g preform
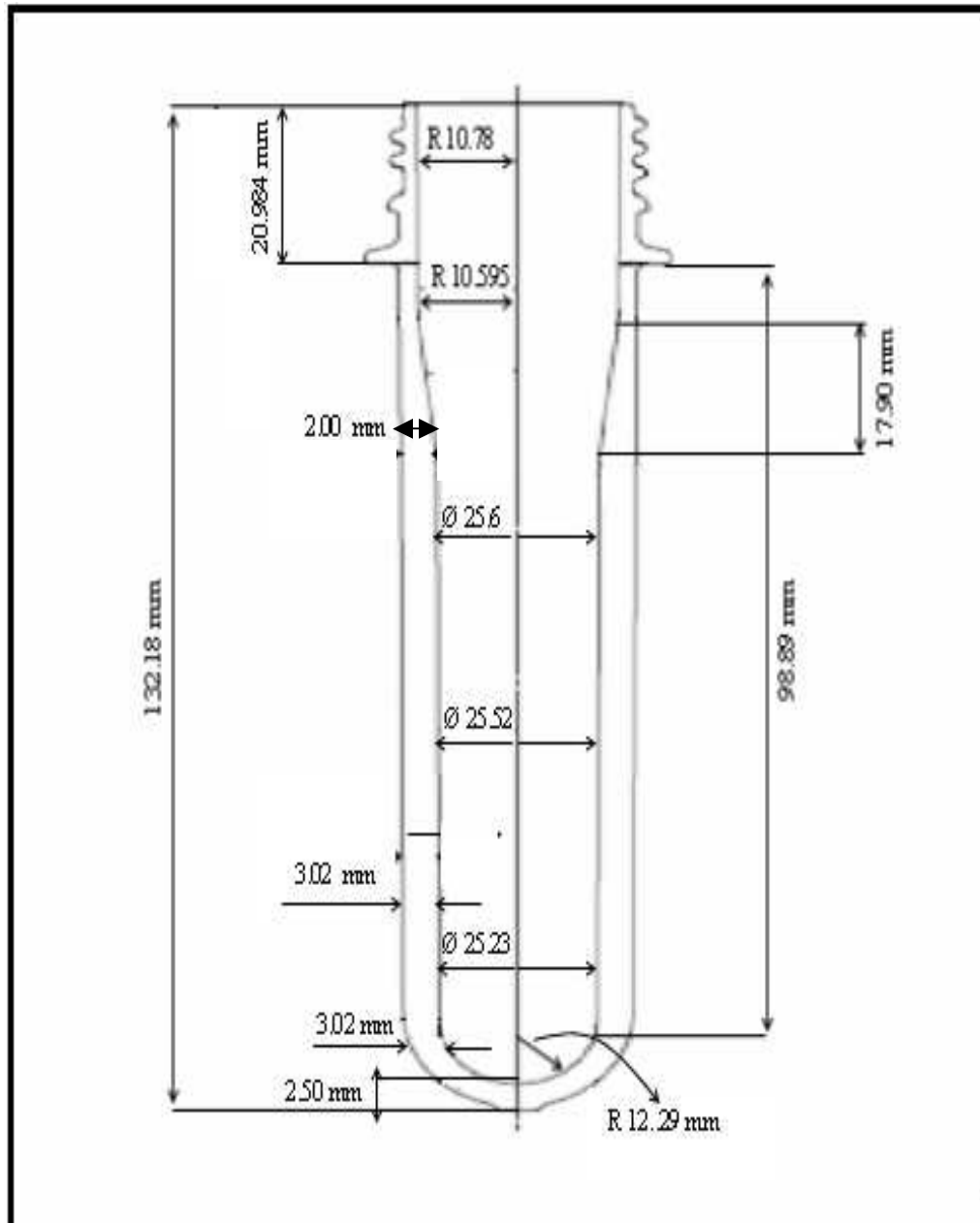
Fig.4-5. Alternative design for the 34 g. preform
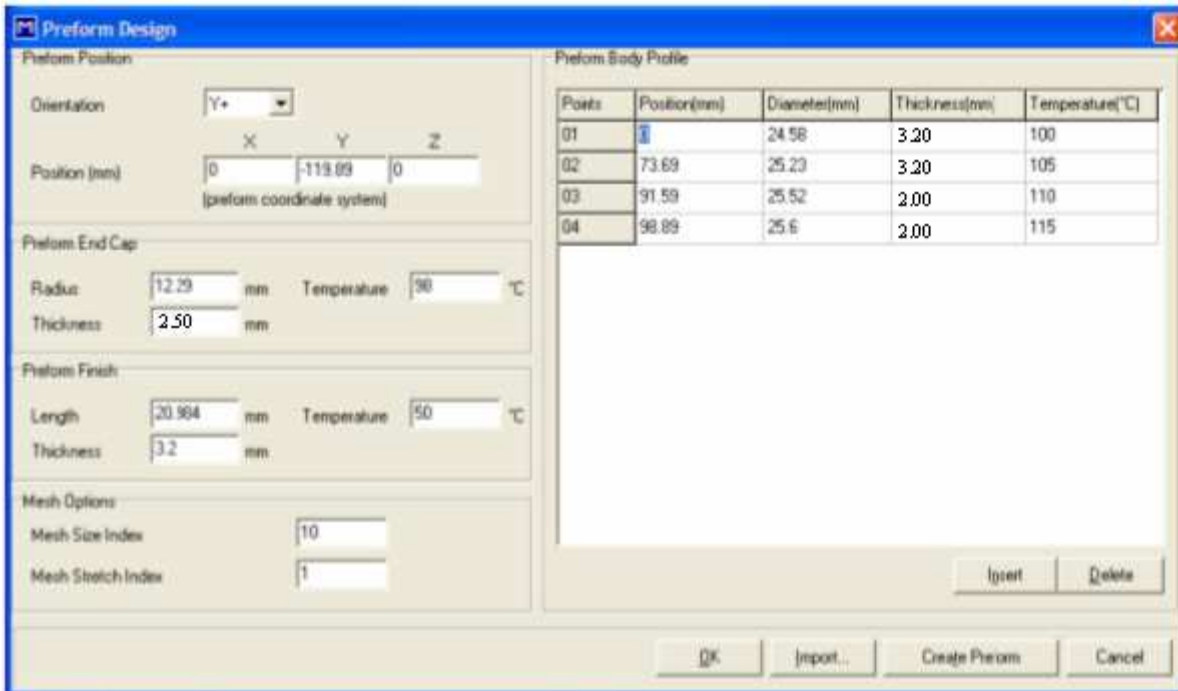
Fig.4-6. Preform design menu in Blow View 8.2 for the 34 g. preform

4.2.4 Temperature profile of the preform

In effect, thickness and temperature profile of the preform are interrelated and they affect

the thickness of the final bottle, especially in the bottom of the bottle [Wang et al., 1998]. The

amount of the PET material being piled at the bottom of the bottle increases linearly with the

decreasing temperature. In this study, two preform temperature profiles were considered; a low

temperature range of 93-110 ^{o}C and a high temperature range of 98-115 ^{o}C. A particular

temperature profile of the preform (fig. 4-7) can be input through Blow View's preform design

menu.

4.2.5 Stretch rod movement

If the stretch rod displacement is not in harmony with other process parameters either the blown

preform ruptures or strain-hardening can not be achieved due to insufficient stretching [McEvoy

et al., 1998]. In this study, the stretch rod movement is adjusted so that the preform stretched

according to that of 'free-blowing' conditions. In order to investigate the effect of the stretch rod motion on the performance of the bottle, the preform was stretched and blown under three different regimes (models).
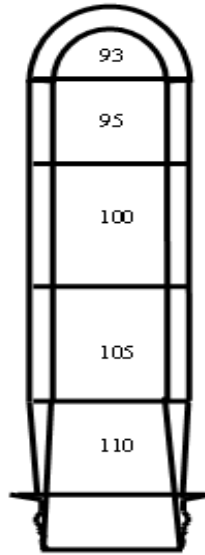
Fig.4-7. Temperature profile of the preform
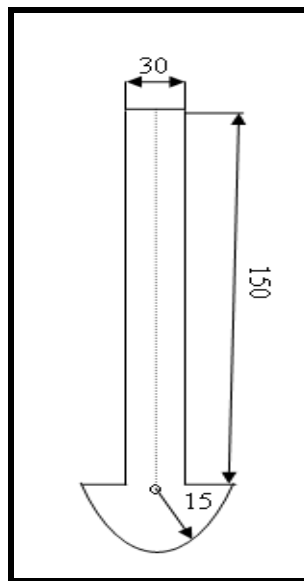
Fig.4-8. Stretch rod dimensions used in this study

The stretch rod design used in this study is given in fig. 4-8. In the simulation, it is assumed friction between the preform and the stretch rod is too small to be considered.

For the first regime described as 'zero stretching' or 'free-blowing' (model-1), the stretch rod was not used in the process and the preform was blown only through the pre-blow pressure.

For the second regime described as '50% stretch' (model-2), the rod stretched the preform just half way down the mold. After that point, the preform was blown by the pre-blow pressure applied inside the preform (fig. 4-9. (a)).

For the third regime described as 'full stretch' (model-3), the preform was stretched by the stretch rod up to the bottom of the bottle mold and the final blow pressure was then applied to complete all bottle corners (fig. 4-9. (b)).
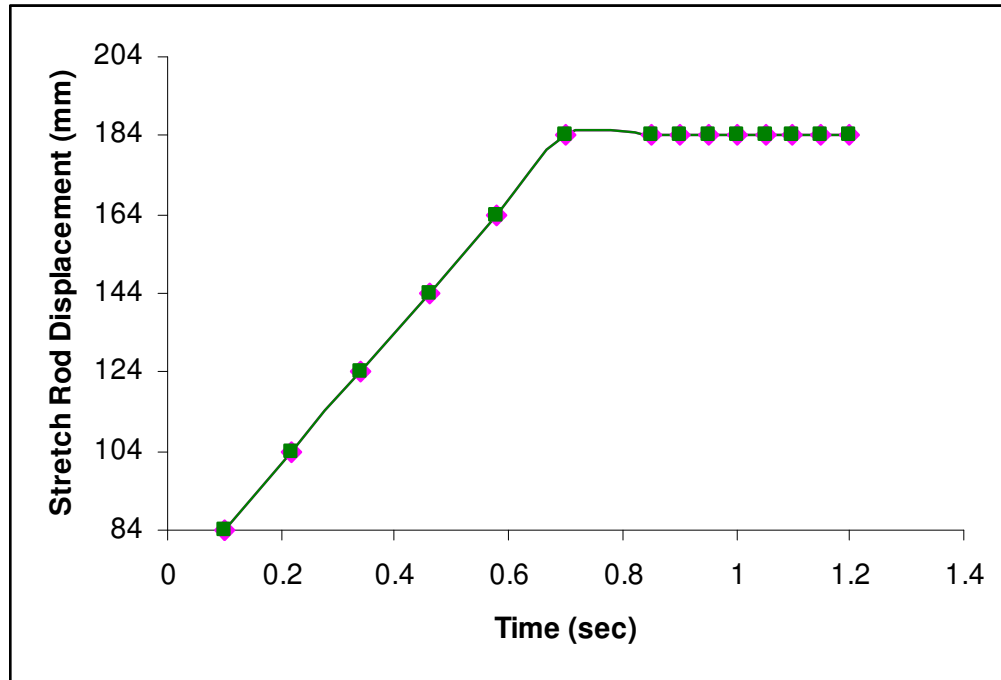
(a)
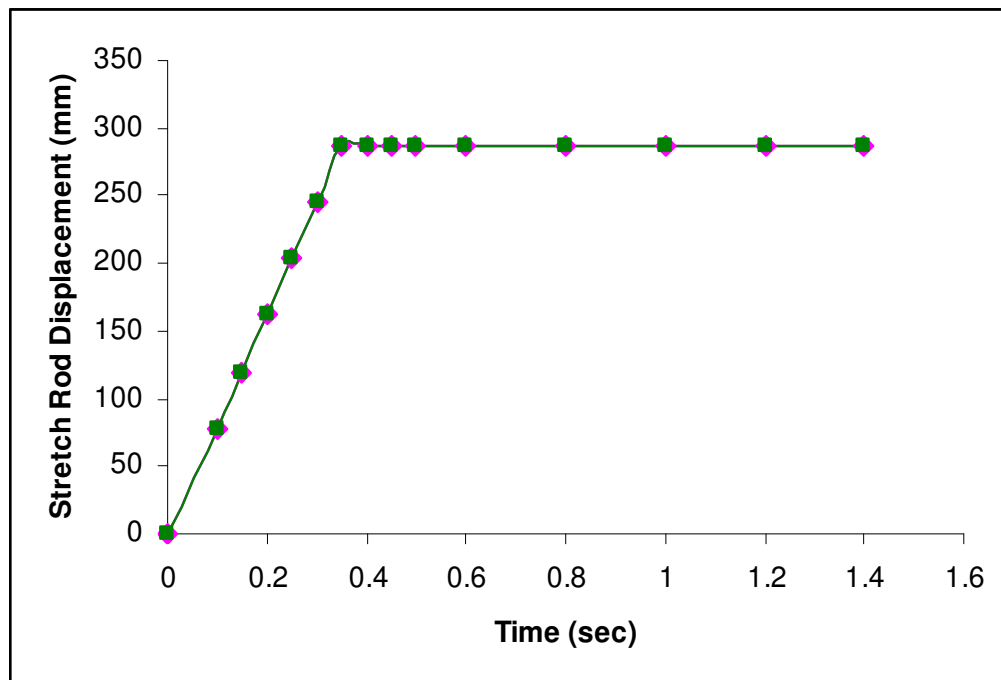
(b)

Fig.4-9. Stretch rod displacement vs. time (a) model-2 (b) model-3

4.2.6 The pressure profile as a function of time

As the preform is stretched by the stretch rod a small amount of 'pre-blow' pressure is applied. A higher pressure which plays a major role in forming the rest of the bottle is applied. The 'pre blow' pressure which is applied only during the time the stretch rod gets up to the base of the bottle is 0.1 to 0.2 MPa, whereas the final pressure can reach up to 4 MPa. The combined duration of these 'blow pressures' define the total processing time [Wang et al., 1998]. The 'pre-blow' and 'final-blow' pressure values were defined so as to comply with the 'free-blowing' just as in the stretch rod movement setting [McEvoy et al., 1998]. Magnitude and timing of the 'pre-blow' and 'final blow' will vary under each 'stretching regime' in accordance with the stretch rod movement and the total processing time as a function of the preform weight, the temperature profile of the preform. The pressure-time profiles of each model are given in fig. 4-10 (a), (b) and (c).
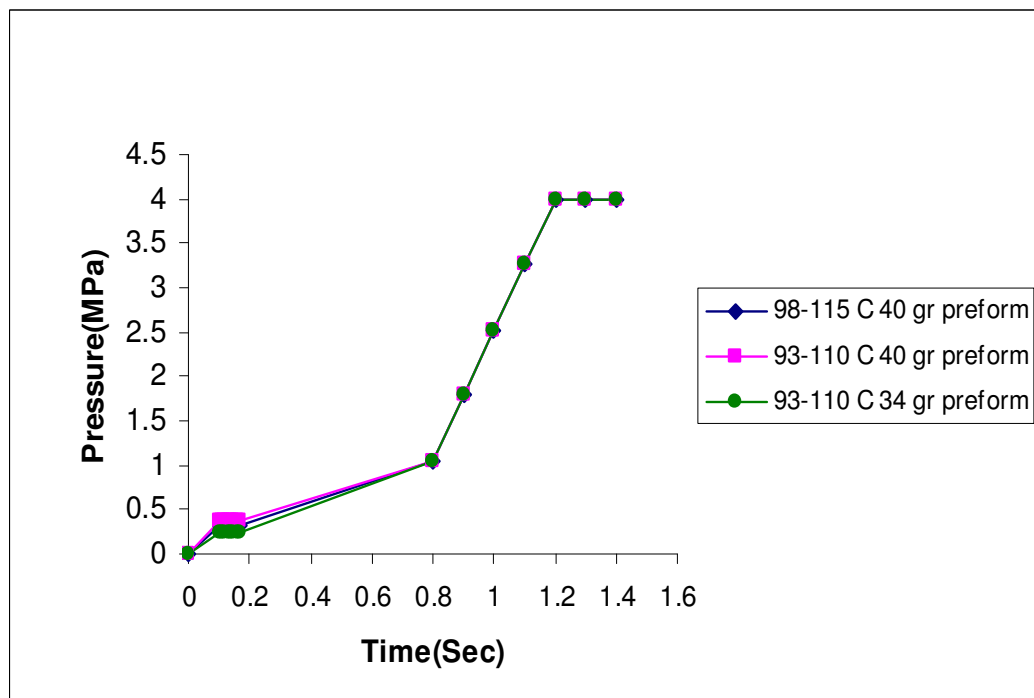
(a)
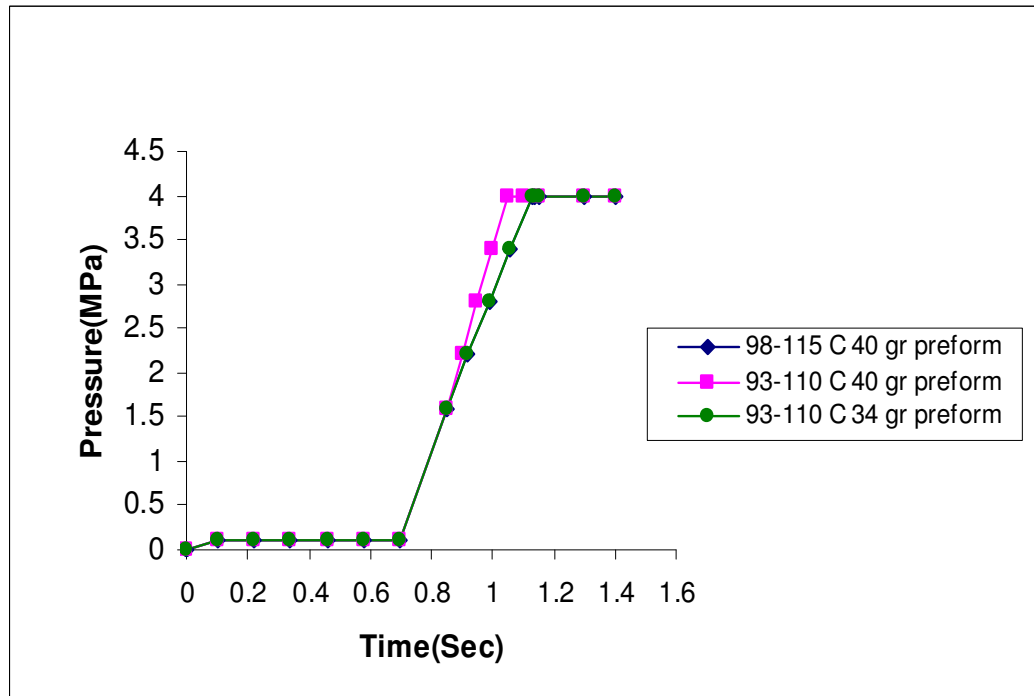
(b)
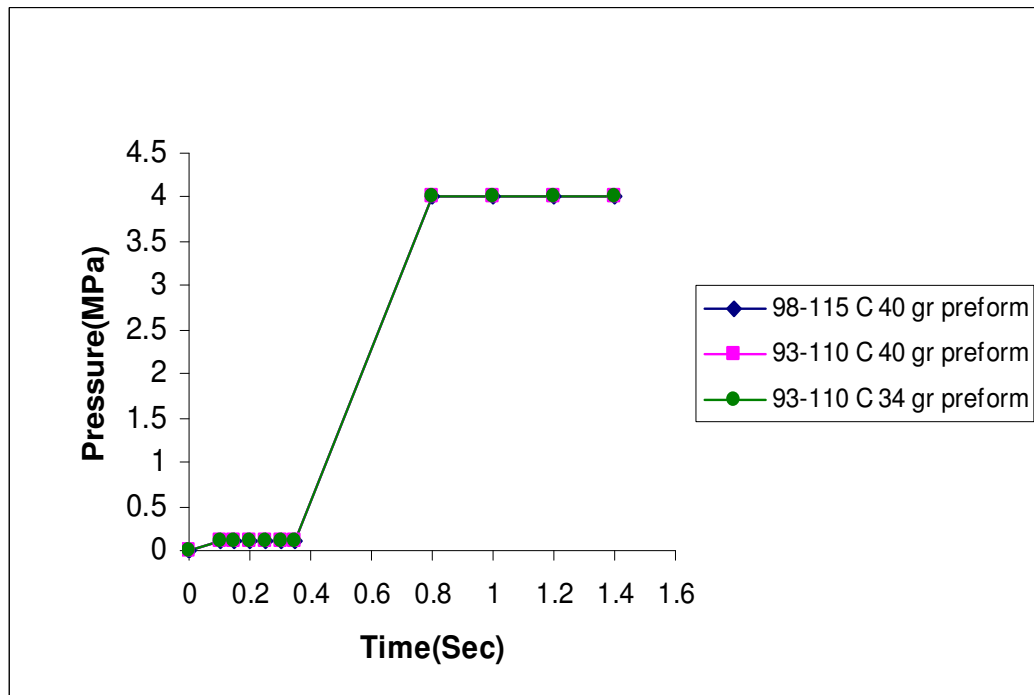
(c)

Fig.4-10. Pressure vs. time profile for (a) model-1 (b) model-2 (c) model-3

4.2.7 ISBM process settings

Both the bottle mould temperature and the stretch rod temperature were set to 30 °C during the process. It was assumed that the stretch rod is made of the aluminum and the heat transfer coefficient for the stretch rod surfaces was taken to be 1000 W/m^2 °C

The ISBM process settings for model-1, model-2 and model-3 are tabulated in Table 4-1, Table 4-2 and Table 4-3 respectively. For each model, two different preform temperature profiles of 108-115 ^{o}C and 103-110 ^{o}C were considered for the 40 g preform; and only low temperature profile of 103-110 ^{o}C was considered for the 34 g preform.

Table 4-1. Processing conditions for model-1

(a) Temperature range 98-115 ^{o}C for 40 g. preform

Step #	Header	Title	Time (sec)	Pressure (MPa)	Mould 1 X	Y	Z	stretch rod X	Y	Z	Conv. IN (Temp, H)		Conv. OUT (Temp, H)	
1	Stretching	Stretch1	0.10	0.32	0.0	0.0	0.0	0.0	-80.0	0.0	20,	5	30,	5
2	Stretching	Stretch2	0.11	0.32	0.0	0.0	0.0	0.0	-80.0	0.0	20,	5	30,	5
3	Stretching	Stretch3	0.12	0.32	0.0	0.0	0.0	0.0	-80.0	0.0	20,	5	30,	5
4	Stretching	Stretch4	0.13	0.32	0.0	0.0	0.0	0.0	-80.0	0.0	20,	5	30,	5
5	Stretching	Stretch5	0.14	0.32	0.0	0.0	0.0	0.0	-80.0	0.0	20,	5	30,	5
6	Stretching	Stretch6	0.15	0.32	0.0	0.0	0.0	0.0	-80.0	0.0	20,	5	30,	5
7	Stretching	Stretch7	0.16	0.32	0.0	0.0	0.0	0.0	-80.0	0.0	20,	5	30,	5
8	Stretching	Stretch8	0.17	0.32	0.0	0.0	0.0	0.0	-80.0	0.0	20,	50	30,	5
9	Blowing	Blow1	0.80	1.056	0.0	0.0	0.0	0.0	-80.0	0.0	20,	50	30,	5
10	Blowing	Blow2	0.90	1.792	0.0	0.0	0.0	0.0	-80.0	0.0	20,	50	30,	5
11	Blowing	Blow3	1.00	2.528	0.0	0.0	0.0	0.0	-80.0	0.0	20,	50	30,	5
12	Blowing	Blow4	1.10	3.264	0.0	0.0	0.0	0.0	-80.0	0.0	20,	50	30,	5
13	Blowing	Blow5	1.20	4.00	0.0	0.0	0.0	0.0	-80.0	0.0	20,	50	30,	5

Temperature Range: 98-115 ºC — Preform Weight: 40 gr.

(b). Temperature range 93-110 ^{o}C for 40 g. preform

Processing Conditions

File   Edit   Simulation   View   Temperature Range: 93-110 ^{o}C   Preform Weight: 40 gr.

Blow

Step #	Header	Title	Time (sec)	Pressure (MPa)	Mould 1			stretch rod			Conv. IN (Temp, H)		Conv. OUT (Temp, H)	
					X	Y	Z	X	Y	Z				
1	Stretching	Stretch1	0.10	0.37	0.0	0.0	0.0	0.0	-80.0	0.0	20,	5	30,	5
2	Stretching	Stretch2	0.11	0.37	0.0	0.0	0.0	0.0	-80.0	0.0	20,	5	30,	5
3	Stretching	Stretch3	0.12	0.37	0.0	0.0	0.0	0.0	-80.0	0.0	20,	5	30,	5
4	Stretching	Stretch4	0.13	0.37	0.0	0.0	0.0	0.0	-80.0	0.0	20,	5	30,	5
5	Stretching	Stretch5	0.14	0.37	0.0	0.0	0.0	0.0	-80.0	0.0	20,	5	30,	5
6	Stretching	Stretch6	0.15	0.37	0.0	0.0	0.0	0.0	-80.0	0.0	20,	5	30,	5
7	Stretching	Stretch7	0.16	0.37	0.0	0.0	0.0	0.0	-80.0	0.0	20,	5	30,	5
8	Stretching	Stretch8	0.17	0.37	0.0	0.0	0.0	0.0	-80.0	0.0	20,	50	30,	5
9	Blowing	Blow1	0.80	1.056	0.0	0.0	0.0	0.0	-80.0	0.0	20,	50	30,	5
10	Blowing	Blow2	0.90	1.792	0.0	0.0	0.0	0.0	-80.0	0.0	20,	50	30,	5
11	Blowing	Blow3	1.00	2.528	0.0	0.0	0.0	0.0	-80.0	0.0	20,	50	30,	5
12	Blowing	Blow4	1.10	3.264	0.0	0.0	0.0	0.0	-80.0	0.0	20,	50	30,	5
13	Blowing	Blow5	1.20	4.00	0.0	0.0	0.0	0.0	-80.0	0.0	20,	50	30,	5

(c). Temperature range 93-110 ^{o}C for 34 gr. preform

Processing Conditions

File   Edit   Simulation   View   Temperature Range: 93-110 ^{o}C   Preform Weight: 34 gr.

Blow

Step #	Header	Title	Time (sec)	Pressure (MPa)	Mould 1			stretch rod			Conv. IN (Temp, H)		Conv. OUT (Temp, H)	
					X	Y	Z	X	Y	Z				
1	Stretching	Stretch1	0.10	0.25	0.0	0.0	0.0	0.0	-80.0	0.0	20,	5	30,	5
2	Stretching	Stretch2	0.11	0.25	0.0	0.0	0.0	0.0	-80.0	0.0	20,	5	30,	5
3	Stretching	Stretch3	0.12	0.25	0.0	0.0	0.0	0.0	-80.0	0.0	20,	5	30,	5
4	Stretching	Stretch4	0.13	0.25	0.0	0.0	0.0	0.0	-80.0	0.0	20,	5	30,	5
5	Stretching	Stretch5	0.14	0.25	0.0	0.0	0.0	0.0	-80.0	0.0	20,	5	30,	5
6	Stretching	Stretch6	0.15	0.25	0.0	0.0	0.0	0.0	-80.0	0.0	20,	5	30,	5
7	Stretching	Stretch7	0.16	0.25	0.0	0.0	0.0	0.0	-80.0	0.0	20,	5	30,	5
8	Stretching	Stretch8	0.17	0.25	0.0	0.0	0.0	0.0	-80.0	0.0	20,	50	30,	5
9	Blowing	Blow1	0.80	1.056	0.0	0.0	0.0	0.0	-80.0	0.0	20,	50	30,	5
10	Blowing	Blow2	0.90	1.792	0.0	0.0	0.0	0.0	-80.0	0.0	20,	50	30,	5
11	Blowing	Blow3	1.00	2.528	0.0	0.0	0.0	0.0	-80.0	0.0	20,	50	30,	5
12	Blowing	Blow4	1.10	3.264	0.0	0.0	0.0	0.0	-80.0	0.0	20,	50	30,	5
13	Blowing	Blow5	1.20	4.00	0.0	0.0	0.0	0.0	-80.0	0.0	20,	50	30,	5

Table 4-2. Processing Conditions for model-2

(a) Temperature range 98-115 $^{\circ}$C for 40 g. preform

Processing Conditions

File   Edit   Simulation   View   Temperature Range: 98-115 $^{\circ}$C   Preform Weight: 40 gr.

Blow

Step #	Header	Title	Time (sec)	Pressure (MPa)	Mould 1 X	Y	Z	stretch rod X	Y	Z	Conv. IN (Temp, H)	Conv. OUT (Temp, H)
1	Stretching	Stretch1	0.10	0.11	0.0	0.0	0.0	0.0	-84.0	0.0	20, 5	30, 5
2	Stretching	Stretch2	0.22	0.11	0.0	0.0	0.0	0.0	-104.0	0.0	20, 5	30, 5
3	Stretching	Stretch3	0.34	0.11	0.0	0.0	0.0	0.0	-124.0	0.0	20, 5	30, 5
4	Stretching	Stretch4	0.46	0.11	0.0	0.0	0.0	0.0	-144.0	0.0	20, 5	30, 5
5	Stretching	Stretch5	0.58	0.11	0.0	0.0	0.0	0.0	-164.0	0.0	20, 5	30, 5
6	Stretching	Stretch6	0.70	0.11	0.0	0.0	0.0	0.0	-184.0	0.0	20, 50	30, 5
7	Blowing	Blow1	0.85	1.60	0.0	0.0	0.0	0.0	-184.0	0.0	20, 50	30, 5
8	Blowing	Blow2	0.92	2.20	0.0	0.0	0.0	0.0	-184.0	0.0	20, 50	30, 5
9	Blowing	Blow3	0.99	2.80	0.0	0.0	0.0	0.0	-184.0	0.0	20, 50	30, 5
10	Blowing	Blow4	1.06	3.40	0.0	0.0	0.0	0.0	-184.0	0.0	20, 50	30, 5
11	Blowing	Blow5	1.13	4.00	0.0	0.0	0.0	0.0	-184.0	0.0	20, 50	30, 5

Table 4-2(b). Temperature range 93-110 $^{\circ}$C for 40 g. preform

Processing Conditions

File   Edit   Simulation   View   Temperature Range: 93-110 $^{\circ}$C   Preform Weight: 40 gr.

Blow

Step #	Header	Title	Time (sec)	Pressure (MPa)	Mould 1 X	Y	Z	stretch rod X	Y	Z	Conv. IN (Temp, H)	Conv. OUT (Temp, H)
1	Stretching	Stretch1	0.10	0.11	0.0	0.0	0.0	0.0	-84.0	0.0	20, 5	30, 5
2	Stretching	Stretch2	0.22	0.11	0.0	0.0	0.0	0.0	-104.0	0.0	20, 5	30, 5
3	Stretching	Stretch3	0.34	0.11	0.0	0.0	0.0	0.0	-124.0	0.0	20, 5	30, 5
4	Stretching	Stretch4	0.46	0.11	0.0	0.0	0.0	0.0	-144.0	0.0	20, 5	30, 5
5	Stretching	Stretch5	0.58	0.11	0.0	0.0	0.0	0.0	-164.0	0.0	20, 5	30, 5
6	Stretching	Stretch6	0.70	0.11	0.0	0.0	0.0	0.0	-184.0	0.0	20, 50	30, 5
7	Blowing	Blow1	0.85	1.60	0.0	0.0	0.0	0.0	-184.0	0.0	20, 50	30, 5
8	Blowing	Blow2	0.90	2.40	0.0	0.0	0.0	0.0	-184.0	0.0	20, 50	30, 5
9	Blowing	Blow3	0.95	3.20	0.0	0.0	0.0	0.0	-184.0	0.0	20, 50	30, 5
10	Blowing	Blow4	1.00	4.00	0.0	0.0	0.0	0.0	-184.0	0.0	20, 50	30, 5
11	Blowing	Blow5	1.05	4.00	0.0	0.0	0.0	0.0	-184.0	0.0	20, 50	30, 5

Table 4-2 (c). Temperature range 93-110 ^{o}C for 34 g. preform

Processing Conditions

File   Edit   Simulation   View   Temperature Range: 93-110 ^{o}C   Preform Weight: 34 gr.

Blow

Step #	Header	Title	Time (sec)	Pressure (MPa)	Mould 1 X	Y	Z	stretch rod X	Y	Z	Conv. IN (Temp, H)		Conv. OUT (Temp, H)	
1	Stretching	Stretch1	0.10	0.11	0.0	0.0	0.0	0.0	-84.0	0.0	20,	5	30,	5
2	Stretching	Stretch2	0.22	0.11	0.0	0.0	0.0	0.0	-104.0	0.0	20,	5	30,	5
3	Stretching	Stretch3	0.34	0.11	0.0	0.0	0.0	0.0	-124.0	0.0	20,	5	30,	5
4	Stretching	Stretch4	0.46	0.11	0.0	0.0	0.0	0.0	-144.0	0.0	20,	5	30,	5
5	Stretching	Stretch5	0.58	0.11	0.0	0.0	0.0	0.0	-164.0	0.0	20,	5	30,	5
6	Stretching	Stretch6	0.70	0.11	0.0	0.0	0.0	0.0	-184.0	0.0	20,	50	30,	5
7	Blowing	Blow1	0.85	1.60	0.0	0.0	0.0	0.0	-184.0	0.0	20,	50	30,	5
8	Blowing	Blow2	0.92	2.20	0.0	0.0	0.0	0.0	-184.0	0.0	20,	50	30,	5
9	Blowing	Blow3	0.99	2.80	0.0	0.0	0.0	0.0	-184.0	0.0	20,	50	30,	5
10	Blowing	Blow4	1.06	3.40	0.0	0.0	0.0	0.0	-184.0	0.0	20,	50	30,	5
11	Blowing	Blow5	1.13	4.00	0.0	0.0	0.0	0.0	-184.0	0.0	20,	50	30,	5

Table 4-3. Processing Conditions for model-3

(a) Temperature range 98-115 ^{o}C for 40 g. preform

Processing Conditions

File   Edit   Simulation   View   Temperature Range: 98-115 ^{o}C   Preform Weight: 40 gr.

Blow

Step #	Header	Title	Time (sec)	Pressure (MPa)	Mould 1 X	Y	Z	stretch rod X	Y	Z	Conv. IN (Temp, H)		Conv. OUT (Temp, H)	
1	Stretching	Stretch1	0.10	0.105	0.0	0.0	0.0	0.0	-77.7	0.0	20,	5	30,	5
2	Stretching	Stretch2	0.15	0.105	0.0	0.0	0.0	0.0	-119.7	0.0	20,	5	30,	5
3	Stretching	Stretch3	0.20	0.105	0.0	0.0	0.0	0.0	-161.7	0.0	20,	5	30,	5
4	Stretching	Stretch4	0.25	0.105	0.0	0.0	0.0	0.0	-203.7	0.0	20,	5	30,	5
5	Stretching	Stretch5	0.30	0.105	0.0	0.0	0.0	0.0	-245.7	0.0	20,	5	30,	5
6	Stretching	Stretch6	0.35	0.105	0.0	0.0	0.0	0.0	-287.7	0.0	20,	50	30,	5
7	Blowing	Blow1	0.80	4.00	0.0	0.0	0.0	0.0	-287.7	0.0	20,	50	30,	5

Table 4-3(b). Temperature range 93-110 ^{o}C for 40 g. preform

Processing Conditions

File   Edit   Simulation   View   Temperature Range: 93-110 ^{o}C   Preform Weight: 40 gr.

Blow

Step #	Header	Title	Time (sec)	Pressure (MPa)	Mould 1			stretch rod			Conv. IN (Temp, H)		Conv. OUT (Temp, H)	
					X	Y	Z	X	Y	Z				
1	Stretching	Stretch1	0.10	0.105	0.0	0.0	0.0	0.0	-77.7	0.0	20,	5	30,	5
2	Stretching	Stretch2	0.15	0.105	0.0	0.0	0.0	0.0	-119.7	0.0	20,	5	30,	5
3	Stretching	Stretch3	0.20	0.105	0.0	0.0	0.0	0.0	-161.7	0.0	20,	5	30,	5
4	Stretching	Stretch4	0.25	0.105	0.0	0.0	0.0	0.0	-203.7	0.0	20,	5	30,	5
5	Stretching	Stretch5	0.30	0.105	0.0	0.0	0.0	0.0	-245.7	0.0	20,	5	30,	5
6	Stretching	Stretch6	0.35	0.105	0.0	0.0	0.0	0.0	-287.7	0.0	20,	50	30,	5
7	Blowing	Blow1	0.80	4.00	0.0	0.0	0.0	0.0	-287.7	0.0	20,	50	30,	5

Table 4-3 (c). Temperature range 93-110 ^{o}C for 34 g. preform

Processing Conditions

File   Edit   Simulation   View   Temperature Range: 93-110 ^{o}C   Preform Weight: 34 gr.

Blow

Step #	Header	Title	Time (sec)	Pressure (MPa)	Mould 1			stretch rod			Conv. IN (Temp, H)		Conv. OUT (Temp, H)	
					X	Y	Z	X	Y	Z				
1	Stretching	Stretch1	0.10	0.105	0.0	0.0	0.0	0.0	-77.7	0.0	20,	5	30,	5
2	Stretching	Stretch2	0.15	0.105	0.0	0.0	0.0	0.0	-119.7	0.0	20,	5	30,	5
3	Stretching	Stretch3	0.20	0.105	0.0	0.0	0.0	0.0	-161.7	0.0	20,	5	30,	5
4	Stretching	Stretch4	0.25	0.105	0.0	0.0	0.0	0.0	-203.7	0.0	20,	5	30,	5
5	Stretching	Stretch5	0.30	0.105	0.0	0.0	0.0	0.0	-245.7	0.0	20,	5	30,	5
6	Stretching	Stretch6	0.35	0.105	0.0	0.0	0.0	0.0	-287.7	0.0	20,	50	30,	5
7	Blowing	Blow1	0.80	4.00	0.0	0.0	0.0	0.0	-287.7	0.0	20,	50	30,	5

4.2.8 Deformation mode of the preform during stretch/preblow

The effect of the processing conditions on the final properties of the bottle is investigated by means of Blow View 8.2 software program. Firstly, the movement of the stretch rod and the temperature on the preform were fixed according to the defined models. The preform was blown while adjusting the pre-blow pressure. When the timing of the stretch rod is not in harmony with the 'pre-blow' pressure, the preform was ruptured through where the preform wall thickness was thinnest, and the software program stopped producing an error message. On the other hand, when the stretch rod movement was very quick, preform stretching did not occur, and the strain-hardening did not happen. That is why; the stretch rod speed should be in harmony with the 'pre-blow' pressure in the duration of ISBM process. Sometimes 'sticking' between the stretch rod and the part of the preform occurred, when the stretch rod and the material were in contact with each other during the initial stretching stage. This issue was resolved either increasing the pre-blow pressure or decreasing the friction constant between aluminum mold and polymer material. At the final blowing stage, when the contact of the PET bottle with the mold was not fully completed, the problem was fixed with the additional increase of the final pressure. In addition, sometimes, when the final-blow pressure is applied, 'bubble formation' has been observed at the bottom of the bottle. This problem was fully fixed applying the final-pressure in a shorter time. The followings are some of the reasons for increasing the level of difficulty of this study:

- ISBM process settings are highly dependant with each other

- The bottle base with petaloid shape is geometrically very complicated

- The PET material physical properties are not constant because they vary depending on the time, strain rate and the ambient conditions.

As the objective of this study is to improve the resistance of the petaloid base of the bottle against environmental stress cracking, attention is concentrated on this region. In this study carried out with the Blow View 8.2, it was aimed for the thickness in the base to be uniform, and for the stress to be minimized. Fig. 4-11, fig. 4-12 and fig. 4-13 show the deformation mode of the preform in nine steps during stretch/pre-blow for each model separately.
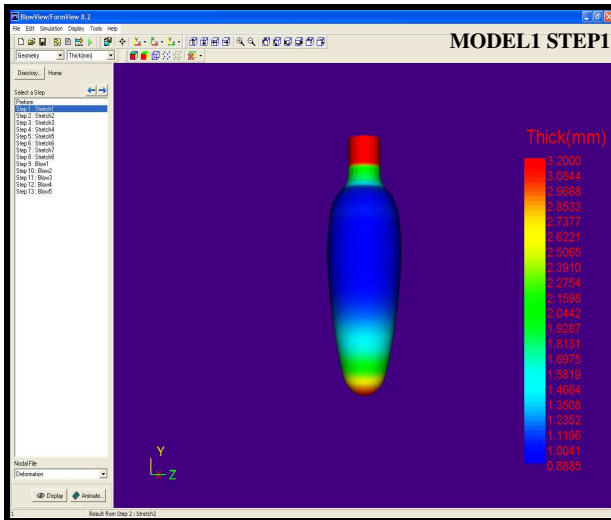
a
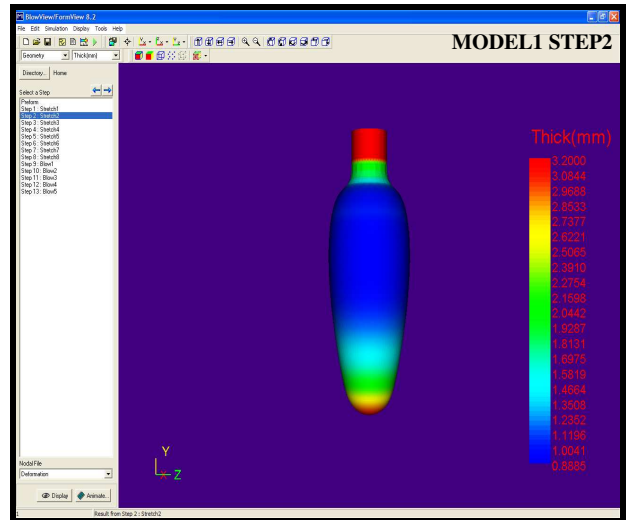
b
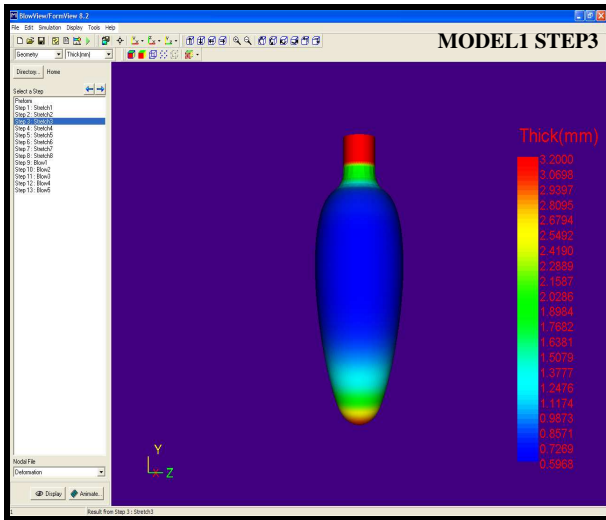
c
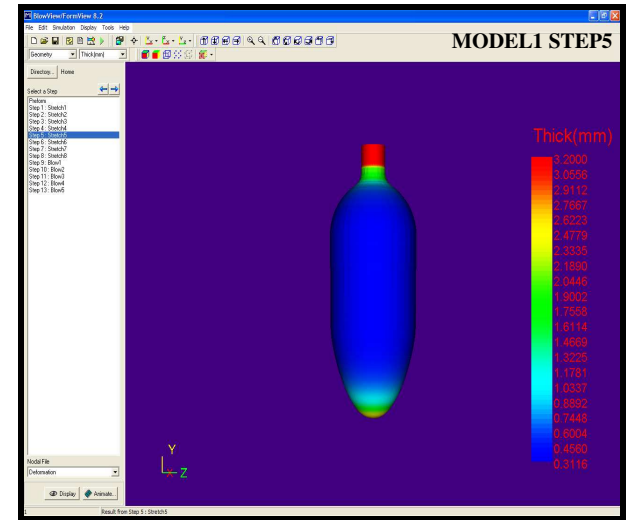
d
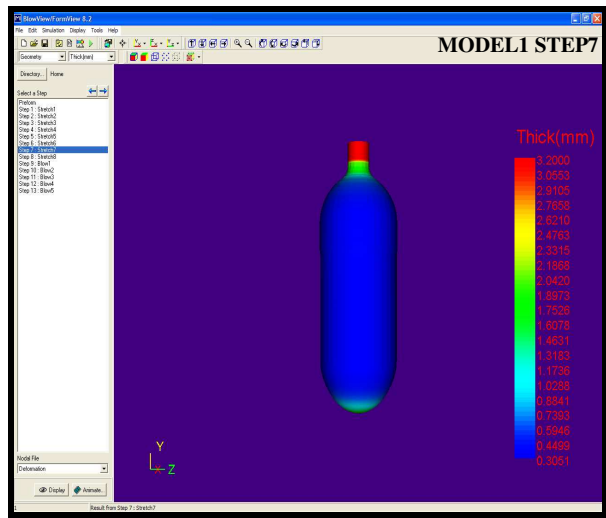
e
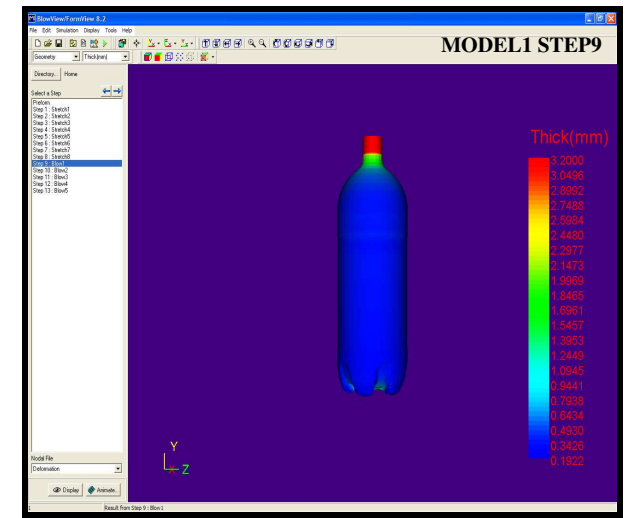
f

Fig.4-11. Preform shapes for Stretch/Pre-blow deformation steps – model-1
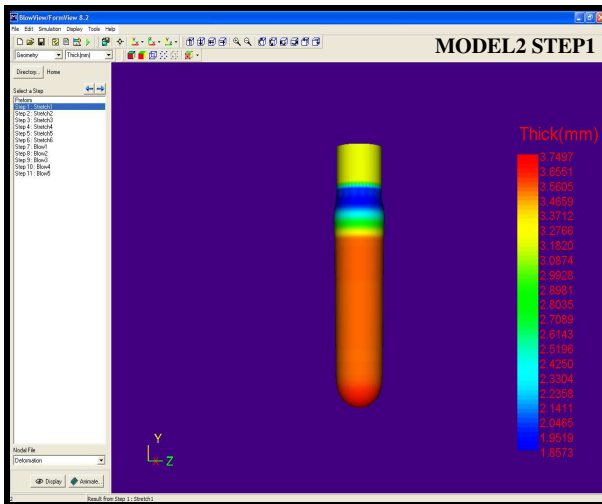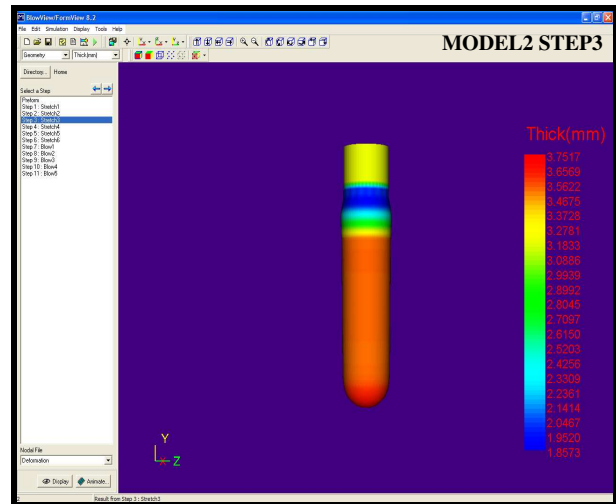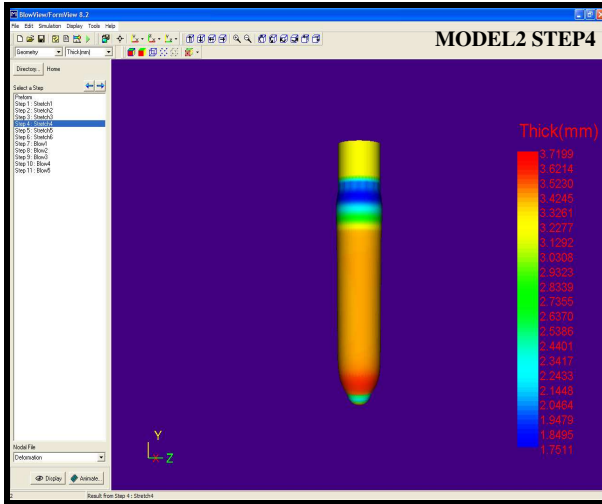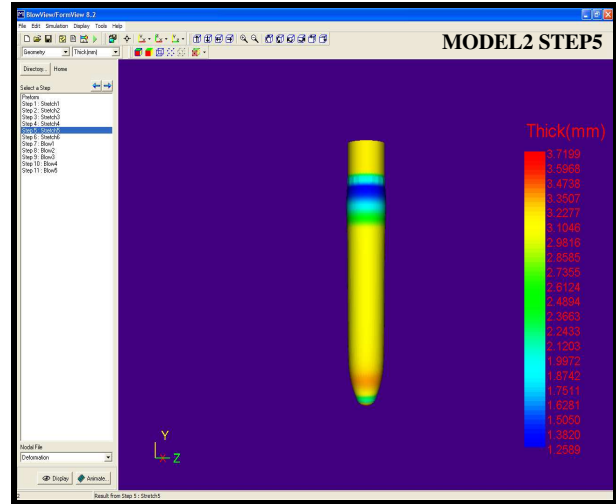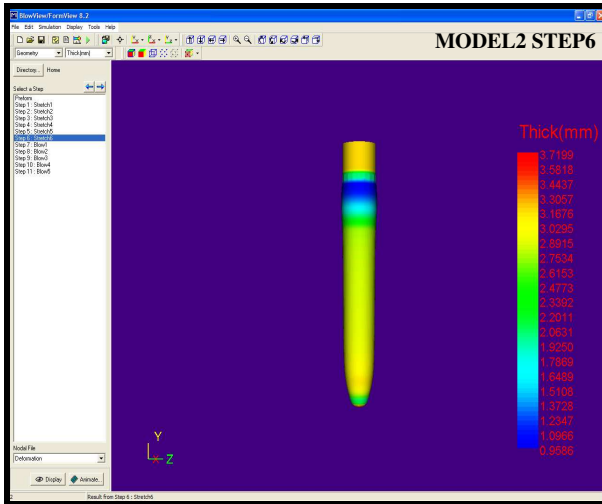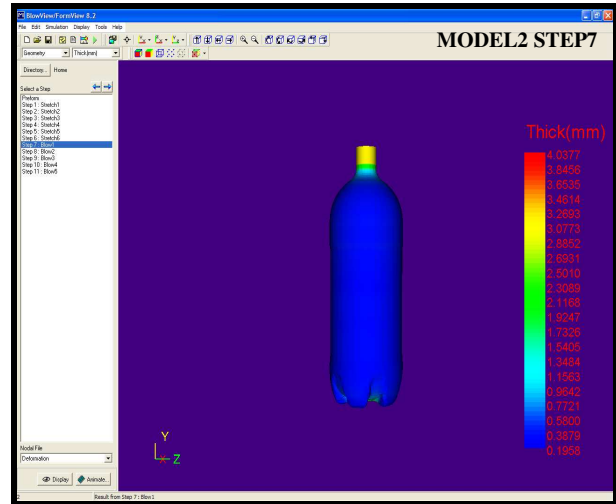
Fig.4-12. Preform shapes for Stretch/Pre-blow deformation steps – model-2
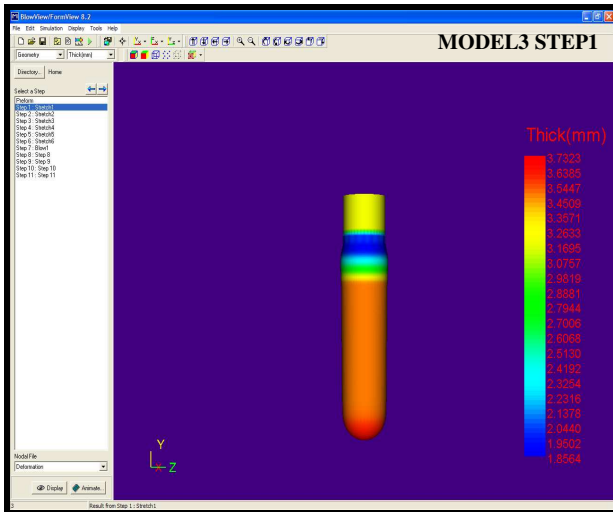
a
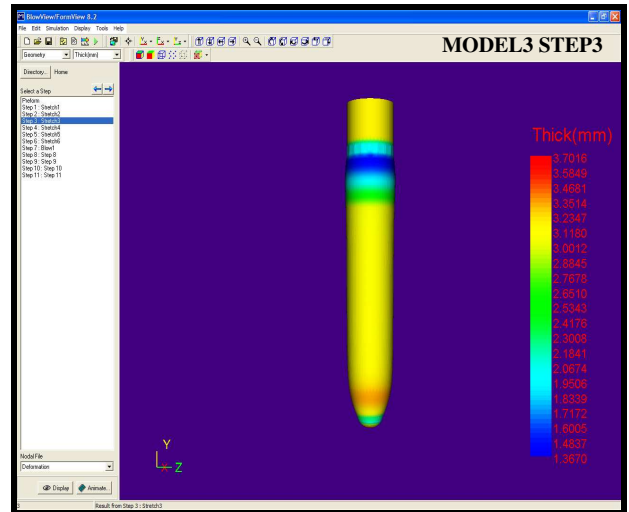
b
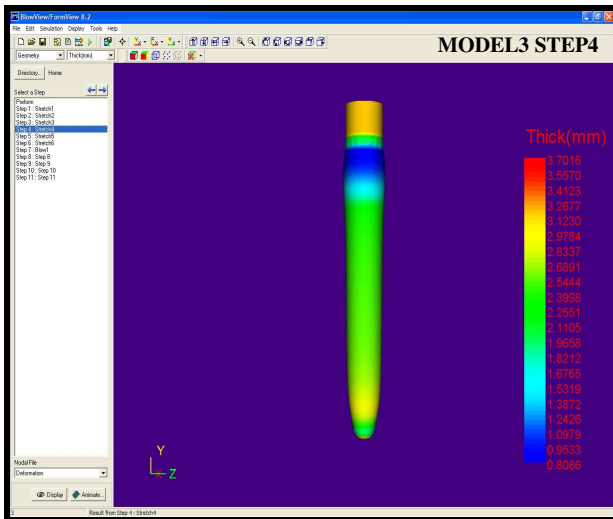
c
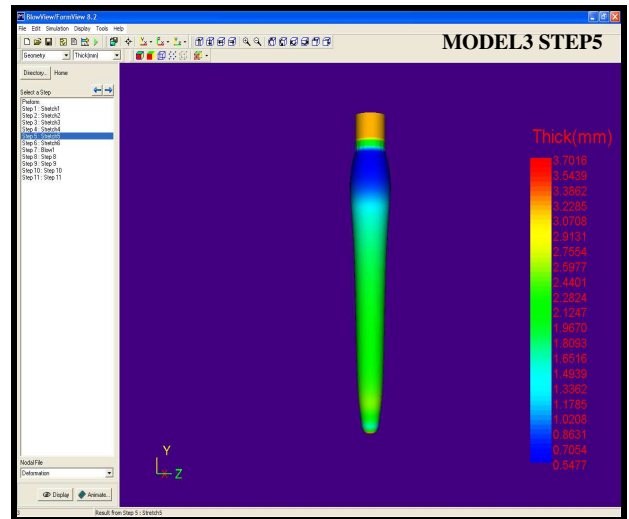
d
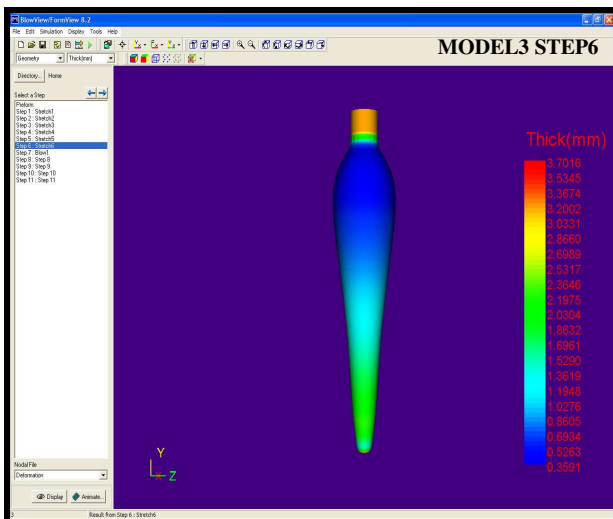
e
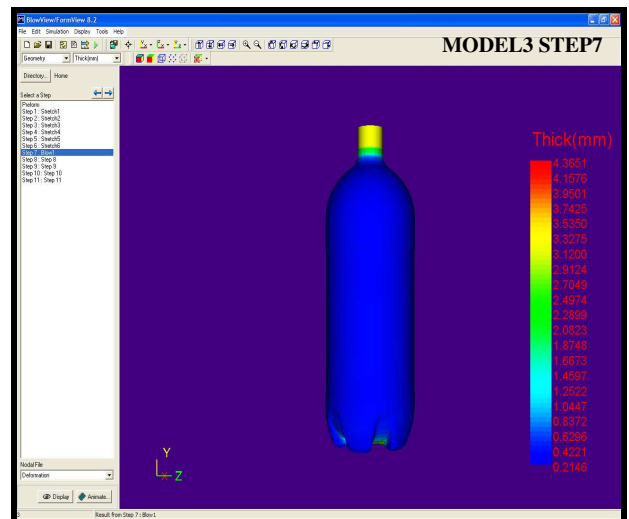
f

Fig.4-13. Preform shapes for Stretch/Pre-blow deformation steps – model-3

4.3 SIMULATION RESULTS WITH BLOW VIEW

4.3.1 Thickness in the bottle base

In this part of the study, the thickness in the bottle base is investigated for all models as a function of the initial temperature profile of the preform and preform weight. The following processing conditions are considered for all three models:

- Temperature profile of 98-115 ^{o}C; 40 g. preform

- Temperature profile of 93-110 ^{o}C; 40 g. preform

- Temperature profile of 93-110 ^{o}C ; 34 g. preform

The results are given in fig. 4-14 (a), (b) and (c) for model-1, model-2 and model-3 respectively; and fig. 4-14 (d) compares the actual (measured) thickness of the optimized bottle base with the simulated thickness values.
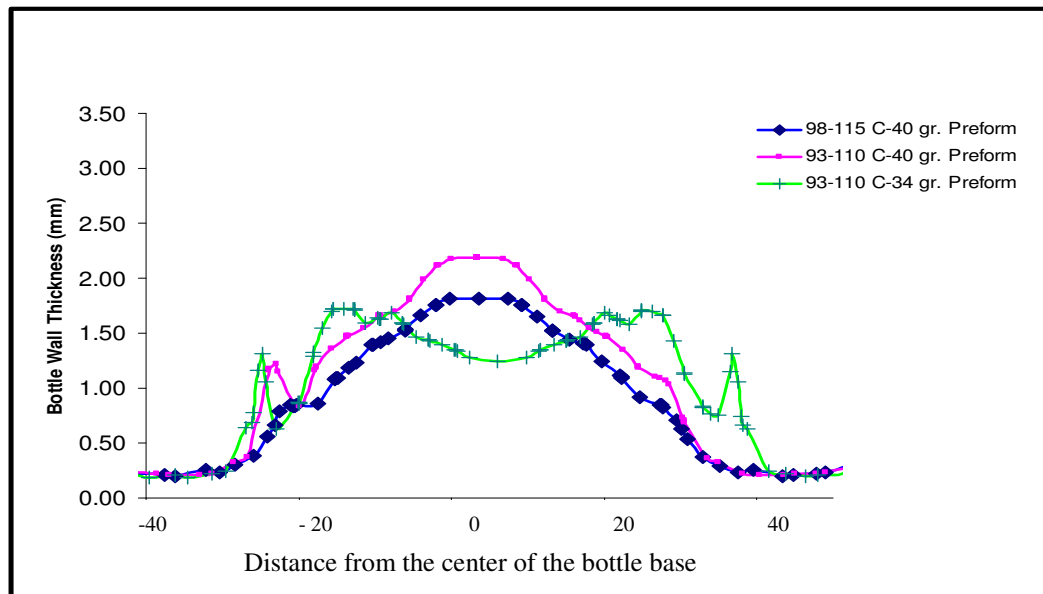
(a)
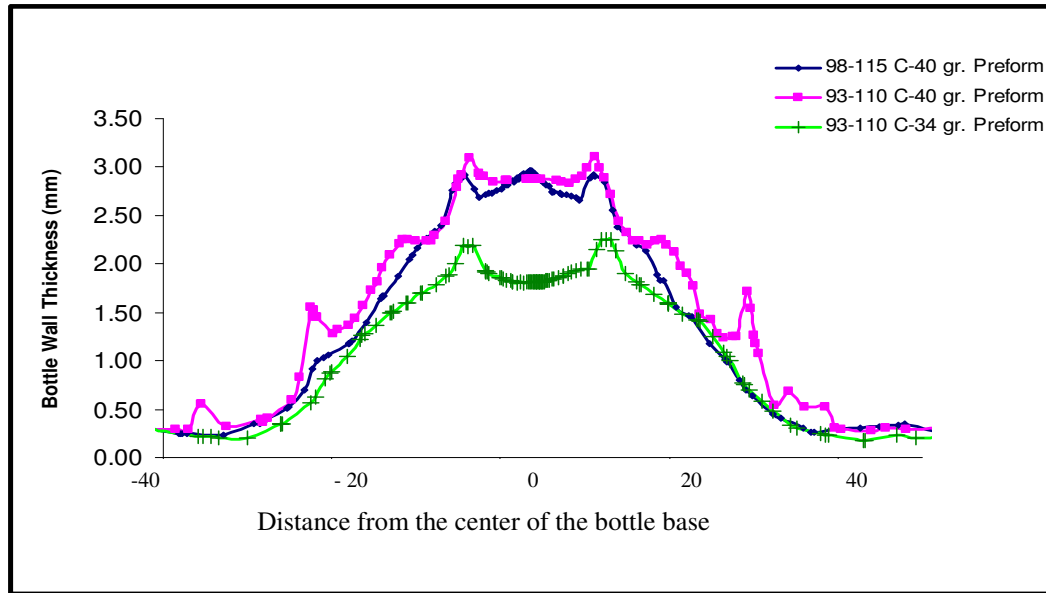
(b)
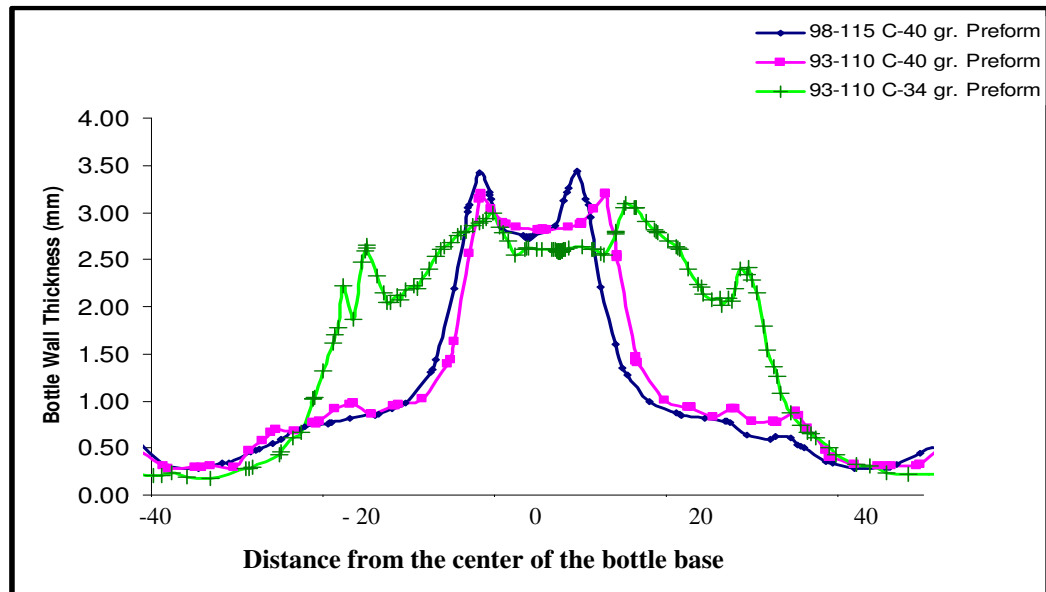
(c)
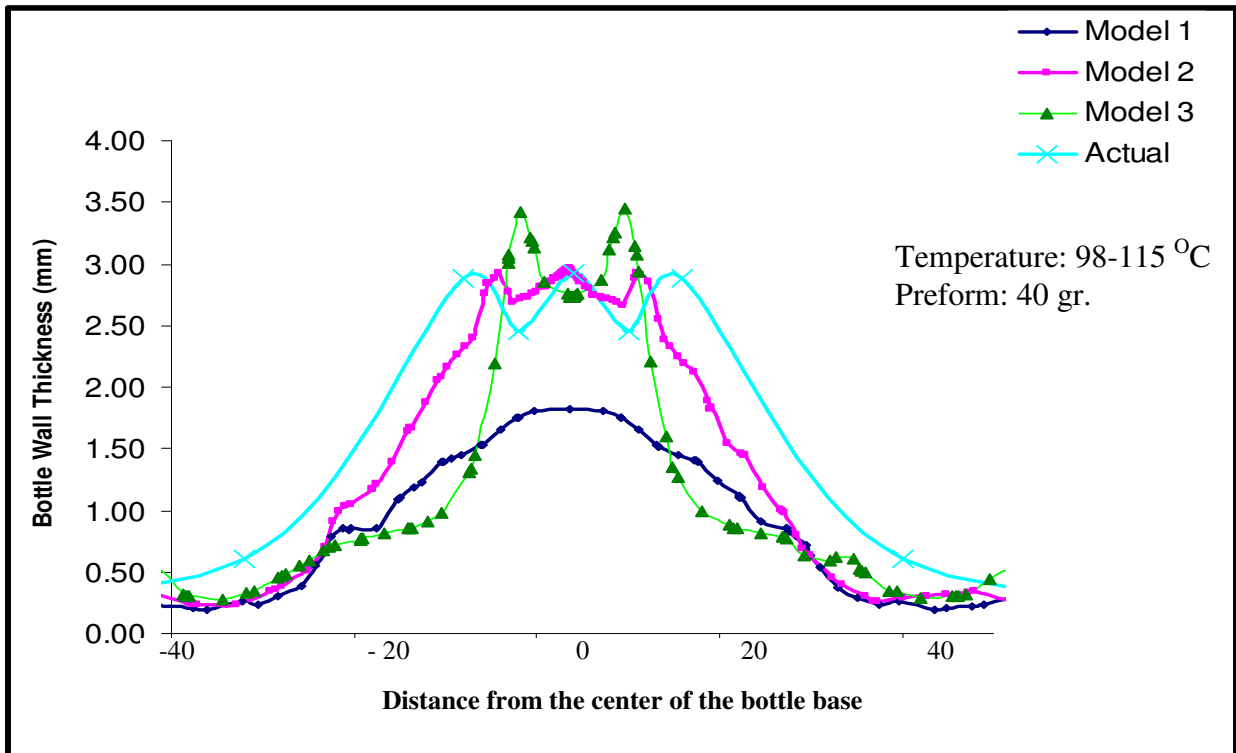
(d)

Fig.4-14. Thickness in the bottle base

(a) model-1 (b) model-2 (c) model-3 (d) comparison of the models

For the three models, the highest base thickness was obtained with model-3, the lowest with model-1. On the other hand, it is found that the uniform thickness in the bottle base was achieved with model-1. The bottle base thickness in the centre region increased as the extent of preform stretching towards the base of the bottle is increased. Hence, the uniformity of the thickness could not be achieved. The highest base thickness was obtained in the central region called 'pinch'. The thickness of the base started to decrease in the direction away from the center of the base, towards the bottle side panels and reached a constant value of 0.3 mm. The abrupt thickness changes in the bottle base tend to increase with the extent of the stretch rod movement; abrupt thickness changes are more prominent with model-3, while no such abrupt thickness changes are observed with model-1. Most importantly, it is observed that the thickness profile achieved by

model-2 processing conditions is very similar to the actual thickness profile of the optimized

bottle base as shown in fig. 4-14(d).

Another observation recorded is that the thickness in the valley and the foot regions of the bottle

base are quite different from each other. The thickest values are found in the centre of the base,

and then in the valley; and the thinnest values are found in the foot section. This can be observed

in simulated thickness values for all three models (fig 4-15 to 4-17). In case of a lower

temperature profile and a lower preform weight, bottle base thickness becomes more uniform.

Temperature Range: 98-115 °C
Preform Weight: 40 g.
(a)

Temperature Range: 93-110 °C
Preform Weight: 40 g.
(b)

Temperature Range: 93-110 °C
Preform Weight: 34 g.
(c)
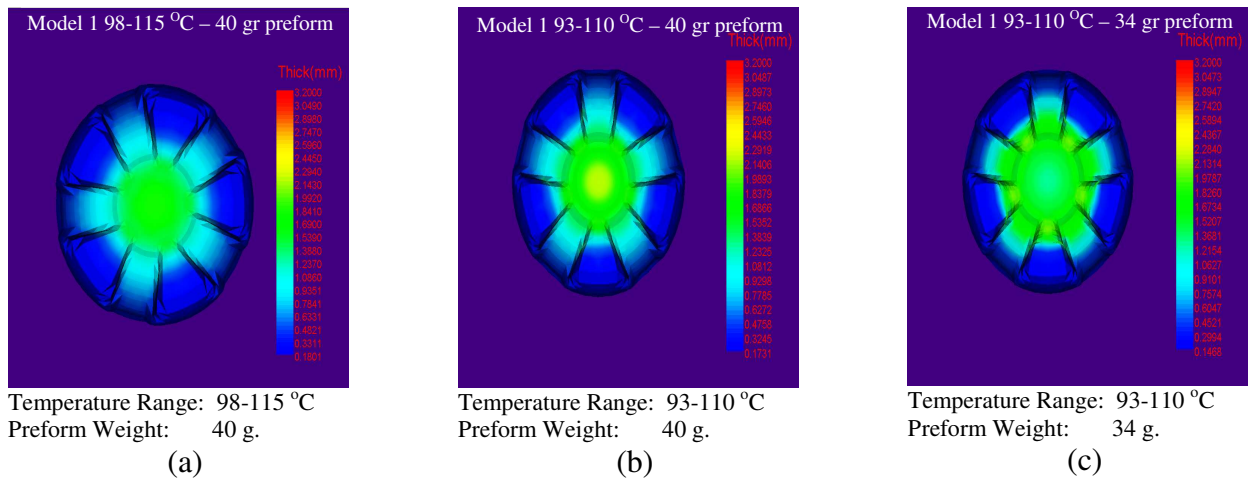
Fig.4-15. Pictures of the thickness distributions at the bottom of the bottle for model-1

Temperature Range: 98-115 °C
Preform Weight: 40 g.
(a)

Temperature Range: 93-110 °C
Preform Weight: 40 g.
(b)

Temperature Range: 93-110 °C
Preform Weight: 34 g.
(c)
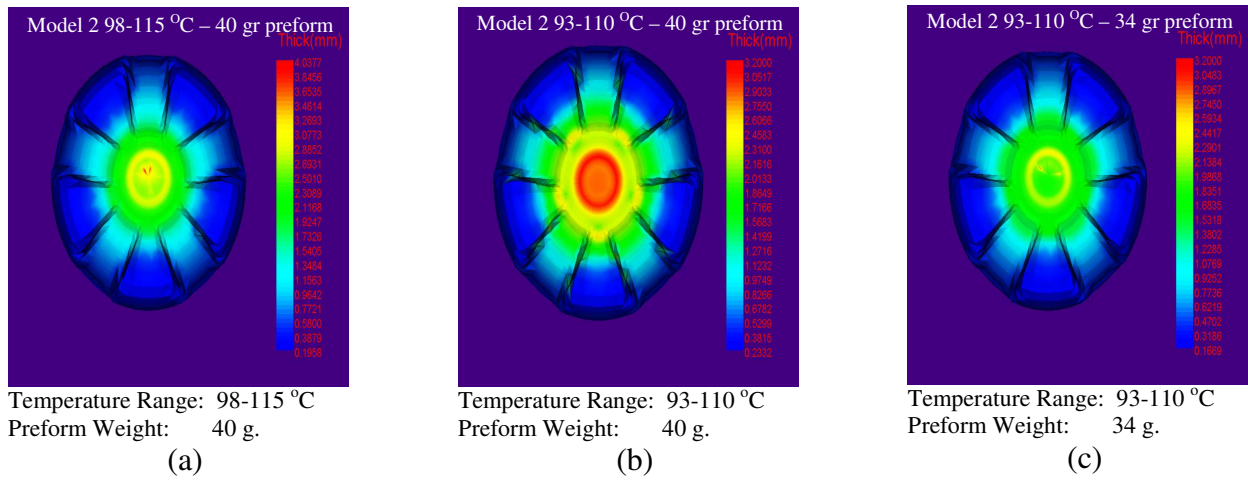
Fig.4-16. Pictures of thickness distributions at the bottom of the bottle for model-2

Temperature Range: 98-115 °C
Preform Weight: 40 g.
(a)

Temperature Range: 93-110 °C
Preform Weight: 40 g.
(b)

Temperature Range: 93-110 °C
Preform Weight: 34 gr.
(c)
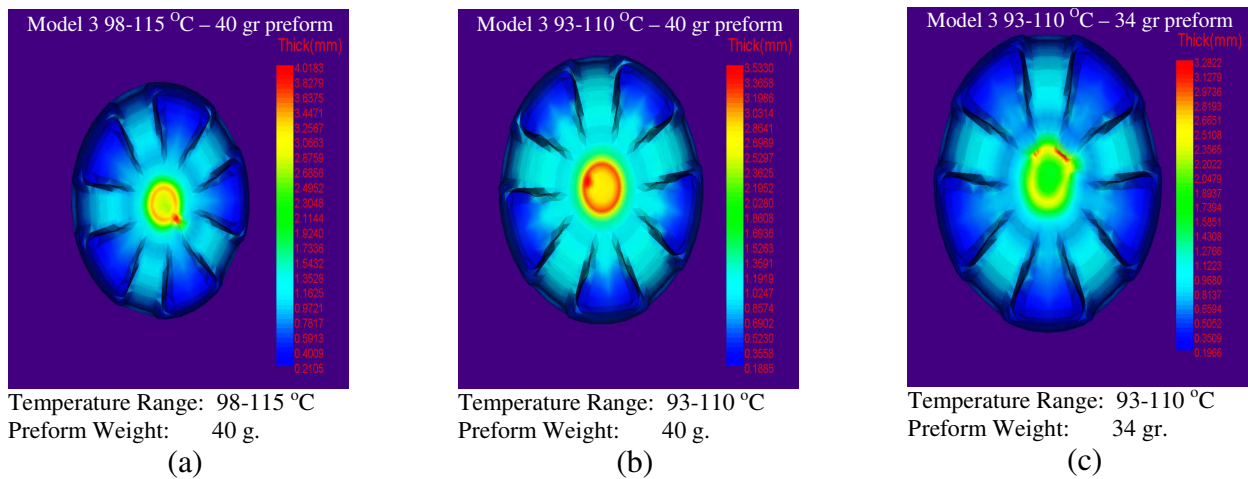
Fig.417. Pictures of the thickness distributions at the bottom of the bottle for model-3

4.3.2 Simulated stress in the bottle base

The simulated stress in the bottle base are studied for two different preform temperature profiles and two different preform weights for each model (Fig 4-18. (a), (b), (c)). Whereas Fig. 4-18. (d) compares the simulated stresses in the bottle base for a high preform temperature profile (98-115 °C) and a heavy preform (40 g) with respect to the three models.
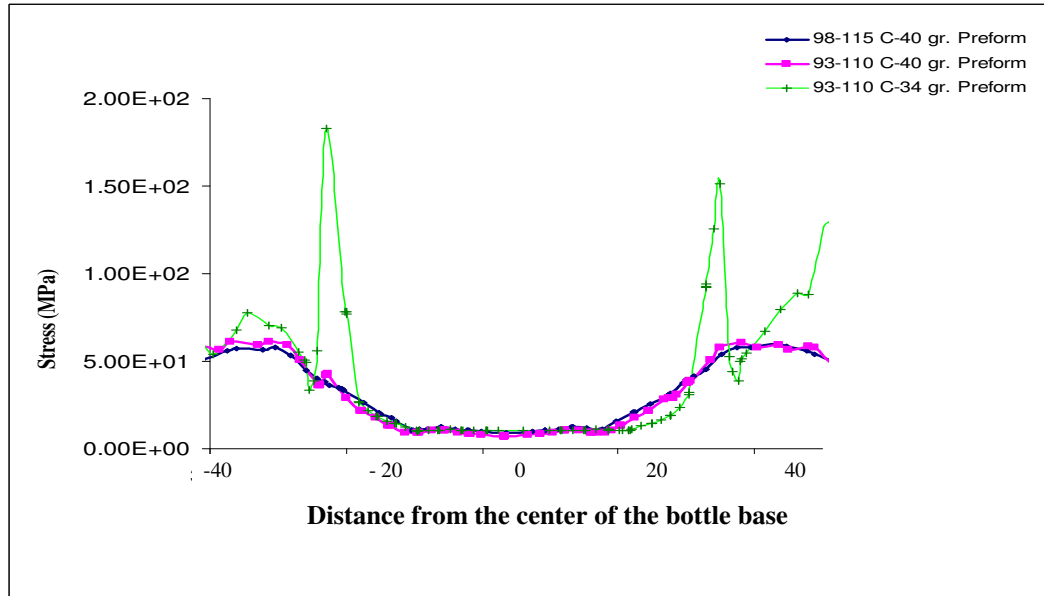
(a)
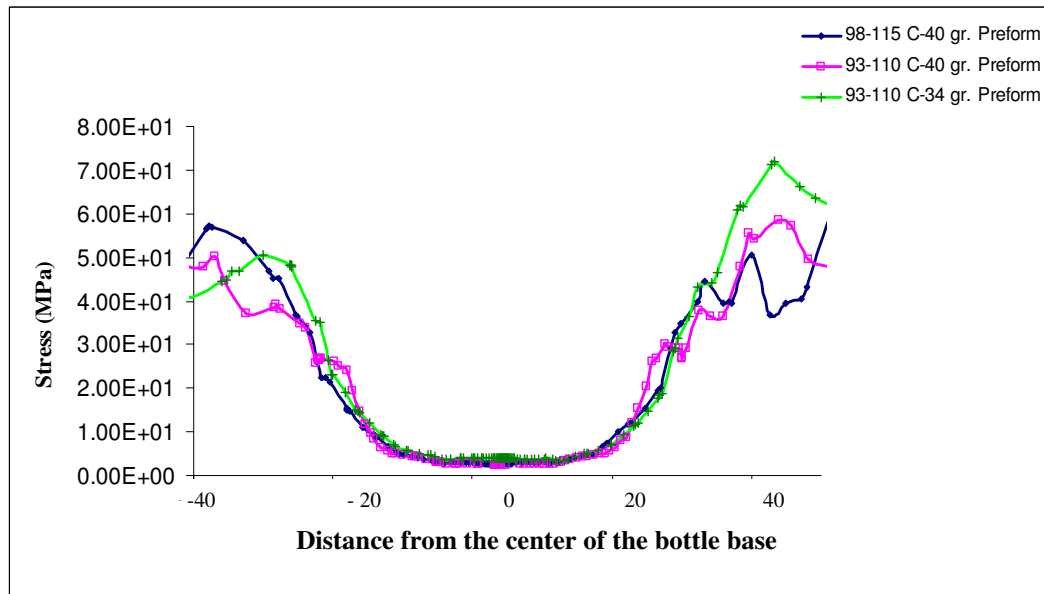
(b)
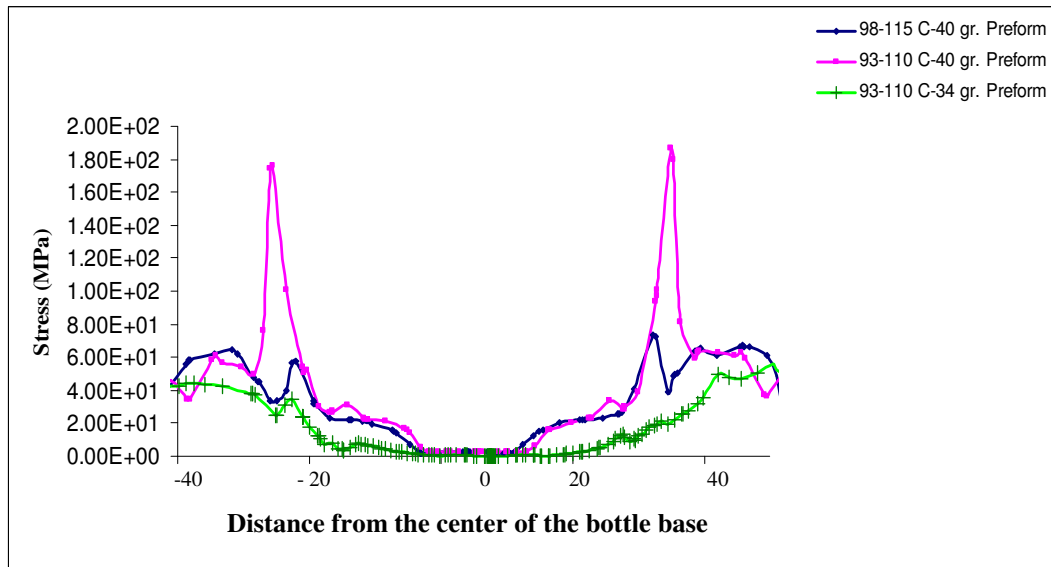
(c)
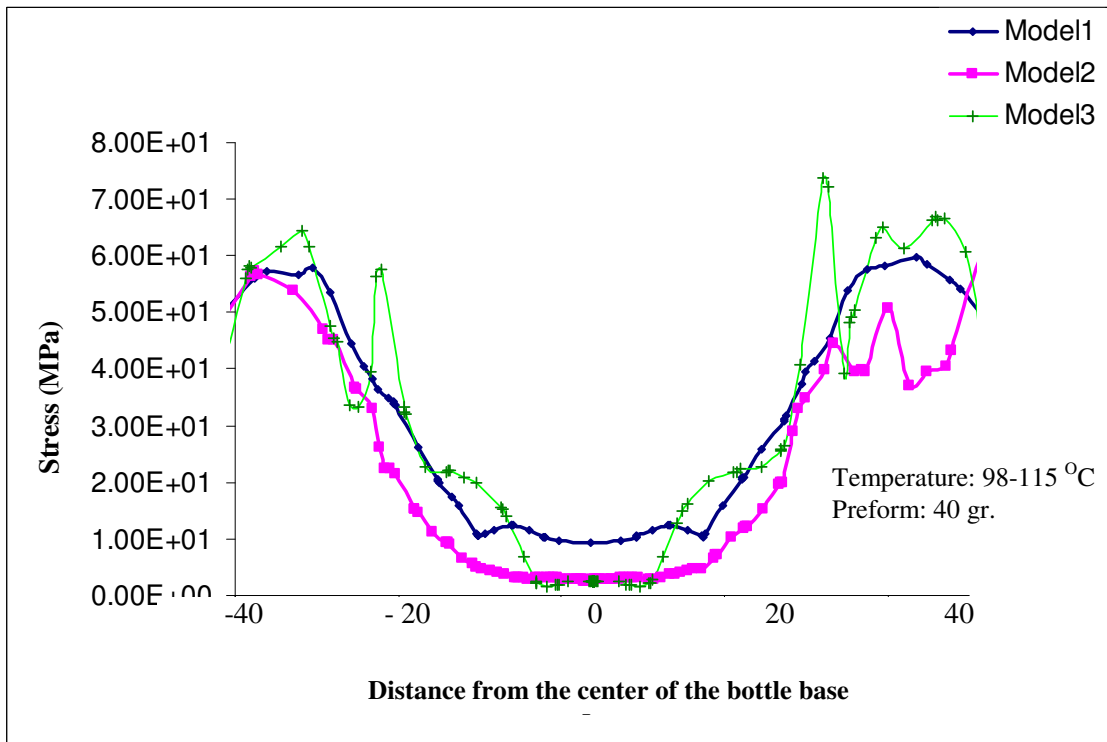
(d)

Fig.4-18. Simulated stress in the bottle base for (a) model-1 (b) model-2

(c) model-3 (d) comparison of the models

The stress in the bottle base is not highly dependant on the preform weight and the initial temperature profile of preform; the stress values are only slightly different from each other. However, when the results are compared with respect to the models, the minimum and maximum stress values in the centre of the base are obtained through model-2 and model-1, respectively (Fig. 4-18(d)). Most importantly, stress is minimized for model-2, which gives the optimum base thickness for the bottles. It can be said that the stretch rod movement has an impact on the stress in the base centre. The highest stress values are in the foot region and the lowest in the centre of the base. This can be observed in simulated stress values for all three models (fig 4-19 to 4-21). As expected there is an inverse relationship between the wall thickness and the stresses in the bottle base.

Temperature Range: 98-115 ^{o}C
Preform Weight: 40 g.
(a)

Temperature Range: 93-110 ^{o}C
Preform Weight: 40 g.
(b)

Temperature Range: 93-110 ^{o}C
Preform Weight: 34 g.
(c)
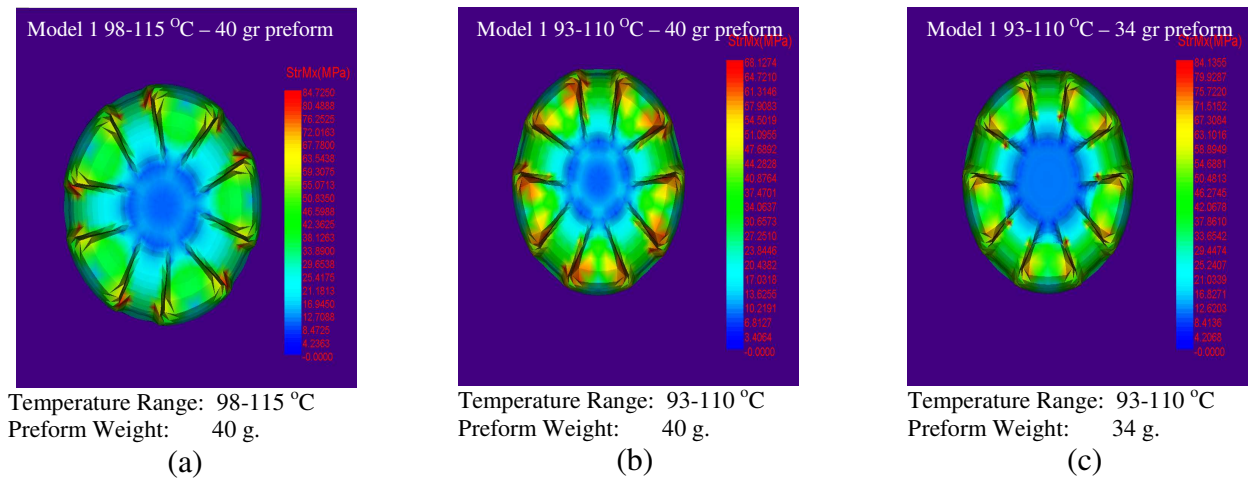
Fig.4-19. Pictures of the stress distributions at the bottom of the bottle for model-1

Temperature Range: 98-115 ^{o}C
Preform Weight: 40 g.
(a)

Temperature Range: 93-110 ^{o}C
Preform Weight: 40 g.
(b)

Temperature Range: 93-110 ^{o}C
Preform Weight: 34 g.
(c)
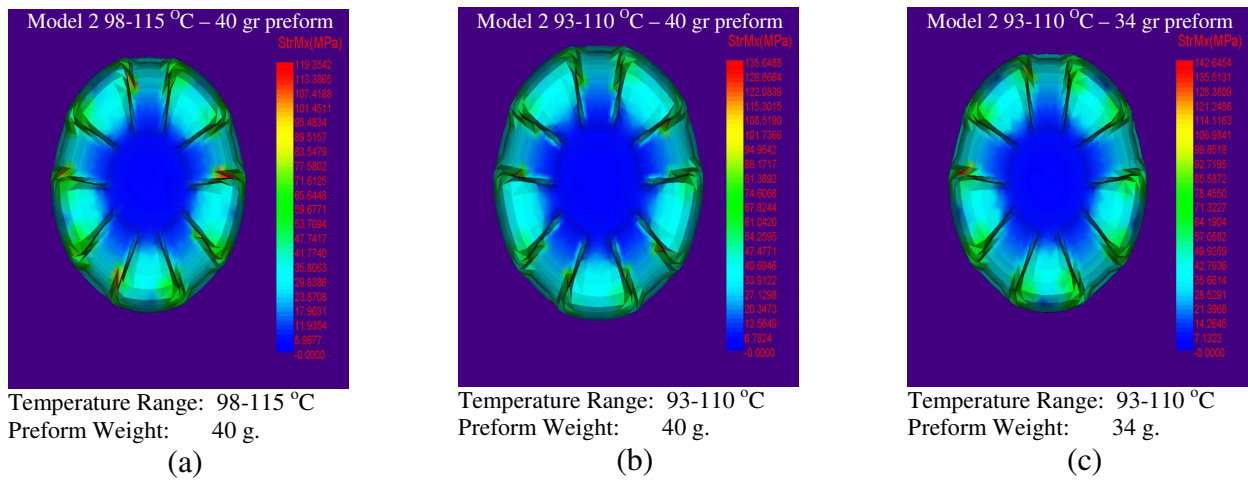
Fig.4-20. Pictures of the stress distributions at the bottom of the bottle for model-2

Temperature Range: 98-115 ^{o}C
Preform Weight: 40 g.
(a)

Temperature Range: 93-110 ^{o}C
Preform Weight: 40 g.
(b)

Temperature Range: 93-110 ^{o}C
Preform Weight: 34 g.
(c)
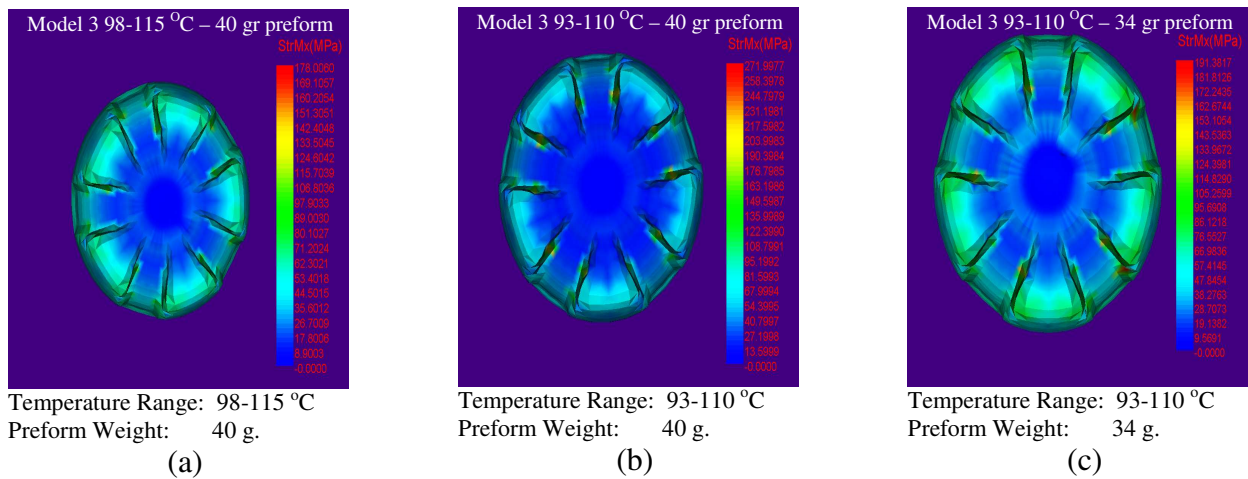
Fig.4-21. Pictures of the stress distributions at the bottom of the bottle for model-3

4.3.3 Simulated crystallinity in the bottle base

The crystallinity in the bottle base are simulated at two different preform temperature profiles and two different preform weights for each model (Fig 4-22 (a), (b), (c)). Fig. 4-22 (d) compares the simulated crystallinity in the bottle base for a high preform temperature profile (98 -115 ^{o}C) and a heavy preform (40 g) for the three models.
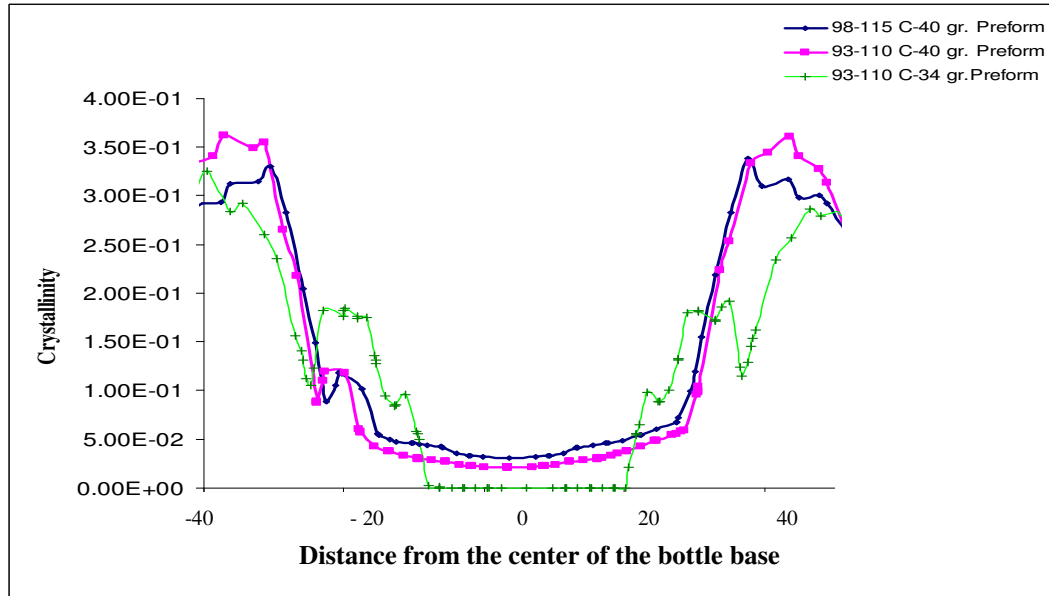
(a)
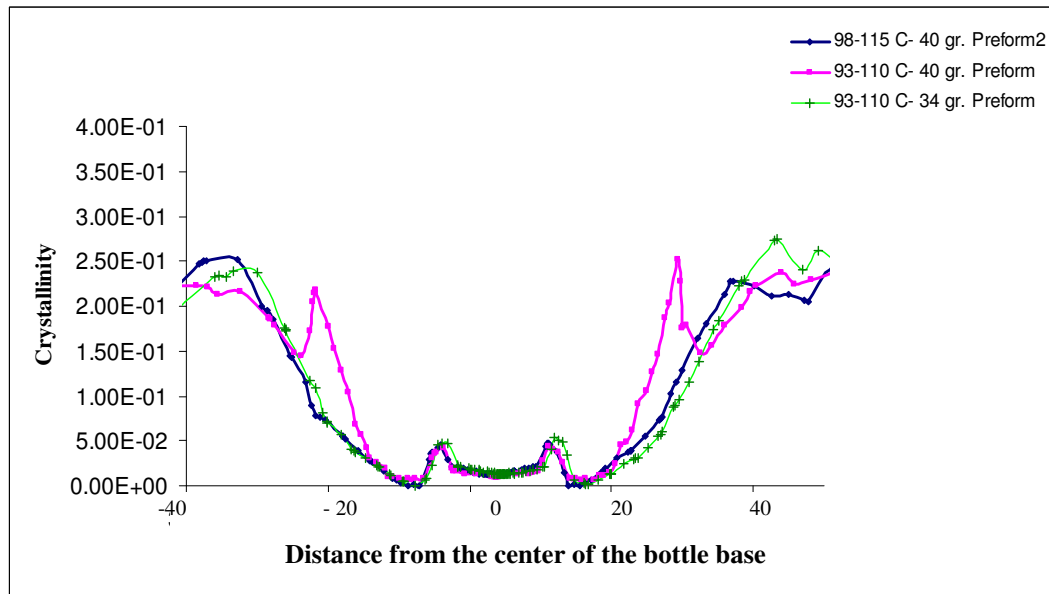
(b)
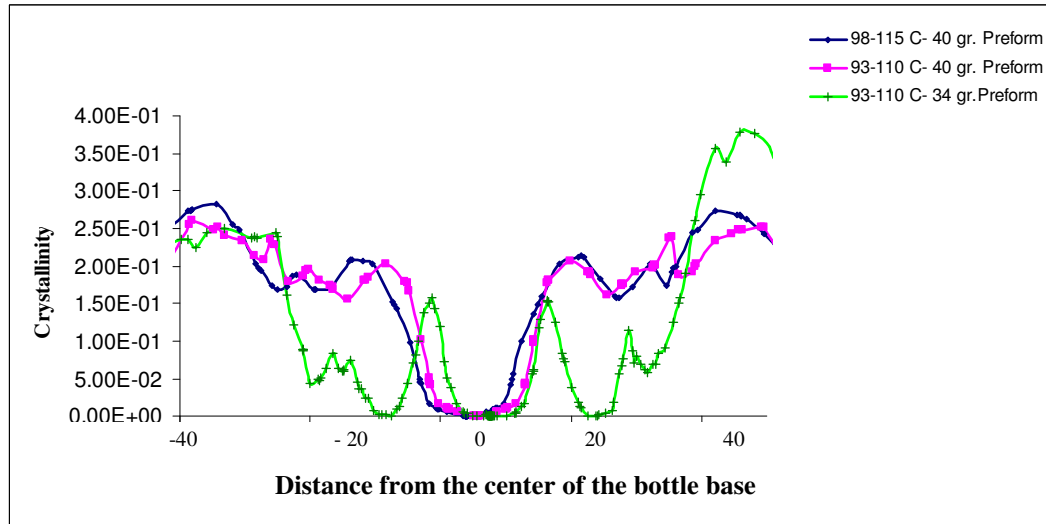
(c)
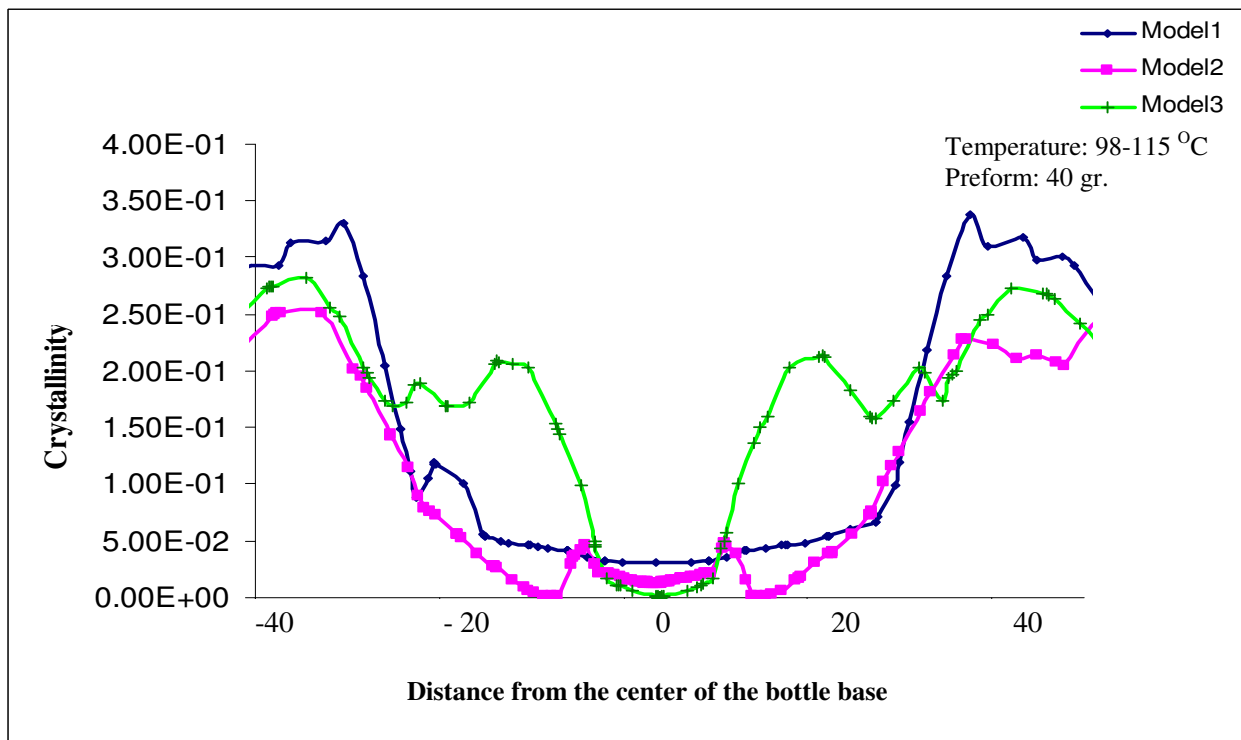
(d)

Fig.4-22. Simulated crystallinity distribution in the bottle base for a) model-1 b) model2

c) model-3 d) comparison of the models

In the center of the bottle base, there are not significant differences in crystallinity as a function of both the preform temperature and the preform weight for all three models. However, there have been certain differences in crystallinity values between the models as shown in fig 4-22 (d). The model-2, which gives the optimum base thickness, results in lowest and most uniform crystallinity values. For all three models, crystallinity increases across the foot/valley sections of the base towards the side panels of the bottle. This can be observed in simulated crystallinity values (fig 4-23 to 4-25).

Temperature Range: 98-115 °C
Preform Weight: 40 g.
(a)

Temperature Range: 93-110 °C
Preform Weight: 40 g.
(b)

Temperature Range: 93-110 °C
Preform Weight: 34 g.
(c)

Fig.4-23. Simulations of the crystallinity in the bottle base; model-1

Temperature Range: 98-115 °C
Preform Weight: 40 g.
(a)

Temperature Range: 93-110 °C
Preform Weight: 40 g.
(b)

Temperature Range: 93-110 °C
Preform Weight: 34 g.
(c)
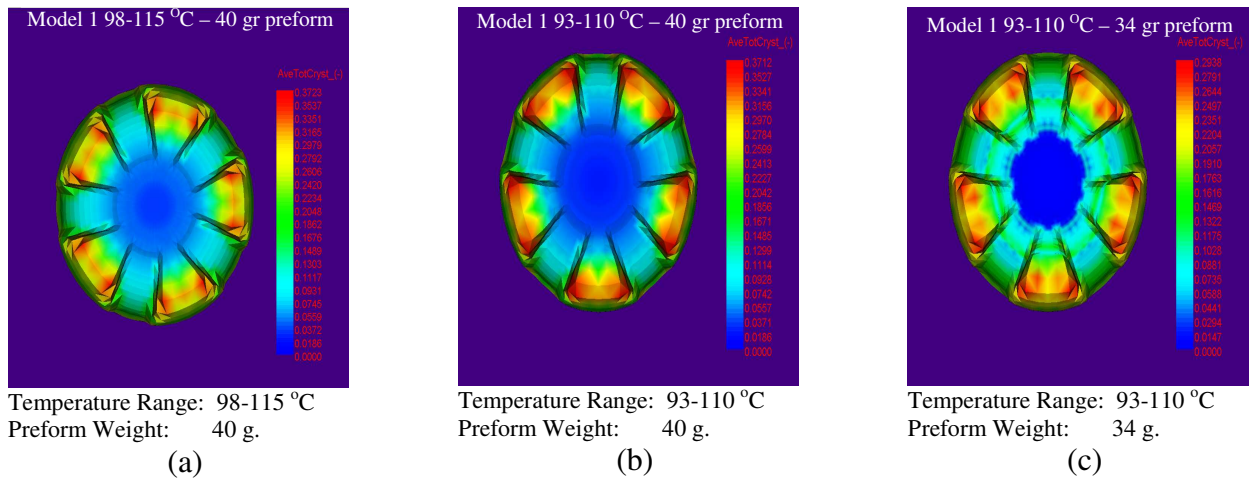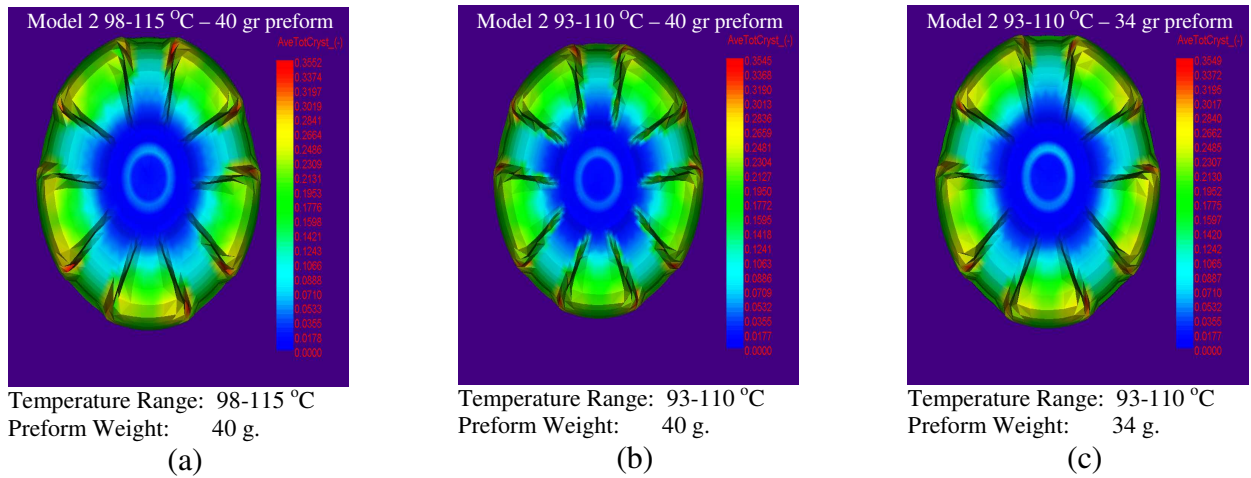
Fig.4-24. Simulations of the crystallinity in the bottle base; model-2

Temperature Range: 98-115 °C
Preform Weight: 40 g.
(a)

Temperature Range: 93-110 °C
Preform Weight: 40 g.
(b)

Temperature Range: 93-110 °C
Preform Weight: 34 g.
(c)
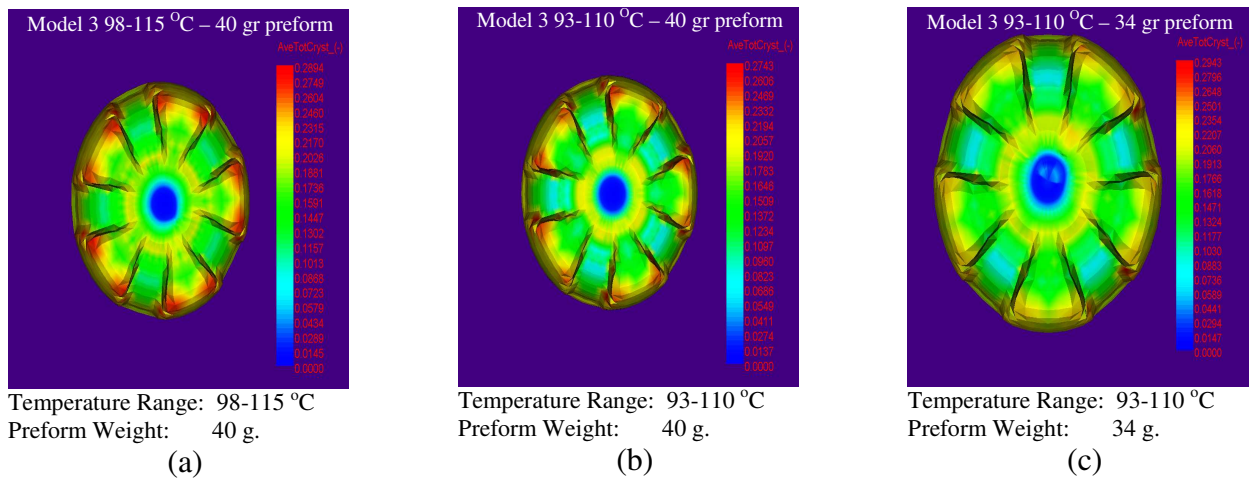
Fig.4-25. Simulations of the crystallinity in the bottle base; model-3

4.3.4 Simulated molecular orientation in the bottle base

The molecular orientation in the bottle base are simulated at two different preform temperature profiles and two different preform weights for each model (Fig 4-26. (a), (b), (c)). Fig. 4-26. (d) compares the simulated molecular orientation in the bottle base for a high preform temperature profile (98 -115 $^{\circ}$C) and a heavy preform (40 g) for the three models.
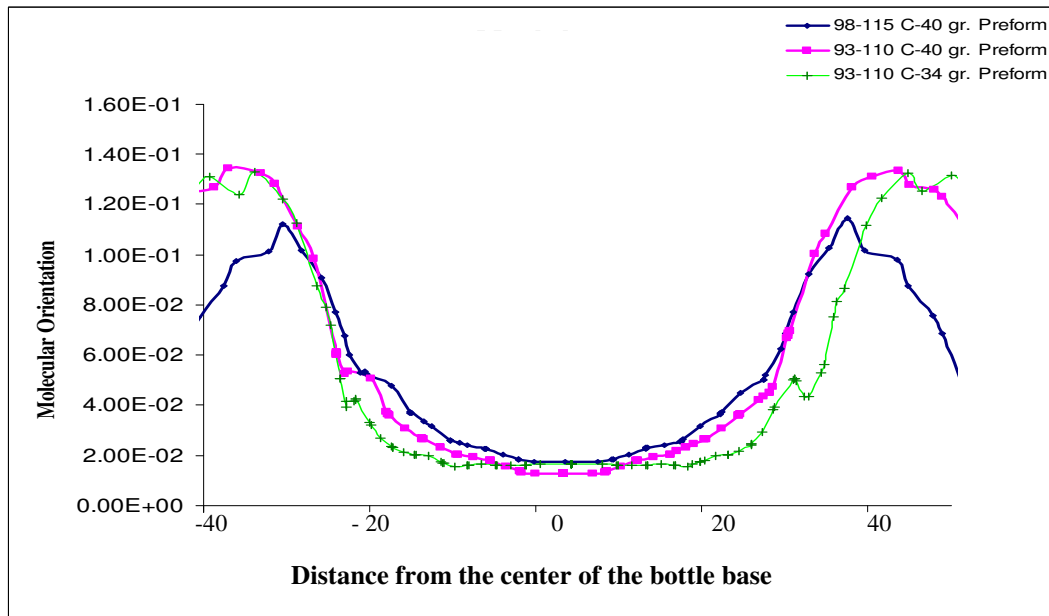
(a)
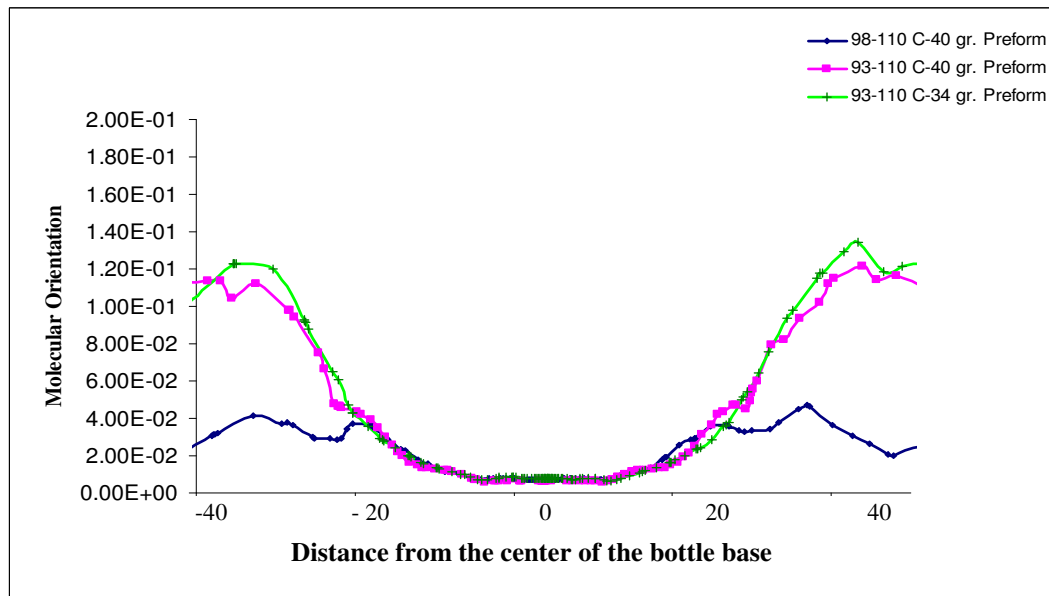
(b)
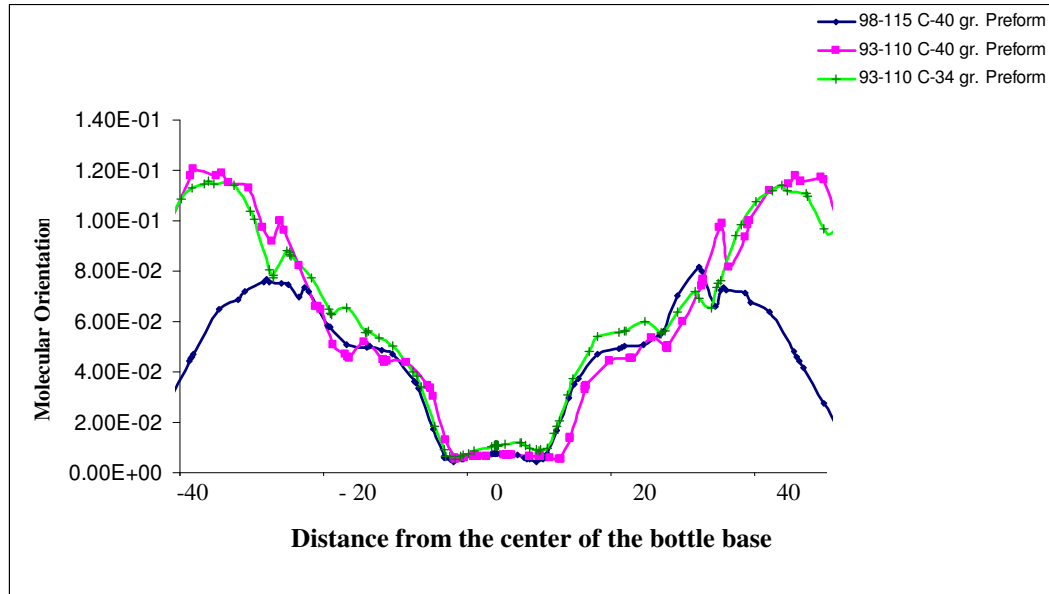
(c)
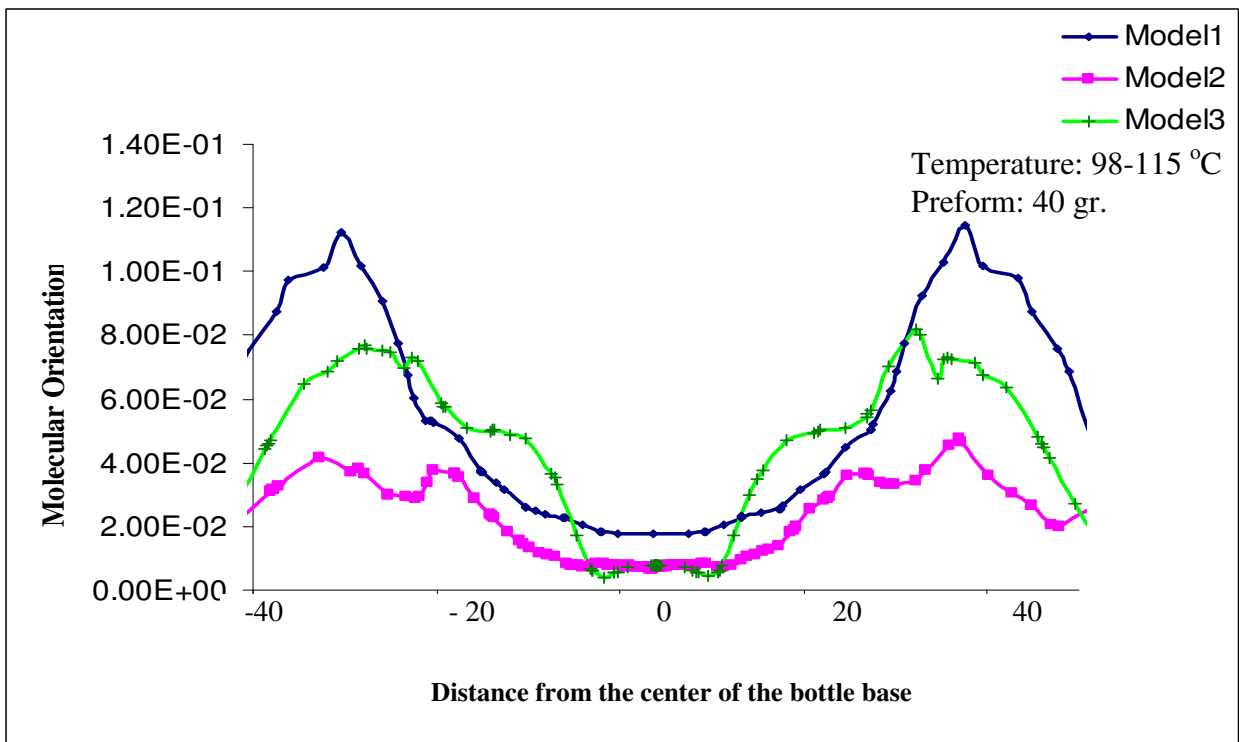
(d)

Fig.4-26. Simulations of molecular orientation in the bottom of the bottle a) model-1 b) model-2

c) model-3 (d) comparison of the models

Molecular orientation increases from the centre of the base towards the side walls of the bottle independent of preform temperature profile and weight. However, the molecular orientation peaks near to the base center in the foot/valley region for high preform temperature profile (98-115 $^{\circ}$C) and heavy preform weight (40 g.). For low temperature profile and light preform, the peak in molecular orientation occurs further down near the side panels of the bottle. It important to note, that the model-2, which gives the optimum base thickness, results in minimum and highly uniform molecular orientation values. For all models, the molecular orientation higher in the foot region of the base compared to the valley; this can be observed in the simulated molecular orientation values (fig 4-27 to 4-29).

Temperature Range: 98-115 °C
Preform Weight: 40 g.
(a)

Temperature Range: 93-110 °C
Preform Weight: 40 g.
(b)

Temperature Range: 93-110 °C
Preform Weight: 34 g.
(c)
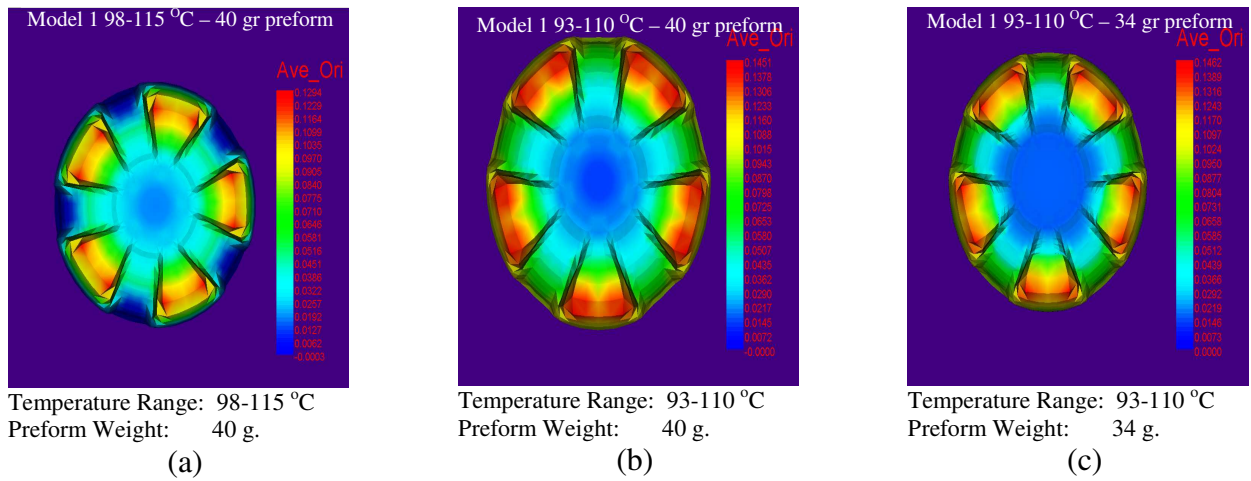
Fig.4-27. Simulation of molecular orientation in the bottle base for model-1

Temperature Range: 98-115 °C
Preform Weight: 40 g.
(a)

Temperature Range: 93-110 °C
Preform Weight: 40 g.
(b)

Temperature Range: 93-110 °C
Preform Weight: 34 g.
(c)
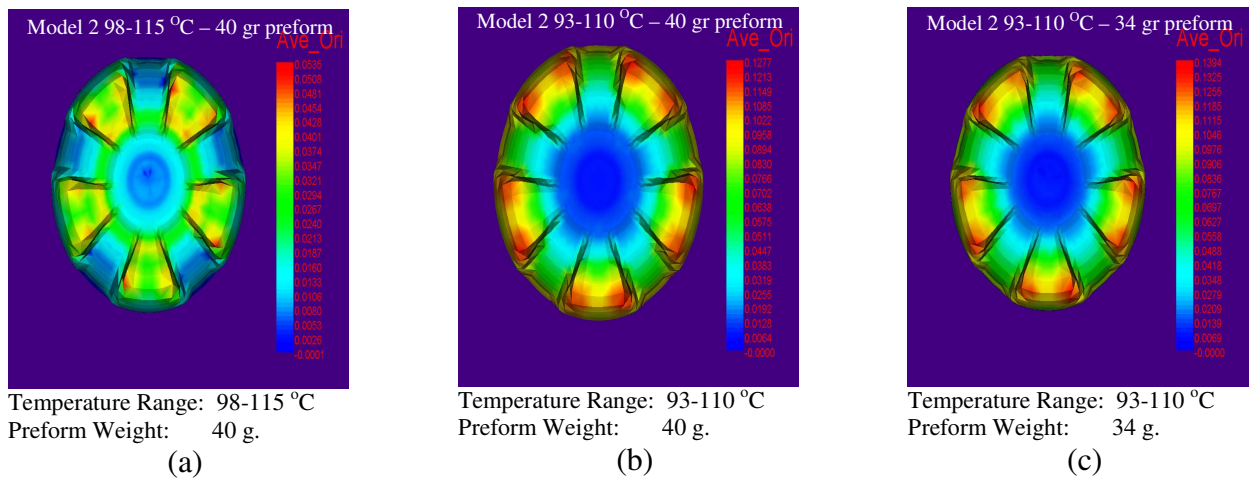
Fig.4-28. Simulation of molecular orientation in the bottle base for model-2

Temperature Range: 98-115 °C
Preform Weight: 40 g.
(a)

Temperature Range: 93-110 °C
Preform Weight: 40 g.
(b)

Temperature Range: 93-110 °C
Preform Weight: 34 g.
(c)
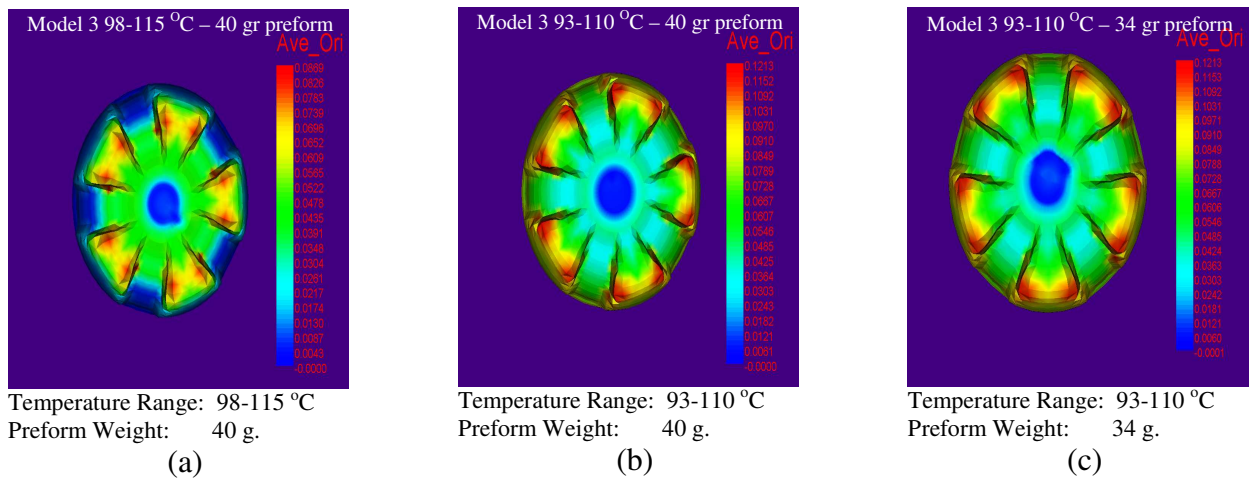
Fig.4-29. Simulation of molecular orientation in the bottle base for model-3

4.3.5 Simulated biaxial ratio in the bottle base

The biaxial ratio in the bottle base are simulated at two different preform temperature profiles and two different preform weights for each model (Fig 4-30. (a), (b), (c)). Fig. 4-30. (d) compares the simulated biaxial ratio in the bottle base for a high preform temperature profile (98 -115 ^{o}C) and a heavy preform (40 g) for the three models.
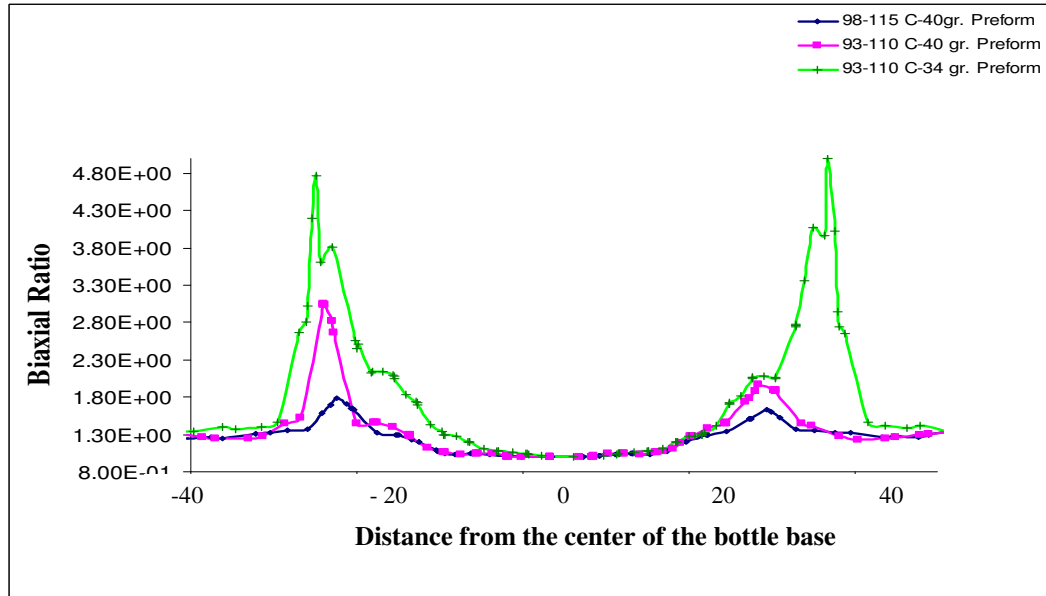
(a)
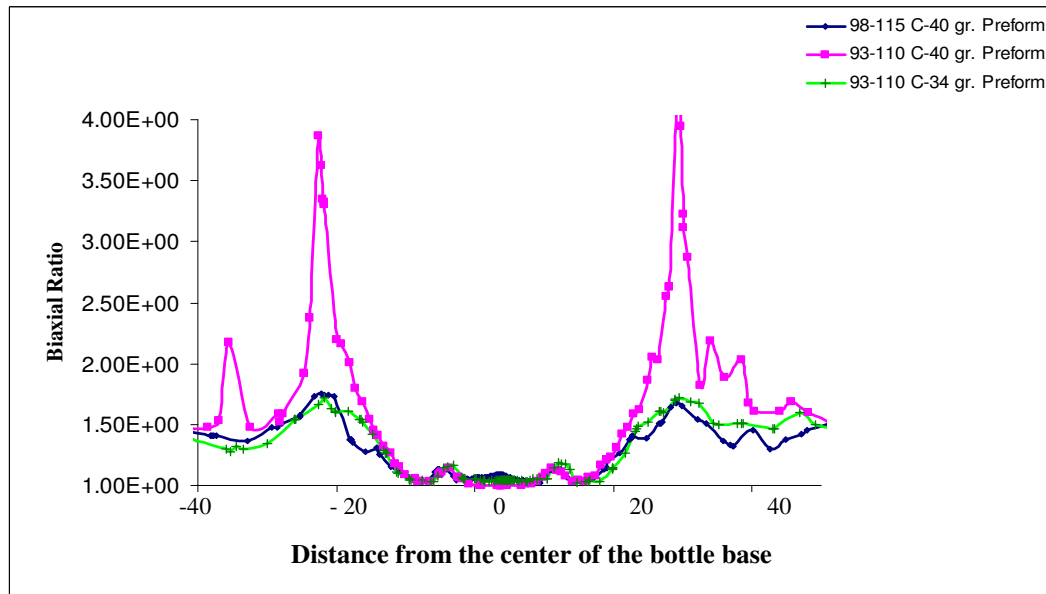
(b)
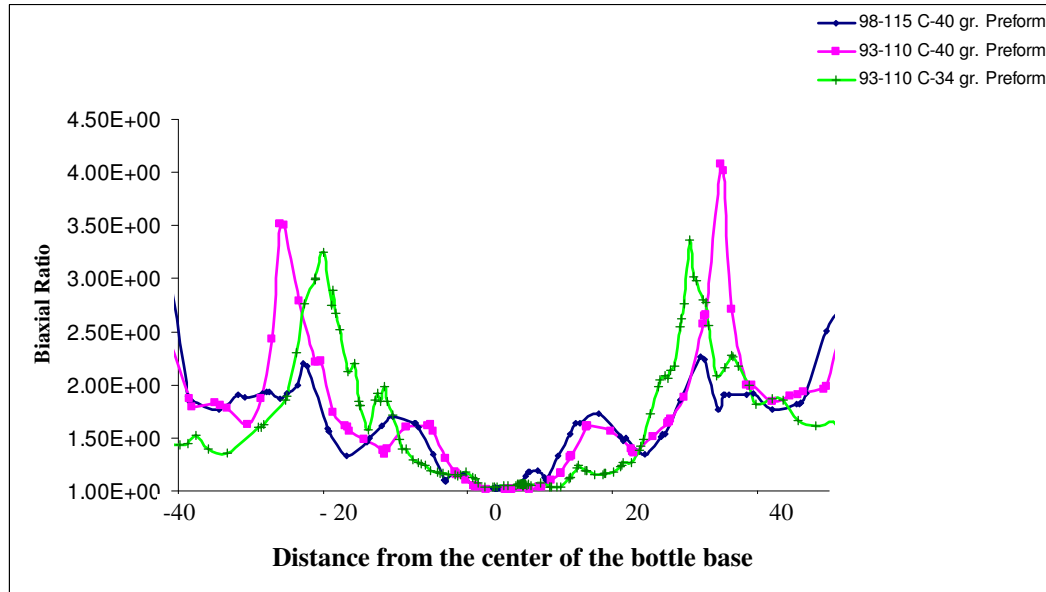
(c)
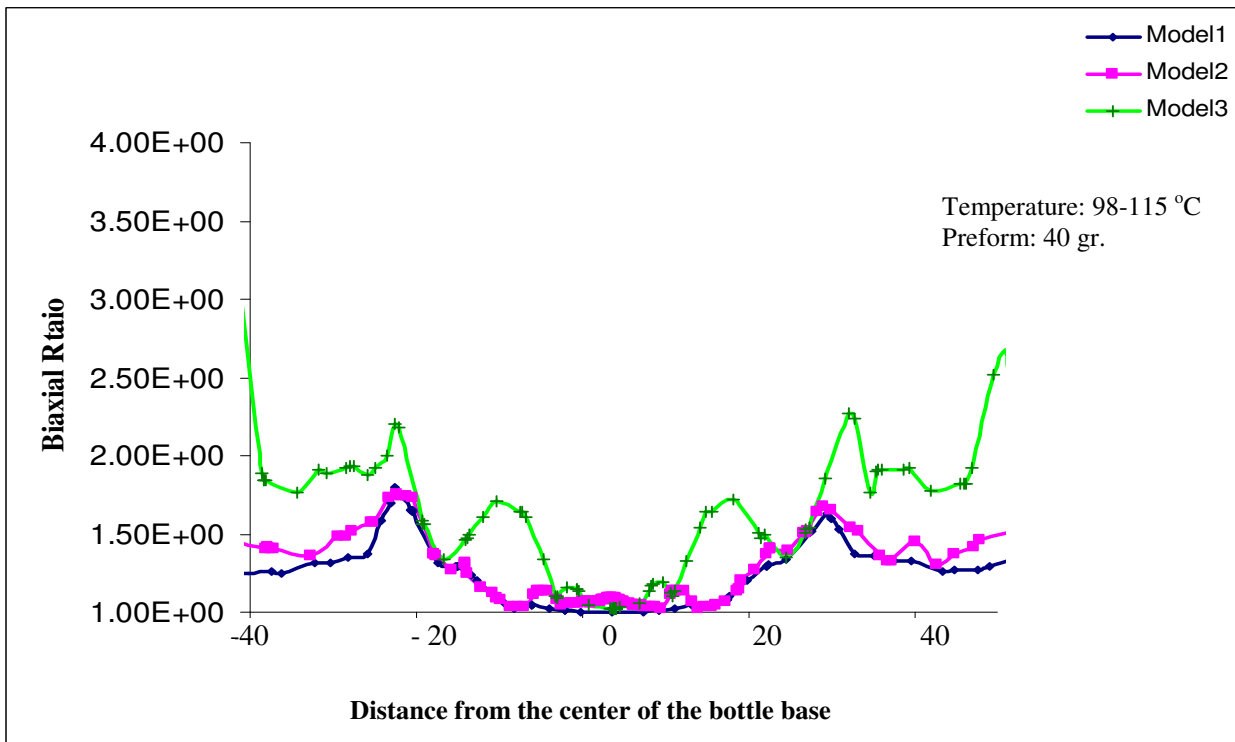
(d).

Fig.4-30. Simulation of biaxial ratio in the bottle base a) model-1 b) model-2

c) model-3 (d) comparison of the models

The biaxial ratio increases from the centre of the base towards the side panels of the bottle for all models. This is because the stretch rod stops at the closed end of the bottle; hence no further axial stretching can take place at the very centre of the base. Whereas, the material in the outer regions away from the centre towards the side wall panels of the bottle, is further stretched radially by the final blow pressure, generating a peak in biaxial ratio in the transition region between the base center and valley/foot region of the base; this can be observed in the simulated biaxial ratio values for all three models. (fig 4-31 to 4-33).

Biaxial ratio increases from the centre of the base towards the side walls independent of processing model used. However, the biaxial ratio peaks in the transition to the foot/valley region for low preform temperature profile (93-110 ^{o}C), low preform weight (34 g) in model-1; and for low preform temperature (93-110 ^{o}C) and high preform weight (40 g) in model-2. For model-3, biaxial ratio peaks in the transition to the foot/valley region at low preform temperature profile (93-110 ^{o}C) independent of preform weight. The model-2, which gives the optimum base thickness, results in minimum and highly uniform biaxial ratio values.

Temperature Range: 98-115 ^oC
Preform Weight: 40 g.
(a)

Temperature Range: 93-110 ^oC
Preform Weight: 40 g.
(b)

Temperature Range: 93-110 ^oC
Preform Weight: 34 g.
(c)
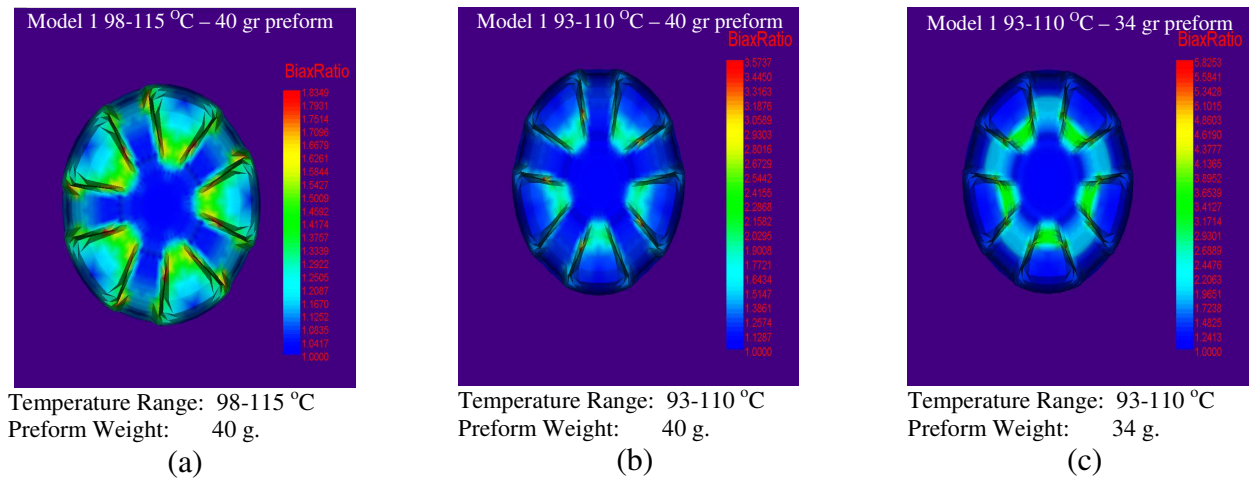
Fig.4-31. Simulations of the biaxial ratios in the bottle base; model-1

Temperature Range: 98-115 ^oC
Preform Weight: 40 g.
(a)

Temperature Range: 93-110 ^oC
Preform Weight: 40 g.
(b)

Temperature Range: 93-110 ^oC
Preform Weight: 34 gr.
(c)
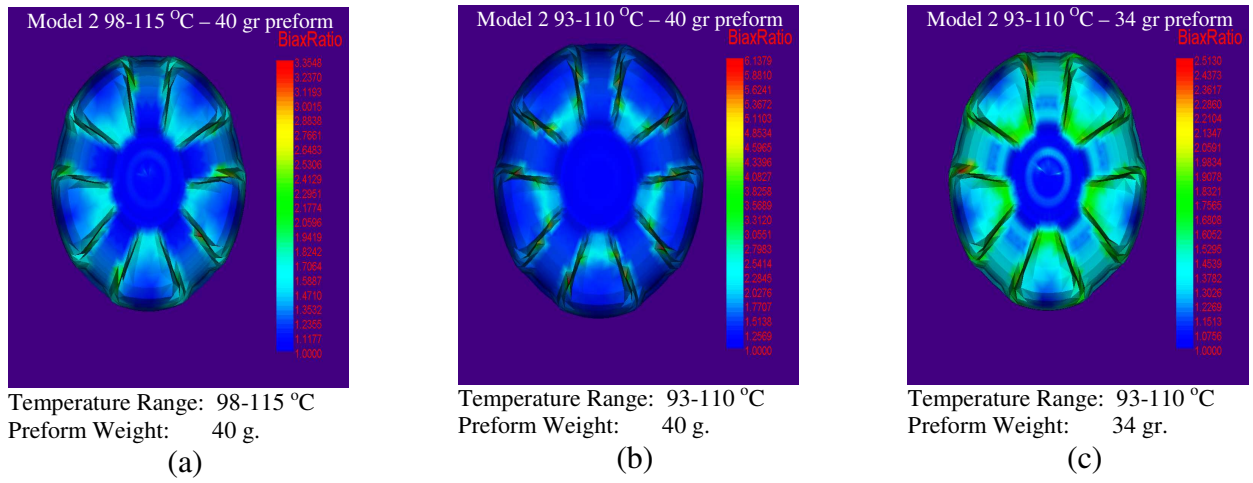
Fig.4-32. Simulations of the biaxial ratios in the bottle base; model-2

Temperature Range: 98-115 ^oC
Preform Weight: 40 g.
(a)

Temperature Range: 93-110 ^oC
Preform Weight: 40 g.
(b)

Temperature Range: 93-110 ^oC
Preform Weight: 34 g.
(c)
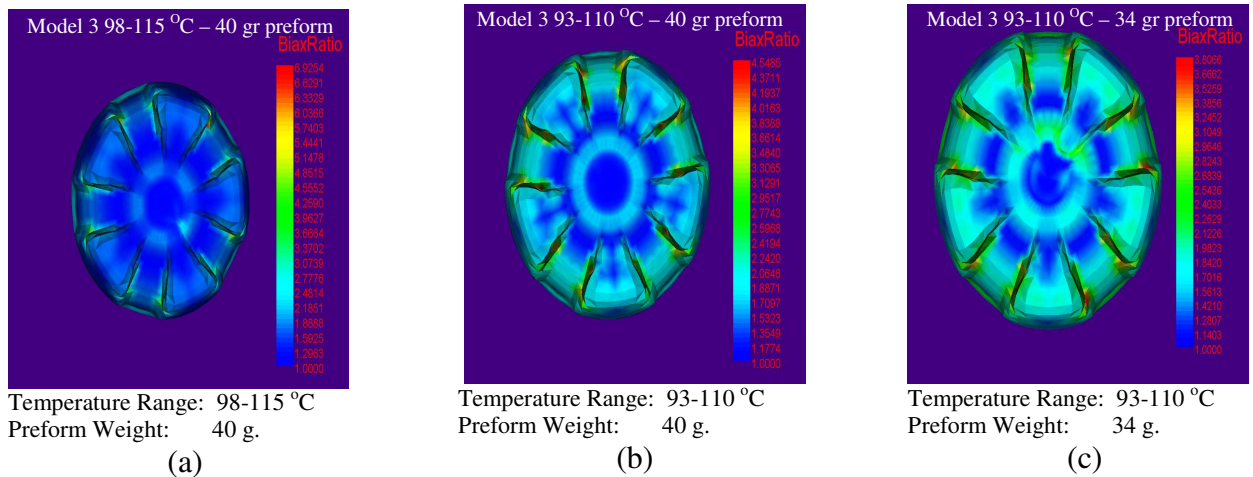
Fig.4-33. Simulations of the biaxial ratios in the bottle base; model-3

4.3.6 The comparison of the simulated properties with respect to the base thickness

The simulated values of the crystallinity, the stress, the molecular orientation and the biaxial ratio are compared with the base thickness of the bottle (fig. 4-34 to fig. 4-37).
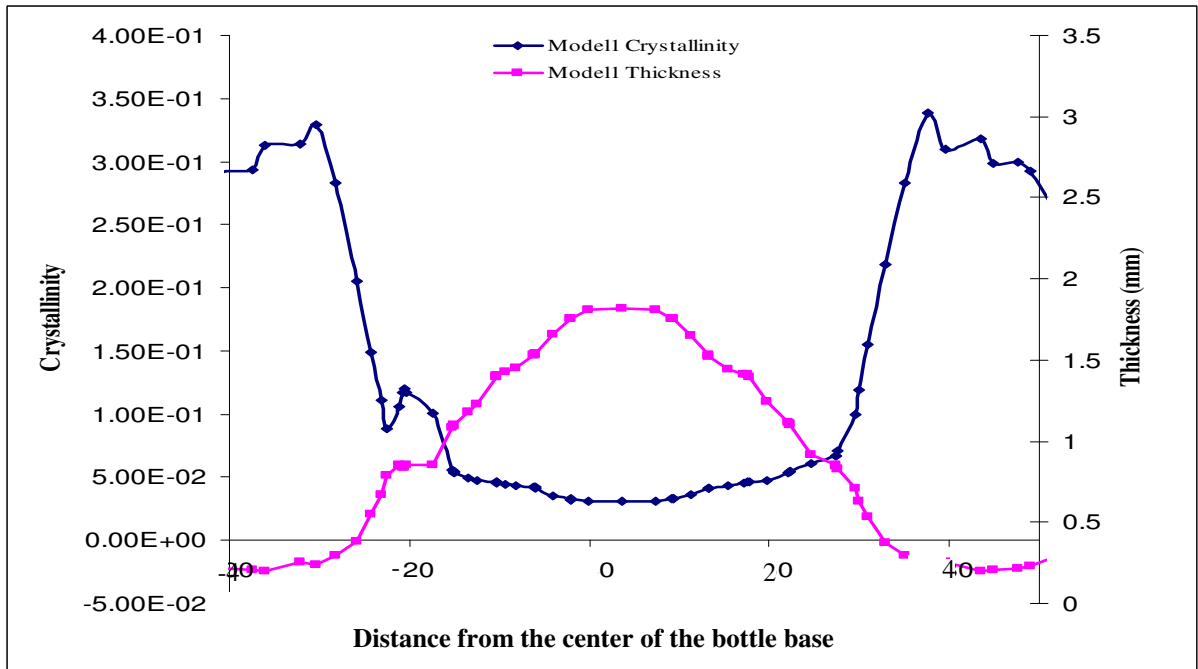
Fig.4-34. The relationship between thickness and crystallinity in the base
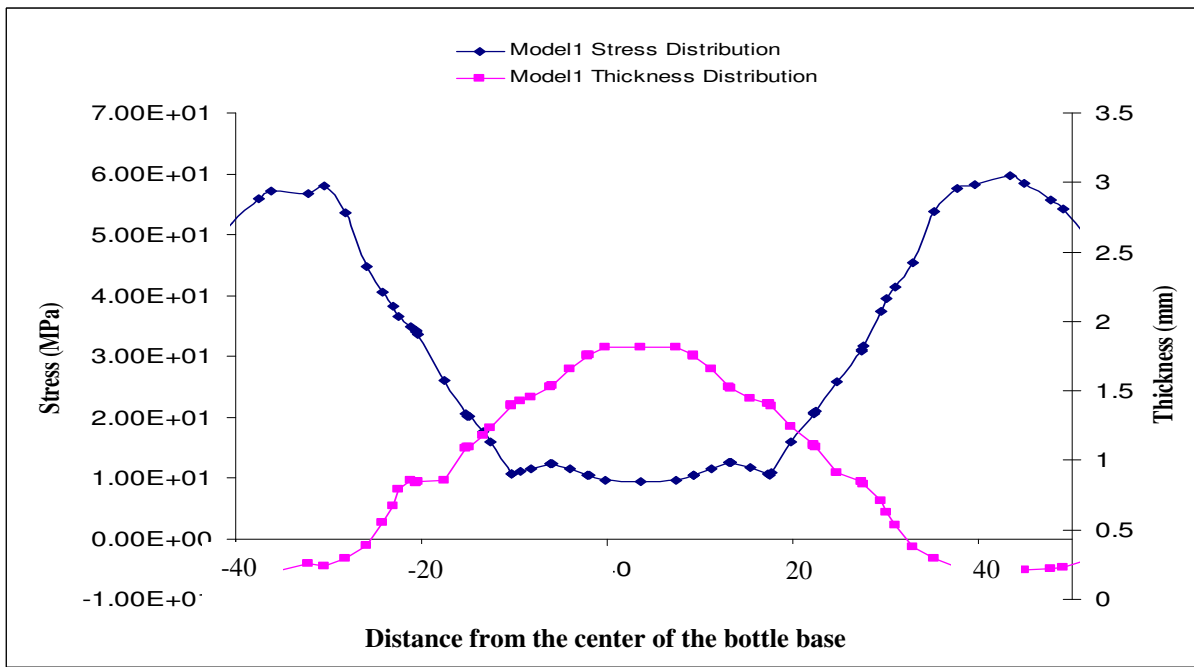
Fig.4-35. The relationship between thickness and stress in the base
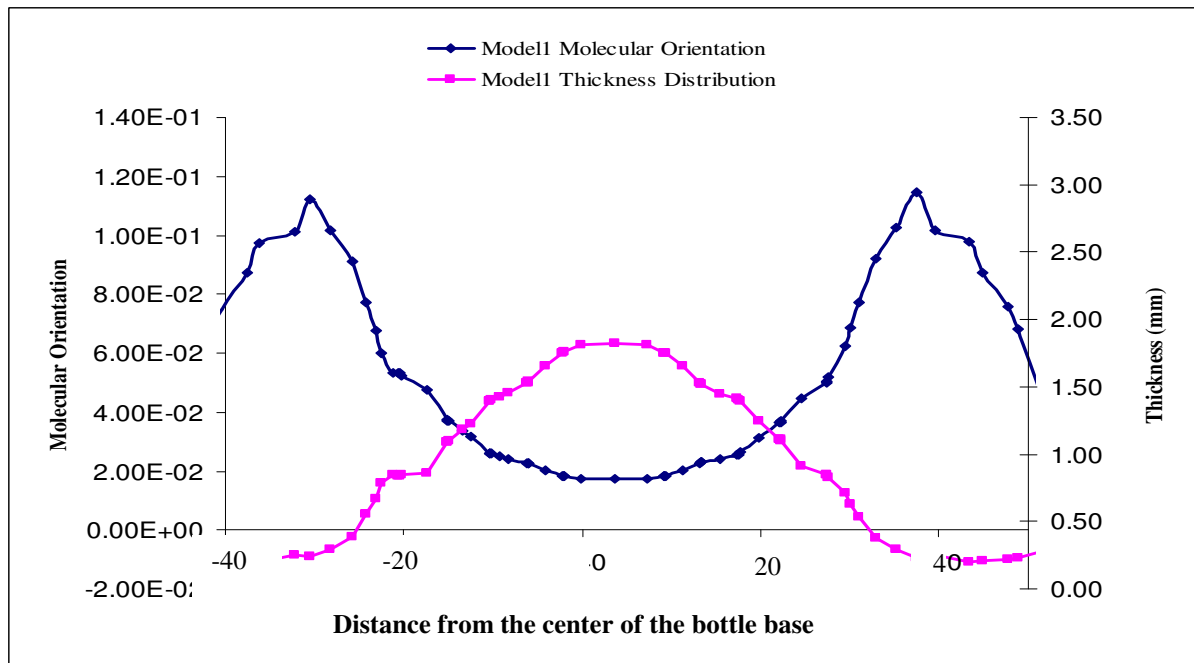
Fig.4-36. The relationship between thickness and molecular orientation in the base
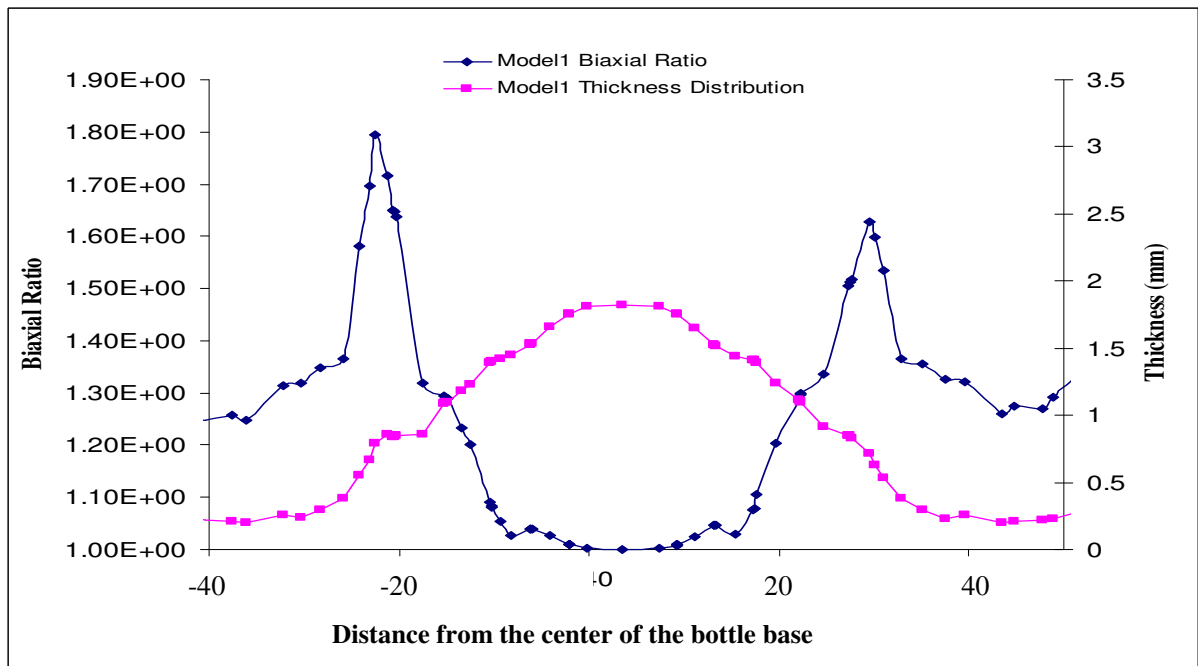
Fig.4-37. The relationship between thickness and biaxial ratio in the base

The crystallinity and the stress decrease with the increasing thickness in the base (fig 4-34 and fig 4-35). Whereas, molecular orientation and biaxial ratio are minimum in the centre of the base and they peak in the transition regions between the centre and the foot/valley region of the base (fig 4-36 and fig 4-37). It was claimed that the circumferential cracks in the bottle are due to the abrupt changes in thickness of the bottle base; the abrupt thickness changes in the base resulted in the abrupt changes in the crystallinity and the molecular orientation; and the transition regions to the valley/foot are the most bi-axially oriented regions of the base [Hanley et al., 2006]. It is confirmed by this simulation, that there is an abrupt change (decrease) in thickness with accompanying changes (increase) in crytallinity and stresses in the base. The molecular orientation and the biaxial ratio peak in the transition regions where the base thickness changes abruptly. In addition, reducing the preform weight from 40 g to 34 g; and processing without the use of the stretch rod caused biaxial ratio to increase; whereas the biaxial orientation ratio somehow decreased with increasing preform temperature profile from 93-110 ^{o}C to 95-115 ^{o}C.

In general, the extent of axial stretching exerted by the rod on the wall panels is higher than the radial stretching carried out by the final pressure in the bottle base. Consequently, the cyrstallinity, molecular orientation and biaxial ratio in the wall panels are expected to be higher than the centre of the bottle base.

4.4 CONCLUSION

In this chapter, the process optimization via the Blow View 8.2 simulation program is explained. In order to achieve a uniform thickness and to minimize stress in the bottle base, two different preform temperature profiles of 93-110 ^{o}C and 98-115 ^{o}C are considered for the 40 g. preform which is currently in use for the production of 1.5 lt. PET bottle. Furthermore, preform weight is reduced to 34 g by changing the standard design. For the new design, only lower preform temperature range of 93-110 ^{o}C is used for the simulation studies. The thickness, stress, crystallinity, molecular orientation, and biaxial ratio in the bottle base are obtained for each processing model. The comments pertaining to each are given under their respective title.

The model-1 introduces highly uniform and minimum wall thickness in the bottle base. In this model, the preform is not stretched due to the stretch rod not being used; excessive PET material is not carried by the rod to the bottle base. Hence, most of the material on the preform walls stays on the side panels of the bottle compared to model-2 and model-3, where stretching relies on the stretch rod movement as well as blow pressure. As the amount of polymer material available in bottle base becomes less, thinner and more uniform thickness is achieved. Whereas for the model-2 and model-3, which depend on the movement of stretch rod, as the amount of the polymer material transported to the bottle base increases, both thicker and less uniform base thickness are obtained. Hence, theoretically, it is more suitable for the stretch rod not to be used in ISBM process in terms of achieving uniform isnd thinner base thickness.

On the other hand, analysis of simulated stress results reveals that, for the model-2, it is possible to minimise stress in the bottle base. Although, preform temperature range and the weight of preform also affect the stress in the bottle base; the thicker the base, the smaller the stress becomes; but the changes in thickness become abrupt with the increasing base thickness and hence the stress cracking may be adversely affected if the strain hardening point has not been reached during stretching of the base. In general, higher stress values are found in the foot and valley regions of the bottle; and the lower stress values are recorded in central region of the base.

For model-2, simulation studies indicate that the crystallinity, biaxial ratio and molecular orientation all decreased at the bottle base while minimizing stress. Although uniformity of the base thickness is not achieved in model-2, as long as the stress in the base is minimized, a non-uniform base thickness may provide the environmental stress crack resistance if the stretching of the base is sufficient to induce strain hardening. Hence, it can be concluded that the injection stretch blow moulding parameters are optimised when the bottle is processed according to the model-2.

Chapter 5

EXPERIMENTAL PROCEDURES AND EVALUATION OF THE OPTIMISED BASE DESIGN

5.1 INTRODUCTION

Injection stretch blow moulded PET bottles are subjected to various performance tests before being qualified for packaging purposes in industry. Whilst the specifics of the quality regime are directly dependant on the type of liquid to be kept in the bottle, the following tests are generally applied:

- Burst Pressure Test

- Top Load Test and Material Distribution

- Environmental Stress Crack Resistance Test

- Crystallinity

- Drop Test

- Permeability to Liquids and Gases

For the purposes of this study the first four tests are regarded as sufficient to assess bottle quality.

In this study, bottle samples of each base design were produced using a two-stage stretch blow machine. 40 g injection molded preforms was used throughout. The process parameters are given in table 5-1.

Table 5-1. Injection stretch blow molding process parameters for the 1.5 lt. bottle

Process Parameters	
SCREW	
Diameter	38 mm
Screw speed	100 rpm
Nozzle Diameter	3 mm
HOT RUNNER BLOCK	
Sprue	275°C
Block	275°C
Nozzle	295°C
BARREL TEMPERATURE	
Front	275°C
Middle	275°C
Rear	270°C
Nozzle	275°C
INJECTION PRESSURE	
Primary	140 Kgf/cm^2
Secondary	60 Kgf/cm^2
Injection speed	200 m/s
STRETCH BLOW MOLDING	
Cold preform temperature	80 °C
Preform re-heat temperature	109 °C
Pre-blow	1.25 MPa
Final blow	4 MPa
Water temperatures	Base: 12°C
	Shell: 12°C
	Oven: 10°C
Machine Oil Temperature	35°C
Stretch Rod Speed	1.0 m/s
Stretch rod outside diameter	14 mm
Process time	2.48 sec.

To investigate the effect of preform temperature, samples of the new (optimised) bottle were produced using preform temperatures of 105, 110, and 115 ^{o}C. The bottles with the optimum base produced under this process operating conditions were fully formed but there has been a slight pearlescence problem for the bottles produced at 105 ^{o}C preform reheat temperature. Also some contact problem was observed on the optimum base of the bottle. Some measures have been taken to eliminate this problem; e.g. reducing the friction between the bottle base and the mold, and removing air pockets that developed between the mold and the bottle surfaces

5.2 EXPERIMENTAL

5.2.1 Burst pressure

Carbonated beverages pressurise the bottle at up to 100psi (7 Bar). The pressurised bottle should not expand excessively, or worse still blow up, at the bottler's filler line.

A number of factors can lead to low bottle burst strength; insufficient wall thickness in some areas due to poor material distribution, wide mould parting lines that may be due to loss of mould compensation (neck, shoulder or side-wall failure), mould damage, etc. Similarly, excessive expansion can occur in the shoulder or panel regions as a result of low section weight or poor material distribution.

AGR Plastics pressure tester, with ramp fill capability. The test head seals the brink of the bottle. The bottle is filled with water and pressurised rapidly to 100 psi. The pressure is then increased at a controlled rate until the bottle fails or the maximum pressure limit of the tester is reached.

5.2.1.1 Apparatus:

In the analyses, AGR Plastic Pressure Tester with Ramp Fill capability is used.

5.2.1.2 Procedure:

a. A reporting system is firstly ensured to input results throughout the conduct of this test. This may be a computer based stored program control system, Excel spreadsheet or manual report form.

b. The "Ramp Fill" mode of testing is selected.

c. The "Initial Pressure" is set at 100 psi and the "Expansion Limit" is set to 'none'.

d. The bottle is positioned into the neck support feature inside the test chamber.

e. The door of the test chamber is closed. There is a safety interlock on the door, if not fully closed, the Burst Tester will not commence testing the bottle.

f. The 'Test Button' is pressed. The test head clamps down and seal the finish of the bottle. The Burst Tester then fills the bottle with water, rapidly increases pressure to the "Initial Pressure" setting and then ramps the pressure up until failure occurs or the maximum pressure limit of the tester is reached.

g. If the bottle bursts, the 'Fail Indicator' lights up in red. The 'Pass Indicator' lights up in green if the bottle does not burst.

h. When the test is completed, the 'test head' rises. The chamber door is opened and the bottle is removed.

i. The "Bottle Pressure" result is recorded.

5.2.2 Top load strength test

5.2.2.1 Apparatus:

Top load strength tests were conducted using the INSTRON 4466 instrument with a system connected to a computer.

5.2.2.2 Procedure:

a.   The bottle to be tested is firstly positioned into the test instrument

b.   A compression force is applied on the top of the bottle

c.   When the bottle is cracked or bended by the force, the test is completed

d.   Maximum load and the load at failure are recorded by computer system.

5.2.3 Material and the weight of bottle sections

In order to measure the material on the bottle, the bottles are sectioned into three parts. These three sections are named as base, centre, top, and these sections' distances from the base are 53.3 mm and 194.3 mm. In this process, it is important that the bottle be separated into its sections by means of an appropriate apparatus that will not allow any material lost. Therefore, conducting this process through a sharp material is an inconvenient method. To this end, an electrical mechanism, which consists of a thin filament that can be heated through electrical current and two folding frames that one of them is mobile and the other one is immobile is used and pictured in fig. 5-1. In addition, there is another cylindrical apparatus in the middle of the mechanism firmly clamping the bottle to be cut. Hence, the bottle sections can be separated from each other by melting the PET material via the hot filament.

The bottle is divided into three sections namely the base, body and top by means of a custom made apparatus as shown in fig. 5-2. The three sections of the bottle, which are shown in fig 5-3, are separately weighted by means of the precision scale and the values are recorded for assessment.
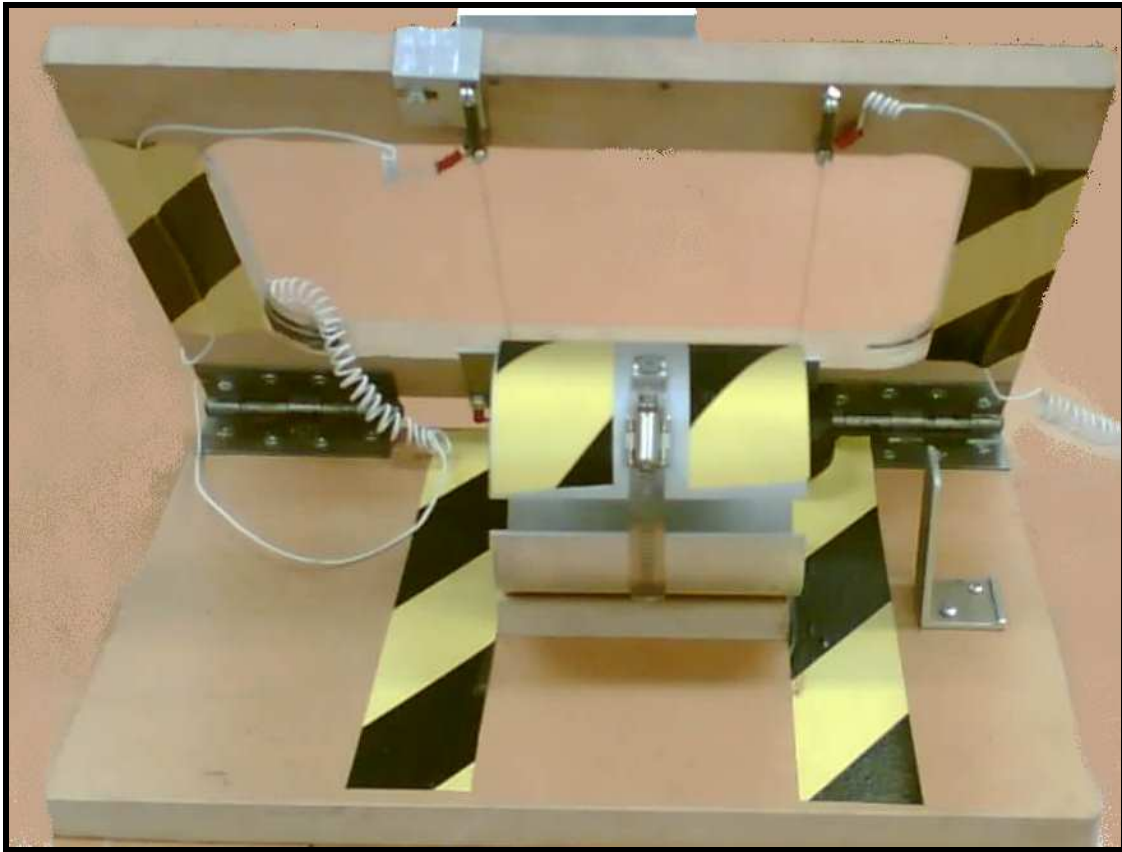
Fig.5-1. Apparatus developed for cutting of PET bottles

Fig.5-2. The base, body and top section of PET bottle

The thickness is very important as well as weight of bottle sections. Especially on the bottle base, increasing the amount of the PET material is to increase the thickness of this section which directly relates to the crack formation in the base. Therefore, the base thickness values for the foot, valley, and central regions of the new and standard bottles (preform reheat temperature 105 ^{o}C) are measured by vernier caliper.

5.2.4 Environmental stress crack resistance tests

5.2.4.1 Apparatus

a. Accelerated Stress Crack Test Unit (ASCRU)

b. Scales

c. 0.20% Sodium Hydroxide Solution (NaOH)

d. Computer

e. DATALYZER SPECTRUM SQC Program

f. Safety Glasses

5.2.4.2 Preparation environmental stress cracking agent

a. Caustic Solution must be prepared using pellets of concentrated NaOH

b. Two grams of NaOH pellets should be added to every 1 liter of cool tap water

5.2.4.3 Procedure

a. All bottles to be analyzed are collected and prepared to analysis

b. It is ensured that drain valves from each compartment are closed

c. Approximately 500ml (enough to immerse the base of the bottle) is added to each compartment

d. Each bottle is labeled and filled to flange with cool tap water

e. Each bottle is attached to the unit by screwing the finish to the metallic caps

f.   Each bottle is placed into appropriate compartment and lid is closed and latches are secured

g.   The unit is switched on.

h.   To initiate each sample, the corresponding start button is pressed and held until it lights up

i.   Undetected leaks are checked at 15 and 30 minutes into the test.

j.   The unit is to display the time when bottle fails. It is allowed for 1 hour for test to complete and then the failure time and location of failure on the base are recorded.

5.2.5 Thermal stability test

The Thermal Stability Test is designed to measure dimensional changes of filled carbonated PET beverage bottles induced by thermal stresses that occur during the life of the filled bottle. Satisfactory Thermal Stability performance is considered as a critical requirement by the bottlers.

A carbonated product exerts pressure on the inside of a bottle; and as temperature increases this internal pressure increases, causing the bottle to expand and creep as function of time. Excessive creep will cause the beverage fill level to drop, which will negatively affect appearance of the package and reduce shelf life of the product.

5.2.5.1 Apparatus:

a.   Separate controlled storage facilities capable of maintaining storage temperatures of 22±1°C and 38±1°C

b.   Height gauge with scribe

c.   Vernier diameter measurement tape (Pi Tape)

d.   Dial or Vernier Calipers

e.   Base clearance gauge

5.2.5.2 Procedure

1. Bottles to be analyzed, as many as required, are selected for this test

2. A height gauge fitted with a scribe to mark the appropriate nominal product fill level onto each bottle is used.

3. Height of all samples to the bottom of the neck support ledge is measured.

4. The label panel diameter of all samples are measured with a Pi tape

5. Pinch diameter and the base diameter are measured with calipers

6. The base clearance of all samples is measured.

7. All bottles are chemically carbonated to a certain target level.

8. All bottles are stored at 22 ± 1°C for 20 - 24 hours.

9. All bottles are transferred to the 38 ±1 °C storage facility and stored for 24 hours.

10. All bottles are removed from the 38°C storage facility and allowed to condition at 22 ± 1°C for 4 hours

11. The bottle perpendicularity, the minimum and maximum heights are measured and the average of the minimum and maximum heights is recorded as the final height.

12. Measurements in the number 5 and 6 are repeated.

13. The "Fill Point Drop' which is the distance between the scribed reference line and the bottom of the product meniscus is measured.

$$\% \text{ Increase} = \frac{(\text{Final height or diameter dimension}) - (\text{Initial empty bottle dimension})}{(\text{Initial empty bottle dimension})} * 100$$

$$\text{Final Pinch / Base Ratio} = \frac{(\text{Final Pinch diameter})}{(\text{Final Base diameter})} * 100$$

5.2.6 Chemical carbonation procedure for thermal test

Carbon Dioxide generation in the CSD bottle is required to carry out the thermal test. In this study, a procedure obtained from packaging companies is employed, which describes a method of carbonation using chemicals to generate the Carbon Dioxide, and it is given concisely as follows.

This procedure is applicable to the carbonation of any rigid container, specifically PET bottles. In addition, the carbonation with PET bottles will be approximately 5% lower than the target level due to the initial bottle expansion and absorption of CO_2 into the bottle wall, at 1–2 days after preparation by this procedure. Therefore, the carbonation level should be 5% higher than the target level.

5.2.6.1 Apparatus:

a.   Laboratory Balance with an accuracy of ± 0.01 gram or better.

b.   Film wrap such as 'Cling' or 'Glad'.

c.   Citric Acid, monohydrate, $COOHCH_2C$ (OH) $COOHCH_2COOH.H_2O$

d.   Sodium Hydrogen Carbonate ($NaHCO_3$) or Sodium Carbonate (Na_2CO_3)

e.   Water at 18 – 23 °C and closures

5.2.6.2 Procedure:

a) Principle:

Carbon dioxide (CO_2) can be generated by the reaction of citric acid and sodium hydrogen carbonate in water according to the chemical equation (1) or citric acid and sodium carbonate in water according to the chemical equation (2).

b) Using sodium hydrogen carbonate:

$3\ NaHCO_2 + COOHCH_2C\ (OH)\ COOHCH_2COOH.H_20$

$$\longrightarrow COONaCH_2\ (OH)\ COONaCH_2COONa + 3\ CO_2 + 3\ H_2O........\ (1)$$

c) Using sodium carbonate:

$3\ Na_2CO_2 + 2\ COOHCH_2C\ (OH)\ COOHCH_2COOH.H_20$

$$\longrightarrow 2\ COONaCH_2\ (OH)\ COONaCH_2COONa + 3\ CO_2 + 3\ H_2O ......\ (2)$$
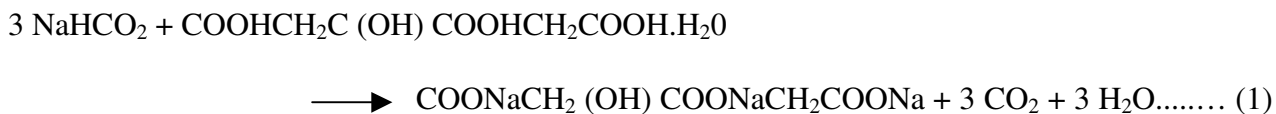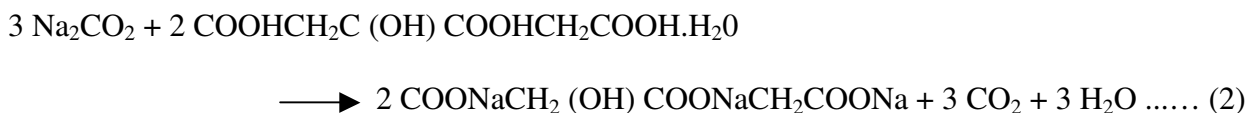
5.2.6.3 Definitions and calculations:

1. Beverage Carbonation is measured in gas volumes:

One gas volume = volume of CO_2 gas at 15.5 ℃ (60 ℉) and 1 atm. pressure that will dissolve in

an equal volume of liquid

E.g.: 1.5 liter bottle at 4.0 volumes = 1.5 x 4.0 = 6.0 liters of CO_2 at 15 ℃ and 1 atm.

a) Calculations using sodium hydrogen carbonate

b) Amount of sodium hydrogen carbonate (base) required:

$W = (Z\ /\ 22.4)\ *\ (Molecular\ Weight\ of\ NaHCO_3 = 84.0)\ *\ Y$

$W = 3.75\ *\ Z\ *\ Y\ grams$

Where:

W = Weight of base (grams)

Z = Brimful capacity of container (liters)

Y = Carbonation required (Gas Volumes)

c) Amount of citric acid required:

$$X = \frac{(1/3) * (W) * (\text{Molecular Weight of Citric Acid} = 210.1)}{\text{Molecular Weight of NaHCO}_3 = 84.0) * 1.08 \text{ (to ensure an excess of acid)}}$$

X = 0.90 * (W) grams

Where:

X = Weight of Acid (gram)

d) Calculations using sodium carbonate

e) Amount of sodium carbonate (base) required:

W = (Z / 22.4) * (Molecular Weight of $Na_2 CO_3$ = 106.0) * Y

W = 4.7 * Z * Y grams

e) Amount of citric acid required:

X = (2/3) * (W) * (Molecular Weight of $COOHCH_2C$ (OH) $COOHCH_2COOH.H_20$ = 210.1/

Molecular Weight of $Na_2 CO_3$ = 106.0) * 1.08 (to ensure an excess of acid)

X = 1.43 * (W) grams

1. The nominal fill level of the bottle is identified, and scribed a line (or mark with permanent marker) at this level onto the bottle

2. The amount of Citric Acid and Sodium Hydrogen Carbonate or Sodium Carbonate required for each bottle are calculated

3. Into an empty bottle, the required amount of Citric Acid to the nearest 0.1 of a gram is weighed and the bottle is filled with water at room temperature just below the fill level.

4. A closure is applied and the bottle is shaked until all Citric Acid is dissolved.

5. The level of the water is adjusted up the fill level marked on the bottle.

6. A piece of film wrap is cut with large enough to be able to roll the base chemical into a cylinder, small enough to pass through the finish opening.

7. The required amount of Sodium Hydrogen Carbonate or Sodium Carbonate is weighed onto the film wrap and rolled to fully encase the chemical.

8. The chemical roll is inserted into the bottle, the bottle is squeezed to remove the headspace air, and a closure is applied.

9. The bottle is vigorously shaked to release the chemical from the fill wrap.

10. After approximately 5 minutes, the bottle is shaked again until the chemicals have been fully dissolved.

5.2.7 Crystallinity

In order to explain the reason for the cracks that occur on the PET bottle base and to explain the differences in the resistance times against ESC, crystallinities at five critical points both in the standard and optimum bottle bases were obtained by Modulated Differential Scanning Calorimetry (MDSC) method (fig. 5-3).

5.2.7.1. Apparatus:

a.   MDSC 2920, TA Instrument.

b.   Laboratory balance with an accuracy of ± 0.0001 gam or better.

c.   Crimped aluminum pans

d.   A clamp to assemble aluminum pans

5.2.7.2. Procedure:

a.   Approximately 10 mg of the sample is cut from the identified points in the bottle base

b.   The sample is accurately weighed and put into the crimple pans

c.   Two heating and cooling cycle between 25 and 280°C are applied on the sample. All heating and cooling rates are 2°C/min with temperature modulation ± 0.5 °C for every 40 sec.
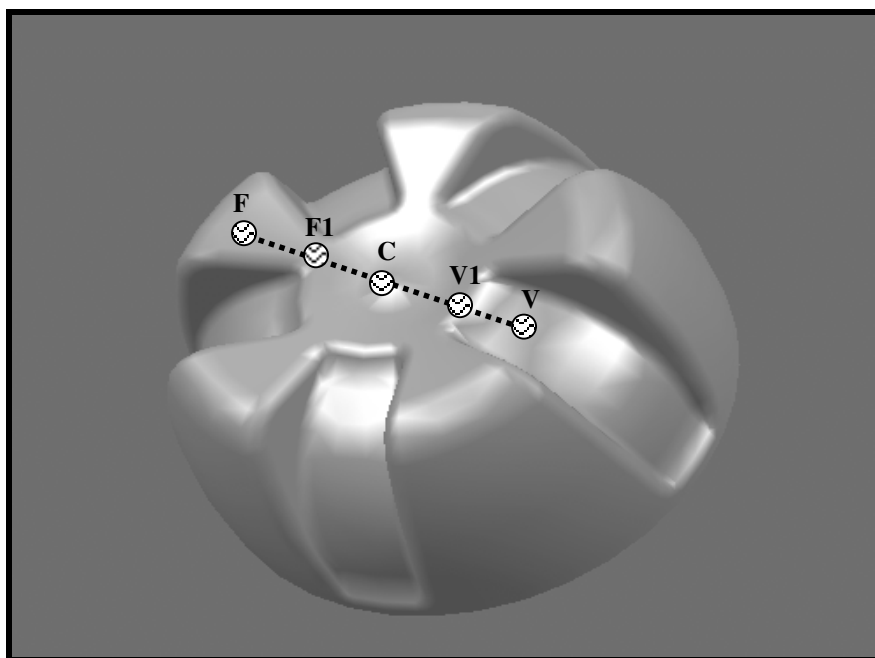
Fig.5-3. Points at which crystallinity values observed by SEM

Table 5-2 Regions and represents used in MDSC

Regions	Represents	Distance from the base center (mm)
Valley	V	30
Transition to valley	V1	13
Centre (Injection point)	C	0
Transition to foot	F1	13
Foot	F	30

5.2.8 Environmental scanning electron microscopy (ESEM) and optical microscopy

In order to explain the mechanism of environmental stress cracking, of the crack morphology both for the standard and the new bottle bases are studied by Environmental Scanning Electron Microscopy (ESEM) and optical microscopy. The specimens used in the analysis were collected from samples tested by the Environmental Stress Crack Resistance (ESCR) tests. The results obtained from this study are based on observation of specimens via Environmental Scanning Electron Microscopy (FEI Quanta 200 ESEM) as shown in fig. 5-4 and Optical Microscopy (Olympus Twin Optic). The observations have been useful in terms of explaining the initial crack location, its direction, appearance of cracks and ultimately shedding a light in the significant difference between the ESCR of the standard and optimized bottles.
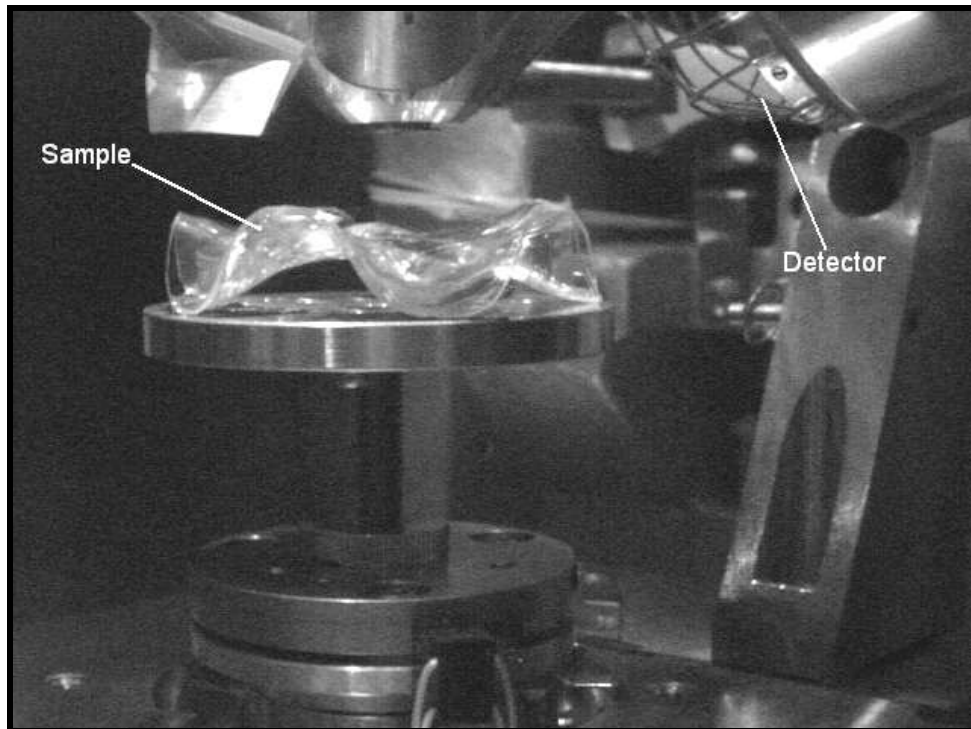
Fig.5-4. ESEM analysis chamber and the sample of the cracked bottle base

Apparatus and accessories used in this study and their settings are as follows:

a.   FEI Quanta 200 ESEM - Scanning Electron Microscope

      (Low Vacuum, High voltage = 15.0 kV, Pressure= 0.5 Torr, Filament current = 2.02 A

      Emission current = 102 μA)

b.   Olympus Twin Optic Optical Microscope

      (zoom magnification=1.8x10, Optic GSWH 10x22)

c.   Kyowa Fibre Optic FL6 light source

d.   Pixelink Digital Image Capture System (resolution 1600x1200 pixels = 2Mp)

5.3 EXPERIMENTAL RESULTS AND DISCUSSION

5.3.1 Burst strength

Burst strength tests both for the standard bottle, were carried out within three days after the

bottles were produced by the stretch blow molding process. In order to determine the effects of

the temperature of the preforms on the performance of the bottles, burst strength test were also

conducted for the new bottles on the new (optimized) bottles which were produced using three

different preform temperatures of 105, 110 and 115 $^{\circ}$C.   These values refer to the average

temperatures on the preform. Whereas, the standard bottles which are currently used in industry

were produced under the standard industrial operating conditions only.

Burst pressures and volumetric expansions are given in table 5-3 and figure 5-5. Burst pressure

indicates the maximum pressure that the bottle can bear, and volumetric expansion gives the

change in volume at the time of failure.

Table 5-3. Burst strength performance of the bottles

	Burst Pressure (psi)	Expansion (ml)
Standard Base	205±02	579±75
Optimum Base	194±02	541±53
Optimum Base (Preform Temp. 105 ^{o}C)	204±18	411±92
Optimum Base (Preform Temp. 110 ^{o}C)	197±02	435±44
Optimum Base (Preform Temp. 115 ^{o}C)	179±04	510±66
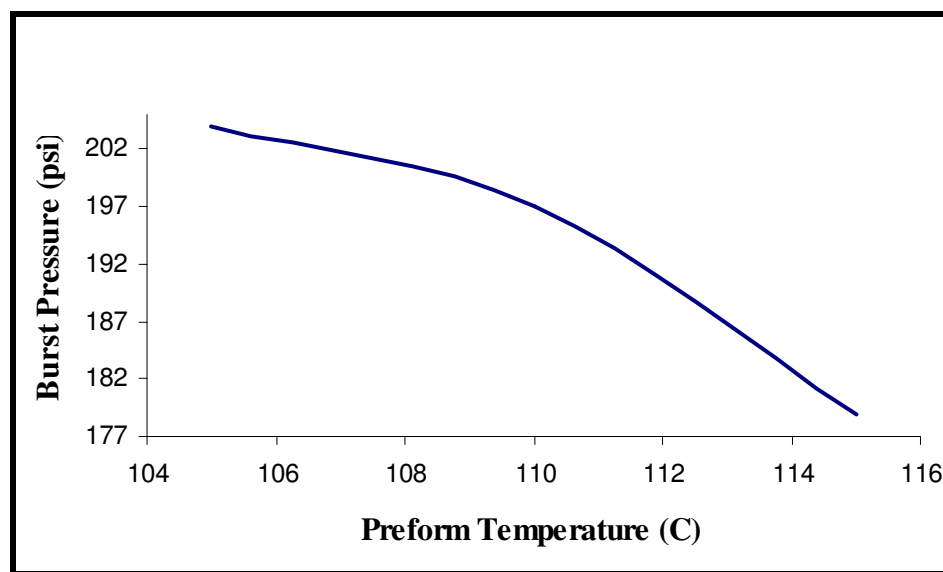
Fig.5-5. Burst strength performance of the bottles

Except for the bottle produced at the preform temperature of 105 ^{o}C, the burst strength and volumetric expansion of the new bottle was reduced relative to the standard bottle. However, considering the standard variation of the results, the differencences between the bottles are not statistically significant.

5.3.2 Top load strength

The top load strength tests were carried out 3 days after the bottles were produced by the Stretch

Blow Molding Process. The results are given in table 5-4 and figure 5-6.

Table 5-4. Top-load performance of the bottles

Max load at buckling/bending (kg)	
Standard Base	31.1±0.6
Optimum Base	29.2±0.5
Optimum Base (Preform Temp. 105 ^{o}C)	31.8±0.4
Optimum Base (Preform Temp. 110 ^{o}C)	33.0±0.3
Optimum Base (Preform Temp. 115 ^{o}C)	33.2±1.0
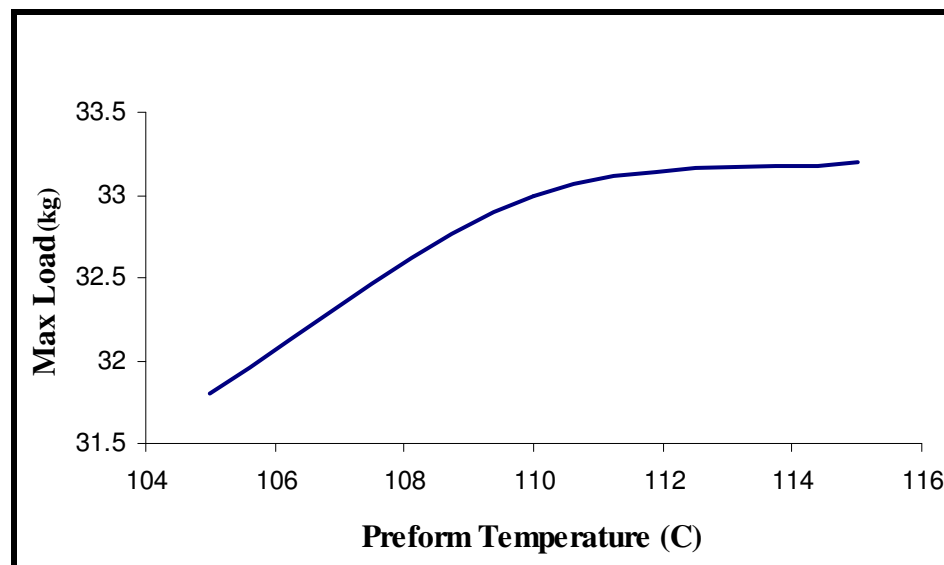
Fig.5-6. Top-load performance of the bottles

When produced under standard operating conditions, the new bottle had lower top load strength than the standard bottle. However, at higher preform temperatures the new bottle showed improved top load strength over the standard bottle; and this improvement increased with increasing preform temperature. This can be explained by referring to bottle section weights in table 5-5 and figure 5-7.

Table 5-5. Bottle section weights

	Base (g)	Centre (g)	Top (g)
Standard Base	11.3	15.0	13.7
Optimum Base	11.8	14.8	13.5
Optimum Base (Preform Temp. 105 ^{o}C)	12.1	14.5	13.4
Optimum Base (Preform Temp. 110 ^{o}C)	11.8	14.8	13.4
Optimum Base (Preform Temp. 115 ^{o}C)	11.6	14.9	13.5
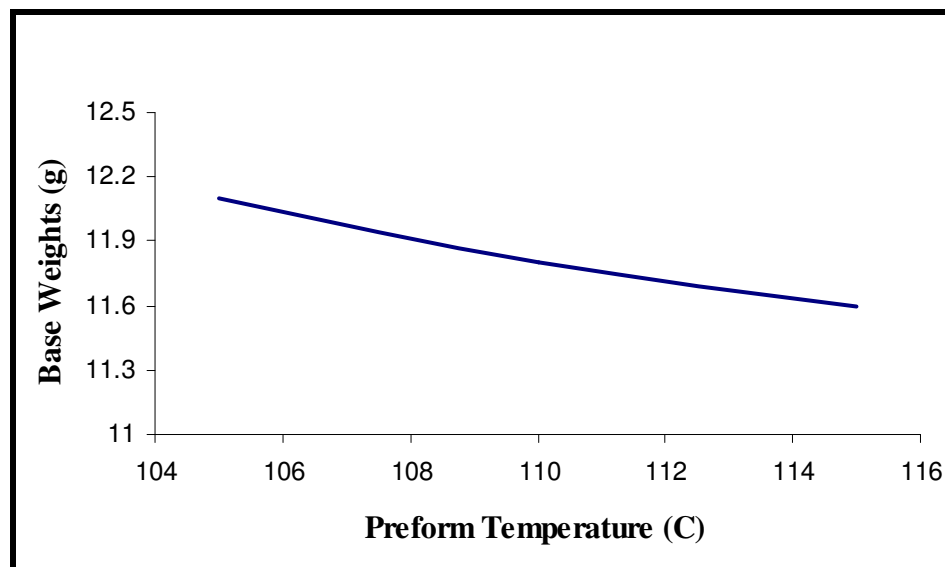
Fig.5-7. Bottle Base weights

The results indicate that in the bottle with the new base design there is slight shift in material distribution from the centre section to the base section; and no change in the top section. Since buckling under top loading is most likely to occur in the centre section, thinning in this region might explain the reduction in top load strength in the new bottle. As the preform temperature is increased, the material in the base move mainly to the centre section with a corresponding increase in top load strength is observed at high preform temperatures for the new bottle with optimized base design.

5.3.3 Environmental stress cracking resistance

The ESCR tests were carried out both on the standard and new bottles just after production and a few days later. To examine the effect of the preform temperature, this test was also conducted on bottles produced at the three different preform temperatures. The results are given in table 5-6 and figure 5-8.

Table 5-6. Accelerated stress crack performance of the bottles

Time to crack development (minutes)	
Standard Base	34±10
Optimum Base	64±18
Optimum Base (Preform Temp. 105 ^{o}C)	92±08
Optimum Base (Preform Temp. 110 ^{o}C)	79±18
Optimum Base (Preform Temp. 115 ^{o}C)	68±15

According to the obtained results, the resistance exhibited against environmental stress cracking has been very high for the optimized bottle base, which is almost 76 percent higher than the standard bottles. Also, resistance that the bottle base exhibits against environmental stress cracking decreased with increase in the preform temperature. This ESCR time is 92 minutes for preform temperature of 105 $^{\circ}$C whilst it is only 68 minutes for preform temperature of 115 $^{\circ}$C. In addition, that ESCR decreases as a function of post-production storage time. Relevant results can be seen in Appendix C in Table C-11, 12 and 13.
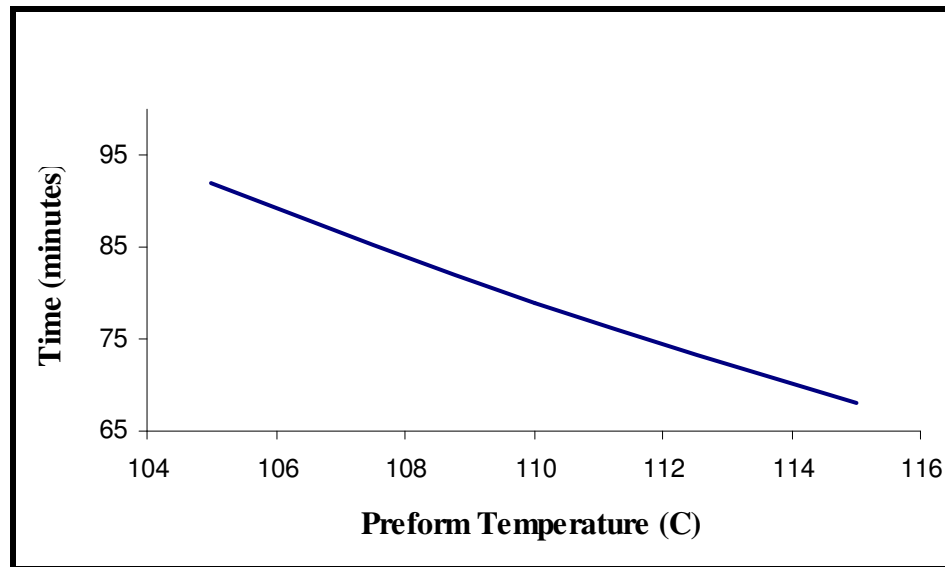
Fig.5-8. Accelerated stress crack performance of the bottles

The cracks occurring at the bottom of the standard and new bottles are shown in Fig. 5-9 and fig.5-10 respectively. In the standard base the cracks developed both radially in the centre of the base (fig.5-9(a)) and diagonally across the base (fig.5-9(b)).

(a)

(b)

Fig.5-9. ESC at the bottom of the bottle with standard base (a) central cracks (b) diagonal cracks

Fig.5-10. ESC at the bottom of the bottle with optimum base

The abrupt changes in thickness are mainly observed in the central region of the base rather than the other regions of the base for both bottles (Fig 5-11). However, the thickness changes on the foot and valley regions are not abrupt but gradual; that is why, the cracks form at the central region for both bottle bases. In addition, it is found that the thickness in the valley region is higher than the foot region for both bottle bases. The resistance to environmental stress cracking increased as a result of optimized base geometry and a lower preform set temperature, causing the base to become thicker than the standard bottles currently used in industry.
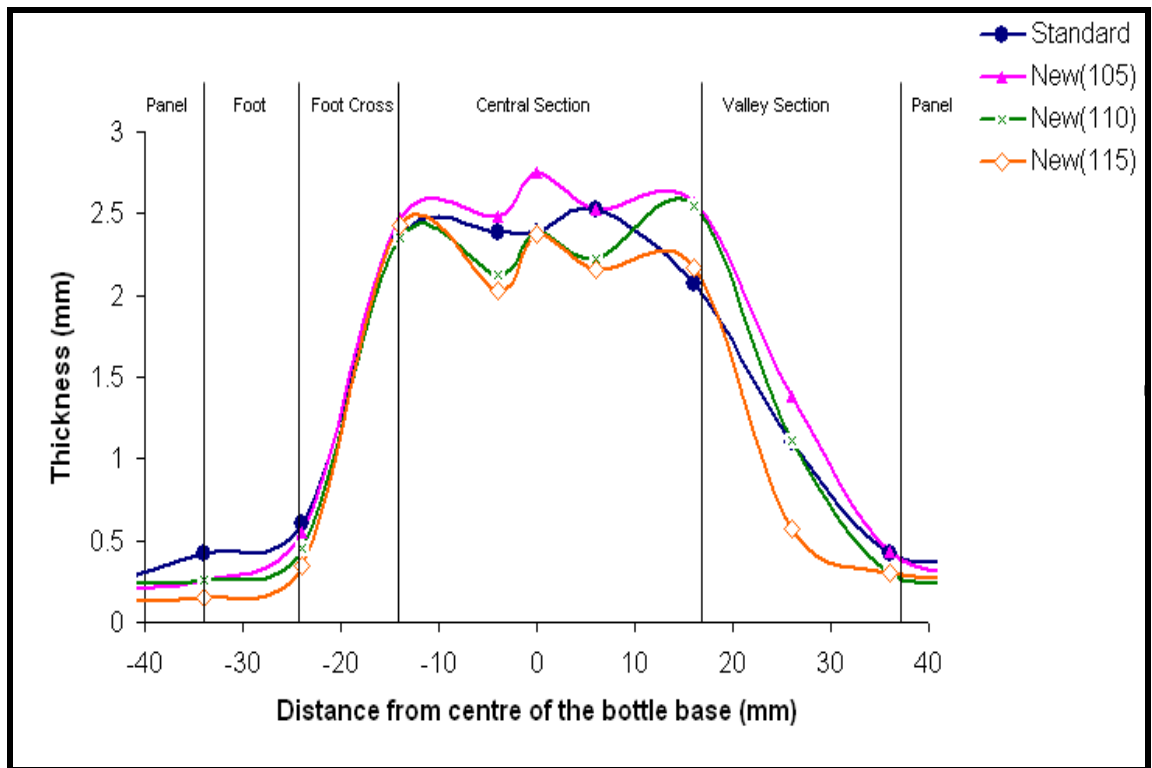
Fig.5-11. Thickness of the bottles with standard and optimized base

5.3.4 Thermal stability of the bottles

Thermal tests were performed for bottles, percentages changes in base clearance, bottle height fill point drop and body diameter are given in Table 5-7 (a) and (b).

Table 5-7. Thermal stability of the bottles; changes in (a) base clearance, bottle height and fill point; (b) body diameter

(a)

	Base Clearance (%)	Bottle Height Growth (%)	Fill Point Drop (mm)
Standard Base	61.1 ± 0.1	2.0 ± 0.06	22.9 ± 1.27
Optimum Base	72.6 ± 0.06	1.6 ± 0.04	21.8 ± 0.20
Optimum Base (Preform Temp. 105 ^{o}C)	81.7 ± 0.07	4.2 ± 0.07	16.6 ± 0.1
Optimum Base (Preform Temp. 110 ^{o}C)	86.7 ± 0.09	4.0 ± 0.06	15.4 ± 0.1
Optimum Base (Preform Temp. 115 ^{o}C)	87.5 ± 0.08	3.9 ± 0.05	16.3 ± 0.1

(b)

	Growth in Diameter (%)		
	Upper Panel	Lower Panel	Base
Standard Base	2.2 ± 0.07	2.4 ± 0.23	1.4 ± 0.46
Optimum Base	2.4 ± 0.09	2.3 ± 0.05	1.6 ± 0.24
Optimum Base (Preform Temp. 105 ^{o}C)	4.4 ± 0.09	4.5 ± 0.22	3.5 ± 0.5
Optimum Base (Preform Temp. 110 ^{o}C)	4.2 ± 0.08	4.0 ± 0.2	2.7 ± 0.6
Optimum Base (Preform Temp. 115 ^{o}C)	4.4 ± 0.08	3.7 ± 0.2	2.6 ± 0.5

The clearance for the bottle with standard base is changed from 7.2 mm to 2.8 mm whereas it changed from 6.2 mm to 1.7 mm for optimized base. However, the percentage change in base clearance is similar for both bottles. As for the relationship of the change of clearance at the

bottle base with the average preform temperature, clearance on the bottle base decreases with the increasing temperature. Furthermore, it is not reasonable to produce bottles with the average preform temperature of above 110 $^{\circ}$C. The excessive concaveness of the base and the loss of self-standing feature of the bottles in an upright position would be problematic.

For the fill point drop result is better for the bottle with the optimized base because the change in this parameter is lower for the newly designed bottle. Similarly growth in body diameter for the upper and lower panels, and the base is close to standard bottle.

5.3.5 Crystallinity

By means of MDSC method, the crystallinity values at critical points in the bottle base are calculated. Resultant heat flow curves in arbitrary units are given at these points for the bottles with standard base and the optimized base as shown in Fig. 5-12 and Fig. 5-13 respectively. From these curves, thermal characteristic such as glass transition temperature (Tg), cold crystallization temperature (T_{cc}), crystallization temperatures (T_c), and melting point (T_m) are obtained and percent crystallinity ($\%\chi$) is calculated.
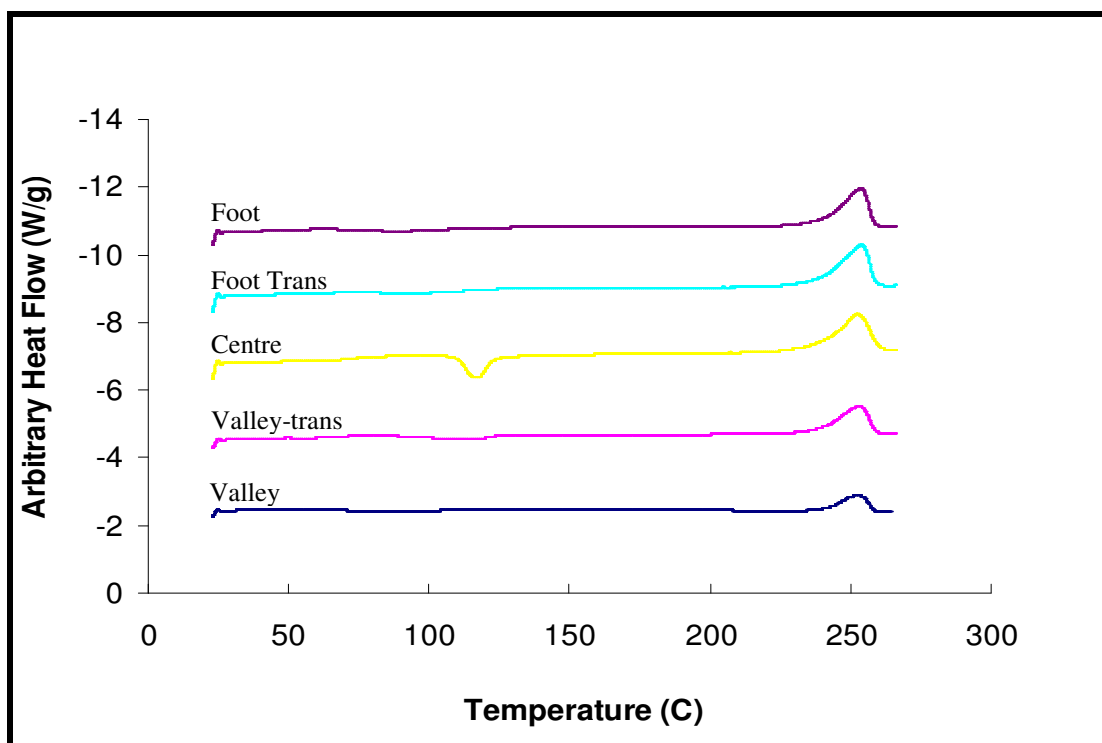
Fig. 5-12 MDSC diagrams of the standard bottle base
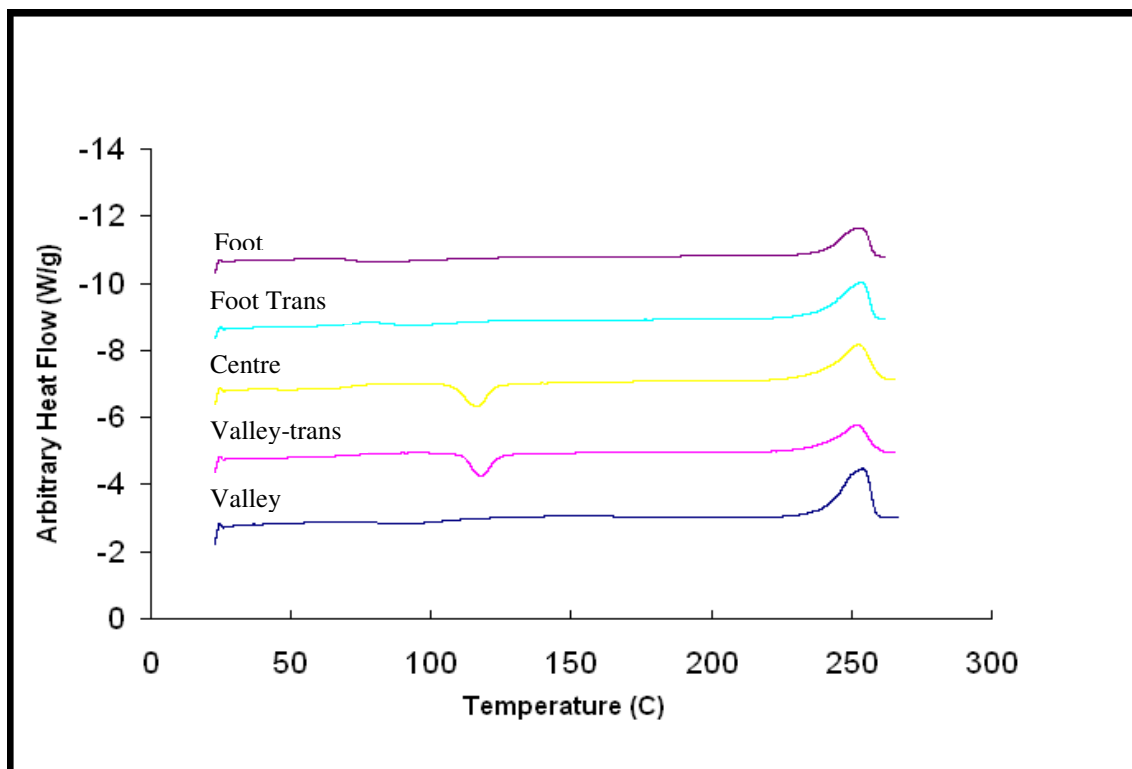
Fig. 5-13 MDSC diagrams of the optimised bottle base

The thermal characterization parameters and percentage crystallinities are given for the standard base and the optimized base in table 5-8 and 5-9 respectively. Glass transition temperatures (T_g), which are related to amorphous structure of the material, vary between 6 ^{o}C and 8 ^{o}C for standard and optimized bottle base respectively; it is not possible to observe any trend. Crystallization temperatures (T_c) are slightly higher for the optimized bottle base compared to the standard base. Similarly, crystallization temperatures (T_c) do not demonstrate a trend either in the standard or in the optimized bottle base. Cold crystallization temperature (T_{cc}) for both bottles shows a significant increase in the base centre and the transition regions. This is also reflected in high percentage crystallinity (% χ) in the centre and the transition regions of the base. For both bottles, base centre virtually indicates an amorphous structure with the χ of 10%.

Table 5-8 Properties of the selected points in the standard bottle base

Location on the base	1st heating					Cooling		2nd heating				χ
	T_g (^{o}C)	T_{cc} (^{o}C)	ΔH_{cc} J/g	T_m (^{o}C)	ΔH_m (J/g)	T_c (^{o}C)	ΔH_c J/g	T_g (^{o}C)	T_{m1} (^{o}C)	T_{m2} (^{o}C)	ΔH_m (J/g)	(%)
Foot	78.4	89.5	5.5	253.6	45.3	201.2	39.8	81.0	242.4	252.7	37.4	43.4
Foot Trans	70.9	90.6	5.9	253.7	43.2	198.9	37.1	79.6	242.3	252.0	35.8	32.2
Centre	73.2	116.8	15.9	252.3	41.7	198.3	37.7	81.7	241.7	252.3	39.2	10.0
Valley Trans	78.4	110.3	9.4	253.0	39.9	198.9	33.4	81.6	241.8	252.0	34.5	23.0
Valley	75.0	88.1	5.9	252.9	44.1	199.4	39.2	79.7	240.6	251.9	37.8	51.8

Table 5-9 Properties of the selected points in the optimum bottle base

Location on the base	1st heating					Cooling		2nd heating				χ
	T_g (°C)	T_{cc} (°C)	ΔH_c J/g	T_m (°C)	ΔH_m (J/g)	T_c (°C)	ΔH_c J/g	T_g (°C)	T_{m1} (°C)	T_{m2} (°C)	ΔH_m (J/g)	(%)
Foot	79.1	77.8	12.8	253.4	45.2	202.5	40.1	78.7	242.9	251.7	36.0	31.2
Foot Trans	75.7	95.9	6.3	253.5	43.3	202.4	35.5	82.1	243.3	252.3	35.9	38.2
Centre	76.5	116.0	18.2	252.4	39.5	201.7	36.9	82.2	243.1	252.3	37.1	14.1
Valley Trans	72.3	114.5	20.1	252.3	41.1	202.8	41.8	80.4	243.7	252.0	38.6	14.4
Valley	78.6	91.2	5.0	253.9	46.3	202.7	41.6	81.8	243.0	252.3	38.5	50.3

Crystallinity values decrease in the direction towards the centre of the base for both bottles as shown in Fig. 5-14. The crystallinity of the optimised base (38.2%) is higher than the standard base (32.2%) for the valley transition region between the centre and the valley; but for the foot transition region between the center and the foot it is not the case; the crystallinity of the optimised base (14.4%) is lower than the standard base (23.0%) in this region. As for the foot region, crystallinity value for the optimised base (50.3%) is similar to that of standard base (51.8%). Nevertheless, it can be said that the crystallinity values across the base are not much different between the two bottles.
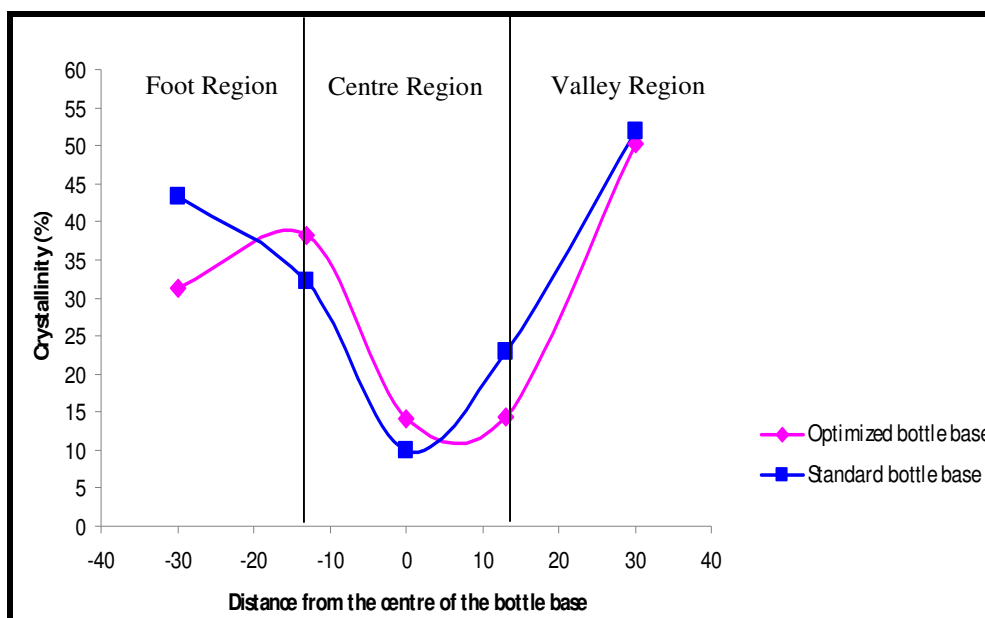
Fig.5-14 Actual crystallinity in the optimum and standard bottle bases

5.3.6. Morphology

Cracks observed in both the standard and the optimized bottle bases are initiated at the injection pin, which acts a stress concentration point, as shown in the optical microcopy image of the bottle base (Fig. 5-15); cracks do not exactly pass through the base centre. The cracks were limited within the central region of the optimised base and did not reach the foot or the valley of the base in the optimised bottle base. Whereas for the standard base, not only central cracks, but in some samples diagonal cracks appeared across the transition regions in the base.

There are clear differences between the appearance of cracks found in the standard and the new bottle base. The cracks in the standard bottle base propagate in a rather straight manner (Fig. 5-16), whereas for the optimized bottle base, cracks take up a spiral form, demonstrating a fibrous appearance (Fig. 5-17). In spite of the fact that both bottles are produced under the same standard process operating conditions and made out of the same material, mechanism of crack appears to be significantly different resulting in significant differences in ESCR times. The crack

propagation mechanisms may be associated with the base properties such as morphology and

crystallinity as well as wall thickness of the base.

Magnification 1.8x10
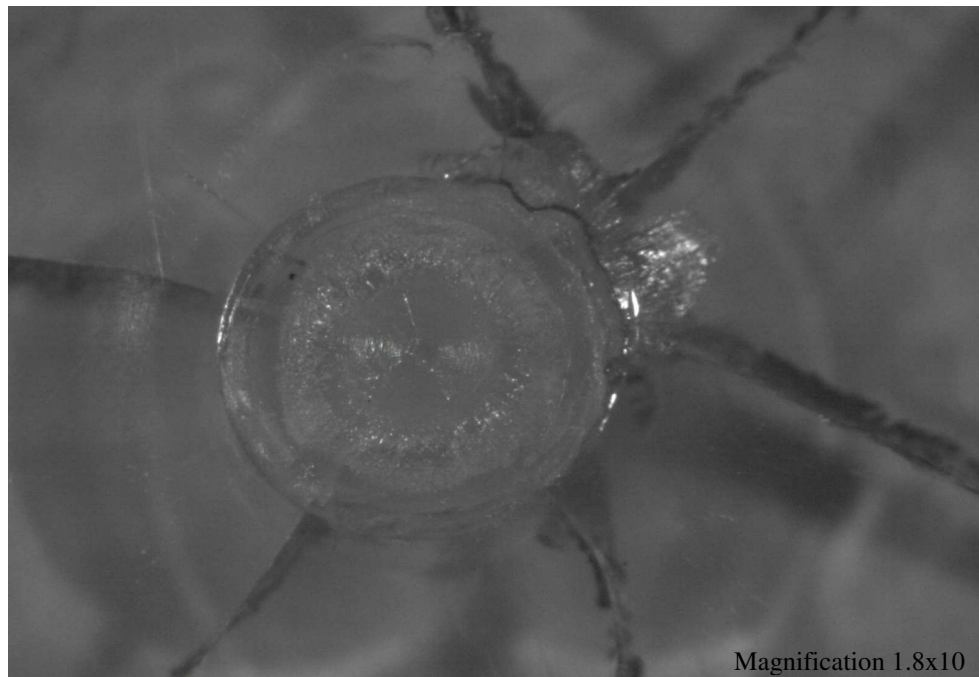
Fig.5-15. Optical microscope images of the cracks around the center of optimum base
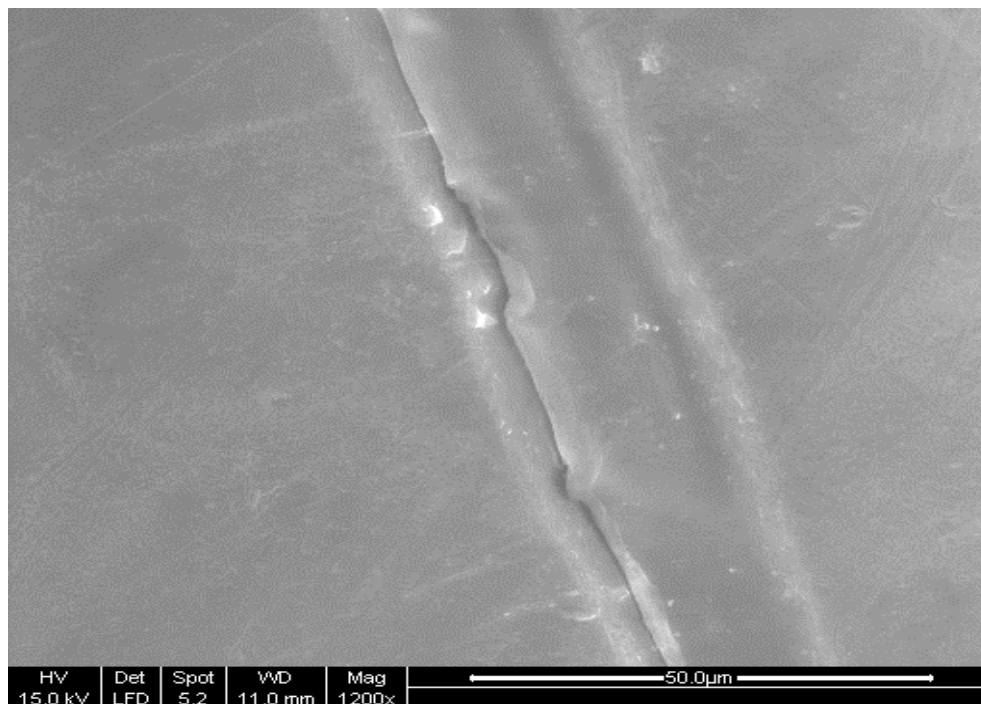
Fig.5-16. SEM image of the crack propagation in the standard bottle base

| HV | Det | Spot | WD | Mag | 500.0μm |
| 15.0 kV | LFD | 4.0 | 13.3 mm | 150x | |
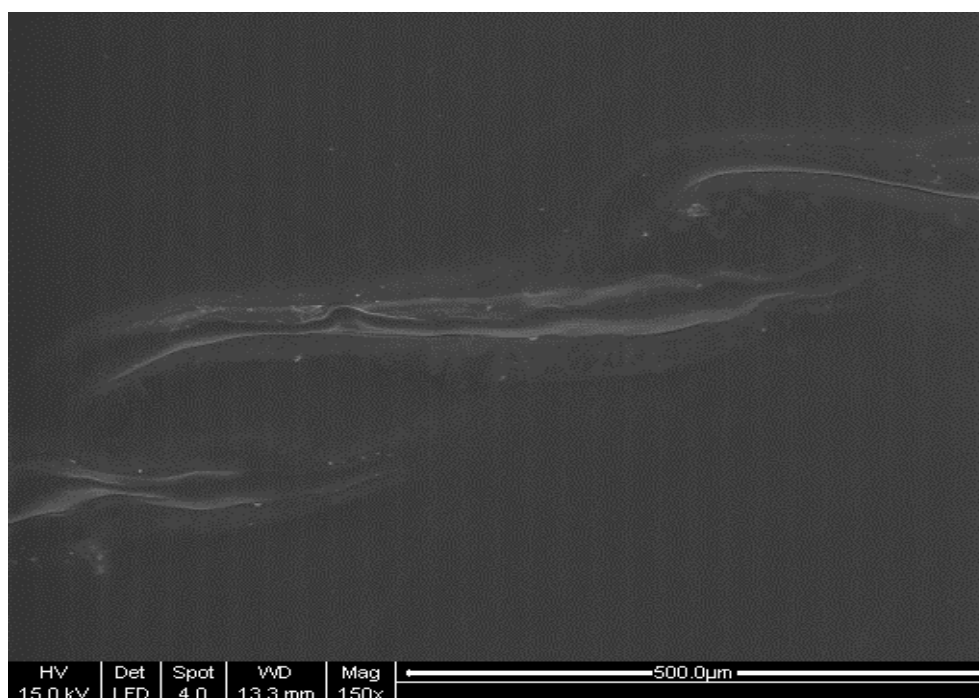
Fig.5-17. SEM image of the crack propagation in the optimized model

5.3.7 Relationship of ESCR to that of physical and mechanical properties of the bottle base

Cracks occur within the central zone of the optimised base design. In this region, the crystallinity values are lower than other regions of the base; hence ESCR should be higher in this region, since the ESCR is expected to increase with the decreasing crystallinity [Brocka et al., 2007]. On the other hand, the highest simulated stress values are found to be in the centre region of the bottle base based on stress simulation conducted via CATIA under the stresses similar to accelerated environmental stress cracking test conditions (Fig. 5-18). The actual thickness in the bottle base which is produced from preforms at an average re-heat temperature of 105 ^{o}C, and the simulated stress of the optimum bottle base are given in figure 5-19. Though the central region of the base is the strongest section based on the thickness, the crack failures have taken place in this region because of higher stress values generated in this region. The other regions are stronger against the ESC because of stress being less. That is why ESC starts within the central region and comes to a stop once reaching the transition zone in the optimized bottles.
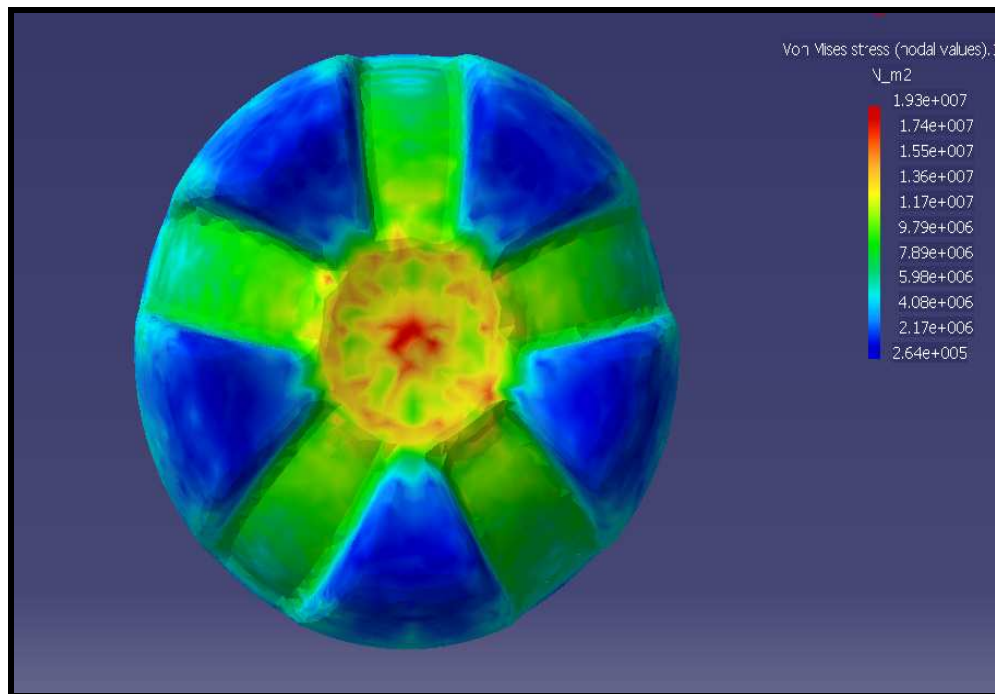
Fig. 5-18 Simulation of the stress in the optimised bottle base under load
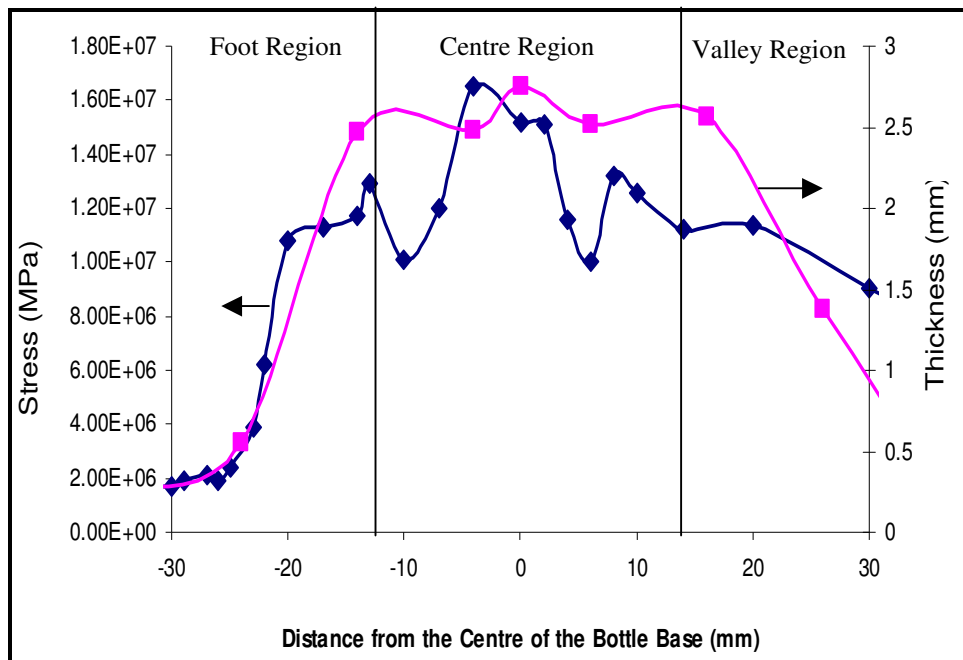
Fig. 5-19 Simulated stress and measured thickness in the optimized bottle base

Fig. 5-20 to Fig. 5-22 shows how the new and the standard base differ in terms crystallinity, molecular orientation and biaxial ratio under optimised processing conditions as defined by model-2. Similar results for other models are given in Appendix B. It can be said that crystallinity, molecular orientation and biaxial ratio increase towards the foot and the valley regions of the bottle base, the magnitude of increase is bigger for the optimised bottle. However, the crystallinity, molecular orientation and biaxial ratio in the standard and optimised base design do not differ in the central region where the environmental stress cracking is mainly observed. This reinforces the hypothesis that in this comparative study, the increase in the ESCR is most likely resulted from the reduction in environmental stress arising from the carbonated soft drink due to modified geometry of the optimised base.
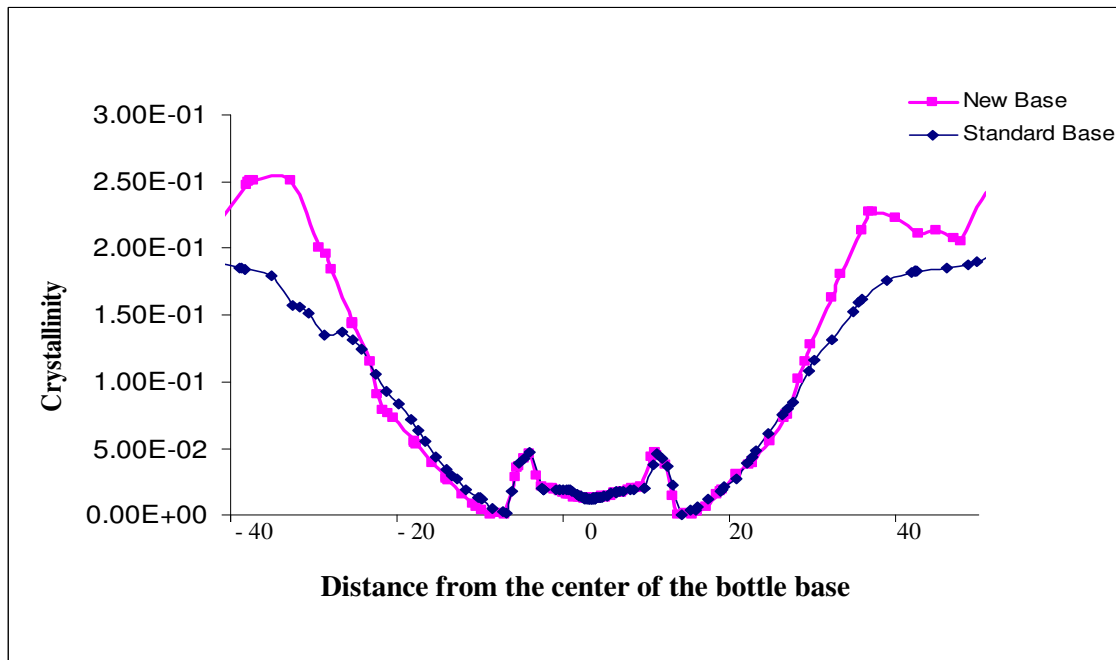
Fig.5-20. Comparison of crystallinity in the new and standard bases; model-2
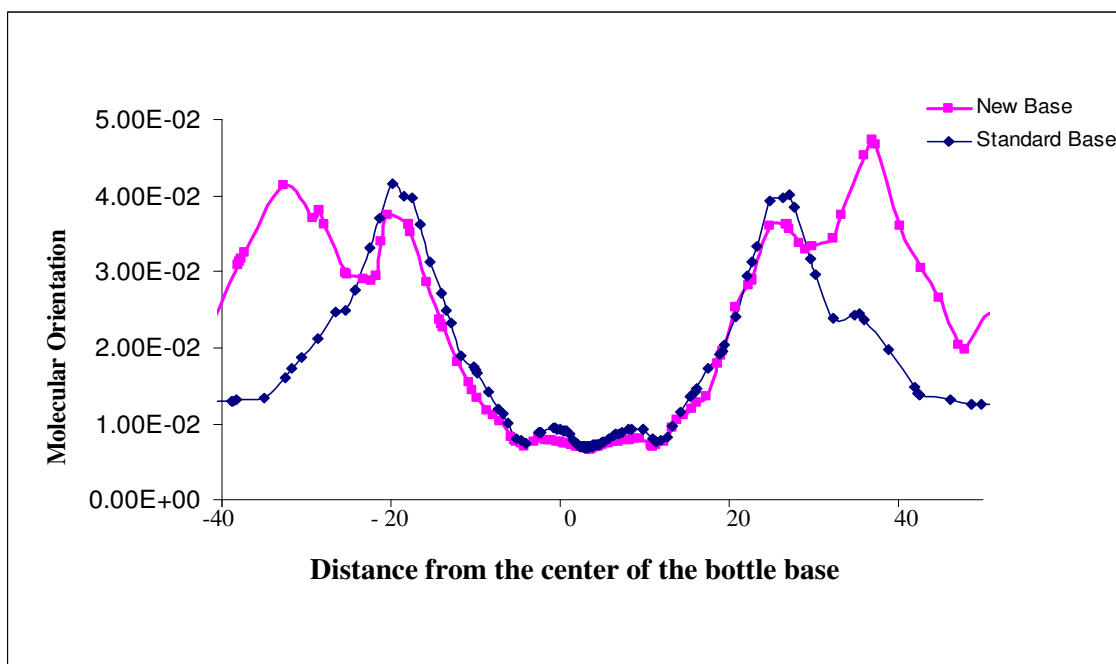
Fig. 5-21. Comparison of molecular orientations in the new and standard bases; model-2
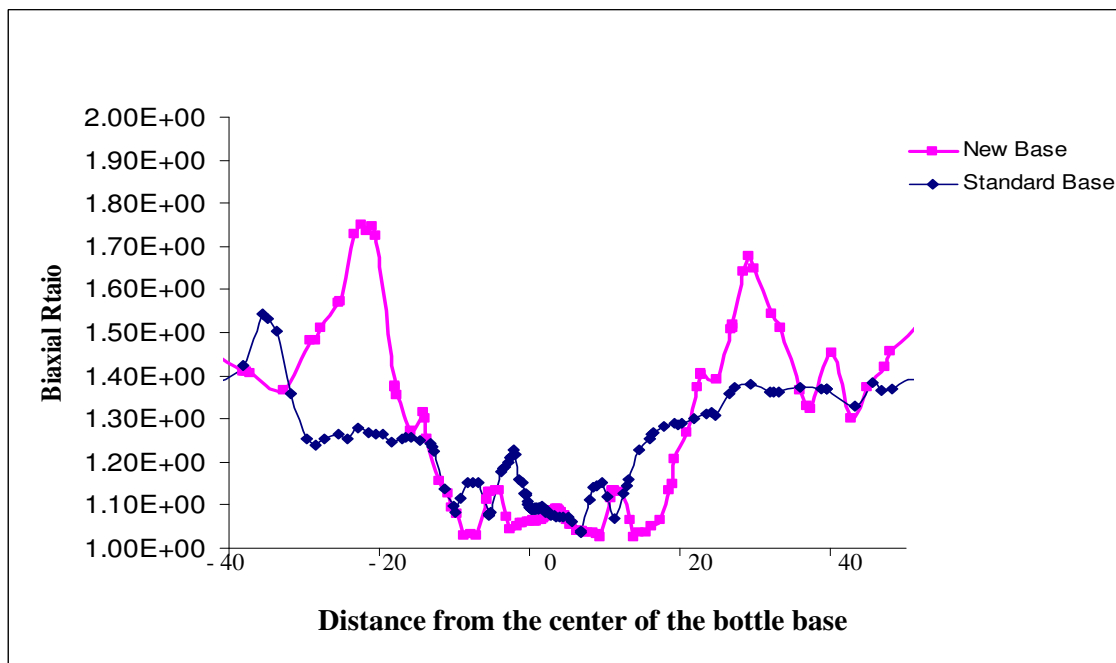
Fig. 5-22. Comparison of biaxial ratios in the new and standard bases; model-2

5.4 CONCLUSION

In this chapter of the study, the physical, mechanical and geometrical changes resulting from the introduction of a new petaloid base are assessed by the appropriate test methods. The results of the performance tests of the optimised bottle base are presented.

According to these results, the optimization study carried out on the petaloid shaped bottle base has been very effective and has significantly increased the ESCR of the bottle. While the amount of material transferred to the base is slightly increased due to the change of geometry of the bottle base equivalent environmental stress reduced at this modified geometry.

While the top load strength increased at standard operating conditions, the burst strength slightly decreased for the new bottle produced at the preform temperatures of 105 $^{\circ}$C, 110 $^{\circ}$C, and 115 $^{\circ}$C. Similarly, thermal stability tests proved that the optimised base did not adversely affect the bottles in terms of thermal stability. So, the optimization process of the petaloid based bottle is successfully completed in terms of preventing the environmental stress cracking.

As for the outcomes achieved by the process parameters change, it is observed that the ESCR reduces with the increasing preform reheat temperature. On the other hand, burst pressure values decreased but top load values increased with the increasing temperature. Furthermore, the clearance value for the optimum base reduced with the increasing temperature. So, one of the most important achievement of this study is that the temperature profile of the preform should be kept as low as possible to ensure high ESCR and to prevent the concaveness at the bottom of the bottle.

Chapter 6

CONCLUSIONS AND SUGGESTIONS FOR

FURTHER WORK

6.1. INTRODUCTION

In this chapter, the overall conclusions obtained from this study are presented and suggestions for further work are explained. Answers to the specific research questions are also given. In this chapter, only the general results are given since the conclusion of each chapter of the thesis has been presented in their respective section in detail.

At the present time, the carbonated soft drinks are generally kept in the containers made from PET material mainly because of its advantageous physical properties. The shapes and sizes of the bottles vary depending on the amount and type of the drink to be stored. Nevertheless, the bottom petaloid shapes of all bottles used for carbonated soft drinks are almost similar to each other. Due to the shape of the bottle base being petaloid, cracks sometimes occur in this base section of the bottles. In this study, the base of the 1500 ml PET bottle has been redesigned optimizing the petaloid shape. According to the obtained results, the base geometry has a significant effect on the environmental stress cracking. As explained in detail in chapter 3, only the valley section of the petaloid base itself does not have a major effect on the cracking. However, this parameter comes into question with other parameters of the petaloid shape. This outcome is related to the research question 1.

The PET bottles are produced by the ISBM process. This process has a number of parameters and each of these parameters significantly affects the cracks occurrence in the bottle base according to the outcomes obtained in chapter 3. Both the injection molding parameters and stretch blow molding (SBM) process parameters are very important for the environmental stress cracking. In this study, it is focused only on the SBM process, which is the second stage in the two-stage processing. The most important parameters to be taken into consideration in SBM process are regarded as the initial temperature profile of the preform, the speed of stretch rod,

magnitude and the timing of the pre-blow and final-blow pressures. Each of them has a significant effect on the environmental stress cracking because they directly affect the amount of the PET material amount in the bottle base and the extent of stretching of the material in the base during the processing. Consequently, the amount of material in the base and the extent of stretching affect the thickness, crystallization, and molecular orientation, biaxial ratio at the bottom of the bottle. The resistance against environmental stress cracking at the bottom of the bottle decreased with increasing initial temperature profile on the preform because of decreasing thickness in the bottle base. On the other hand, crystallization and molecular orientation increased together with the increasing temperature according to the results obtained through the Blow View 8.2 simulation program (Research question 2).

The cracks occurring in the base also depend on the process conditions, material properties, and storage conditions. The PET bottles of 1.5 it that are produced in SBM process are exposed to the environmental stress cracking tests in certain time intervals. After the production, the passing time caused the resistance that the bottle base exhibits against environmental stress cracking to decrease. The maximum resistance is achieved in the tests performed just after the production (Research question 6).

In order to be able to compare the new and standard bottle base with each other, bottles are produced at the same standard processing process conditions used in industry. In addition, the samples for the optimum based bottle are produced at three different initial temperatures profiles on the preform with the aim of defining the temperature effects on the bottle. Top load strength, burst pressure strength, thermal stability, environmental stress crack resistance, and crystallinity and morphology studies are conducted on all bottles. According to the results obtained, the ESCR of the bottle with optimized base is significantly higher than the standard based bottle,

whereas nearly all performance test results are similar to the standard based bottle's values (Research question 6, 7).

The optimization process of the petaloid base of the 1500 ml PET bottle is carried out by means of CATIA V5 R14 version software program. In this optimization process, the base geometry is targeted to result in minimum stress in the bottle base and ECHIP-7 software program is used to assess the results found through CATIA V5 R14. In conclusion, the optimization process is completed by means of Catia V5 R14 and Echip-7 software programs, and the resistance of the bottle base against environmental stress cracking is significantly enhanced. Stress analysis and design process with Catia V5 are conducted conveniently because the software program allowed both the mesh geometry to be easily generated and the material properties to be fully entered. Catia V5 R14 software is therefore an appropriate program for stress analysis and design process (Research question 8 and 9).

Both the preform design and the initial temperature effect on the physical properties of the bottle are predicted by means of Blow View 8.2 software program. To this end, the weight of preform is decreased and the preform design is altered accordingly. In addition, the physical changes occurring especially in the bottle base are observed. According to the obtained results, as the preform weight decreases, the thickness of the bottom of the bottle decreases and the other parameters such as crystallinity, molecular orientation, and biaxial ratio also changed. In this study, there has not been an opportunity to investigate the effect of the low weight preform on ESCR (Research question 10).

6.2. SUGGESTIONS FOR FURTHER WORK

The following suggestions will be useful in terms of understanding this environmental stress crack phenomenon occurring on the bottle base.

1- In order to observe the effects of the preform produced at various injection pressures and mold temperature on ESCR, some preform samples can be produced by changing ISBM process settings.

2- Other geometrically modified preform samples can be produced to compare the changes on the bottle base in terms of the thickness, crystallinity, molecular orientation, and ESCR. The preform weight may be reduced modifying its design and wall thickness so the thickness in the bottle base is uniform and minimum. I suggest focusing on minimum stress.

3- In order to investigate the effects of the bottle mold temperature on the physical properties, the bottle samples can be produced with various mold surface temperatures and then ESCR tests can be performed.

4- This study has focused on two stage ISBM process where preform is reheated. A single stage ISBM process should be considered because one stage ISBM is becoming widespread. The bottles produced with both methods can be compared with each other in terms of ESCR.

5- Three different models are developed for SBM process in this study but these models could not be applied to SBM process due to the lack of machinery, which was available for experimental work, produced pressure was well above the pressure considered for the models. Therefore, bottle samples can be produced under these three processing models by improving technical facility.

REFERENCES

REFERENCES

Alfonso, G.C., Verdona, M.P., Wasiak A. (1978), "Crystallization Kinetics of Oriented Poly(Ethylene Terephthalate) from the Glassy State", *Polymer*, **19**, 711–716.

ASTM (2005), "Standard Test Method for Environmental Stress-Crack Resistance of Blow-Molded Polyethylene Containers; D2561-95(2005) - Procedure B", American Society for Testing and Materials, Philadelphia, USA

ASTM (2000), "Standard Test Methods for Density and Specific Gravity (Relative Density) of Plastics by Displacement; D792-00", *American Society for Testing and Materials*, Philadelphia, USA

Awaja, F., Pavel, D. (2005),"Recycling of PET", *European Polymer Journal*, **41**, 2614–2634.

Azar, A. A., Biddlestone, F., Hay, J. N., Haward, R. N. (1983), "The Effect of Physical Aging on The Properties of Poly(Ethylene Terephthalate)", *Polymer*, **24**, 1245-1251.

Baczek, S. (2003), "Low Shear In-Mould Decoration-Processes For The Manufacture Of Three-Dimensional Molded Interconnect Devices (3D-MID), *Conference Proceedings, SPE ANTEC*, Nashville, USA.

Ballman, R. L., Shusman, T. (1959), "Easy Way to Calculate Injection Molding Set-up Time", *Modern Plastics*, 126, 130-131

Benning, C. J. (1983), "Plastic Films for Packaging", Lancaster, Pennsylvania, Technomic Publishing Co.

REFERENCES

Berens, A. R., Hodge, I. M. (1984), "Effects of Stress and Vapor Exposure Before and During Aging on Enthalpy Relaxation of Poly(Vinyl Chloride)", *Polymer Engineering Science*, **24**, 1123-1129.

Bernier, G. A., Kambour, R. P. (1968), "The Role of Organic Agents in the Stress Crazing and Cracking of Poly(2, 6-dimethyl-l, 4-phenylene oxide)", *Macromolecules*, **1**, 393-400.

Bird, R. B., Stewart, W. E., Lightfoot, E. N. (1960), "Transport Phenomena", New. York, USA, John Wiley and Sons.

Bjorksten, J., Tovey, H., Harker, B., Henning, J. (1956), "Polyesters and their Applications", London, UK., Chapman and Hall.

Blundell, D. J., Oldman, R. J., Fuller, W. (1999), "Orientation and Crystallization Mechanisms During Fast Drawing of Poly(Ethylene Terephthalate) ", *Polymer Bulletin*, **42**, 357-363.

Blundell, D. J., Mahendrasingam, A., Martin, C. (2000), "Orientation Prior to Crystallization During Drawing of Poly(Ethylene Terephthalate)", *Polymer*, **41**, 7793-7802.

Bonnebat, C., Roullet, G., de Vries, A. J. (1981), "Biaxially Oriented Poly(Ethylene Terephthalate) Bottles: Effects of Resin Molecular Weight on Parison Stretching Behavior", *Polymer Engineering Science*, **21**,189-195.

Boyer, R. F. (1975), "Glassy Transitions in Semi-Crystalline Polymers" *Journal Polymer Science Symposium*, **50**, 189-242

Briston, J. (1992), "Advances in Plastics Packaging Technology", Surrey, UK., Pira International.

Brocka, Z., Schmactenberg, E., Ehrenstein, G. W. (2007), "Radiation Cross Linking Engineering Thermoplastic for Tribological Applications", *Conference Proceedings, SPE ANTEC*, Cincinnati, USA

Brody, A. (2001), "Strategies for Polyester Packaging", Food Technology, **55**, 68-69.

Brooks, D. W., Giles, G. A. (2002), "PET Packaging Technology", Sheffield, Academic Press.

BSDA: British Soft Drinks Association, 2000, found at http://www.britishsoftdrinks.com/htm/qa/ai_carbon.htmi

Bur, A. J., Wang, F. W., Thomas, C. L., Rose, J. L. (1994), "In-Line Optical Monitoring of Polymer Injection Molding", *Polymer Engineering Science*, **34**, 671-679.

Busch, J. V., Field, F. R., Rosato, D. V. (1988), "Computer Aided Part Cost Analysis for Injection Molding", *Conference Proceedings, SPE ANTEC*, Boston, USA

Cakmak, M., Spruiell, J. E., White, J. L. (1984), "A Basic Study of Orientation in Poly(Ethylene Terephthalate) Stretch-Blow Molded Bottles", *Polymer Engineering Science*, **24**, 1390-1395.

Canadas, J. C., Diego, J. A., Mudarra, M., Belana, J. (1998), "Comparative TSPC, TSDC and DSC Physical Aging Studies on PET-a", *Polymer*, **39**, 2795-2801.

REFERENCES

Carslaw H. S., Jaeger, J. C. (1959), "Conduction of Heat in Solids", Oxford, UK, Clarendon Press.

Chang, S., Sheau, M. F., Chen, S. M. (1983), "Solid-State Polymerization of Poly(Ethy1ene Terephthalate)", *Journal Applied Polymer Science*, **28**, 3289-3300.

Chevalier, L. (1999), "Influence of Microstructure Evolution on Mechanical Strength of Blown Poly(Ethylene Terephthalate)", *Plastics Rubber and Composites*, **28**, 385-392.

Chevalier, L., Linhone, C., Regnier, G. (1999), "Induced Crystallinity During Stretch–Blow Moulding Process and Its Influence on Mechanical Strength of Poly(Ethylene Terephthalate) Bottles", *Plastics Rubber and Composites*, **28**, 393-400.

Choi, B. H., Weinhold, J., Reuschle, D., Kapur, M. (2007), "Investigation of Fracture Mechanism of HDPE Subjected to Environmental Stress Cracking", *Conference Proceedings, SPE ANTEC*, Cincinnati, USA.

Cobbs, W. H., Jr., Burton, R. L. (1953), "Crystallization of Polyethylene Terephthalate", *Journal of Polymer Science*, **10**, 275-290.

Collins, E. A., Bares, J., Billmeyer, F. W. (1973), "Experiments in Polymer Science", New York, USA, John Wiley and Sons.

Chua, C. K., Lye, S. L. (1998), "Parametric Modelling of Drinking Bottles", *Integrated Manufacturing Systems*, **9**, 99–108.

REFERENCES

Crawford, R. J. (1987), "Plastic Engineering", Pergamon Press, Second Edition

DeGroot, J. A., Doughty, A. T., Stewart, K. B., Patel, R. M. (1994),"Effects of Cast Film Fabrication Variables on Structure Development and Key Stretch Film Properties", *Journal Applied Polymer Science*, **52**, 365-376.

Dietzel, H., Schumann, J., Muller, K. (1991), "Calculating the cooling and sealing times analytically", *Kunststoffe*, **81**, 1138-1140.

Dixon, E. R., Jackson, J. B. (1968), "The Inter-relation of Some Mechanical Properties with Molecular Weight and Crystallinity in Poly(Ethylene Terephthalate)", *Journal of Material Science*, 3, 464-470.

Dominghaus, H. (1993), "Plastic for Engineering: Materials, Properties, Applications", New York, USA, Hanser Publishers.

Dorkenoo, K. D., Pfromm, P. H. (1999), "Experimental Evidence and Theoretical Analysis of Physical Aging in Thin and Thick Amorphous Glassy Polymer Films", *Journal Polymer Science, Part B: Polymer Physic*, **37**, 2239-2251.

Dubay, R., Bell, A. C. (1998), "An Experimental Comparison Of Cooling Time for Cylindrical Plastic Components Using Heat Conduction Models In the Non-Conservative Forms', *Polymer Engineering Science*, **38**, 1048-1059.

REFERENCES

Dumbleton, J. H. (1968), "Influence of Crystallinity and Orientation on Sonic Velocity and Birefringence in Poly(Ethylene Terephthalate) Fibers", *Journal of Polymer Science*, **6**, 795-800.

Ehrenstein, G. W. (2001), "Polymer Materials-Structure-Properties-Applications", Munich, Germany, Hanser Publishers.

Erwin, L., Pollock, M. A., Gonzalez, H. (1983),"Blowing of Oriented PET Bottles: Predictions of Free Blown Size and Shape", *Polymer Engineering Science*, **23**, 826-829.

Everall, N., MacKerron, D., Winter, D. (2002), "Characterization of Biaxial Orientation Gradients in Poly(Ethylene Terephthalate) Films and Bottles Using Polarized Attenuated Total Reflection FTIR Spectroscopy ", *Polymer*, **43**, 4217-4223.

Evstatiev, M., Fakirov, S., Apostolov, A., Hristov, H., Schultz, J. M. (1992) "Structure and Mechanical Properties of Highly Oriented Poly(Ethylene Terephthalate) Films" *Polymer Engineering and Science*, **32**, 964-970.

Fan, G., Di Maio L., Incarnato, L., Scafato, P., Acierno, D. (2000), "The Relative Significance of Biaxial Stretch Ratio Effects on The Permeability of Oriented PET Film", *Packaging Technology and Science*, **13**, 123-132.

Fellers, J. F., Kee, B. F. (1974), "Crazing Studies of Polystyrene. I. A New Phenomenological Observation", *Journal Applied Polymer Science*, **18**, 2355-2365.

REFERENCES

Gauvin, C., Thibault, F., Laroche, D. (2003), "Optimization of Blow Molded Part Performance Through Process Simulation", *Polymer Engineering Science*, **43**, 1407-1414.

George G. A., O'Shea, M. S. (1990), "The Effect of Morphology on The Environmental Degradation of Nylon 6 Under Tensile Load", Polymer Degradation and Stability, **28,** 289-310.

Gibbs, M. (1989), *Conference Proceedings, SPE ANTEC*, New York, USA.

Groeninckx, G., Berghmans, H., Overbergh, N., Smets, G. (1974), "Crystallization of Poly(Ethylene Terephthalate) Induced by Inorganic Compounds. I. Crystallization Behavior from the Glassy State in a Low-Temperature Region", *Journal polymer Science, Polymer Physic*, **12**, 303-316.

Groeninckx, G., Berghmans, H., Smets, G. (1976), **"**Morphology and Modulus-Temperature Behavior of Semicrystalline Poly(Ethylene Terephthalate) (PET)", *Journal of Polymer Science, Polymer Physic*, **14**, 591-602.

Han, W. H., McKenna, G. B. (1997), "Plasticizer Effects on Physical Aging of Epoxy", Conference Proceedings, SPE ANTEC, Toronto, Canada..

Hanley, T., Sutton, D., Cookson, D., Koisor, E., Knott, R. (2006), "Molecular Morphology of Petaloid Bases of PET Bottles: A Small-Angle X-Ray Scattering Study", *Journal of Polymer Science*, **99**, 3328-3335.

Hartwig, K., Michaeli, W. (1995), "Modelling and simulation of the injection stretch-blow molding process", *Conference Proceedings, SPE ANTEC*, Boston, USA

REFERENCES

Hatakeyama, T., Quinn, F.X. (1994), "Thermal Analysis: Fundamentals and Applications to Polymer Science", New York, USA, John Wiley & Sons Inc.

Hittmair, P., Ullman, R. (1962)," Environmental Stress Cracking of Polyethylene", *Journal Applied Polymer Science*, **6**, 1-14.

Howard, J. B. (1959), "A Review of Stress Cracking in Polyethylene", *SPE Journal*, **15**, 397- 409

Howard, J. B., Martin, W. M. (1960), "Effects of Thermal History on Some Properties of Polyethylene", *SPE journal*, **16**, 407-412.

Huang, H. X., Yin, Z. S., Liu, J. H. (2006),"Visualization Study and Analysis on Preform Growth in Polyethylene Terephthalate Stretch Blow Molding", *Journal Applied Polymer Science*, **103**, 564-573.

Hutchinson, J. M. (1995), "Physical Aging of Polymers", *Progress in Polymer Science*, **20**, 703-760.

Illers, H., Breuer, H. (1963),"Molecular Motions in Polyethylene Terephthalate", *Journal of Colloid Science*, **18**, 1-31.

Imbalzano, J. F., Washburn, D. N., Mehta, P.M. (1991), "Permeation and Stress Cracking of Fluoropolymers", *Chemical Engineering*, **1**, 105-108.

Ito, E. (1974), "Studies of The Amorphous Region of Polymers. I. Relationship Between the Change of Structure and Glass-Transition Temperature in Drawn Poly(Ethylene Terephthalate)", *Journal of Polymer Science, Polymer Physic*, **12**, 1477-1483.

Jabarin, S.A. (1982), "Optical Properties of Thermally Crystallized Poly(Ethylene Terephthalate)", *Polymer Engineering and Science*, **22**, 815-820.

Jabarin, S.A. (1984), "Orientation Studies of Poly(Ethylene Terephthalate)", *Polymer Engineering and Science*, **24,** 376-384.

Jabarin, S. A., Lofgren, E. A. (1986), "Effect of Water Absorption on Physical Properties of High Nitrile Barrier Polymers", *Polymer Engineering Science*, **26**, 405-409.

Jabarin, S. A., Lofgren, E. A. (1986), "Effects of Water Absorption on Physical Properties and Degree of Molecular Orientation of Poly (Ethylene Terephthalate)", *Polymer Engineering Science*, **26**, 620-625.

Jabarin, S. A. (1987), "Crystallization Kinetics of Polyethylene Terephthalate. I. Isothermal Crystallization from The Melt", *Journal Applied Polymer Science*, **34(1),** 85-96.

Jabarin, S. A. (1987), "Crystallization Kinetics of Polyethylene Terephthalate. II. Dynamic Crystallization of PET", *Journal Applied Polymer Science*, **34**, 97-102.

Jabarin, S. A. (1987),"Crystallization Kinetics of Poly(Ethylene Terephthalate). III. Effect of Moisture on The Crystallization Behavior of PET from The Glassy State", *Journal Applied Polymer Science*, **34**, 103-108.

Jabarin, S.A. (1992), "Strain-Induced Crystallization of Poly(Ethylene Terephthalate)", *Polymer Engineering and Science*, **32,** 1341-1349.

Jabarin, S. A., Lofgren, E. A. (1992), "Environmental Aging and Stress-Cracking of Poly(ethylene Terephthalate)", Polymer Engineering Science, **32**, 146-156.

Jabarin, S. A. (1998), "PET Technology and Processing Textbook", Toledo University Press.

Jabarin, S. A. (2003), "Advances in Barrier Concepts for Improved Rigid Packaging', *Conference Proceedings, SPE ANTEC*, Nashville, USA.

Joao, B. P. Soares, Abbott, R. F., Kim, J. D. (2000), "Environmental stress cracking resistance of polyethylene: The use of CRYSTAF and SEC to establish structure-property relationships", *Journal of Polymer Science Part B: Polymer Physics*, **38**, 1267-1275.

Joel, R. F. (1995), "Polymer Science and Technology", Englewood Cliffs, New Jersey, USA, Prentice Hall PTR

Kabanemi, K. K., He´tu, J. F., Derdouri, A. (2002) "Design Sensitivity Analysis Applied to Injection Molding for Optimization of Gate Location and Injection Pressure", *Symposium Proceedings, National Research Council of Canada (NRC)*, Boucherville, Canada

Kefalas, V. A. (1995), "Solvent Crazing as A Stress-Induced Surface Adsorption and Bulk Plasticization Effect", *Journal Applied Polymer Science*, **58**, 711-717.

Keller, K., Lester, G. R. (1954), Philosophical Transactions of the Royal Society of London. Series B, Biological Sciences, London, UK, **A247**, 1-34.

REFERENCES

Keller, A. (1955),"The Spherulitic Structure of Crystalline Polymers. Part I. Investigations with The Polarizing Microscope", *Polymer Science*, **17(84)**, 291-308.

Konno, M., Cui, A., Nishiwaki, N., Hori, S. (1993), "Measurement of The Polymer Melt Temperature in Injection Molding Machine by Using Ultrasonic Technique", *Conference Proceedings, SPE ANTEC*, New Orleans, USA.

Lai, G. Y., Rietveld, J. X. (1996), "Role of Polymer Transparency and Temperature Gradients in The Quantitative Measurement of Process Stream Temperature During Injection Molding via IR Pyrometry", *Polymer Engineering Science*, **36**,1755-1768.

Laroche, D., DiRaddo, R. W., Pecora, L. (1995), "Closed-loop optimization and integrated analysis of the blow moulding process", *Conference Proceedings, Numiform*, New York, USA

Launay, A., Thominette, F., Verdu, J. (1999), "Water Sorption in Amorphous Poly(Ethylene Terephthalate)", *Journal Applied Polymer Science*, **73**, 1131-1137.

Lebaudy, Ph., Grenet, J. (2001),"Heating Simulation of Multilayer Preforms", *Journal of Applied Polymer Science*, **80**, 2683-2689.

Lee D. K., Soh, S. K. (1996), "Prediction of Optimal Preform Thickness in Blow Molding", *Polymer Engineering Science*, **36**, 1513-1520.

Lee, S. C., Min, B, G. (1999), "Depression of Glass Transition Temperature Due to The Chain Extension in Glassy State", *Polymer*, **40**, 5445-5448.

REFERENCES

Leigner, F. P. (1985), "Free-Blown PET Preforms Characterize Blown Bottles", *Plastics Engineering* **41**, 47-51.

Liang J. Z., Ness, J. N. (1996), "The Calculation of Cooling Time in Injection Moulding", *Journal Material Processing Technology*, **57**, 62-64.

Lofgren, E. A., Jabarin, S. A. (1994), "Polarized Internal Reflectance Spectroscopic Studies of Oriented Poly(Ethylene Terephthalate)", *Journal Applied Polymer Science*, **51**, 1251-1267.

Lu, X., Hay, J. N. (2000), "The Effect of Physical Aging on The Rates of Cold Crystallization of Poly(Ethylene Terephthalate)", *Polymer*, **41**, 7427-7436.

Lu, X. F., Hay, J. N. (2001), "Isothermal Crystallization Kinetics and Melting Behaviour of Poly(Ethylene Terephthalate)", *Polymer*, **42**, 9423-9431.

Lustiger, A., Markham, R. L. (1983), "Importance of Tie Molecules in Preventing Polyethylene Fracture Under Long-Term Loading Conditions", *Polymer*, **24**, 1647-1654.

Lustiger, A. (1986), "Failure of Plastics", Munich, Germany, Hanser Publishers.

Lyu, M. Y., Pae, Y. (2003), "Bottom Design of Carbonated Soft Drink Poly(Ethylene Terephthalate) Bottle to Prevent Solvent Cracking", *Journal of Apply Polymer Science*, **88**, 1145-1152.

REFERENCES

Mahendrasingam, A., Martin, C., Fuller, W., Blundell, D. J, (1999), "Effect of Draw Ratio and Temperature on The Strain-Induced Crystallization of Poly (Ethylene Terephthalate) at Fast Draw Rates", *Polymer*, **40**, 5553-5565.

Mahendrasingam, A., Blundell, D. J., Martin, C. (2000),"Influence of Temperature and Chain Orientation on The Crystallization of Poly(Ethylene Terephthalate) During Fast Drawing", *Polymer*, **41**, 7803-7814.

Marco, Y., Chevalier, L., Poitou, A. (2002), "Induced Crystallization and Orientation of Poly(Ethylene Terephthalate) During Uniaxial and Biaxial Elongation", *Macromolecule Symposium*, **185**, 15-34.

Mark, H. F., Bikales, N. M., Overberger, C. G., Menges, G. (1985), "Organophosphorus polymers", *Encyclopedia of Polymer Science and Engineering*, **10**, 595-618.

Martin, L., Stracovsky, D., Laroche, D., Bardetti, A., Ben-Yedder, R., DiRaddo, R. (1999), "Modeling and Experimental Validation of The Stretch Blow Moulding of PET", *Conference Proceedings, SPE ANTEC*, New York, USA

Maruhashi, Y., Asada, T. (1996), "Structure and Properties of Biaxially Stretched Poly(Ethylene Terephthalate) Sheets", *Polymer Engineering and Science*, **36**, 483-494.

Maruhashi, Y. (2001), "Structure and Physical Properties of Biaxially Stretched Polyethylene Terephthalate Sheets Under Different Heat-Set and Stretch Conditions", *Polymer Engineering and Science*, **41**, 2194-2199.

REFERENCES

Masood, S. H., Keshavamurthy, V. (2005), "Development of Collapsible PET Water Fountain Bottles", *Journal of Materials Processing Technology*, **162**, 83-89.

McCaig, M. S., Paul, D. R. (2000), "Effect of Film Thickness on the Changes in Gas Permeability of a Glassy Polyarylate Due To Physical Aging. Part I. Experimental Observations", *Polymer*, **41**, 629-637.

McCaig, M. S., Paul, D. R., Barlow, J. W. (2000), "Effect of Film Thickness on the Changes in Gas Permeability of a Glassy Polyarylate Due to Physical Aging Part II. Mathematical Model", *Polymer*, **41**, 639-648.

McCrun, N. G., Buckley, C. P., Bucknall, C. B. (1997), "Principles of Polymer Engineering", Oxford, UK., Oxford University Press.

McEvoy, J. P. (1997), "Computer Aided Design for Injection Blow Molded Plastic Containers", PhD Thesis, The Queen's University Belfast, UK

McEvoy, J. P., Armstrong, C. G., Crawford, R. J. (1998),"Simulation of the Stretch Blow Moulding Process of PET Bottles", Advances *in Polymer Technology*, **17**, 339-352.

Menary, G. H., Armstrong, C. G., Crawford, R. J., McEvoy, J. P. (2000),"Modelling of Poly(Ethylene Terephthalate) In Injection Stretch-Blow Moulding", *Plastic Rubber Composite*, **29**, 360-370.

REFERENCES

Menary, G. H. (2001), "Modelling Injection Stretch Blow Moulding and The Resulting 'In Service' Performance of PET Bottles", Belfast, UK., The Queen's University Press.

Menges, G., Michaeli, W., Mohren, P. (2001) "How to Make Injection Molds", Munich, Germany, Hanser Publishers.

Migler, K. B., Bur, A. J. (1998), "Fluorescence Based Measurement of Temperature Profiles During Polymer Processing", Polymer Engineering Science, **38**, 213-221.

Miller, M. L. (1966), "The Structure of Polymers", New York, USA, Reinhold Publishing Corp.

Misra, A., Stein, R. S. (1972), "Light Scattering Studies of The Early Stages of The Crystallization of Poly(Ethylene Terephthalate)", *Journal of Polymer Science Part B: Polymer Letters* , **10**, 473-477.

Misra, A., Stein, R. S. (1975),"Stress-Induced Crystallization of Poly(Ethylene Terephthalate)", *Journal Polymer Science, Polymer Physic*, **17**, 235-257.

Mitra, D., Misra, A. (1988),"Study on the Effect of Dibenzylidene Sorbitol as A Nucleating Agent on the Crystallization and Morphology of Poly(Ethylene Terephthalate)**",** *Journal Applied Polymer Science*, **36**, 387-402.

Monteix, S., Schmidt, F., Le Maoult, Y., Ben Yedder, R., Diraddo, R. W., Laroche, D. (2001),"Experimental Study and Numerical Simulation Of Preform or Sheet Exposed to Infrared Radiative Heating", *Journal of Materials Processing Technology*, **119**, 90-97.

Moore, R. S., O'Loane, K., Shearer, J. C. (1981), "Fourier Transform Infrared Characterization of Conformational Changes in Amorphous Poly(ethylene Terephthalate) During Volume Recovery", *Polymer Engineering Science*, **21**, 904-906.

Moskala, E. J. (1998), "A Fracture Mechanics Approach to Environmental Stress Cracking in Poly(Ethylene-Terephthalate)", *Polymer*, **39**, 675-680.

Munk, P., Aminabhavi, T.M. (2002), "Introduction to Macromolecular Science", New York, USA, John Wiley & Sons, Inc.

Newman, S., Cox, W.P. (1960), "The Glass Temperature of Semicrystalline Polymers", *Journal of Polymer Science*, **46**, 29-49.

Nyugen, K. T., Prystay, M. (1978), "An Inverse Method for Estimation of the Initial Temperature Profile and Its Evolution in Polymer Processing", *International Journal of Heat and Mass Transfer*, **42**, 1969-1978.

Ohlberg, S. M., Roth, J., Raff, R. A. V. (1959), "Relationship between impact strength and spherulite growth in linear polyethylene", *Journal Applied Polymer Science*, **1**, 114-120.

Osborn, K.R., Jenkins, W.A. (1992), "Plastic Films: Technology and Packaging Application", Lancaster, Pennsylvania, Technomic Publishing Co.

Ozawa, T. (1971),"Kinetics of Non-Isothermal Crystallization", *Polymer*, **12(3)**, 150-158.

Peterlin, A. (1975),"Environmental Effects on Low Temperature Crazing of Crystalline Polymers", *Journal Polymer Science Symposium*, **50**, 243-264.

Pfromm, P. H., Koros, W. J. (1995), "Accelerated Physical Ageing of Thin Glassy Polymer Films: Evidence from Gas Transport Measurements", *Polymer*, **36**, 2379-2387.

Pham, X. T., Thibault, F., Lim, L. T. (2004), "Modeling and Simulation of Stretch Blow Molding of Polyethylene Terephthalate", *Polymer Engineering and Science*, **44**, 1460-1472

Reading M., Price, D. M., Orliac, H. (2001), "Measurement of Crystallinity in Polymers Using Modulated Temperature Differential Scanning Calorimetry", *Materials Characterization by Dynamic and Modulated Thermal Analytical Techniques*, **ASTM STP 1402**, 17-31.

Rietsch, F. (1990), "Strain-Induced Crystallization of Oriented Poly (Ethylene Terephthalate): Influence on the Tensile Yield Stress Behaviour", *European Polymer*, **26**, 1077.

Rietveld, J. X., Lai, G. Y. (1994), "Inverse Method for Obtaining The Temperature Profile Within A Mold via IR Pyrometry", Conference *Proceedings, SPE ANTEC*, San Francisco, USA.

Robertson, G.L. (1993), "Food Packaging: Principles and Practice", New York, USA, Marcel Dekker Inc.

Rosato, D.V., Rosato, D.V. (1989), "Blow Molding Handbook", Oxford, UK., Oxford University Press.

REFERENCES

Rosato, D. V. (1998), "Blow Molding Handbook", Cincinnati, USA, Hanser/Gardner Publications Inc.

Roseblade, R. J. (1983), "The Effect of Injection Moulding Processing Parameters on the Environmental Stress Cracking Resistance of Polycarbonate Mouldings", Ascot Vale, Vic., Australia, Materials Research Laboratories

Rybnikar, F. (1960),"Secondary Crystallization of Polymers", *Journal of Polymer Science*, **44**, 517-522.

Salem, D.R. (1998), "Microstructure Development during Constant-Force Drawing of Poly(Ethylene Terephthalate) Film", *Polymer*, **39**, 7067-7077.

Salem, D. R. (1999), "Orientation and Crystallization in Poly(Ethylene Terephthalate) during Drawing at High Temperatures and Strain Rates", *Polymer Engineering and Science*, **39**, 2419-2430.

Sathyanarayana, P. M., Shariff, G., Thimmegowda, M. C., Ramani, R., Ranganathaiah, C., Ashalatha, M. B., (2002), "Structural Relaxation in Poly(Ethylene Terephthalate) Studied by Positron Annihilation Lifetime Spectroscopy", *Polymer International*, **51**, 765-771.

Satoto, R., Morikawa, J., Hashimoto, T. (1999), "Thermally Stimulated Current Studies on Molecular Relaxation and Blow Moulding of Poly(Ethylene Terephthalate)", *Polymer International*, **48**, 509-514.

REFERENCES

Schmidt, P. G. (1963), "Polyethylene Terephthalate Structural Studies", Journal Polymer Science, **A1**, 1271-1292.

Schmidt, F. M., Agassant, J. F., Bellet, M., Desoutter, L. (1966), "Viscoelastic Simulation of PET Stretch/Blow Molding", *Journal Non-Newtonian Fluid Mechanic*, **64**, 19-42.

Schmidt, L. R., Carley, J. F. (1975)"Biaxial stretching of heat-softened plastic sheets: Experiments and results", *Polymer Engineering Science*,**15**, 51-62.

Schmidt, F. M., Agassant, J. F., Bellet, M. (1998), "Experimental Study and Numerical Simulation of The Injection Stretch/Blow Molding Process", *Polymer Engineering and Science*, **38**, 1399-1412.

Shanahan, M. E. R., Chen-Fargheon, C., Schultz, J. (1980), "The Influence of Spherulitic Size on The Environmental Stress Cracking of Low Density Polyethylene", *Makromolekular Chemie*, 181, 1121-1126.

Smith, D. E., Chen, C. J., Usman, M., Koskey, J. (1997), "Multi-Gate Injection Molding Process Optimization Using Design Sensitivity. Analysis", American Society Mechanical Engineering, New York, USA

Starkweather, H. W., JR., Moore, G. E., Hansen, J. E., Roder, T. M., Brooks, R. E. (1956), "Effect of Crystallinity on The Properties of Nylons " *Journal of Polymer Science*, **21**, 189-204.

Starkweather, H. W., Richard, J. R., Brooks, R. E. (1959), "Effect of Spherulites on The Mechanical Properties of Nylon 66", *Journal Applied Polymer Science*, **1**, 236-239.

Stelson, K. A. (2003), "Calculating Cooling times for Polymer Injection Moulding", *Proceedings of the institution of Mechanical Engineers*, **217**, 709-713

Sternstein, S. S., Ongchin, L., Silverman, A. (1968), "Craze Formation and Shear Yielding Considered for Glassy Polymers in terms of Stress Field Requirements", Journal Polymer Science Symposium, 7, 175-199.

Strebel, J. J., Moet, A, (1995), "The Effects of Annealing on Fatigue Crack Propagation in Polyethylene", *Journal Polymer Science, Polymer Physic*, **33**, 1969-1984

Strebel, J. J., Benson, M. (1996),"The Effect of Processing Variables on The Environmental Stress Crack Resistance of Blow-Molded Polyethylene Bottles", *Polymer Engineering And Science*, **36**, 1266-1271.

Strobl, G. (1997), "The Physics of Polymers: Concepts for Understanding Their Structures and Behavior" Berlin, Germany, Springer.

Struik, L. C. E. (1978), "Physical Aging of Amorphous Polymer and other Materials", Amsterdam, Elsevier applied science publishers.

Stuart, B. (2002), "Polymer Analysis", New York, USA, John Wiley & Sons

REFERENCES

Sun, N., Yang, J., Shen, D. (1999), "The Effect of Water Absorption on The Physical Ageing of Amorphous Poly(Ethylene Terephthalate) Film", *Polymer*, **40**, 6619-6622.

Sűvegh, K., Zelkó, R. (2002), "Physical Ageing of Poly(vinylpyrrolidone) under Different Humidity Conditions", *Macromolecules*, **35**, 795-800.

Tant, M. R., Wikes, G. L. (1981), "An Overview of The Non-Equilibrium Behavior of Polymer Glasses", Polymer Engineering Science, **21**, 874-895.

Tant, M. R., Wilkes, G. L. (1981), "Physical Aging Studies of Semi-crystalline Poly(ethylene Terephthalate)", *Journal Applied Polymer Science*, **26**, 2813-2825.

Thibault, F., Malo, A., Lanctot, B., Diraddo, R. (2007), "Preform shape and operating condition optimization for the stretch blow molding process", *polymer engineering science*, **47**, 289-301

VanderPlaats, G. N. (1999), "Numerical Optimization Techniques for Engineering Design", Colorado Springs, USA, VanderPlaats Research & Development Inc.

Van Dijk, R. (1997), "FEA as A Design Tool", *Packaging Today Europe*, **1**, 40-44.

Varma, P., Lofgren, E.A., Jabarin, S.A. (1998), "Properties and Kinetics of Thermally Crystallized Orientated Poly(Ethylene Terephthalate) (PET) I: Kinetics of Crystallization", *Polymer Engineering and Science*, **38**, 237-244.

REFERENCES

Venkateswaran, G., Cameron, M. R., Jabarin, S. A. (1998), "Effects of Temperature Profiles Through Preform Thickness on The Properties of Reheat-Blown PET Containers", *Advances in Polymer Technology*, **17**, 237-349.

Von Mises, R. (1913), "Mechanik der Festen Korper im plastisch deformablen Zustand", *Nachr. Math. Phys.*, **1**, 582–592.

Wadley, H. N. G., Norton, S. J., Mauer, F., Droney, B. (1986), "Ultrasonic Measurement of Internal Temperature ", Philosophical Transactions of the Royal Society of London Series, London, UK, **A320**, 341-361.

Walter Michaeli, E. H. (2004)," Saving Time by Foam Injection Molding", *Conference Proceedings, SPE ANTEC*, Chicago, USA.

Wang, S., Makinouchi, A., Nakagawa, T. (1998), "Three-Dimensional Viscoplastic FEM Simulation of a Stretch Blow Molding Process", *Advances in Polymer Technology*, **17**, 189-202.

Wang, S., Makinouchi, A., Okamoto, M., Kotaka, T., Maeshima, M., Ibe, N., Nakagawa, T. (2000), "Viscoplastic Material Modelling for the Stretch Blow Moulding Simulation", *International Polymer Processing*, **15**, 166-175.

Wang, S., Makinouchi, A., Okamoto, M., Kotaka, T., Maeshima, M., Ibe, N., Nakagawa, T. (1999), "3D FEM Simulation of the Stretch Blow Molding Process with A Two-Stage Material Model", *Conference Proceedings, SPE ANTEC*, New York, USA.

REFERENCES

Ward, I.M.   (1975), "Structure and Properties of Oriented Polymers", New York, USA, John Wiley and Sons

Wellinghoff, S., Baer, E. (1975), "The Mechanism of Crazing in Polystyrene" *Journal Macromolecular Science–Physic*, **11**, 367-387

Wright, D. C., Gotham, K. V. (1983),"Solvent-Crazing Criteria", Polymer Engineering Science, **23**, 135-139.

Wright, D. (1996), "Environmental Stress Cracking of Plastics", Shawbury, UK, Rapra Technology Ltd

Xinhai, Z., Guogun, Z., Guangchun, W., Tonghai, W. (2006), "Sensitivity Analysis Based Multiple Objective Preform Die Shape Optimal Design in Metal Forging", J. Mater. Sci. Technol., **22**, 273-278.

Xu, H., Kazmer, D. A. (1999), "Stiffness Criterion for Cooling Time Estimation", *International Polymer Processing*, **14**, 103-108

Yaffe, M. B., Kramer, E. J. (1981), "Plasticization Effects on Environmental Craze Microstructure", Journal of Material Science, **16**, 2130-2136.

Yang, Z. J., Harkin-Jones, E. M. A., Armstrong, C. G., Menary, G. H. (2004), "Finite Element Modelling of Stretch-Blow Molding of PET Bottles Using Buckley Model: Plant Tests and

Effects of Process Conditions and Material Parameters", *Journal of Process Mechanical Engineering*, **218**, 237-250.

Yang, Z. J., Jones, E. H., Menary, G. H., Armstrong, C. G. (2004), "A Non-Isothermal Finite Element Model for Injection Stretch-Blow Molding of PET Bottles with Parametric Studies", *Polymer Engineering Science*, **44**, 1379-1390.

Yilmazer, U., Xanthos, M., Bayram, G., Tan, V.(2000), "Viscoelastic Characteristics of Chain Extended/Branched and Linear Polyethylene Terephthalate Resins", *Journal of Applied Polymer Science*, **75**, 1371-1377.

Yu, C. J., Sunderland, J. E. (1992), "Determination of Ejection Temperature and Cooling Time in Injection Molding", *Polymer Engineering Science*, **32**, 191-197.

Zagarola, S. W. (1998), "Designing PET Preform Injection Molding Process for The Lightest Practical Weight Offers Opportunities for Improved Productivity and Quality", *Conference Proceedings, SPE ANTEC*, Atlanta, USA.

Zagarola, S. W. (2000), "Blow and Injection Molding Process Set-Ups Play a Key Role in Stress Crack Resistance for PET Bottles for Carbonated Beverages', *Conference Proceedings, SPE ANTEC*, Orlando, USA.

Zelkó, R., Süvegh, K., Marton, S., Rácz, I. (2000), "Effects of Storage Conditions on the Free Volume of Polyvinylpyrrolidone: Comparison of Positron Lifetime Data with the Tensile Strength of Tablets", *Pharmaceutical Research*, **17**, 1030-1032.

Zhao, J., Wang, J., Li, C., Fan, Q. (2002), "Study of The Amorphous Phase in Semi-crystalline Poly(Ethylene Terephthalate) Via Physical Aging", *Macromolecules*, **35**, 3097-3103.

APPENDICES

In appendix A section, the statistic values that belong to the optimum Von Mises stress analysis carried out through CATIA V5 R14 version are given in tables. The statistical values are for the optimum stress analysis conducted under the internal pressure of 0.4 MPa and optimum base dimensions optimized by ECHIP-7.

Table A-1. Mesh entities and sizes

Entity	Size
Nodes	35732
Elements	119467

Table A-2. Element type

Connectivity	Statistic
TE4	119467 (100.00%)

Table A-3. Element Quality

Criterion	Good	Poor	Bad	Worst	Average
Skewness	113915 (95.35%)	5421 (4.54%)	131 (0.11%)	0.993	0.450
Distortion (deg)	79651 (66.67%)	34992 (29.29%)	4824 (4.04%)	62.962	30.300
Stretch	119421 (99.96%)	46 (0.04%)	0 (0.00%)	0.178	0.623
Min. Length (mm)	119467 (100.00%)	0 (0.00%)	0 (0.00%)	0.556	1.670
Max. Length (mm)	119467 (100.00%)	0 (0.00%)	0 (0.00%)	5.310	3.123
Shape Factor	119402 (99.95%)	65 (0.05%)	0 (0.00%)	0.160	0.675
Length Ratio	119440 (99.98%)	27 (0.02%)	0 (0.00%)	6.570	1.944
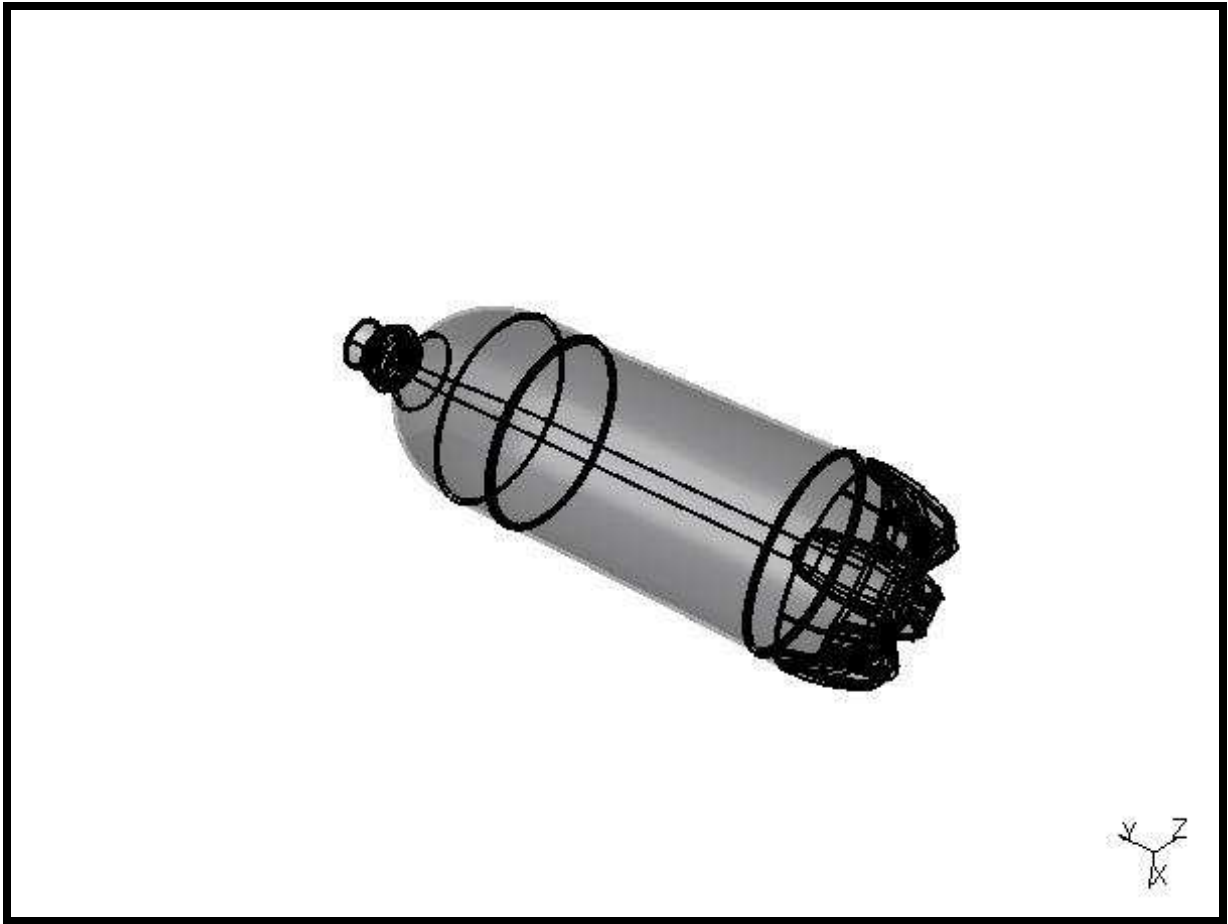
Fig.A-1. Boundary conditions on the bottle

Table A-4. Structure Computation results

Number of nodes	35732
Number of elements	119467
Number of D.O.F	107196
Number of Contact relations	0
Number of Kinematic relations	0
Linear tetrahedron	119467

Table A-5. Restraint computation results

Name: Restraint Set	1
Number of S.P.C	1563

Table A-6. Applied load-1 computation results

Fx (N)	0.04106
Fy (N)	-151.3
Fz (N)	0.008740
Mx (N.m)	0.0001245
My (N.m)	-00009121
Mz (N.m)	-0.001402

Table A-7. Stiffness computation results

Number of lines	107196
Number of coefficients	1893765
Number of blocks	4
Maximum number of coefficients per bloc	499992
Total matrix size Mb	22.08

Table A-8. Singularity computation results

Number of local singularities	0
Number of singularities in translation	0
Number of singularities in rotation	0
Generated constraint type	MPC

Table A-9. Constraint computation results

Number of constraints	1563
Number of coefficients	0
Number of factorized constraints	1563
Number of coefficients	0
Number of deferred constraints	0

Table A-10. Direct method computation results

Name	StaticSet.1
Restraint	RestraintSet.1
Load	LoadSet.1
Strain Energy	1.350e+000 J
Equilibrium	

Table A-11. Factorized computation results

Method	SPARSE
Number of factorized degrees	105633
Number of supernodes	7191
Number of overhead indices	546522
Number of coefficients	20605248
Maximum front width	1680
Maximum front size	1412040
Size of the factorized matrix (Mb)	157.206
Number of blocks	21
Number of Mflops for factorization	1. 155e+004
Number of Mflops for solve	8. 295e+001
Minimum relative pivot	1. 019e-002

Table A-12. Applied forces computation results

Components	Applied Forces	Reactions	Residual	Relative Magnitude Error
Fx (N)	4.1058e-002	-4.1058e-002	3.2193e-011	9.9400e-013
Fy (N)	-1.5128e+002	1.5128e+002	-1.7337e-011	5.3531e-013
Fz (N)	8.7403e-003	-8.7403e-003	-1.8613e-010	5.7472e-012
Mx (Nxm)	1.2454e-004	-1.2454e-004	1.8579e-011	2.0913e-012
My (Nxm)	-9.1206e-005	9.1206e-005	2.1079e-012	2.3727e-013
Mz (Nxm)	-1.4019e-003	1.4019e-003	9.8382e-012	1.1074e-012

Fig.A-2. Deformed mesh on the bottle under the internal pressure of 0.4 MPa.
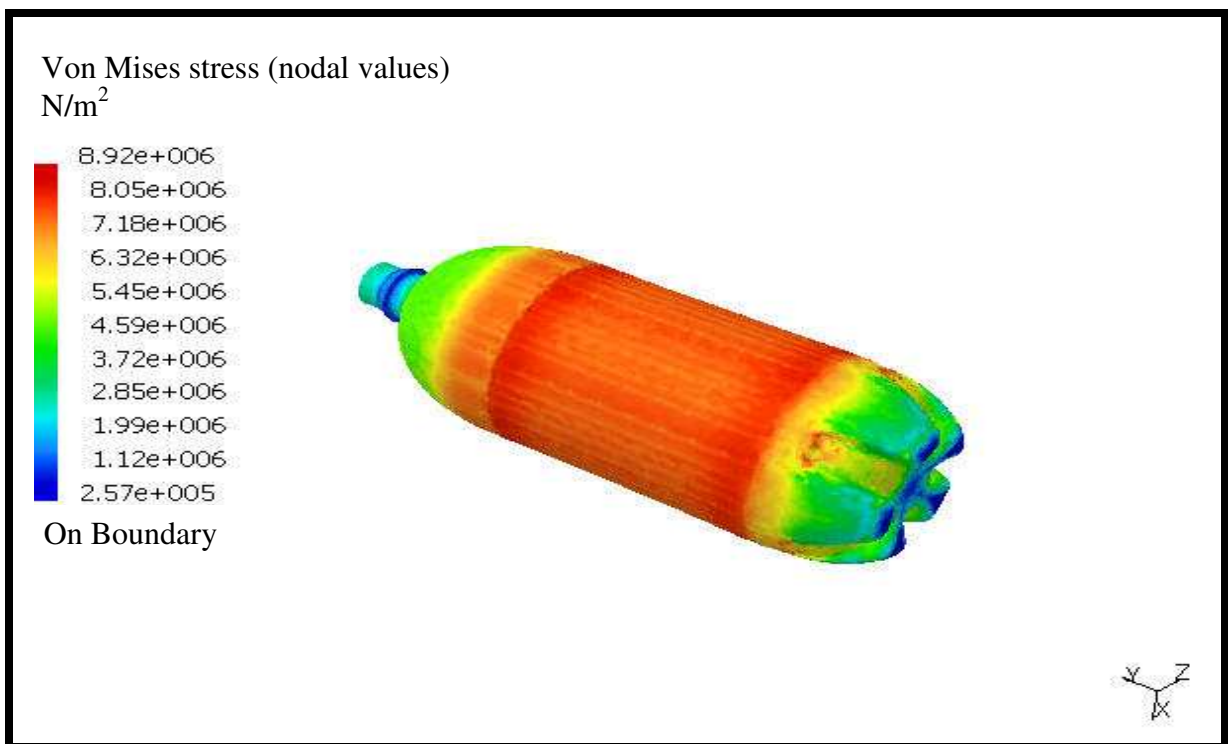
Fig.A-3. Optimum Von Mises stress for the internal pressure of 0.4 MPa.

Table A-13. Von Mises stress values for the pressure of 0.4 MPa. at different wall thickness

			Von Mises Stress values (MPa)					
Bottle wall thickness (mm)			0.5		1		2	
Foot Length (mm)	Valley width (mm)	Clearance (mm)	Max	Min	Max	Min	Max	Min
16	1	3	40.30	0.12	18.20	0.13	8.63	0.16
16	1	10	39.10	0.10	20.00	0.15	8.66	0.25
16	1	17	39.80	0.17	22.10	0.33	10.20	0.28
16	4.667	12.333	49.10	0.14	23.40	0.25	9.36	0.21
16	6.5	3	48.10	0.05	22.60	0.14	9.59	0.05
16	6.5	10	45.70	0.11	20.70	0.30	9.83	0.11
16	6.5	17	46.40	0.61	22.80	1.16	10.90	0.69
16	12	3	55.20	0.10	27.60	0.16	11.50	0.09
16	12	10	54.80	0.18	23.90	0.27	10.60	0.16
16	12	17	50.50	0.19	23.70	0.22	10.50	0.26
24.333	4.667	7.667	44.30	0.07	22.70	0.12	8.97	0.12
28.5	1	3	39.80	0.10	22.00	0.13	9.01	0.13
28.5	1	17	40.30	0.33	19.50	0.65	9.75	0.40
28.5	6.5	10	50.10	0.10	19.70	0.17	10.10	0.15
28.5	6.5	17	51.20	0.05	21.60	0.77	11.00	0.39
28.5	12	3	50.90	0.08	29.30	0.14	12.60	0.10
28.5	12	10	49.70	0.10	22.30	0.26	11.10	0.32
28.5	12	17	46.00	1.15	25.80	0.50	10.80	0.62
32.667	4.667	7.667	49.50	0.12	23.10	0.13	9.75	0.14
32.667	8.333	3	52.00	0.11	27.10	0.14	11.30	0.12
41	1	3	51.50	0.12	26.20	0.12	10.50	0.13
41	1	10	49.10	0.09	21.10	0.13	9.96	0.15
41	1	17	48.40	0.20	24.20	0.16	11.50	0.35
41	6.5	3	57.30	0.07	28.70	0.13	11.70	0.14
41	8.333	12.333	54.50	0.12	26.90	0.14	10.60	0.13
41	12	3	60.20	0.09	32.10	0.13	13.60	0.15
41	12	10	54.80	0.11	29.20	0.13	13.90	0.20
41	12	17	51.40	0.26	25.50	0.19	11.30	0.15

Table A-14. Von Mises stress values for the pressure of 0.6 MPa. at different wall thickness

			Von Mises Stress Values (MPa)					
Bottle wall thickness (mm)			0.5		1		2	
Foot Length (mm)	Valley width (mm)	Clearance (mm)	Max	Min	Max	Min	Max	Min
16	1	3	60.40	0.17	27.30	0.20	12.90	0.24
16	1	10	58.60	0.15	30.00	0.22	13.00	0.38
16	1	17	59.70	0.26	33.20	0.50	15.20	0.41
16	4.667	12.333	73.70	0.22	35.00	0.31	14.00	0.31
16	6.5	3	72.20	0.08	33.90	0.21	14.40	0.07
16	6.5	10	68.60	0.17	31.00	0.45	14.70	0.16
16	6.5	17	69.60	0.91	34.20	1.75	16.30	1.04
16	12	3	82.80	0.14	41.50	0.24	17.30	0.13
16	12	10	82.20	0.27	35.80	0.40	15.90	0.25
16	12	17	75.80	0.29	35.60	0.33	15.70	0.39
24.333	4.667	7.667	66.50	0.11	34.10	0.18	13.40	0.19
28.5	1	3	59.70	0.16	32.90	0.20	13.50	0.19
28.5	1	17	60.40	0.49	29.20	0.98	14.60	0.60
28.5	6.5	10	75.10	0.15	29.60	0.26	15.10	0.23
28.5	6.5	17	76.80	0.07	32.30	1.16	16.40	0.58
28.5	12	3	76.40	0.12	44.00	2.09	18.80	0.15
28.5	12	10	74.50	0.14	33.50	0.38	16.60	0.47
28.5	12	17	69.00	1.72	38.70	0.75	16.20	0.93
32.667	4.667	7.667	74.20	0.18	34.70	0.20	14.60	0.21
32.667	8.333	3	78.00	0.17	40.60	0.21	17.00	0.19
41	1	3	77.30	0.18	39.20	0.19	15.70	0.20
41	1	10	73.70	0.14	31.60	0.20	14.90	0.22
41	1	17	72.70	0.30	36.30	0.25	17.30	0.52
41	6.5	3	85.90	0.11	43.00	0.19	17.60	0.21
41	8.333	12.333	81.80	0.19	40.30	0.21	15.90	0.20
41	12	3	90.40	0.14	48.20	0.20	20.40	0.23
41	12	10	82.20	0.16	43.80	0.19	20.90	0.30
41	12	17	77.10	0.39	38.30	0.29	17.00	0.23
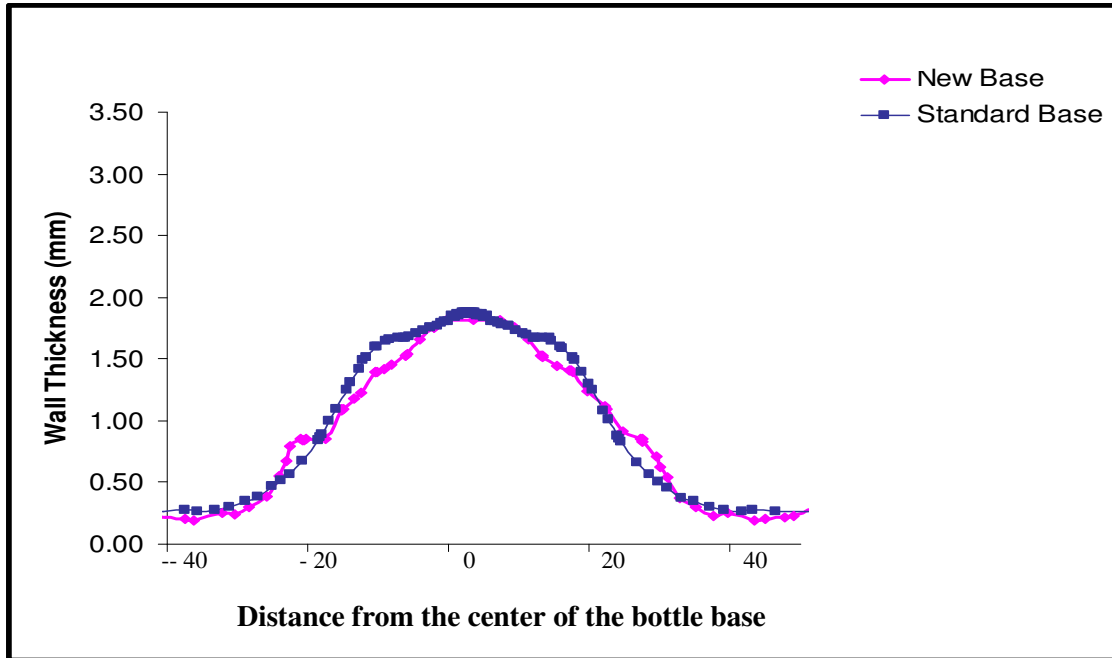
Fig. B-1(a). Comparison of thickness profile of the optimised and standard bases; model-1
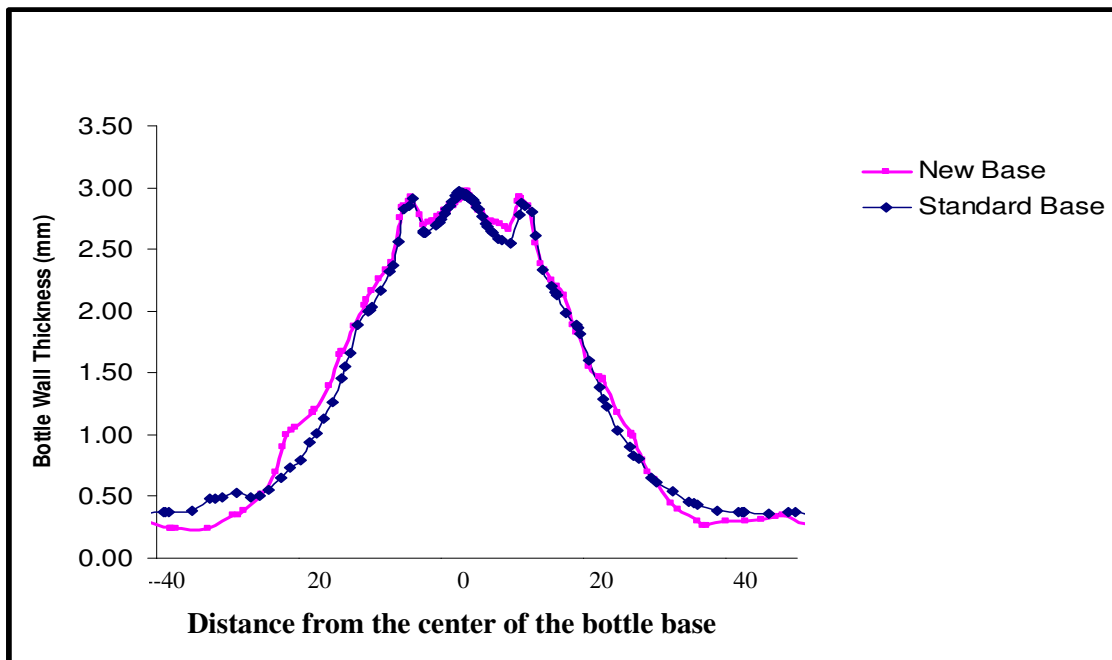
Fig. B-1(b). Comparison of thickness profile of the optimised and standard bases; model-2
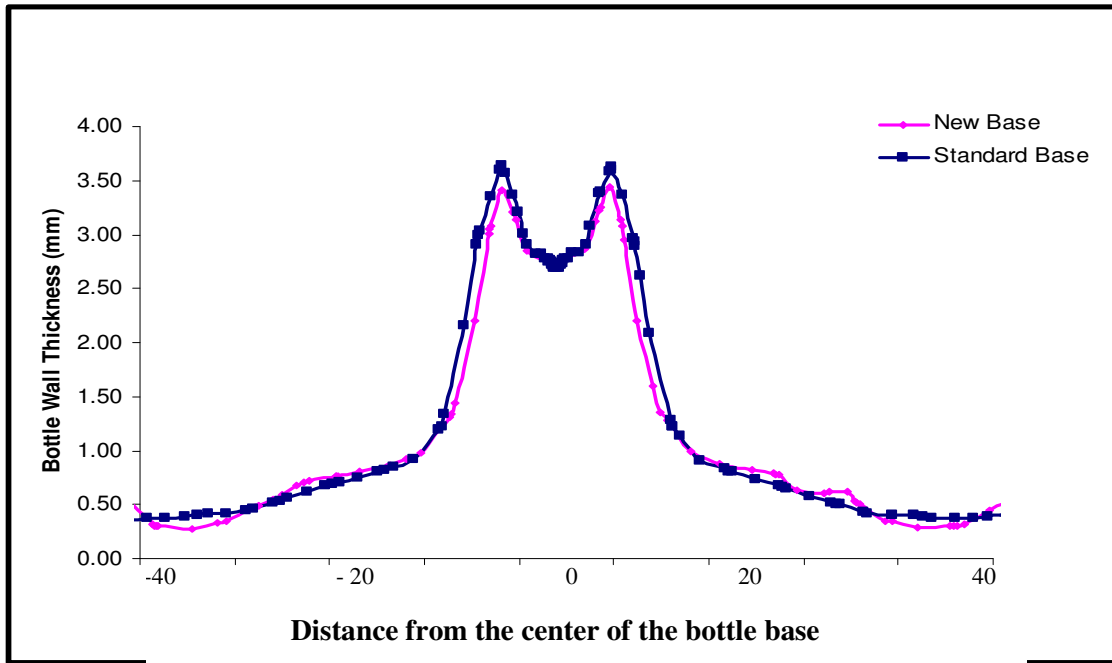
Fig. B-1(c). Comparison of thickness profile of the optimised and standard bases; model-3
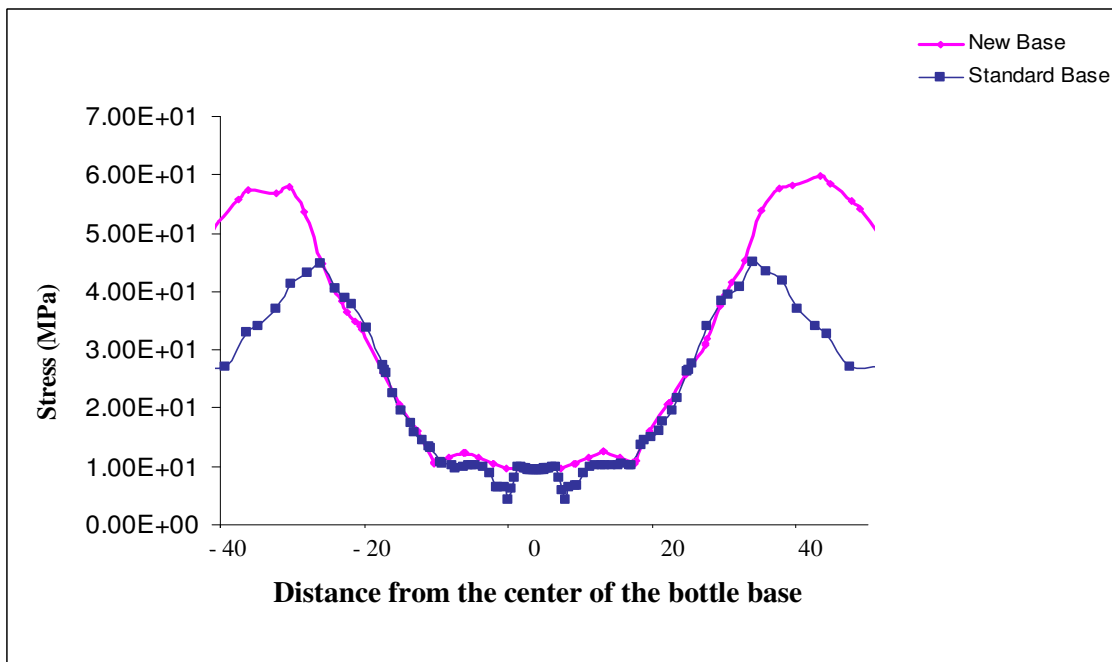
Fig.B-2.(a) Comparison of stress profile of the optimised and standard bases; model-1
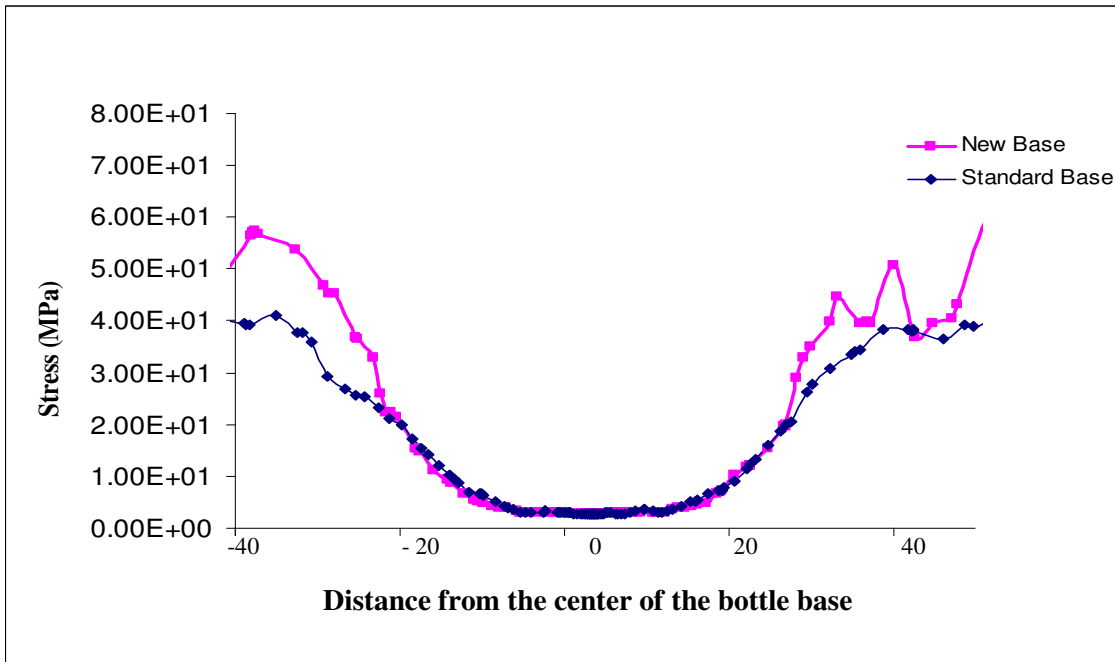
Fig.B-2(b). Comparison of stress profile of the optimized and standard bases; model-2
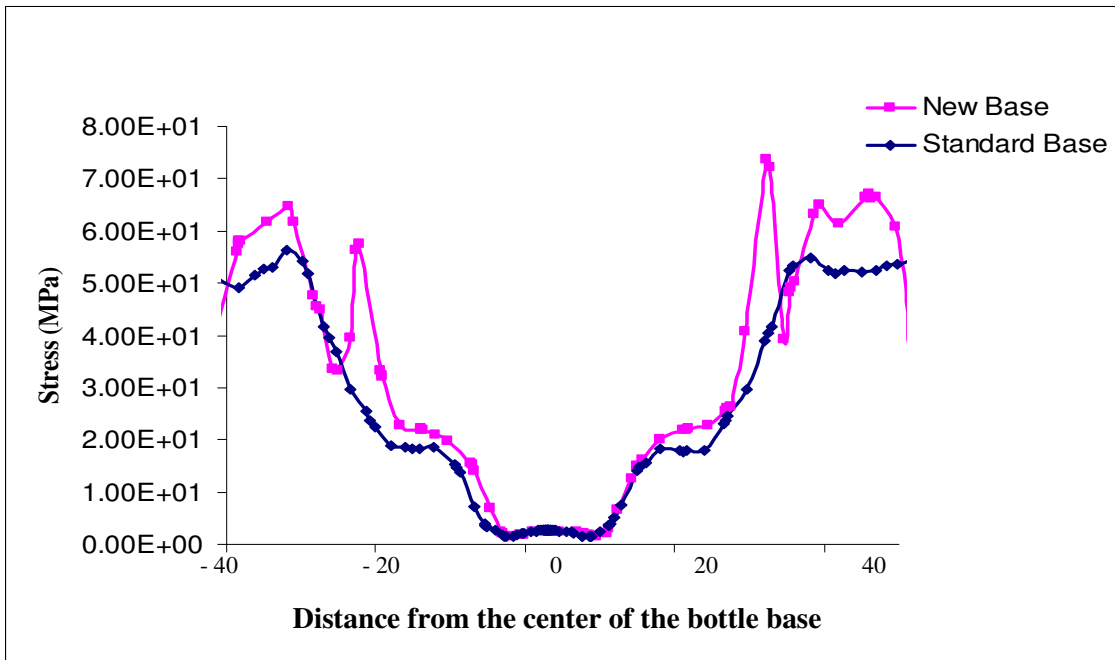
Fig.B-2(c). Comparison of stress profile of the optimised and standard bases; model-3
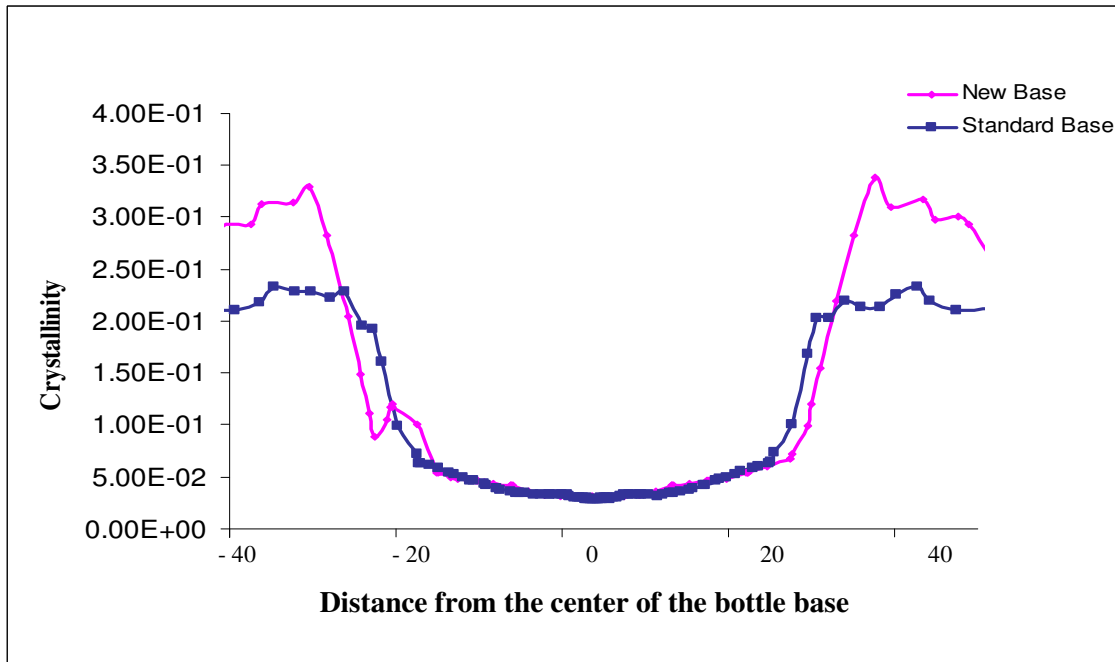
Fig.B-3.(a) Comparison of crystallinity of the optimised and standard bases; model-1
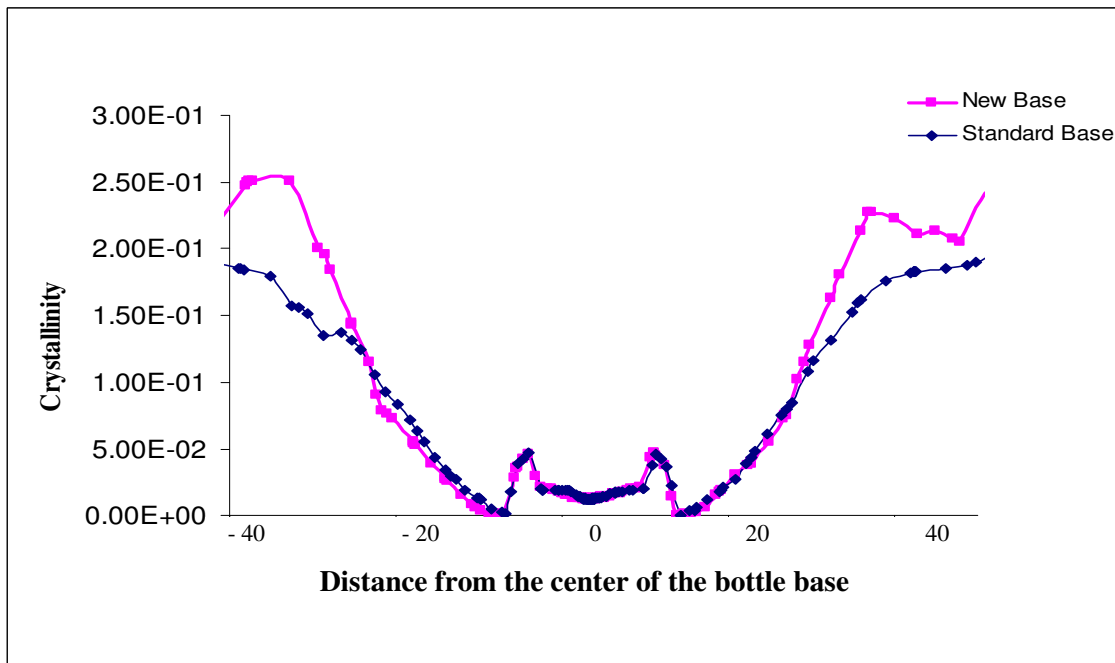
Fig.B-3(b). Comparison of crystallinity of the optimised and standard bases for model-2
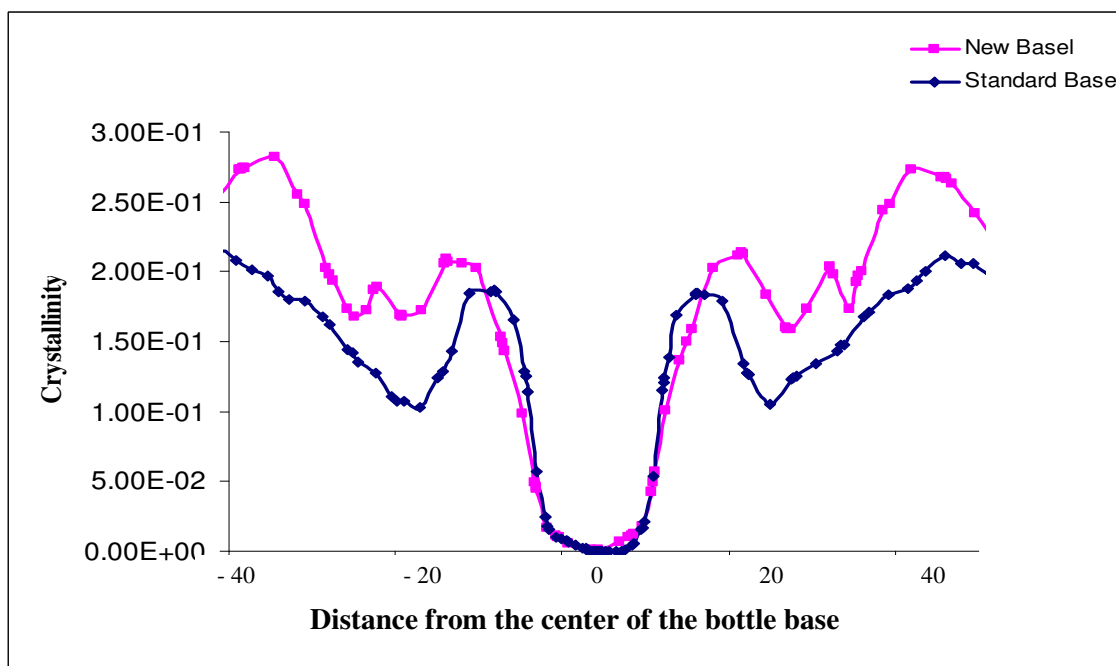
Fig.B-3(c). Comparison of crystallinity of the optimised and standard bases for model-3
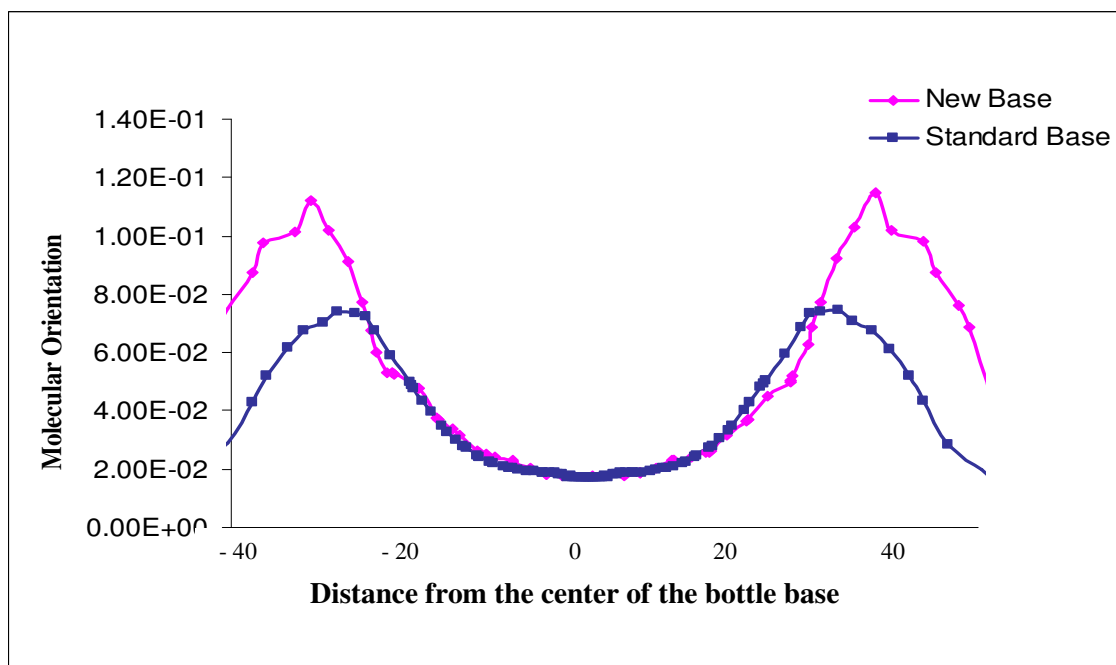
Fig.B-4. (a).Comparison of molecular orientations of the optimized and standard bases; model-1
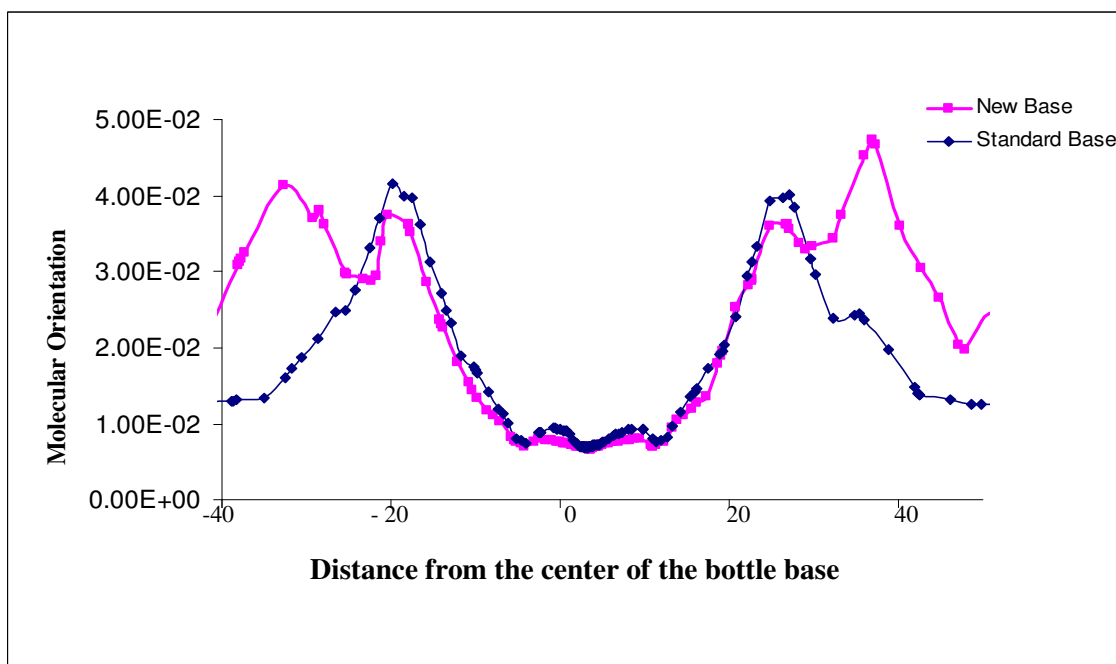
Fig.B-4(b). Comparison of molecular orientations of the optimized and standard bases; model-2
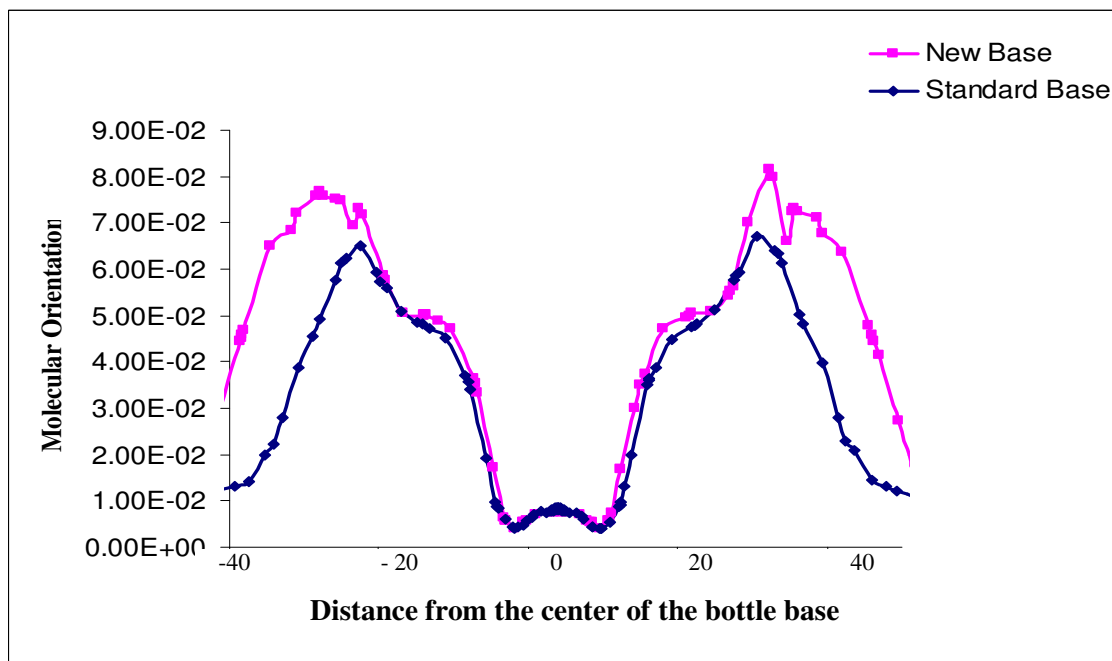
Fig.B-4(c). Comparison of molecular orientations of the optimized and standard bases; model-3
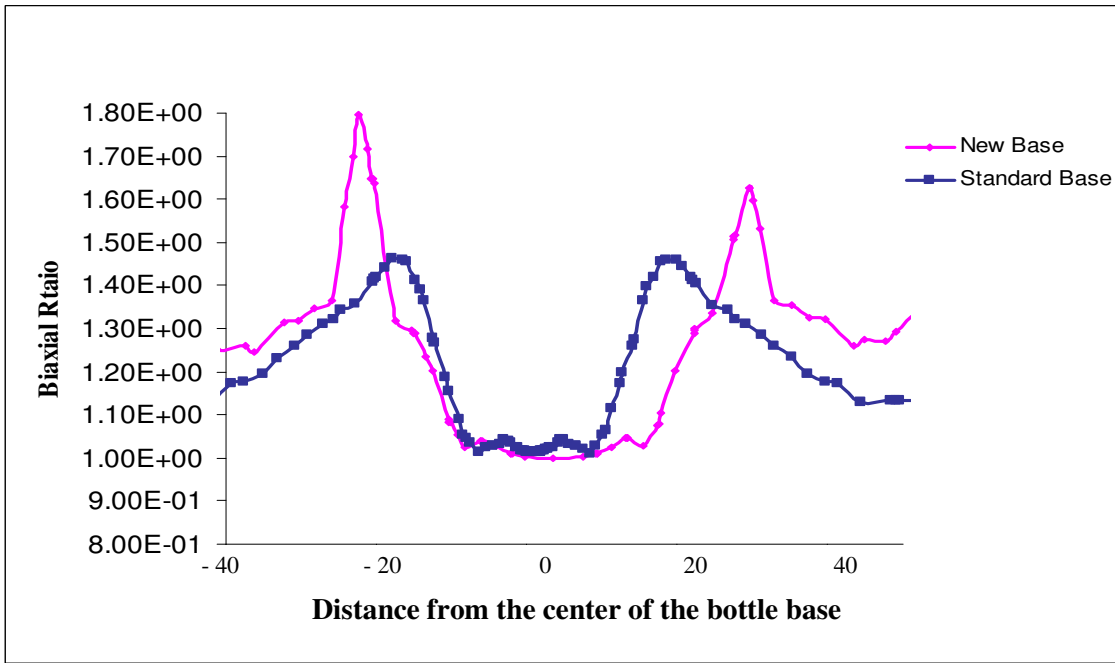
Fig.B-5.(a) Comparison of biaxial ratios of the optimized and standard bases; model-1
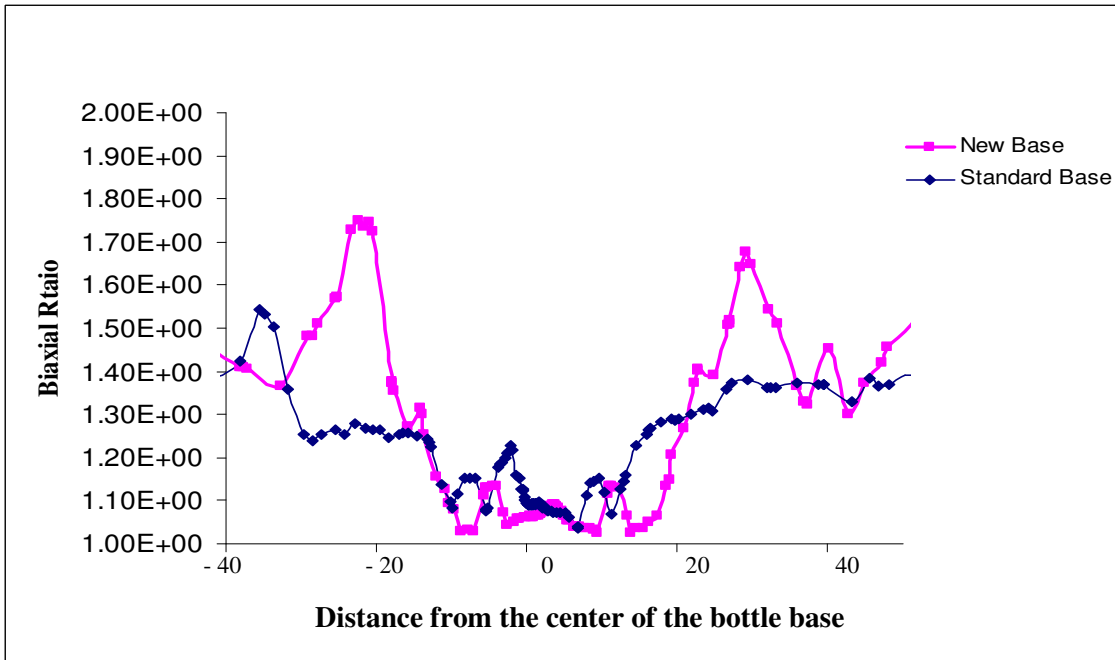
Fig. B-5(b). Comparison of biaxial ratios of the optimized and standard bases; model-2
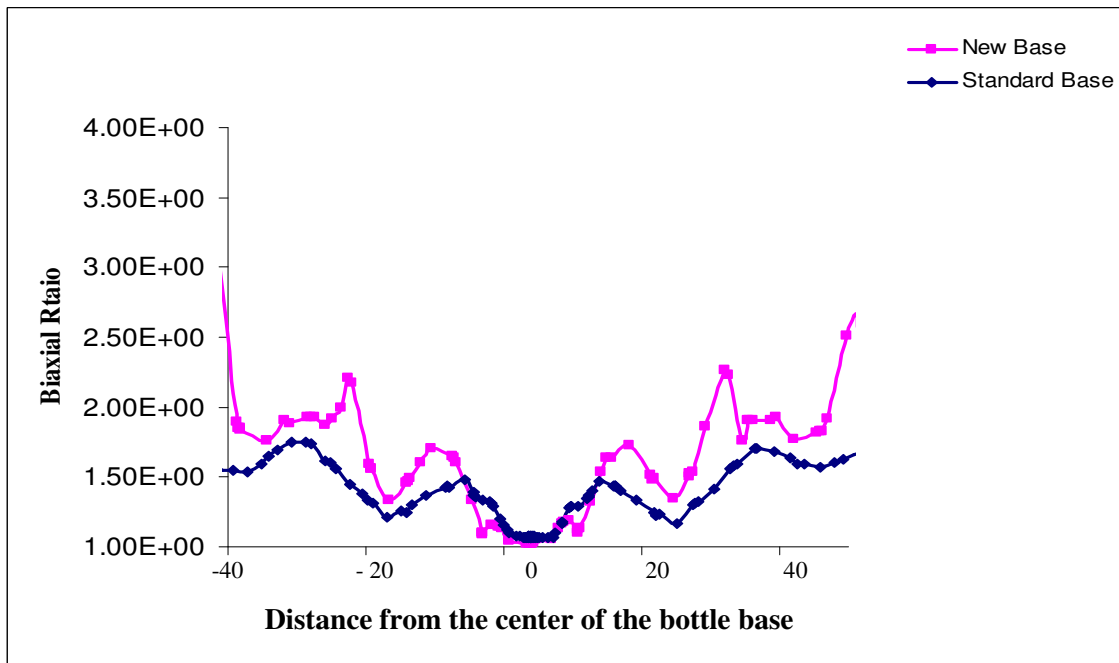
Fig.B-5(c). Comparison of biaxial ratios of the optimized and standard bases; model-3

Table C-1. Bottle burst pressure values for the bottle with standard base

Standard Base			
	Burst	Expansion	Time
Samples	(psi)	(ml)	(seconds)
1	202	678	39
2	203	663	38
3	207	508	33
4	204	531	35
5	205	577	37
6	207	518	35
Average	205	579	36
Std Dev	2	75	2

Table C-2. Bottle burst pressure values for the bottle with standard base

Optimum base			
	Burst	Expansion	Time
Samples	(psi)	(ml)	(seconds)
1	192	516	33
2	193	494	32
3	198	610	35
4	193	590	34
5	195	556	33
6	195	478	31
Average	194	541	33
Std Dev	2	53	1

The following tests were carried out within 2 hours after the bottles were produced by Stretch

Blow Molding Process.

Table C-3. Bottle burst pressure values for the bottle with optimum base;

preform reheat temperature of 105 ^{o}C

105 ^{o}C Preform Set-point			
Samples	Burst (psi)	Expansion (ml)	Time (seconds)
1	209	428	33
2	210	486	35
3	210	444	33
4[*]	151[*]	155[*]	22[*]
5	207	392	32
6	212	498	35
7	213	471	34
8	203	383	31
9	212	426	33
10	209	423	33
11	210	414	32
Average	204	411	32
Std Dev	18	92	4

([*]) This bottle failed in the base whilst all other bottles failed in the panel area as is normal for good bottle production.

Table C-4. Bottle burst pressure values for the bottle with optimum base; preform reheat

temperature of 110 ^{o}C

110 ^{o}C Preform Set-point			
Samples	Burst (psi)	Expansion (ml)	Time (seconds)
1	198	415	32
2	199	451	33
3	195	424	32
4	199	433	33
5	194	409	31
6	197	343	30
7	196	433	32
8	197	458	32
9	196	485	31
10	197	501	33
Average	197	435	32
Std Dev	2	44	1

Table C-5. Bottle burst pressure values for the bottle with optimum base; preform reheat

temperature of 115 ^{o}C

	115 ^{o}C Preform Set-point		
	Burst	Expansion	Time
Samples	(psi)	(ml)	(seconds)
1	179	492	32
2	179	508	32
3	176	631	34
4	175	480	32
5	178	488	32
6	182	578	34
7	177	520	31
8	181	407	28
9	173	438	28
10	186	561	34
Average	179	510	32
Std Dev	4	66	2

Table C-6. Top load test and section weights of the bottle with standard base

	Standard Base			
	Top Load	Section Weights (g)		
Samples	Peak (Kg)	Base	Centre	Top
1	30.3	11.3	15.0	13.6
2	31.8	11.3	15.0	13.7
3	31.3	11.3	15.1	13.7
4	31.1	11.4	15.0	13.6
5	30.5	11.4	15.0	13.7
6	31.3	11.3	15.0	13.8
Average	31.1	11.3	15.0	13.7
Std Dev	0.6	0.1	0.0	0.1

Table C-7. Top load test and section weights of the bottle with optimum base

Optimum base				
	Top Load	Section Weights (g)		
Samples	Peak (Kg)	Base	Centre	Top
1	29.6	11.8	14.7	13.4
2	29.7	11.8	14.7	13.6
3	28.7	11.9	14.8	13.4
4	29.4	11.7	14.7	13.6
5	28.5	11.7	14.8	13.6
6	29.4	11.6	14.8	13.6
Average	29.2	11.8	14.8	13.5
Std Dev	0.5	0.1	0.1	0.1

Table C-8. Top loads and section weights of the bottle with optimum base;

preform reheat temperature of 105 ^{o}C

105 ^{o}C Preform Set-point				
	Top Load	Section Weights (g)		
Samples	Peak (Kg)	Base	Centre	Top
1	31.6	12.1	14.5	13.4
2	32.6	12.2	14.5	13.4
3	31.6	12.1	14.6	13.5
4	31.6	12.1	14.5	13.4
5	31.8	12.2	14.5	13.4
6	31.7	12.1	14.6	13.5
Average	31.8	12.1	14.5	13.4
Std Dev	0.4	0.0	0.1	0.1

Table C-9. Top loads and section weights of the bottle with optimum base;

preform reheat temperature of 110 ^{o}C

	Top Load	Section Weights (g)		
110 ^{o}C Preform Set-point				
Samples	Peak (Kg)	Base	Centre	Top
1	32.8	11.8	14.8	13.4
2	33.6	11.7	14.8	13.4
3	33.1	11.8	14.8	13.6
4	33.0	11.8	14.7	13.4
5	32.8	11.7	14.8	13.4
6	33.0	11.8	14.7	13.4
Average	33.0	11.8	14.8	13.4
Std Dev	0.3	0.0	0.1	0.1

Table C-10. Top loads and section weights of the bottle with optimum base;

preform reheat temperature of 115 ^{o}C

	Top Load	Section Weights (g)		
115 ^{o}C Preform Set-point				
Samples	Peak (Kg)	Base	Centre	Top
1	34.2	11.5	15.1	13.5
2	34.3	11.7	14.8	13.6
3	31.9	11.6	14.9	13.5
4	33.4	11.6	15.0	13.5
5	32.2	11.7	14.9	13.6
6	33.2	11.5	14.8	13.5
Average	33.2	11.6	14.9	13.5
Std Dev	1.0	0.1	0.1	0.0

Table C-11. Accelerated stress crack resistance for off-machine performance

ACCELERATED STRESS CRACK PERFORMANCE (minutes)		
Samples	Standard Base	Optimum base
1	61	66
2	51	58
3	25	87
4	49	77
5	47	71
6	21	82
Average	42	74
Std Dev	16	11

Table C-12. Accelerated stress crack resistance a few days after blow molding

ACCELERATED STRESS CRACK PERFORMANCE (minutes)		
Samples	Standard Base	Optimum base
1	32	68
2	36	73
3	44	64
4	14	75
5	36	61
6	37	53
7	31	50
8	27	66
9	31	67
10	48	60
Average	34	64
Std Dev	10	18

Table C-13 ASC Resistance to the average temperatures for the optimum base less than 24 hours

after blow molding

ACCELERATED STRESS CRACK PERFORMANCE (minutes)			
Samples	105 ^{o}C	110 ^{o}C	115 ^{o}C
1	83	103	48
2	101	69	75
3	91	67	57
4	87	81	81
5	100	60	83
6	81	86	46
7	98	63	79
8	93	61	73
9	85	113	84
10	103	82	52
Average	92	79	68
Std Dev	8	18	15

Table C-14. Thermal stability test for the 1500 ml. bottle with standard base

1500 ml. BOTTLE WITH STANDARD BASE									
Sample Number	Bottle Height (mm) (to bottom of flange)		Bottle Diameters (at locations defined in specifications sheet)						Base Clearance
			Upper Panel		Lower Panel		Base		
	Initial	Final	Initial	Final	Initial	Final	Initial	Final	(Initial)
1	274.2	279.8	90.9	93.0	91.0	93.4	92.6	93.9	7.2
2	274.3	280.0	91.0	93.0	90.9	93.0	92.1	93.9	7.0
3	274.2	279.6	91.0	93.0	91.0	93.0	93.0	93.9	7.3
Average	274.2	279.8	91.0	93.0	91.0	93.1	92.6	93.9	7.2
St. Dev	0.06	0.20	0.07	0.02	0.04	0.25	0.42		0.15
Minimum	274.2	279.6	90.9	93.0	90.9	93.0	92.1	93.9	7.0
Maximum	274.3	280.0	91.0	93.0	91.0	93.4	93.0	93.9	7.3
Sample Number	Fill Point Drop (mm) Final	Perpendicularity Final	Base Clearance Final	Height Growth (percent)	Growth in Diameters percent)			Pinch / Base Ratio (if applicable)	
					Upper Panel	Lower Panel	Base	Initial	Final
1	24.3		2.8	2.0	2.3	2.6	1.4	98.3	99.5
2	22.4		2.9	2.1	2.2	2.3	1.9	98.7	99.0
3	21.9		2.7	2.0	2.2	2.2	1.0	97.8	99.0
Average	22.9		2.8	2.0	2.2	2.4	1.4	98.3	99.2
St. Dev	1.27		0.10	0.06	0.07	0.23	0.46	0.42	0.26
Minimum	21.9		2.7	2.0	2.2	2.2	1.0	97.8	99.0
Maximum	24.3		2.9	2.1	2.3	2.6	1.9	98.7	99.5

Table C-15. Thermal stability test for the 1500 ml. bottle with optimum base

1500 ml. BOTTLE WITH OPTIMUM BASE									
Sample Number	**Bottle Height (mm) (to bottom of flange)**		**Bottle Diameters (at locations defined in specifications sheet)**						**Base Clearance**
			Upper Panel		**Lower Panel**		**Base**		
	Initial	**Final**	**Initial**	**Final**	**Initial**	**Final**	**Initial**	**Final**	**(Initial)**
1	273.8	278.3	91.0	93.3	91.1	93.2	92.8	94.1	6.2
2	273.9	278.3	91.1	93.3	91.0	93.2	92.3	94.0	6.3
3	273.9	278.5	91.2	93.3	91.1	93.2	92.5	94.2	6.2
Average	**273.9**	**278.4**	**91.1**	**93.3**	**91.1**	**93.2**	**92.6**	**94.1**	**6.2**
St. Dev	**0.06**	**0.12**	**0.10**	**0.04**	**0.07**	**0.03**	**0.24**	**0.13**	**0.06**
Minimum	**273.8**	**278.3**	**91.0**	**93.3**	**91.0**	**93.2**	**92.3**	**94.0**	**6.2**
Maximum	**273.9**	**278.5**	**91.2**	**93.3**	**91.1**	**93.2**	**92.8**	**94.2**	**6.3**
Sample Number	**Fill Point Drop (mm) Final**	**Perpendicularity Final**	**Base Clearance Final**	**Height Growth (percent)**	**Growth in Diameters Percent**			**Pinch / Base Ratio (if applicable)**	
					Upper Panel	**Lower Panel**	**Base**	**Initial**	**Final**
1	21.6		1.7	1.6	2.5	2.3	1.3	98.1	99.1
2	21.8		1.6	1.6	2.4	2.4	1.7	98.5	99.2
3	22.0		1.7	1.7	2.3	2.3	1.8	98.5	99.0
Average	**21.8**		**1.7**	**1.6**	**2.4**	**2.3**	**1.6**	**98.4**	**99.1**
St. Dev	**0.20**		**0.06**	**0.04**	**0.09**	**0.05**	**0.24**	**0.22**	**0.11**
Minimum	**21.6**		**1.6**	**1.6**	**2.3**	**2.3**	**1.3**	**98.1**	**99.0**
Maximum	**22.0**		**1.7**	**1.7**	**2.5**	**2.4**	**1.8**	**98.5**	**99.2**

Table C-16. Thermal stability test for the 1500 ml. bottle with optimum base preform reheat temperature of 105 ^{o}C

1500 ml. BOTTLE WITH OPTIMUM BASE (105 ^{o}C)									
Sample Number	Bottle Height (mm) (to bottom of flange)		Bottle Diameters (at locations defined in specifications sheet)						Base Clearance
			Upper Panel		Lower Panel		Base		
	Initial	Final	Initial	Final	Initial	Final	Initial	Final	(Initial)
1	273.2	284.5	91.4	95.2	91.4	95.5	93.0	96.3	6.0
2	273.2	285.0	91.4	95.5	91.4	95.5	93.0	96.2	6.1
Average	273.2	284.8	91.4	95.4	91.4	95.5	93.0	96.3	6.0
St. Dev	0.00	0.35	0.00	0.23	0.00	0.00	0.00	0.11	0.07
Minimum	273.2	284.5	91.4	95.2	91.4	95.5	93.0	96.2	6.0
Maximum	273.2	285.0	91.4	95.5	91.4	95.5	93.0	96.3	6.1
Sample Number	Fill Point Drop (mm) Final	Perpendicularity Final	Base Clearance Final	Height Growth (percent)	Growth in Diameters percent)			Pinch / Base Ratio (if applicable)	
					Upper Panel	Lower Panel	Base	Initial	Final
1	17.0		1.0	4.1	4.2	4.5	3.6	98.2	99.1
2	16.2		1.2	4.3	4.5	4.5	3.4	98.3	99.4
Average	16.6		1.1	4.2	4.4	4.5	3.5	98.2	99.3
St. Dev	0.57		0.12	0.13	0.25	0.00	0.11	0.06	0.21
Minimum	16.2		1.0	4.1	4.2	4.5	3.4	98.2	99.1
Maximum	17.0		1.2	4.3	4.5	4.5	3.6	98.3	99.4

Table C-17. Thermal stability test for the 1500 ml. bottle with optimum base preform reheat temperature of 110 ^{o}C

1500 ml. BILLBOARD WITH OPTIMUM BOTTLE BASE (110 ^{o}C)									
Sample Number	Bottle Height (mm) (to bottom of flange)		Bottle Diameters (at locations defined in specifications sheet)						Base Clearance
			Upper Panel		Lower Panel		Base		
	Initial	Final	Initial	Final	Initial	Final	Initial	Final	(Initial)
1	274.0	285.0	91.4	95.2	91.4	95.2	93.0	95.5	5.8
2	274.0	285.0	91.4	95.2	91.4	94.9	93.0	95.5	6.1
Average	274.0	285.0	91.4	95.2	91.4	95.1	93.0	95.5	6.0
St. Dev	0.00	0.00	0.00	0.00	0.00	0.23	0.00	0.00	0.17
Minimum	274.0	285.0	91.4	95.2	91.4	94.9	93.0	95.5	5.8
Maximum	274.0	285.0	91.4	95.2	91.4	95.2	93.0	95.5	6.1
Sample Number	Fill Point Drop (mm) Final	Perpendicularity Final	Base Clearance Final	Height Growth (percent)	Growth in Diameters percent)			Pinch / Base Ratio (if applicable)	
					Upper Panel	Lower Panel	Base	Initial	Final
1	15.2		1.0	4.0	4.2	4.2	2.7	98.4	99.7
2	15.6		0.5	4.0	4.2	3.8	2.7	98.6	99.3
Average	15.4		0.8	4.0	4.2	4.0	2.7	98.5	99.5
St. Dev	0.28		0.36	0.00	0.00	0.25	0.00	0.14	0.24
Minimum	15.2		0.5	4.0	4.2	3.8	2.7	98.4	99.3
Maximum	15.6		1.0	4.0	4.2	4.2	2.7	98.6	99.7

Table C-18. Thermal stability test for the 1500 ml. bottle with optimum base preform reheat temperature of 115 ^{o}C

1500 ml. BOTTLE WITH OPTIMUM BASE (115 ^{o}C)									
Sample Number	Bottle Height (mm) (to bottom of flange)		Bottle Diameters (at locations defined in specifications sheet)						Base Clearance
			Upper Panel		Lower Panel		Base		
	Initial	Final	Initial	Final	Initial	Final	Initial	Final	(Initial)
1	274.6	285.0	91.7	95.5	91.7	94.7	93.0	95.4	5.5
2	274.6	285.5	91.7	96.0	91.4	95.1	93.0	95.4	5.7
Average	274.6	285.3	91.7	95.8	91.6	94.9	93.0	95.4	5.6
St. Dev		0.35		0.34	0.23	0.22			0.11
Minimum	274.6	285.0	91.7	95.5	91.4	94.7	93.0	95.4	5.5
Maximum	274.6	285.5	91.7	96.0	91.7	95.1	93.0	95.4	5.7
Sample Number	Fill Point Drop (mm) Final	Perpendicularity Final	Base Clearance Final	Height Growth (percent)	Growth in Diameters percent)			Pinch / Base Ratio (if applicable)	
					Upper Panel	Lower Panel	Base	Initial	Final
1	15.5		0.8	3.8	4.2	3.3	2.6	98.6	99.3
2	17.0		0.6	4.0	4.7	4.0	2.6	98.4	99.7
Average	16.3		0.7	3.9	4.4	3.7	2.6	98.5	99.5
St. Dev	1.06		0.13	0.13	0.37	0.50		0.14	0.23
Minimum	15.5		0.6	3.8	4.2	3.3	2.6	98.4	99.3
Maximum	17.0		0.8	4.0	4.7	4.0	2.6	98.6	99.7
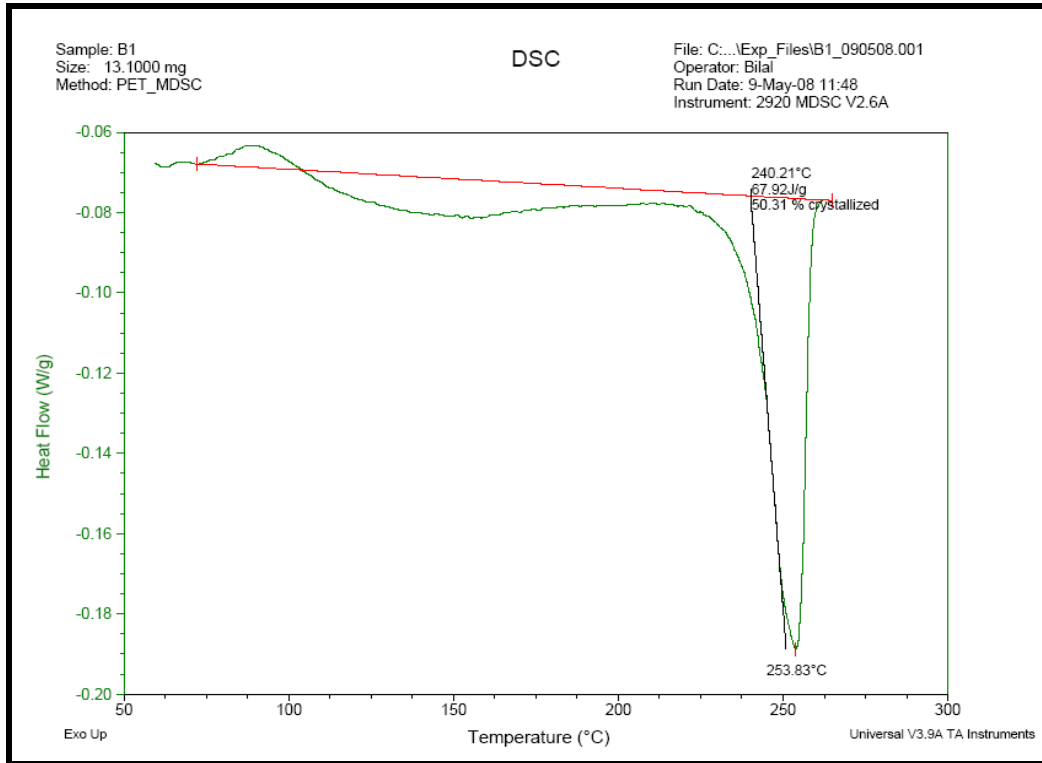
Fig.D-1(a). Heat flow curve; and cystallinity of the optimised base design at the valley region

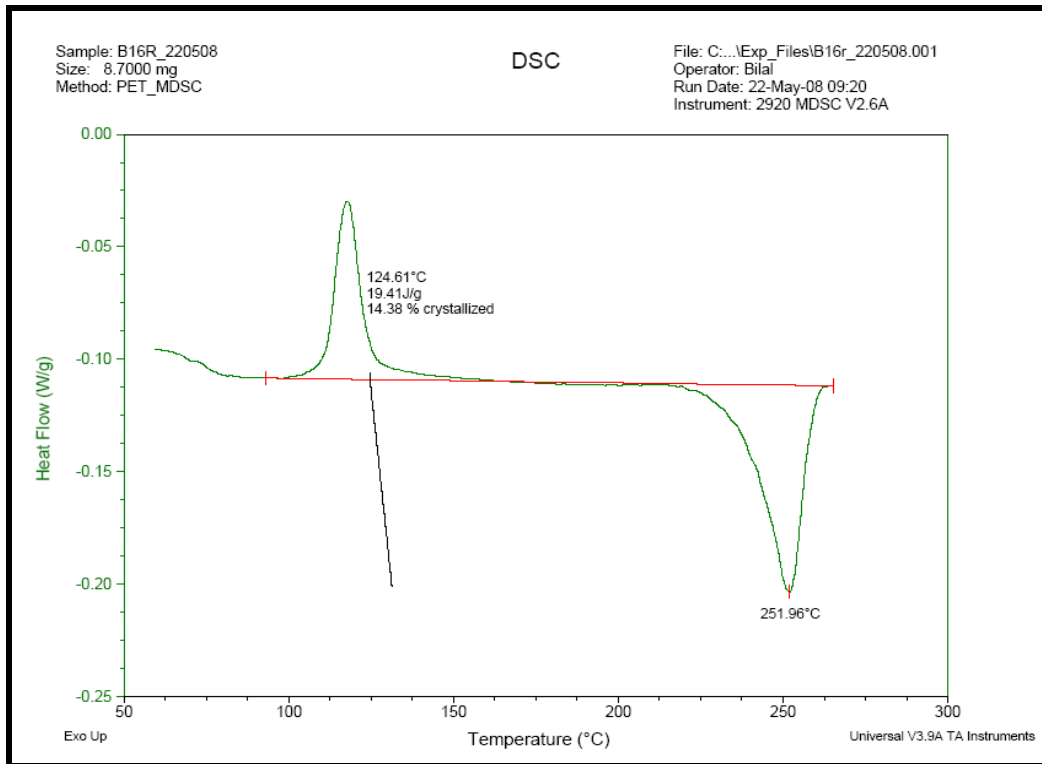
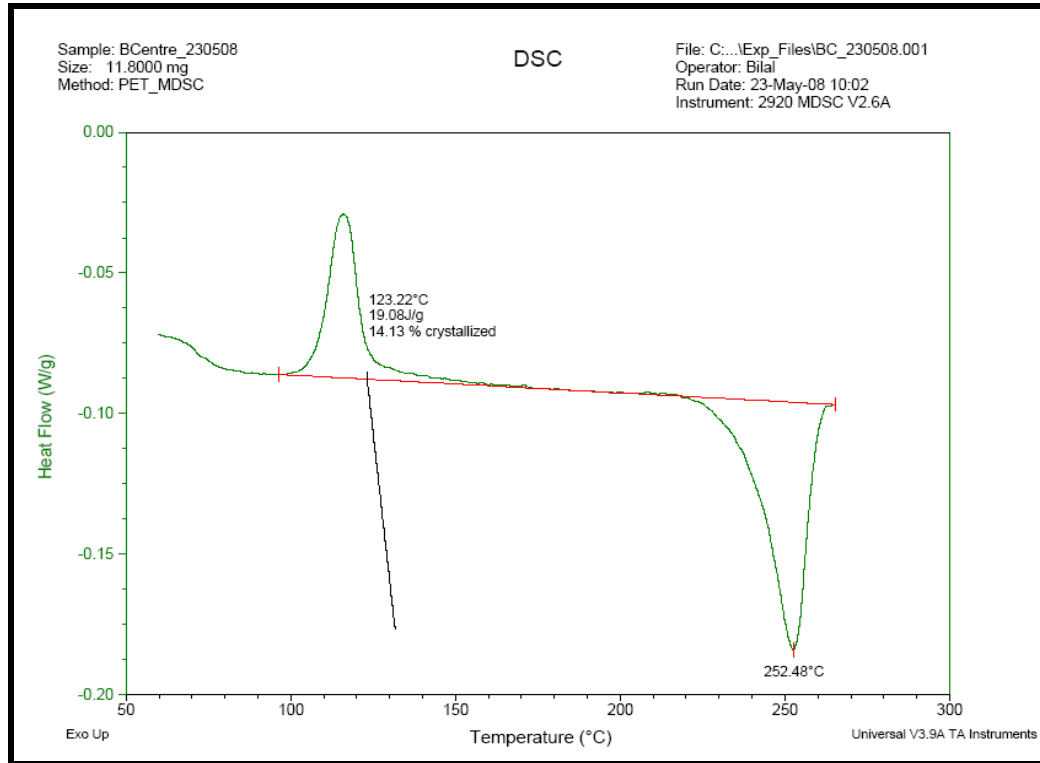Fig.D-1(b). Heat flow curve; and cystallinity of the optimised base design at the valley transition

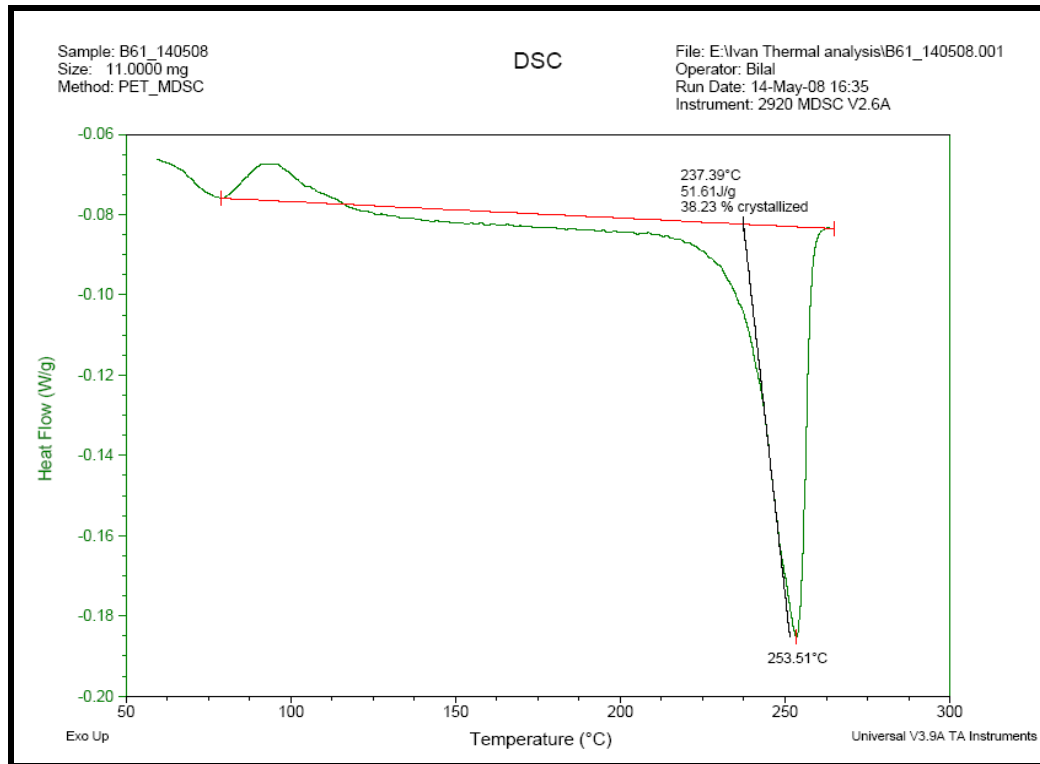Fig.D-1(c). Heat flow curve; and cystallinity of the optimised base design at the centre region

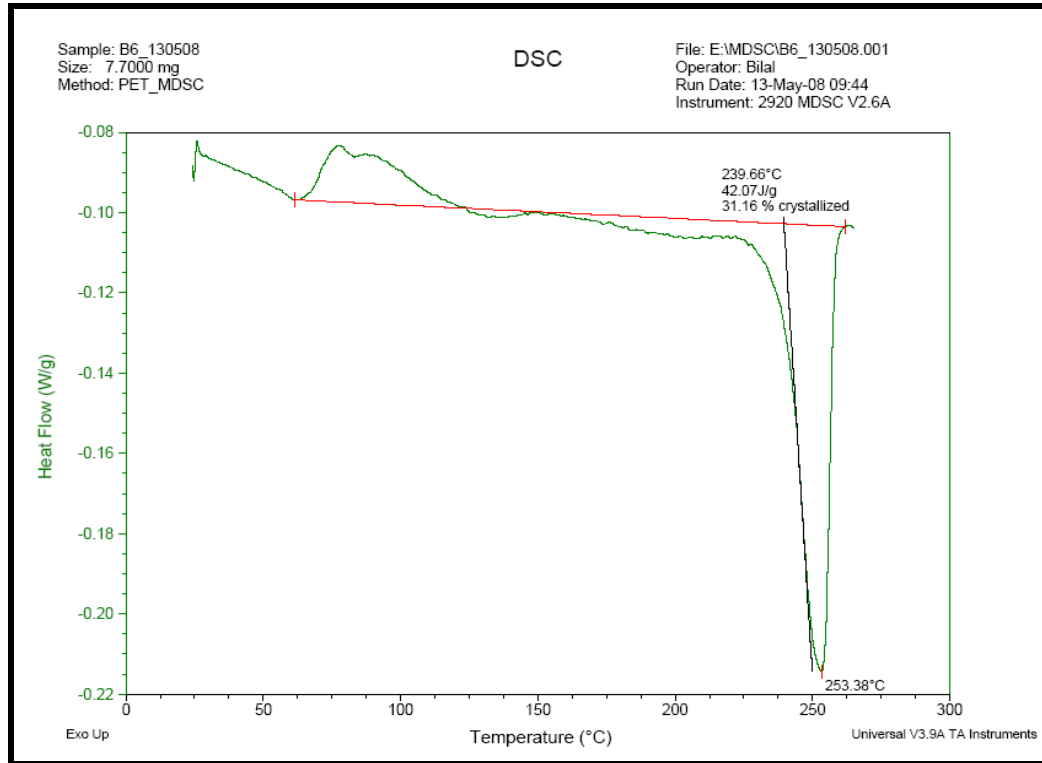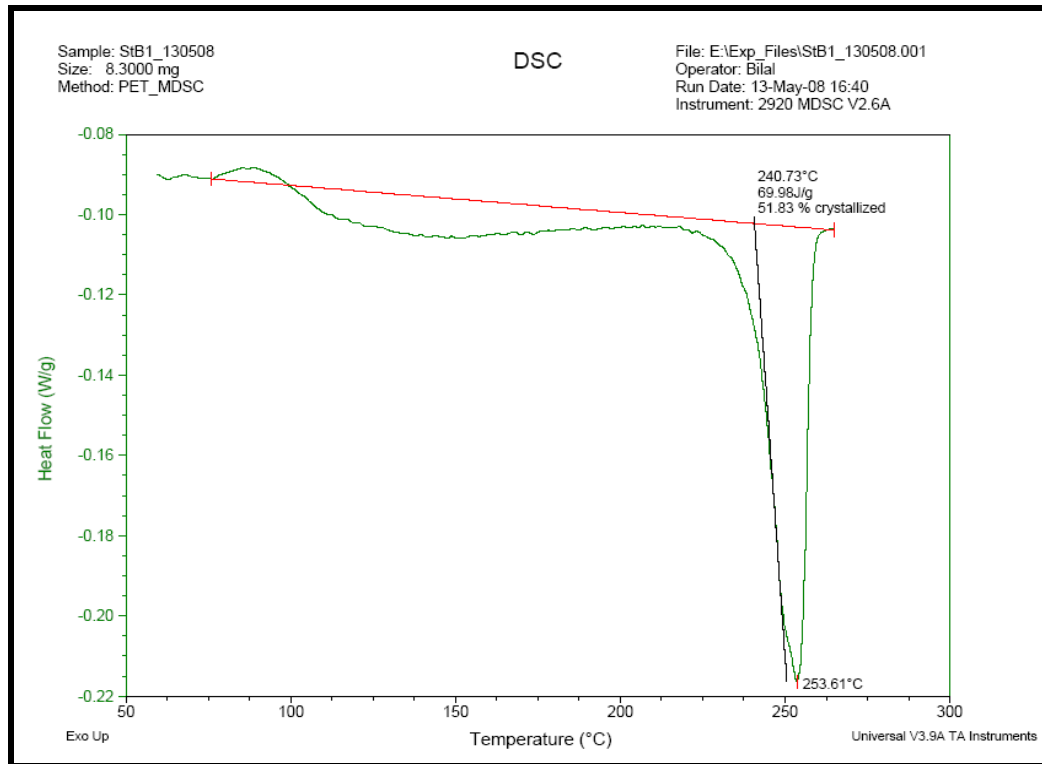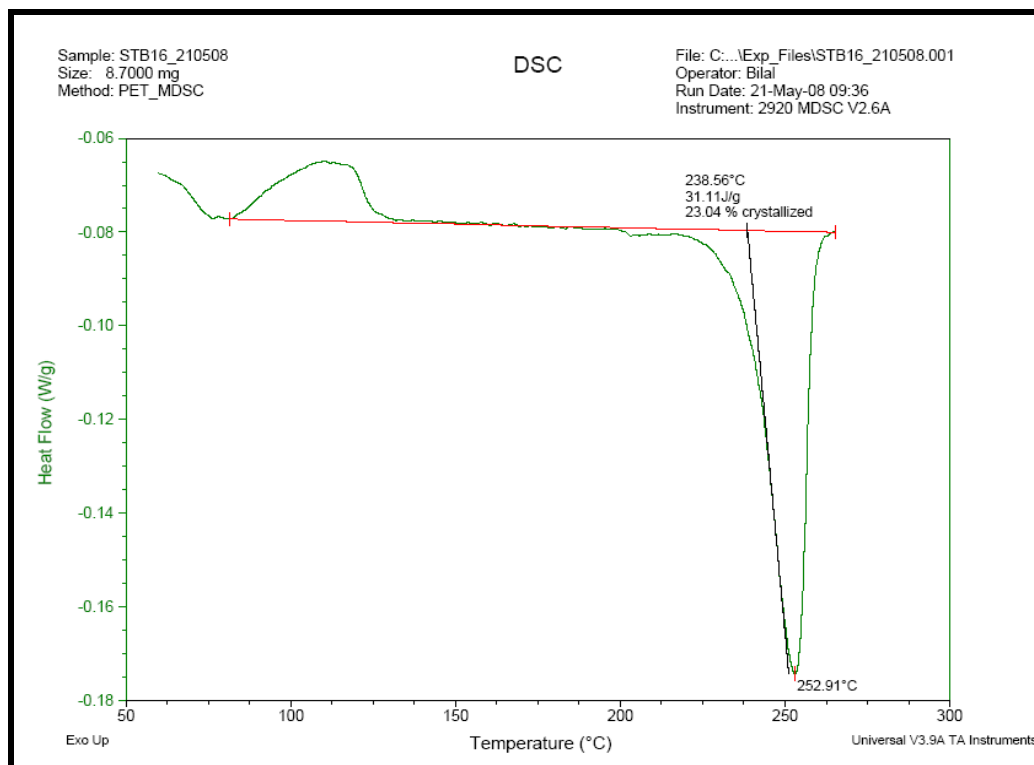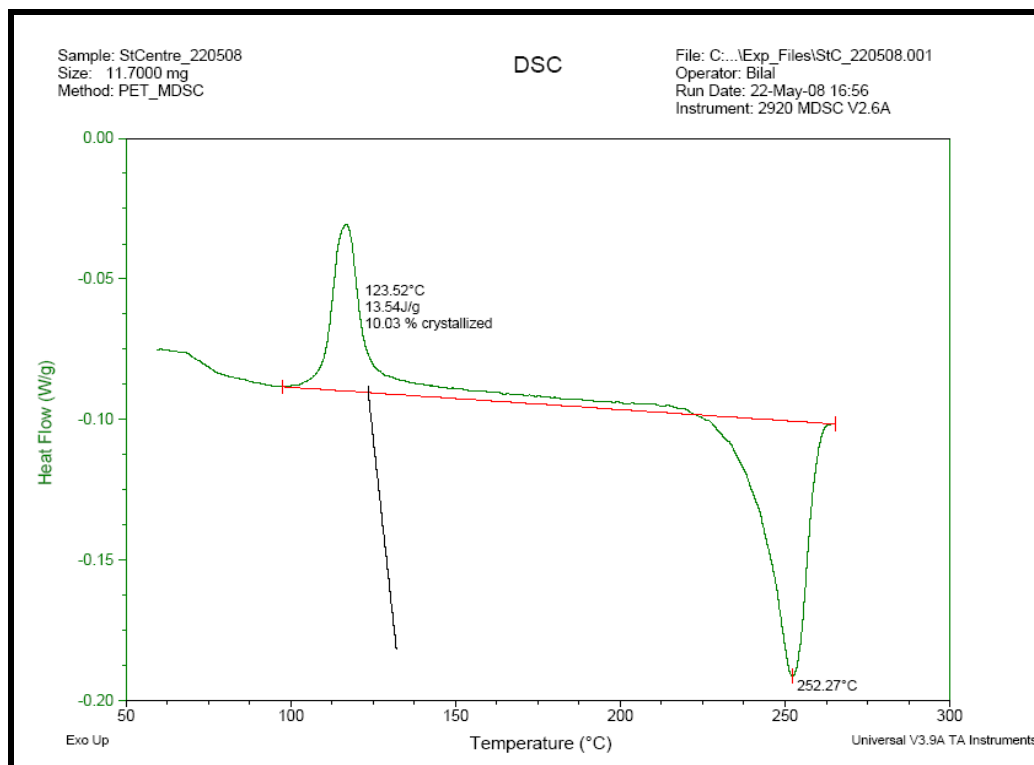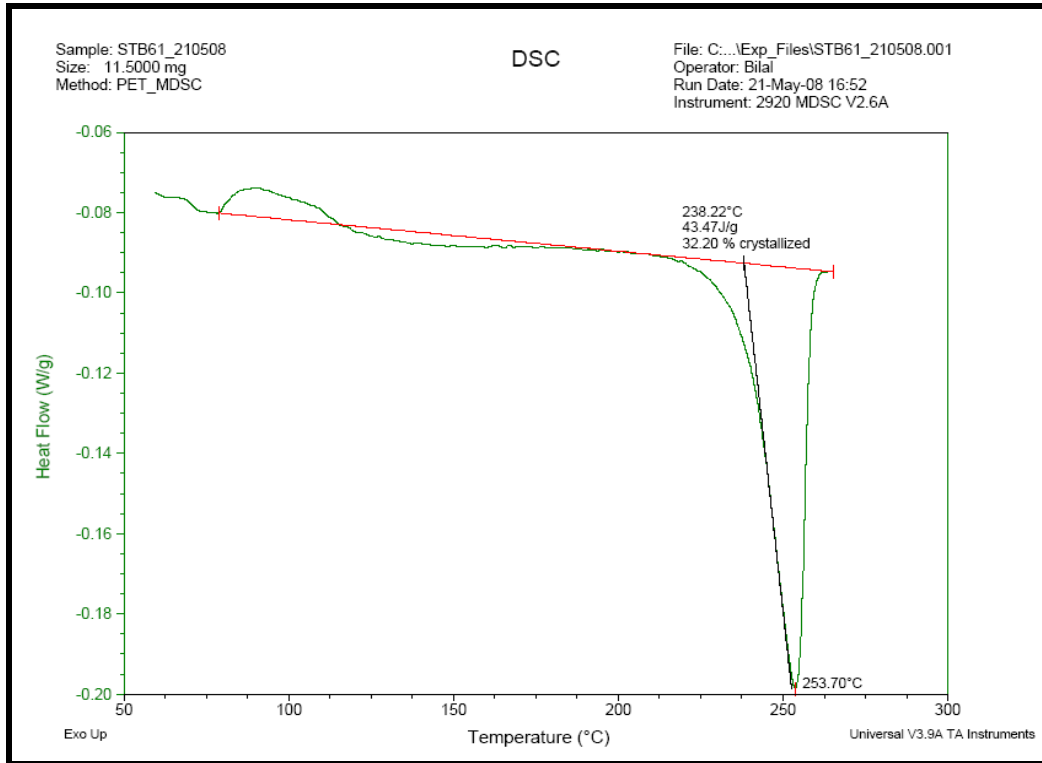Fig.D-1(d). Heat flow curve; and cystallinity of the optimised base design at the foot transition

Fig.D-1(e). Heat flow curve; and cystallinity of the optimised base design at the foot region

Fig.D-2(a). Heat flow curve; and cystallinity of the standard base design at the valley region

Fig.D-2(b). Heat flow curve; and cystallinity of the standard base design at the valley transition
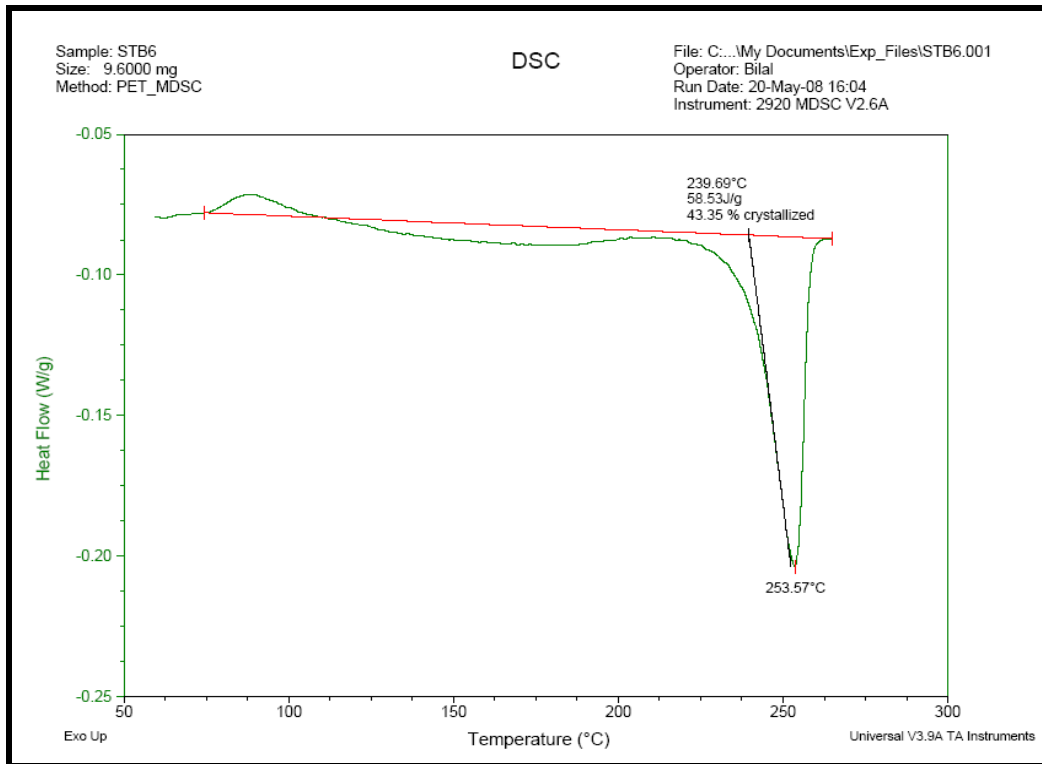

Fig.D-2(c). Heat flow curve; and cystallinity of the standard base design at the centre region

Fig.D-2(d). Heat flow curve; and cystallinity of the standard base design at the foot transition

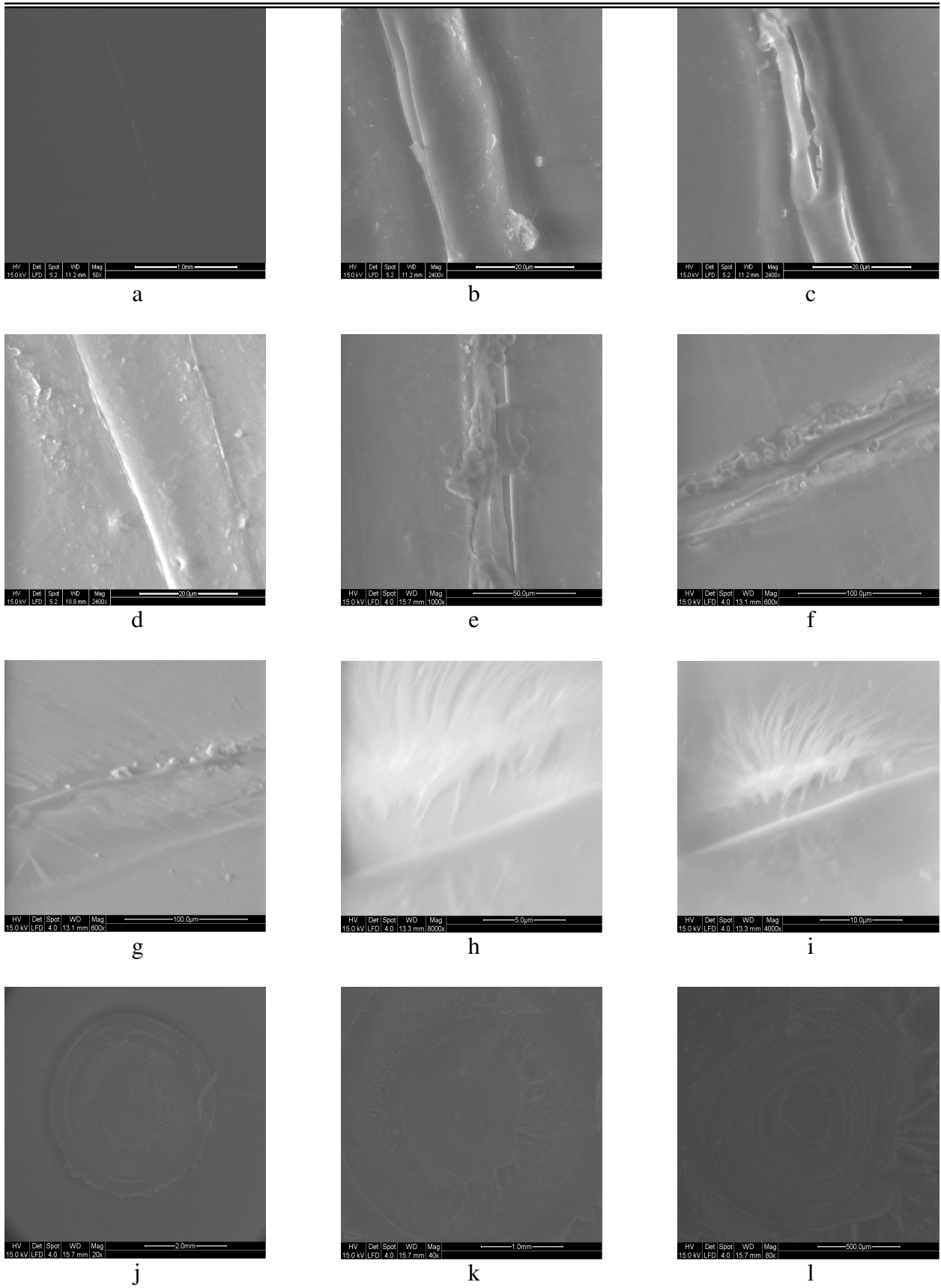Fig.D-2(e). Heat flow curve; and cystallinity of the standard base design at the foot region

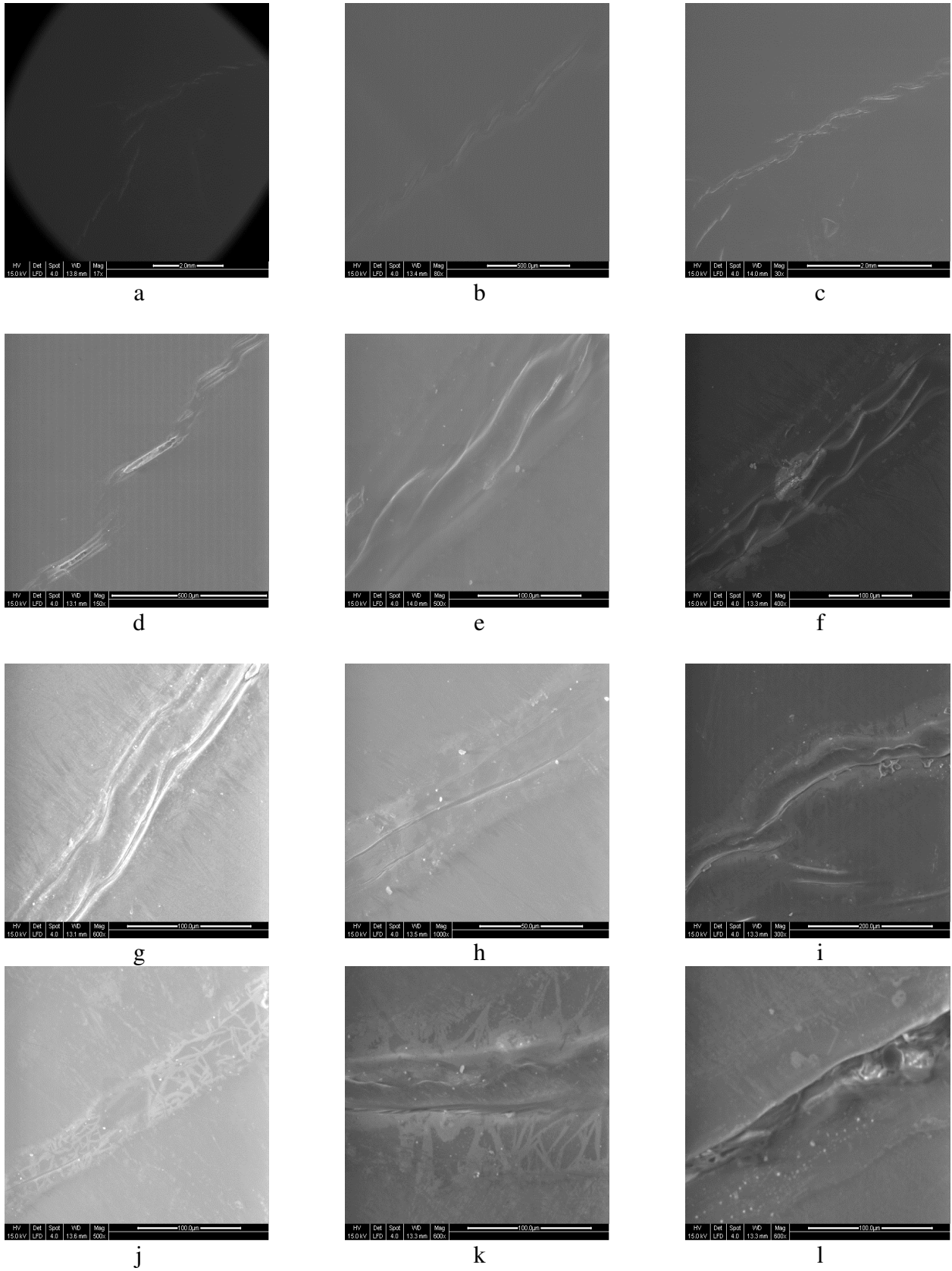Fig.E-1. SEM Images of the cracked bottle base with standard design

a

b

c

d

e

f

g

h

i

j

k

l

Fig.E-2. SEM Images of the cracked bottle base with optimized design
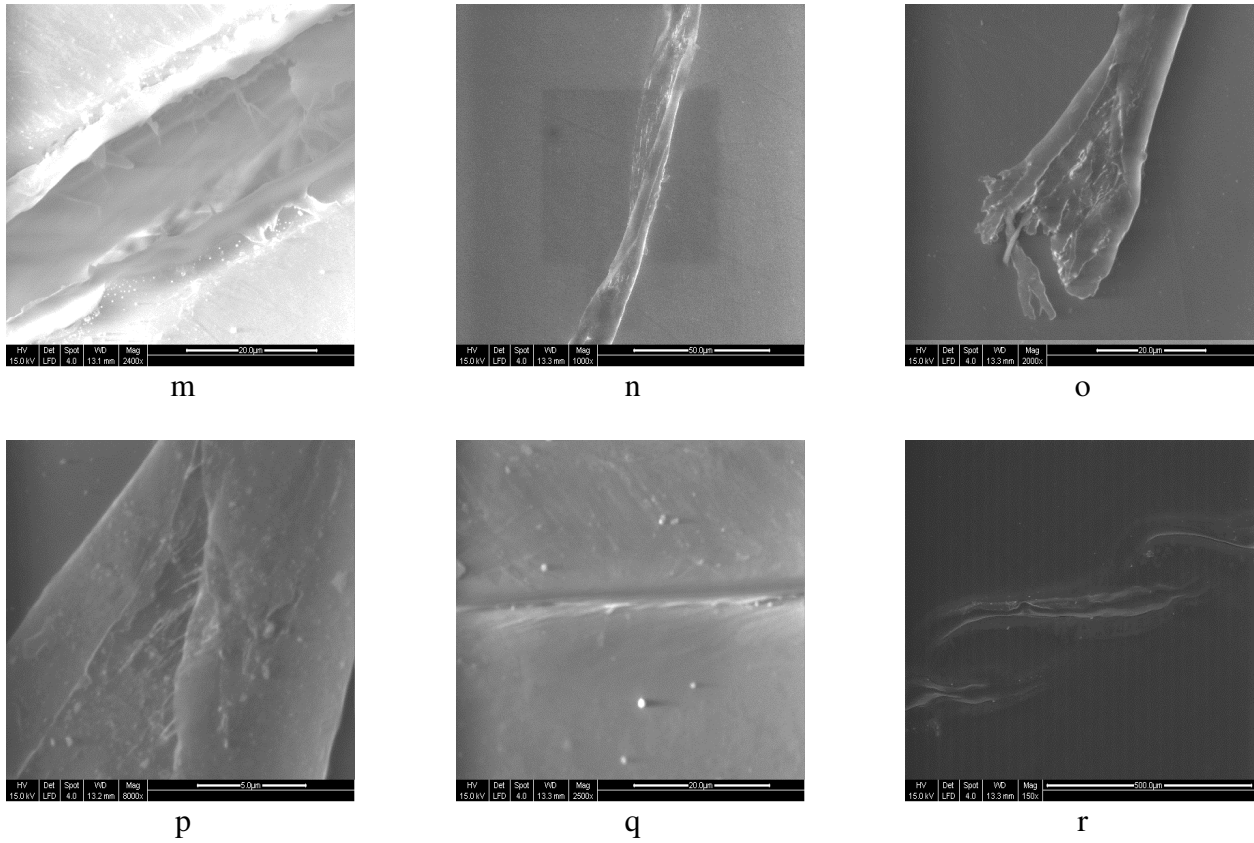
m

n

o

p

q

r

Fig.E-2. SEM Images of the cracked bottle base with optimized design (continue)